

Supporting Information for

**Efficient Copolymerization of Acrylate and Ethylene with Neutral P, O-Chelated Nickel Catalysts: Mechanistic Investigations of Monomer Insertion and Chelate Formation**

Shuoyan Xiong<sup>†1</sup>, Manar M. Shoshani<sup>†1</sup>, Xinglong Zhang<sup>†1</sup>, Heather A. Spinney<sup>2</sup>, Alex J.

Nett<sup>2</sup>, and Briana S. Henderson<sup>2</sup>, Thomas F. Miller III<sup>\*1</sup>, and Theodor Agapie<sup>\*1</sup>

\*To whom correspondence should be addressed, E-mail: agapie@caltech.edu,  
tfm@caltech.edu

<sup>1</sup>Division of Chemistry and Chemical Engineering, California Institute of Technology, Pasadena, California 91125, United States

<sup>2</sup>Chemical Science, Core R&D, Dow, Midland, Michigan 48667, United States

*Experimental details for*

**Part A: Ligands and metal complexes**

1. Synthesis of ligands and metal complexes	S2
2. NMR characterization of ligands and metal complexes	S16
3. Solution-state NMR characterization and discussion of <b>5</b>	S26
4. Crystallographic information	S31

**Part B: Ethylene/tBA copolymerization**

5. Conditions and results.	S38
6. NMR Characterization of ethylene/tBA copolymers	S47
7. GPC curves of ethylene/tBA copolymers	S51

**Part C: Kinetic studies**

8. Kinetic measurements	S54
9. DFT calculations	S76
10. Computational investigation in isomerization	S112
11. Discussion of experimental and computational kinetic studies	S121

*References*

S129

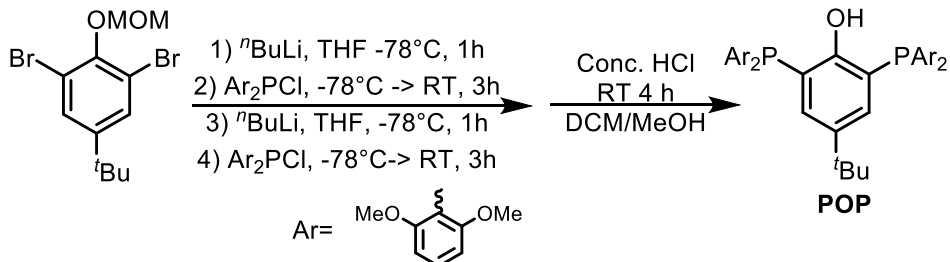
## *Experimental details for:*

### *Part A: Ligands and Metal Complexes*

#### *1. Synthesis of ligands and metal complexes*

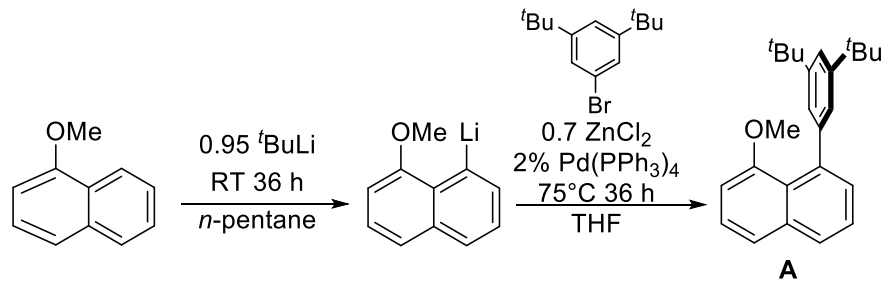
##### **General Considerations**

All air- and water-sensitive compounds were manipulated under N<sub>2</sub> or Ar using standard Schlenk or glovebox techniques. The solvents for air- and moisture-sensitive reactions were dried over sodium benzophenone ketyl or calcium hydride or by the method of Grubbs.<sup>1</sup> Deuterated solvents were purchased from Cambridge Isotopes Lab, Inc.; C<sub>6</sub>D<sub>6</sub>, and C<sub>7</sub>D<sub>8</sub> was dried over a purple suspension with Na/benzophenone ketyl and vacuum transferred; C<sub>6</sub>D<sub>5</sub>Cl was dried over CaH<sub>2</sub> for greater than 24 h, vacuum transferred, and passed over an activated alumina plug. Ethylene (99.999%) for kinetic experiments was purchased from Matheson Tri-Gas and used without further purification. 2,6-lutidine was dried with sieves and distilled over AlCl<sub>3</sub> to remove 3-picoline and 4-picoline. t-Butyl acrylate were dried over 4 Å sieves for greater than 72h, vacuum transferred, and passed over an activated alumina plug. Acrylates used in kinetic studies contain 200~300 ppm of monomethyl ether hydroquinone as inhibitor. Dimethoxybenzene, 1-methoxynaphthalene, and pyridine were dried over calcium hydride and vacuum-transferred or distilled prior to use. 3,5-ditertbutylbromobenzene was dried by heating at 70 °C under vacuum for 16 hours. 2.5 M <sup>7</sup>BuLi, BBr<sub>3</sub>, Br<sub>2</sub>, ZnCl<sub>2</sub>, and palladium-tetrakis(triphenylphosphine) were purchased from Sigma-Aldrich and used without further purification. Bis(dimethoxyphenyl)phosphine chloride,<sup>2</sup> 1,3-dibromo-5-(tert-butyl)-2-(methoxymethoxy)benzene,<sup>3</sup> NiMe<sub>2</sub>TMEDA,<sup>4</sup> and Nipy<sub>2</sub>(CH<sub>2</sub>Si(CH<sub>3</sub>)<sub>3</sub>)<sup>5</sup> were synthesized according to literature procedures. All <sup>1</sup>H, <sup>13</sup>C, and <sup>31</sup>P spectra of organic and organometallic compounds were recorded on Varian Mercury 300, Varian INOVA-400, or 500, or Bruker Cryoprobe 400 spectrometers. <sup>1</sup>H and <sup>13</sup>C chemical shifts are reported relative to residual solvent resonances.



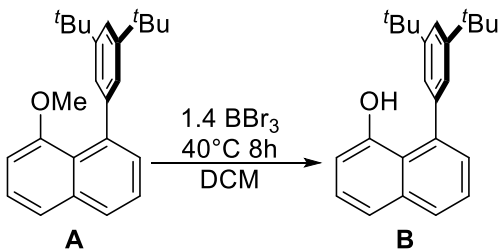
**POPH:** A Schlenk flask fitted with a screw-in Teflon stopper was charged with a solution of 1,3-dibromo-5-(tert-butyl)-2-(methoxymethoxy)benzene (3.52 g, 10.0 mmol) in THF (40 mL) and cooled to -78 °C under nitrogen. A hexane solution of *n*-butyllithium (4 mL, 2.5 M, 10.0 mmol) was added dropwise via syringe. After stirring for an additional 30 min at -78 °C, a solution of bis(2,6-dimethoxyphenyl)phosphine chloride (3.41 g, 10.0 mmol) in THF (20 mL) was added dropwise via cannula. After complete addition, the reaction was allowed to warm up to room temperature and stirred for an additional 3 h, yielding a yellow solution. The reaction was then cooled to -78 °C and a hexane solution of *n*-butyllithium (4 mL, 2.5 M, 10.0 mmol) was added dropwise via syringe. After stirring for an additional 30 min at -78 °C, a solution of bis(2,6-dimethoxyphenyl)phosphine chloride (3.41 g, 10.0 mmol) in THF (20 mL) was added dropwise via cannula. After complete addition, the reaction was allowed to warm up to room temperature and stirred for an additional 3 h, yielding a bright orange solution. The volatiles were then removed under vacuum. The pale yellow residue was dissolved in degassed CH<sub>2</sub>Cl<sub>2</sub> (20 mL) and degassed MeOH (10 mL) followed by the addition of concentrated aqueous HCl (5 mL). The resulting mixture was degassed immediately via three freeze-pump-thaw cycle with a liquid nitrogen bath. After stirring for 4 h under room temperature, volatiles were removed under vacuum. In a N<sub>2</sub>-filled glovebox (no exclusion of water), the resulting pale-yellow residue was taken up in CH<sub>2</sub>Cl<sub>2</sub> (40 mL), washed with saturated aqueous solutions of K<sub>2</sub>CO<sub>3</sub> (3 x 10 mL) and NH<sub>4</sub>Cl (3 x 10 mL), dried over MgSO<sub>4</sub>,

and filtered through Celite. The volatiles were removed under reduced pressure. In a glovebox (exclusion of water and oxygen), the resulting pale-yellow solid was dissolved in ether and filtered through Celite. The volatile materials were removed once more under vacuum and the resulting mixture was washed by hexanes (10 mL) and the solid was collected via vacuum filtration, yielding 2,6-bis(bis(2',6'-dimethoxyphenyl)phosphino)-4-tert-butylphenol (**POPH**) (1.68g, 22% yield) as a white powder.  $^1\text{H}$  NMR (400 MHz,  $\text{C}_6\text{D}_6$ ):  $\delta$  7.56–7.54 (d,  $^3J_{\text{HH}} = 8.4$  Hz, 2H, PhH), 7.50 (s, 1H, OH), 7.03–6.99 (t,  $^4J_{\text{HH}} = 8.4$  Hz, 4H, PhH), 6.26–6.23 (dd,  $^3J_{\text{HH}} = 8.4$  Hz,  $^3J_{\text{HH}} = 2.6$  Hz, 8H, PhH), 3.13 (s, 24H, OCH<sub>3</sub>), 1.17 (s, 9H, C(CH<sub>3</sub>)<sub>3</sub>);  $^{13}\text{C}\{\text{H}\}$  NMR (101 MHz,  $\text{C}_7\text{D}_8$ ):  $\delta$  162.88 (d,  $^2J_{\text{CP}} = 8.7$  Hz, 8C, aryl-C), 159.45 (t,  $^2J_{\text{CP}} = 13.1$  Hz, 2C, aryl-C), 139.30 (t,  $^3J_{\text{CP}} = 6.1$  Hz, 2C, aryl-C), 131.18 (d,  $J_{\text{CP}} = 21.7$  Hz, 2C, aryl-C), 129.27 (s, 4C, aryl-C), 122.32 (d,  $^2J_{\text{CP}} = 13.1$  Hz, 2C, aryl-C), 115.57 (d,  $J_{\text{CP}} = 27.3$  Hz, 4C, aryl-C), 104.55 (s, 8C, aryl-C), 55.48 (s, 24C, OCH<sub>3</sub>), 34.31 (s, 1C, C(CH<sub>3</sub>)<sub>3</sub>), 32.01 (s, 9C, C(CH<sub>3</sub>)<sub>3</sub>);  $^{31}\text{P}\{\text{H}\}$  NMR (121 MHz,  $\text{C}_6\text{D}_6$ ):  $\delta$  -55.61 (s).

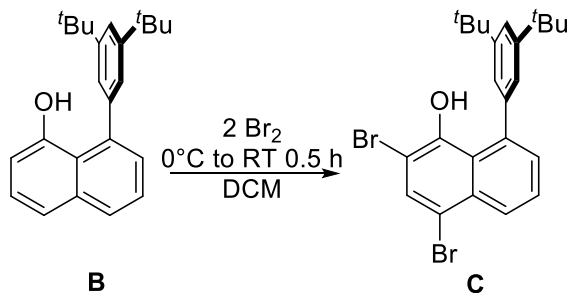


**8-(3,5-di(tert-butyl)phenyl)-1-methoxynaphthalane:** To a solution of 1-methoxynaphthalene (7.21 g, 45.60 mmol) in *n*-pentane (75 ml) in a Teflon-fitted Schlenk tube was added tert-butyl lithium (2.87 g, 45.30 mmol). The solution was stirred in the glovebox for 36 h and the resulting yellow suspension was passed through a frit. The collected yellow solid was washed with *n*-pentane (2 x 50 mL) and dried under vacuum. The lithium salt was then collected (7.20 g, 96.2% yield) and used without further purification. The lithium

salt (5.25 g, 32.0 mmol) was dissolved in THF (100mL). ZnCl<sub>2</sub> (3.04 g, 22.4 mmol) was then added as a solid to the stirring solution over the course of 15 minutes. The resultant cloudy pale-yellow solution was stirred for an additional 0.5 h. Palladium-tetrakis(triphenylphosphine) (740 mg, 0.64 mmol) and 3,5 di-tertbutyl-bromobenzene (8.61 g, 32.0 mmol) were then added as solids to the stirring solution. The Schlenk tube was then sealed and transferred to the Schlenk line and equipped with a reflux condenser. The solution was heated at 75 °C for 36 hours, under an N<sub>2</sub> atmosphere, and then cooled to room-temperature at which point distilled water (25 mL) was added. The suspension was transferred to a round bottom flask and the THF was evaporated on a rotary evaporator. The crude material was then extracted with dichloromethane (3 x 100 mL), washed with H<sub>2</sub>O (3 x 40 mL), and then dried with MgSO<sub>4</sub>. After filtering, the volatiles were removed and the crude pale-yellow oil (9.65g, 87.1 % yield) was used without further purification. Confirmation of product assignment was determined by <sup>1</sup>H NMR spectroscopy. <sup>1</sup>H NMR (400 MHz, CDCl<sub>3</sub>): δ 7.80 (dd, <sup>3</sup>J<sub>HH</sub> = 8. Hz, <sup>4</sup>J<sub>HH</sub> = 1.3 Hz, 1H, PhH), 7.50 (d, <sup>3</sup>J<sub>HH</sub> = 8.3 Hz, 1H, PhH), 7.47 (dd, <sup>3</sup>J<sub>HH</sub> = 8.3 Hz, <sup>3</sup>J<sub>HH</sub> = 7.3 Hz, 1H, PhH), 7.38 (apparent t, <sup>3</sup>J<sub>HH</sub> = 8.0 Hz, 1H, PhH), 7.36 (t, <sup>4</sup>J<sub>HH</sub> = 1.9 Hz, 1H, PhH), 7.33 (dd, <sup>3</sup>J<sub>HH</sub> = 7.2 Hz, <sup>4</sup>J<sub>HH</sub> = 1.3 Hz, 1H, PhH), 7.17 (d, <sup>4</sup>J<sub>HH</sub> = 1.9 Hz, 2H, PhH), 6.77 (d, <sup>3</sup>J<sub>HH</sub> = 7.8 Hz, 1H, PhH), 3.45 (s, 3H, OCH<sub>3</sub>), 1.36 (s, 18H, 'Bu).

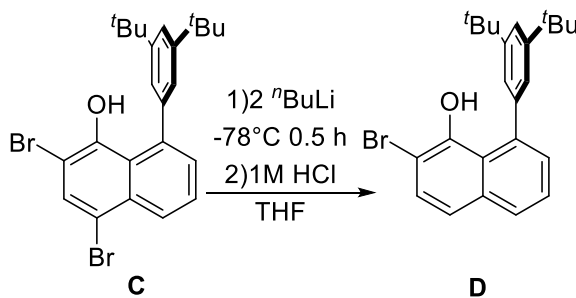


**8-(3,5-di(tert-butyl)phenyl)-1-naphthol:** To a two-neck round bottom flask equipped with a reflux-condenser, and solid **A** (9.65 g, 27.9 mmol) was added anhydrous dichloromethane (200 mL) via cannula transfer. The round bottom was then cooled to – 78 °C and  $\text{BBr}_3$  (3.43 mL, 36.3 mmol) was added to the stirring solution using two separate syringes. The solution was then warmed to room temperature and then heated to 40 °C and stirred for an additional 8 hours. The light brown solution was then cooled to 0 °C and distilled water was carefully added to quench the excess  $\text{BBr}_3$ . The organic fraction was then separated, and the aqueous fraction was further extracted with dichloromethane (2 x 50 mL). The organic fractions were combined and washed with water (3 x 30 mL), and then dried with  $\text{MgSO}_4$ . After filtration, the solution was filtered through a plug of silica and washed with additional dichloromethane. All volatiles were then removed and the crude pale-yellow solid E (8.50 g, 91.5 % yield) was used without further purification. Confirmation of product assignment was determined by  $^1\text{H}$  NMR spectroscopy.  $^1\text{H}$  NMR (400 MHz,  $\text{CDCl}_3$ ):  $\delta$  7.86 (dd,  $^3J_{\text{HH}} = 8.2$  Hz,  $^4J_{\text{HH}} = 1.3$  Hz, 1H, PhH), 7.56 (t,  $^4J_{\text{HH}} = 1.9$  Hz, 1H, PhH), 7.35-7.52 (overlapping multiplets, 3H, PhH), 7.34 (d,  $^4J_{\text{HH}} = 1.9$  Hz, 2H, PhH), 7.24 (dd,  $^3J_{\text{HH}} = 7.0$  Hz,  $^3J_{\text{HH}} = 1.3$  Hz, 1H, PhH), 6.91 (dd,  $^3J_{\text{HH}} = 7.5$  Hz,  $^4J_{\text{HH}} = 1.3$  Hz, 1H, PhH), 5.90 (s, 1H, OH), 1.37 (s, 18H,  $^3\text{Bu}$ ).

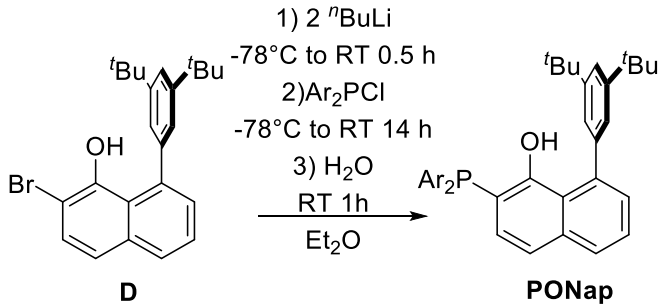


**8-(3,5-di(tert-butyl)phenyl)-2,4-dibromo-1-mnaphthol:** A solution of **B** (8.50 g, 25.5 mmol) in dichloromethane (250 mL) and transferred to a two-neck round bottom flask equipped with a pressure equalizing dropping funnel. To the dropping funnel was added 2 equivalents of bromine (2.62 mL, 50.9 mmol) as a solution in dichloromethane (10 mL). Connected through tubing, is an oil bubbler and a saturated aqueous solution of NaOH. Compressed air was pushed through the apparatus to allow for efficient quenching of the formed HBr. The reaction vessel was cooled to 0 °C and the solution of bromine was slowly added via dropping funnel over the course of 0.5 hours. After complete addition of bromine, the cooling bath was removed, and the reaction was stirred at room temperature for an additional 0.5 hours. A saturated solution of sodium thiosulfate was then added to the stirring solution and the organic layer was separated. The aqueous layer was further extracted with dichloromethane (2 x 150 mL) and the organic layers were combined and washed with water (3 x 100 mL). After collecting the organic layer, the solution was filtered through a plug of silica which was washed with additional dichloromethane. All volatiles were then removed from the solution and the pale-yellow solid **C** (9.06 g, 70.5 % yield) was used without further purification. Confirmation of product assignment was determined by <sup>1</sup>H NMR spectroscopy.

<sup>1</sup>H NMR (400 MHz, CDCl<sub>3</sub>): δ 8.28 (d, <sup>3</sup>J<sub>HH</sub> = 8.5 Hz, 1H, PhH), 7.95 (s, 1H, PhH), 7.59 (dd, <sup>3</sup>J<sub>HH</sub> = 8.5 Hz, <sup>3</sup>J<sub>HH</sub> = 8.0 Hz, 1H, PhH), 7.57 (t, <sup>4</sup>J<sub>HH</sub> = 1.9 Hz, 1H, PhH), 7.34 (d, <sup>3</sup>J<sub>HH</sub> = 7.0 Hz, 1H, PhH), 7.28 (d, <sup>4</sup>J<sub>HH</sub> = 1.9 Hz, 2H, PhH), 6.34 (s, 1H, OH), 1.36 (s, 18H, <sup>t</sup>Bu).

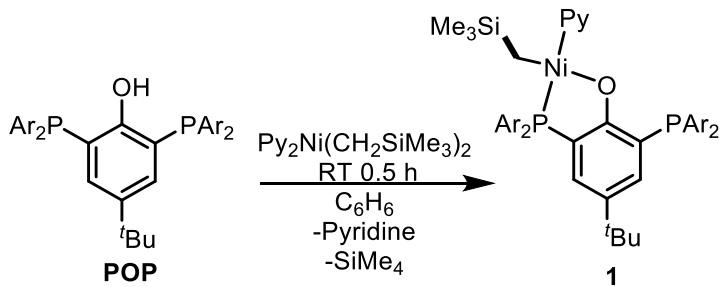


**8-(3,5-di(tert-butyl)phenyl)-2-bromo-1-naphthol:** A solution of **C** (9.06g, 18.5 mmol) in anhydrous THF (150 mL) in a two-neck round bottom equipped with a stir bar is cooled to -78 °C. To this stirring solution is added 2 equivalents of *n*-butyl-lithium (13.3 mL, 2.5 M, 37.0 mmol) dropwise, via syringe. The solution was left stirring at -78 °C for 0.5 h, at which point the solution was quickly transferred to a stirring solution of 1M HCl (50 mL). The resulting solution was allowed to warm to room temperature and was stirred for an additional 0.5 hours. The solution was extracted with dichloromethane (3 x 200 mL), and the combined organics were washed with water (3 x 100 mL). The combined organics were then dried with MgSO<sub>4</sub>, filtered, and evaporated to afford the crude product **D** which was further purified by column chromatography in hexanes (5.3 g, 69.7 % yield) to obtain a white solid. <sup>1</sup>H NMR (400 MHz, CDCl<sub>3</sub>): δ 7.82 (dd, <sup>3</sup>J<sub>HH</sub> = 8.3 Hz, <sup>4</sup>J<sub>HH</sub> = 1.3 Hz, 1H, PhH), 7.60 (d, <sup>3</sup>J<sub>HH</sub> = 8.70 Hz, 1H, PhH), 7.55 (t, <sup>4</sup>J<sub>HH</sub> = 1.8 Hz, 1H, PhH), 7.47 (dd, <sup>3</sup>J<sub>HH</sub> = 8.1 Hz, <sup>3</sup>J<sub>HH</sub> = 7.0 Hz, 1H, PhH), 7.38 (d, <sup>3</sup>J<sub>HH</sub> = 8.70 Hz, 1H, PhH), 7.30 (d, <sup>4</sup>J<sub>HH</sub> = 1.8 Hz, 2H, PhH), 7.27 (dd, <sup>3</sup>J<sub>HH</sub> = 7.0 Hz, <sup>4</sup>J<sub>HH</sub> = 1.3 Hz, 1H, PhH), 6.33 (s, 1H, OH), 1.38 (s, 18H, 'Bu); <sup>13</sup>C{<sup>1</sup>H} NMR (101 MHz, C<sub>6</sub>D<sub>6</sub>): δ 151.79 (s, 2C, Aryl-C), 150.61 (s, 1C, Aryl-C), 141.38 (s, 1C, Aryl-C), 138.11 (s, 1C, Aryl-C), 135.31 (s, 1C, Aryl-C), 132.41 (s, 1C, Aryl-C), 130.86 (s, 1C, Aryl-C), 129.44 (s, 1C, Aryl-C), 128.74 (s, 1C, Aryl-C), 125.53 (s, 1C, Aryl-C), 124.19 (s, 2C, Aryl-C), 122.77 (s, 1C, Aryl-C), 122.41 (s, 1C, Aryl-C), 121.91 (s, 1C, Aryl-C), 106.92 (s, 1C, Aryl-C), 35.07 (s, 1C, CH(CH<sub>3</sub>)<sub>3</sub>), 31.44 (s, 6C, CH(CH<sub>3</sub>)<sub>3</sub>).



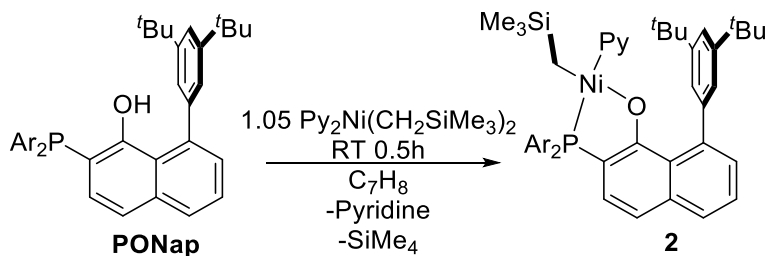
**PONapH:** In a glovebox, a stirring solution of **D** (600 mg, 1.46 mmol) in diethyl ether (10 mL) was cooled to -78 °C prior to the dropwise addition to 2 equivalents of *n*-butyl-lithium (1.1 mL, 2.5 M, 2.92 mmol). The solution was warmed to room temperature and the resulting suspension was stirred for 0.5 hours. The suspension was then cooled to -78 °C and a solution for di(2,6 dimethoxyphenyl)phosphine chloride (497 mg, 1.46 mmol) in THF (5 mL) was added dropwise. The resulting solution was allowed to warm to room temperature slowly over the course of 14 hours. In a glovebox containing degassed protic solvents, under an N<sub>2</sub> atmosphere, water (10 mL) was added to the suspension and stirred for one hour. The pale-yellow suspension was extracted with Et<sub>2</sub>O (2 x 25 mL) and the organic fractions were combined and washed with H<sub>2</sub>O (3 x 5 mL). The organic fractions were combined, dried with MgSO<sub>4</sub>, flited, and evaporated to afford the crude product which was recrystallized from a saturated solution of Et<sub>2</sub>O at -40°C for 16h (240 mg, 25.8 % yield) to afford pure **PONapH**.  
<sup>1</sup>H NMR (400 MHz, C<sub>6</sub>D<sub>6</sub>): δ 7.81 (dd, <sup>3</sup>J<sub>HH</sub> = 8.4 Hz, <sup>4</sup>J<sub>HP</sub> = 5.4 Hz, 1H, PhH), 7.60 (dd, <sup>3</sup>J<sub>HH</sub> = 8.4 Hz, <sup>4</sup>J<sub>HH</sub> = 1.4 Hz, 1H, PhH), 7.48 (t, <sup>4</sup>J<sub>HH</sub> = 1.8 Hz, 1H, PhH), 7.34 (d, <sup>4</sup>J<sub>HH</sub> = 2.0 Hz, 2H, PhH), 7.23 (dd, <sup>3</sup>J<sub>HH</sub> = 7.1 Hz, <sup>4</sup>J<sub>HH</sub> = 1.4 Hz, 1H, PhH), 7.18 (d, <sup>3</sup>J<sub>HH</sub> = 7.1 Hz, 1H, PhH), 7.16 (d, <sup>3</sup>J<sub>HH</sub> = 7.5 Hz, 1H, PhH), 7.00 (t, <sup>3</sup>J<sub>HH</sub> = 8.2 Hz, 2H, PhH), 6.20 (dd, <sup>3</sup>J<sub>HH</sub> = 8.2 Hz, <sup>4</sup>J<sub>HP</sub> = 2.9 Hz, 4H, PhH), 3.05 (s, 12H, OCH<sub>3</sub>), 1.24 (s, 18H, <sup>t</sup>Bu); <sup>31</sup>P{<sup>1</sup>H} NMR (121 MHz, C<sub>6</sub>D<sub>6</sub>): δ -65.68 (s, 1P). <sup>13</sup>C{<sup>1</sup>H} NMR (101 MHz, C<sub>6</sub>D<sub>6</sub>): δ 162.83 (d, J<sub>CP</sub> = 8.12 Hz, 2C, Aryl-C), 156.10 (d, J<sub>CP</sub> = 20.3 Hz, 1C, Aryl-C), 149.66 (s, 2C, Aryl-C), 144.28 (s, 1C, Aryl-C), 140.10

(d,  $J_{CP} = 2.5$  Hz, 1C, Aryl-C), 136.68 (s, 1C, Aryl-C), 132.30 (d,  $J_{CP} = 8.4$  Hz, 1C, Aryl-C), 129.72 (s, 1C, Aryl-C), 129.01 (s, 1C, Aryl-C), 128.60 (s, 4C, Aryl-C), 125.18 (s, 1C, Aryl-C), 124.47 (s, 2C, Aryl-C), 122.28 (d,  $J_{CP} = 1.9$  Hz, 1C, Aryl-C), 120.34 (s, 1C, Aryl-C), 120.21 (d,  $J_{CP} = 6.9$  Hz, 1C, Aryl-C), 118.96 (d,  $J_{CP} = 3.7$  Hz, 1C, Aryl-C), 113.93 (d,  $J_{CP} = 19.1$  Hz, 1C, Aryl-C), 104.57 (d,  $^4J_{CP} = 4.0$  Hz, 4C, Aryl-C), 55.45 (s, 4C, OCH<sub>3</sub>), 35.01 (s, 2C, CH(CH<sub>3</sub>)<sub>3</sub>), 31.73 (s, 6C, CH(CH<sub>3</sub>)<sub>3</sub>).



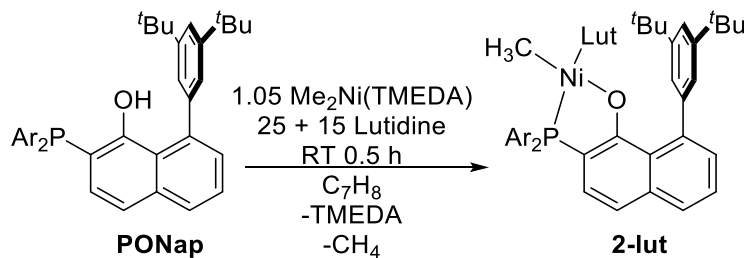
**POP-Ni(py)(CH<sub>2</sub>SiMe<sub>3</sub>) (1):** In the glove box, to a solution of Py<sub>2</sub>Ni(CH<sub>2</sub>SiMe<sub>3</sub>)<sub>2</sub> (22 mg, 0.0593 mmol) in benzene (2 ml) in a vial was added a solution of **POPH** (42.83 mg, 0.0563 mmol) in benzene (4 ml). The mixture was stirred for 2 h under room temperature, forming a red-brown solution. Volatile materials were removed under vacuum and the residue was extracted with diethyl ether three times and dried in vacuo to provide the complex **1** (44 mg, 76%) as a yellowish solid. <sup>1</sup>H NMR (400 MHz, C<sub>6</sub>D<sub>6</sub>): δ 8.94–8.92 (m, 2H, PhH), 7.47–7.43 (m, 1H, PhH), 7.08–7.04 (t, <sup>3</sup>J<sub>HH</sub> = 8.2 Hz, 2H, PhH), 7.04–7.00 (t, <sup>3</sup>J<sub>HH</sub> = 8.2 Hz, 2H, PhH), 6.95–6.92 (m, 1H, PhH), 6.83–6.79 (m, 1H, PhH), 6.47–6.43 (m, 2H, PhH), 6.34–6.32 (dd, <sup>3</sup>J<sub>HH</sub> = 8.2 Hz, <sup>4</sup>J<sub>HH</sub> = 2.2 Hz, 4H, PhH), 6.29–6.26 (dd, <sup>3</sup>J<sub>HH</sub> = 8.2 Hz, <sup>4</sup>J<sub>HH</sub> = 3.5 Hz, 4H, PhH), 3.36 (s, 12H, OCH<sub>3</sub>), 3.28 (s, 12H, OCH<sub>3</sub>), 1.13 (s, 9H, C(CH<sub>3</sub>)<sub>3</sub>), 0.12 (s, 9H, Si(CH<sub>3</sub>)<sub>3</sub>), -0.71–-0.74 (d, <sup>3</sup>J<sub>HP</sub> = 8.7 Hz, 2H, NiCH<sub>2</sub>Si); <sup>13</sup>C{<sup>1</sup>H} NMR (101 MHz, C<sub>6</sub>D<sub>6</sub>): 163.88 (d, <sup>2</sup>J<sub>CP</sub> = 9.1 Hz, 4C, Ar-C), 161.77 (d, <sup>2</sup>J<sub>CP</sub> = 1.5 Hz, 4C, Ar-C), 151.61 (m, 3C, Ar-C), 135.58 (s, 1C, Ar-C), 130.43 (m, 1C, Ar-C), 130.10 (s, 2C, Ar-C), 129.18 (s, 2C, Ar-C),

128.54 (s, 2C, Ar-C), 128.26 (m, 4C, Ar-C), 123.07 (d,  $^3J_{CP} = 1.9$  Hz, 2C, Ar-C), 118.65 (s, 1C, Ar-C), 112.77 (m, 1C, Ar-C), 105.04 (s, 4C, Ar-C), 104.74 (d,  $^3J_{CP} = 4.1$  Hz, 4C, Ar-C), 55.91 (s, 6C, OCH<sub>3</sub>), 55.90 (s, 6C, OCH<sub>3</sub>), 55.40 (s, 12C, OCH<sub>3</sub>), 34.10 (s, 1C, C(CH<sub>3</sub>)<sub>3</sub>), 31.98 (s, 9C, C(CH<sub>3</sub>)<sub>3</sub>), 2.15 (s, 9C, SiMe<sub>3</sub>), -18.25 (d,  $^2J_{CP} = 29.0$  Hz, 1C, NiCH<sub>2</sub>Si);  $^{31}P\{^1H\}$  NMR (121 MHz, C<sub>6</sub>D<sub>6</sub>):  $\delta$  -5.31 (d,  $^4J_{PP} = 8.9$  Hz, 1P), -52.09 (d,  $^4J_{PP} = 8.9$  Hz, 1P). Anal. Calcd(%): C, 62.33; H, 6.46; N, 1.73. Found(%): C, 61.82; H, 6.33; N, 1.18.



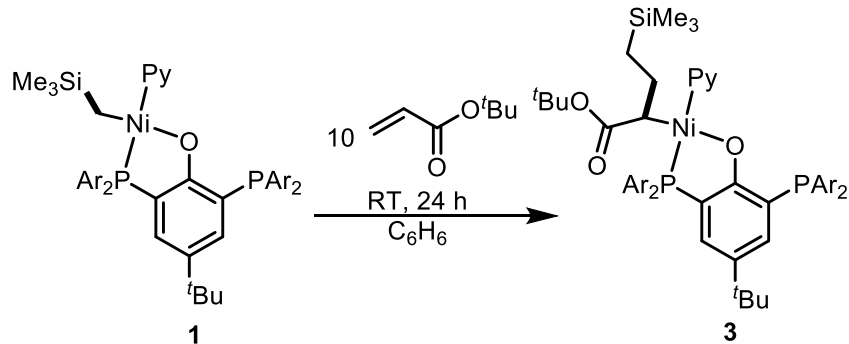
**PONap-Ni (2):** This complex was synthesized via a similar route for **1** and as isolated in 65% yield.  $^1H$  NMR (400 MHz, C<sub>6</sub>D<sub>6</sub>):  $\delta$  8.45 (2<sup>nd</sup> order multiplet AA'BB', 2H, PhH), 7.89(dd,  $^3J_{HH} = 8.3$  Hz,  $^4J_{HP} = 10.1$  Hz, 1H, PhH), 7.65 (dd,  $^3J_{HH} = 8.0$  Hz,  $^4J_{HH} = 1.4$  Hz, 1H, PhH), 7.44 (d,  $^4J_{HH} = 1.8$  Hz, 2H, PhH), 7.31 (t,  $^4J_{HH} = 1.8$  Hz, 1H, PhH), 7.24 (t,  $^3J_{HH} = 7.3$  Hz, 1H, PhH), 7.16 (dd,  $^3J_{HH} = 7.0$  Hz,  $^4J_{HH} = 1.4$  Hz, 1H, PhH), 6.95-7.10 (overlapping multiplets, 4H, PhH), 6.87 (tt,  $^3J_{HH} = 7.7$  Hz,  $^4J_{HH} = 1.7$  Hz 1H, p-H C<sub>5</sub>H<sub>5</sub>N), 6.57 (t,  $^3J_{HH} = 7.2$  Hz, 2H, PhH), 6.20 (dd,  $^3J_{HH} = 7.2$  Hz,  $^4J_{HP} = 3.6$  Hz, 4H, PhH), 3.18 (s, 12H, OCH<sub>3</sub>), 1.32 (s, 18H, 'Bu), -0.24 (s, 9H, SiMe<sub>3</sub>), -0.68 (d,  $^3J_{HP} = 9.0$  Hz, 2H, Ni-CH<sub>2</sub>);  $^{13}C\{^1H\}$  NMR (101 MHz, C<sub>6</sub>D<sub>6</sub>):  $\delta$  173.82 (d,  $J_{CP} = 23.9$  Hz, 1C, Aryl-C), 161.92 (d,  $J_{CP} = 1.4$  Hz, 2C, Aryl-C), 151.21 (d,  $J_{CP} = 1.3$  Hz, 2C, Aryl-C), 148.06 (s, 2C, Aryl-C), 146.88 (s, 1C, Aryl-C), 142.40 (d,  $J_{CP} = 2.3$  Hz, 1C, Aryl-C), 139.54 (d,  $J_{CP} = 1.6$  Hz, 1C, Aryl-C), 135.25 (s, 1C, Aryl-C), 130.36 (s, 1C, Aryl-C), 129.67 (s, 1C, Aryl-C), 129.28 (d,  $J_{CP} = 1.4$  Hz, 1C, Aryl-C), 125.51 (s, 1C, Aryl-C), 125.06 (s, 2C, Aryl-C), 123.87 (d,  $J_{CP} = 1.6$  Hz, 4C, Aryl-C),

118.84 (s, 1C, Aryl-C), 117.69 (d,  $^2J_{CP} = 56.8$  Hz, 2C, Aryl-C), 112.82 (d,  $J_{CP} = 8.1$  Hz, 1C, Aryl-C), 111.97 (d,  $^2J_{CP} = 49.5$  Hz, 2C, Aryl-C), 104.78 (d,  $^4J_{CP} = 4.0$  Hz, 4C, Aryl-C), 55.43(s, 4C, OCH<sub>3</sub>), 35.00 (s, 2C, CH(CH<sub>3</sub>)<sub>3</sub>), 32.05 (s, 6C, CH(CH<sub>3</sub>)<sub>3</sub>), 2.23 (s, 3C, SiMe<sub>3</sub>), -16.91 (d,  $^2J_{CP} = 31.1$  Hz, 1C, Ni-CH<sub>2</sub>);  $^{31}P\{^1H\}$  NMR (121 MHz, C<sub>6</sub>D<sub>6</sub>):  $\delta$  -5.94 (s, 1P). Anal. Calcd(%): C, 68.37; H, 7.03; N, 1.63. Found(%): C, 68.27; N, 6.79; N, 1.29.



**PONap-Ni(lut)(Me)(2-lut):** In the glove box, to a thawing solution of NiMe<sub>2</sub>(TMEDA) (38 mg, 0.19 mmol) in toluene(2 mL) was add a thawing solution of **PONapH** (120 mg, 0.19 mmol) and 25 equivalents of 2,6-lutidine (448 mg, 4.71 mmol) in toluene (2 mL). The strongly colored yellow solution was stirred while warming to room temperature for 10 minutes. While arming, 15 additional equivalents of 2,6-lutidine (268 mg, 2.82 mmol) were added and the solution was stirred at room temperature for an additional 0.5 h. All volatiles were removed from solution which was triturated with hexanes (3 x 10 mL). The resulting residue was fractioned with *n*-pentane (12 mL) and toluene (8 mL), and the volatiles were subsequently removed from the toluene fraction yielding spectroscopically pure **2-lut** (98 mg, 63.6 % yield).  $^1H$  NMR (400 MHz, C<sub>6</sub>D<sub>6</sub>):  $\delta$  7.83 (t,  $^3J_{HH} = 9.2$  Hz, 1H, PhH), 7.64 (dd,  $^3J_{HH} = 7.5$  Hz, 1H, PhH), 7.03-7.18 (overlapping multiplets, 5H, PhH), 7.01 (d,  $^3J_{HH} = 8.1$  Hz, 1H, PhH), 6.96 (t,  $^4J_{HH} = 7.3$  Hz, 1H, PhH), 6.39 (d,  $^3J_{HH} = 7.6$  Hz, 2H, PhH), 6.27 (dd,  $^3J_{HH} = 8.0$  Hz,  $^4J_{HP} = 3.4$  Hz, 4H, PhH), 3.22 (s, 6H, (C<sub>5</sub>H<sub>3</sub>N)(CH<sub>3</sub>)<sub>2</sub>), 3.21 (s, 12H, OCH<sub>3</sub>), 1.25 (s, 18H,

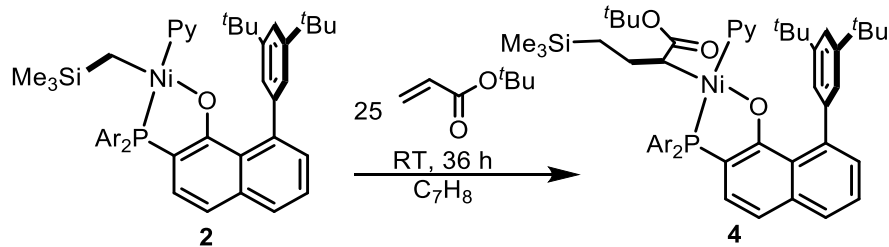
<sup>1</sup>Bu), -0.92 (d, <sup>3</sup>J<sub>HP</sub> = 6.4 Hz, 3H, Ni-CH<sub>3</sub>); <sup>31</sup>P{<sup>1</sup>H} NMR (121 MHz, C<sub>6</sub>D<sub>6</sub>): δ -5.60. Anal. Calcd(%): C, 70.60; H, 6.91; N, 1.72. Found(%): C, 69.56; H, 6.79; N, 1.29.



**POP-Ni(py)(CCO)(3):** In a glove box, to a yellow solution of **1** (49 mg, 0.050 mmol) in benzene (5 mL) was added 10 equivalents of tertbutyl acrylate (64 mg, 0.5 mmol). After 24 h, all volatiles were removed under vacuum and the residue was triturated with cold pentane (3 x 5 mL). The remaining residue was then dried under vacuum to afford crude **3** as an orange solid (16.5 mg, 28%). <sup>31</sup>P{<sup>1</sup>H} NMR (121 MHz, C<sub>6</sub>D<sub>6</sub>): δ -6.62 ~ -7.26 (broad m), δ -52.85 ~ -53.45 (broad m).

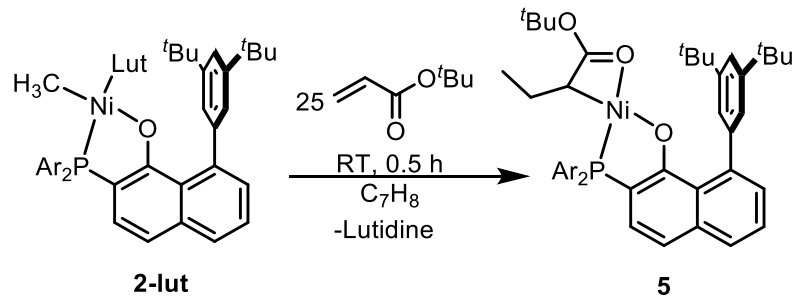
Since only broad peaks were observed in <sup>1</sup>H NMR of **3** and addition of excess pyridine could sharpen peaks in <sup>1</sup>H NMR (Figure S2.17). Integrable NMR spectra of **3** were collected with 2 equiv. of additional pyridine. <sup>1</sup>H NMR (400 MHz, C<sub>6</sub>D<sub>6</sub>): δ 8.56-8.77 (overlapping multiplets, 4H, bound and free pyridine-H), δ 7.33 (d, <sup>3</sup>J<sub>HH</sub> = 16 Hz, 2H, PhH), 7.00-7.12 (overlapping multiplets, 5H, PhH), 6.92 (broad s, 1H, free pyridine-H), 6.85 (broad s, 1H, PhH), 6.42-6.68 (overlapping multiplets, 4H, bound and free pyridine-H), 6.20-6.36 (d, overlapping multiplets, 8H, PhH), 3.59 (broad s, 6H, OCH<sub>3</sub>), 3.26 (s, 6H, OCH<sub>3</sub>), 3.26 (t, <sup>3</sup>J<sub>HH</sub> = 12.8 Hz, 1H, nickel-CH), 3.20 (s, 6H, OCH<sub>3</sub>), 3.12 (s, 6H, OCH<sub>3</sub>), 1.99 (td, <sup>3</sup>J<sub>HH</sub> = 12.8 Hz, <sup>3</sup>J<sub>HH</sub> = 3.2 Hz, 1H, nickel-alkyl), 1.12 (s, 9H, OC(CH<sub>3</sub>)<sub>3</sub>), 1.09 (s, 9H, C(CH<sub>3</sub>)<sub>3</sub>), 1.02 (s, 1H, nickel alkyl), 0.69 (td, <sup>3</sup>J<sub>HH</sub> = 12.8 Hz, <sup>3</sup>J<sub>HH</sub> = 3.2 Hz, 1H, nickel-alkyl), 0.25 (s, 1H, nickel-

alkyl), 0.06 (s, 9H, Si(CH<sub>3</sub>)<sub>3</sub>); <sup>31</sup>P{<sup>1</sup>H} NMR (121 MHz, C<sub>6</sub>D<sub>6</sub>): δ -6.80 (d, <sup>4</sup>J<sub>PP</sub> = 7.3 Hz, 1P), -53.17 (d, <sup>4</sup>J<sub>PP</sub> = 7.3 Hz, 1P).



**PONap-Ni(py)(CCO)(4):** To a solution of **2** (135 mg, 0.157 mmol) in toluene (5 mL), in a glove box, was added 25 equivalents of tertbutyl acrylate (503.1 mg, 3.93 mmol). After 36 h, all volatiles were removed from the solution and the residue was triturated with hexanes (3 x 5 mL). The remaining residue was then fractioned with *n*-pentane (5 mL) and diethyl ether (10 mL). The diethyl ether fraction was evaporated to afford crude **4** (63 mg, 40.6 % yield).  
<sup>1</sup>H NMR (400 MHz, C<sub>7</sub>D<sub>8</sub>): δ 8.65 (broad s, W<sub>1/2</sub> = 36.8 Hz, 2H, *o*-pyridine), 7.65 (d, <sup>3</sup>J<sub>HH</sub> = 8.1 Hz, 1H, PhH), 7.60 (broad m, 1H, PhH), 7.38 (s, 2H, PhH), 7.26 (t, <sup>3</sup>J<sub>HH</sub> = 7.1 Hz, 1H, PhH), 6.99-7.19 (overlapping multiplets, 5H, PhH), 6.96 (d, <sup>3</sup>J<sub>HP</sub> = 8.4 Hz, 2H, PhH), 6.70 (broad s, W<sub>1/2</sub> = 27.5 Hz, 2H, PhH), 6.33 (broad d, <sup>3</sup>J<sub>HH</sub> = 7.8 Hz, 2H, PhH), 6.26 (d, <sup>3</sup>J<sub>HH</sub> = 7.8 Hz, 2H, PhH), 3.47 (s, 6H, OCH<sub>3</sub>), 3.36 (s, 1H, Ni-CH), 3.24 (s, 6H, OCH<sub>3</sub>), 1.47 (s, 18H, tBu), 1.32 (broad s, 9H, W<sub>1/2</sub> = 64 Hz, O'tBu), 0.92 (t, <sup>3</sup>J<sub>HH</sub> = 6.6 Hz, 2H, Ni-alkyl), 0.67 (broad multiplet, W<sub>1/2</sub> = 31 Hz, 1H, Ni-alkyl), 0.31 (s, 1H, Ni-alkyl), -0.03 (s, 9H, SiMe<sub>3</sub>); <sup>31</sup>P{<sup>1</sup>H}

NMR (121 MHz, C<sub>6</sub>D<sub>6</sub>): δ -6.15 (broad s, W<sub>1/2</sub> = 37.1 Hz, 1P)



**PONap-Ni (CCO): (5)** Complex **5** was synthesized and purified in a similar way to **4** with the exception of using **2-lut** as the precursor. The reaction was completed in 0.5 h and was isolated in 70 % yield.  $^1\text{H}$  NMR (400 MHz,  $\text{C}_6\text{D}_6$ ):  $\delta$  7.68 (dd,  $^3J_{\text{HH}} = 7.7$  Hz,  $^4J_{\text{HP}} = 1.8$  Hz, 1H, PhH), 7.63 (dd,  $^3J_{\text{HH}} = 7.4$  Hz,  $^3J_{\text{HH}} = 10.8$  Hz, 1H, PhH), 7.56 (s, 2H, PhH), 7.47 (broad multiplet, 1H, PhH), 7.26-7.37 (overlapping multiplets, 2H, PhH), 6.99-7.07 (overlapping multiplets, 4H, PhH), 6.22 (dd,  $^3J_{\text{HH}} = 8.4$  Hz,  $^4J_{\text{HP}} = 3.8$  Hz, 2H, PhH), 6.16 (dd,  $^3J_{\text{HH}} = 8.2$  Hz,  $^4J_{\text{HP}} = 3.8$  Hz, 2H, PhH), 3.27 (s, 6H,  $\text{OCH}_3$ ), 3.15 (broad s,  $W_{1/2} = 15$  Hz, 6H,  $\text{OCH}_3$ ), 2.09 (broad m, 1H, Ni-CH), 1.54 (broad s,  $W_{1/2} = 15$  Hz, 18H, 'Bu), 1.47 (s, 9H, O'Bu), 1.19 (broad multiplet, 1H, Ni-CH-CHH), 0.81-0.86 (overlapping multiplets, 4H, Ni-CH-CH<sub>2</sub>-CH<sub>3</sub> + Ni-CH-CHH-CH<sub>3</sub>);  $^{13}\text{C}\{\text{H}\}$  NMR (101 MHz,  $\text{C}_6\text{D}_6$ ):  $\delta$  174.93 (d,  $J_{\text{CP}} = 22.5$  Hz, 2C, Aryl-C), 161.97 (d,  $J_{\text{CP}} = 2.0$  Hz, 2C, Aryl-C), 161.86 (broad s, 1C, Aryl-C), 147.72 (multiplet, 1C, Aryl-C), 145.70 (s, 1C, Aryl-C), 143.49 (multiplet, 1C, Aryl-C), 139.28 (s, 1C, Aryl-C), 131.21 (s, 1C, Aryl-C), 131.13 (s, 1C, Aryl-C), 128.88 (s, 2C, Aryl-C), 127.09 (s, 2C, Aryl-C), 126.42 (d,  $J_{\text{CP}} = 11.4$  Hz, 1C, Aryl-C), 126.13 (s, 2C, Aryl-C), 119.15 (s, 1C, Aryl-C), 112.78 (d,  $J_{\text{CP}} = 8.7$  Hz, 1C, Aryl-C), 108.25 (d,  $J_{\text{CP}} = 53.1$  Hz, 1C, Aryl-C), 104.55 (d,  $J_{\text{CP}} = 4.4$  Hz, 2C, Aryl-C), 104.30 (d,  $J_{\text{CP}} = 4.4$  Hz, 2C, Aryl-C), 55.86 (s, 1C, OC(CH<sub>3</sub>)<sub>3</sub>), 55.47 (s, 2C, OCH<sub>3</sub>), 55.43 (s, 2C, OCH<sub>3</sub>), 35.05 (s, 2C, CH(CH<sub>3</sub>)<sub>3</sub>), 32.19 (s, 6C, CH(CH<sub>3</sub>)<sub>3</sub>), 28.86 (s, 3C, OC(CH<sub>3</sub>)<sub>3</sub>), 21.90 (d,  $^2J_{\text{CP}} = 25.5$  Hz, 1C, Ni-CH), 20.06 (d,  $^3J_{\text{CP}} = 3.3$  Hz, 1C, Ni-CHCH<sub>2</sub>), 14.62 (s, 1C, Ni-CHCH<sub>2</sub>CH<sub>3</sub>);  $^{31}\text{P}\{\text{H}\}$  NMR (121 MHz,  $\text{C}_7\text{D}_8$ , 193 K):  $\delta$  -6.57 (broad s, 39.5 Hz, 1P);  $^{31}\text{P}\{\text{H}\}$  NMR (121 MHz,  $\text{C}_7\text{D}_8$ , 193 K):  $\delta$  -6.53 (broad s, 27.5 Hz, 1P), -8.08 (s, 1P). Anal. Calcd(%): C, 68.83; H, 7.10; N, 0. Found(%): C, 67.44; H, 6.89; N, 0.2.

**2. NMR characterization of ligands and metal complexes**

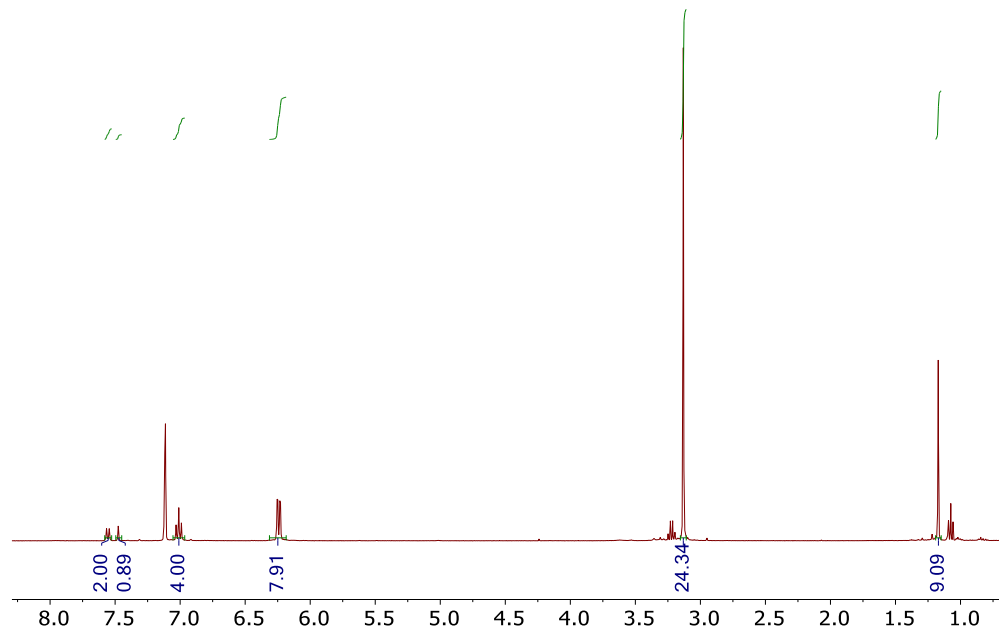


**Figure S2.1.**  $^1\text{H}$  NMR spectrum of **POPH** in  $\text{C}_6\text{D}_6$ .

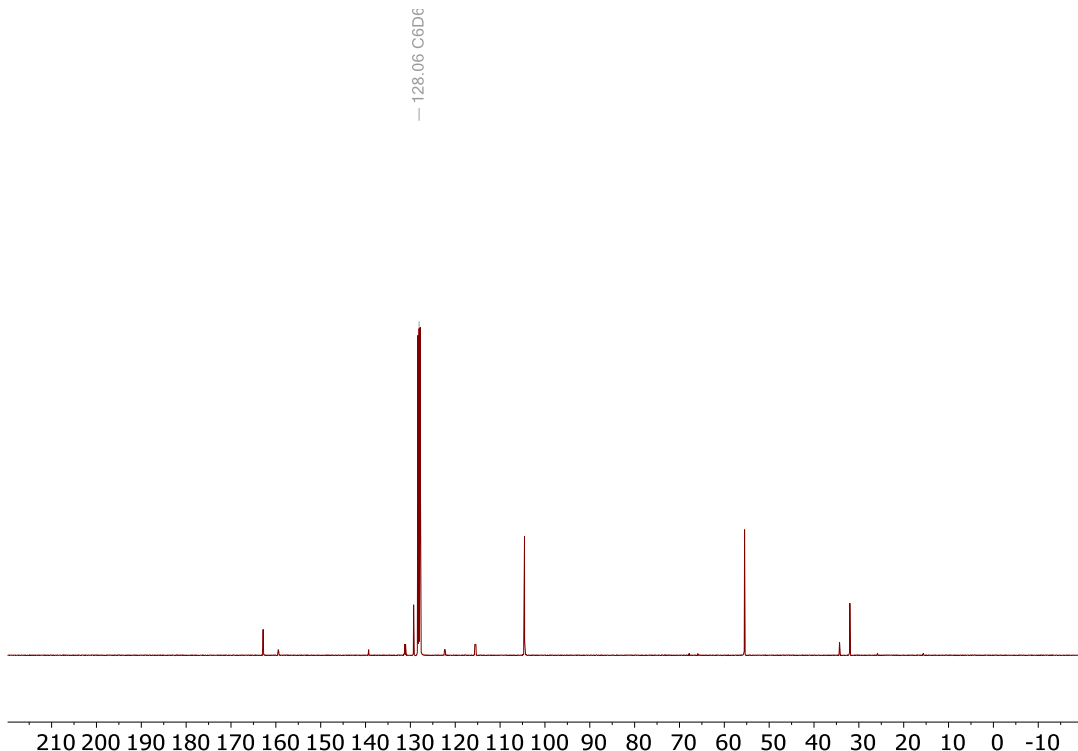


**Figure S2.2.**  $^{13}\text{C}\{\text{H}\}$  NMR of **POPH** in  $\text{C}_6\text{D}_6$ .

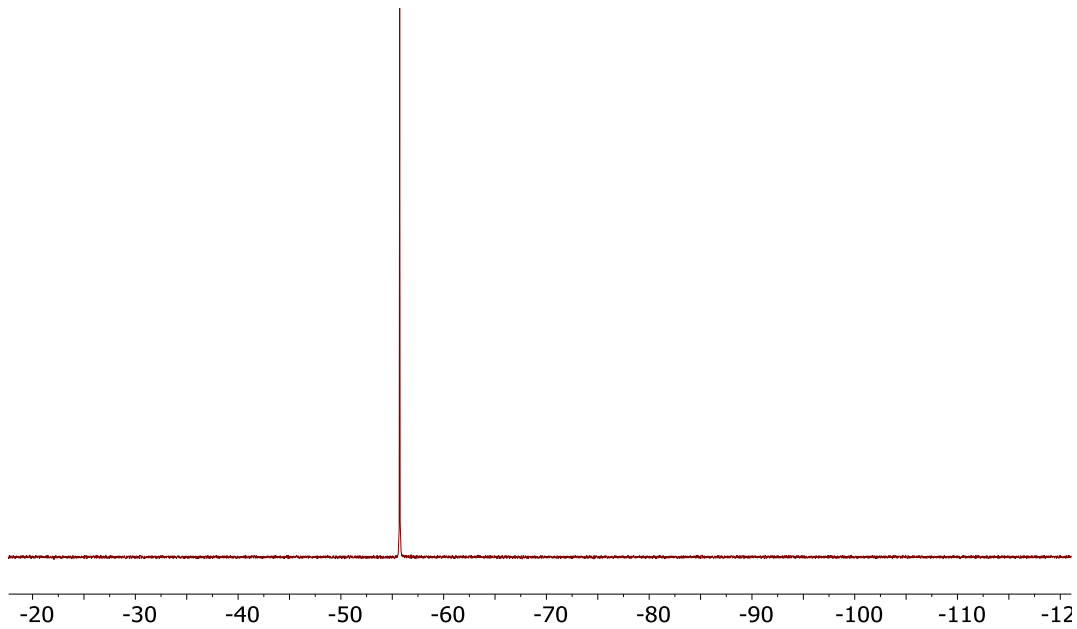


**Figure S2.3.**  $^{31}\text{P}\{\text{H}\}$  NMR spectrum of **POPH** in  $\text{C}_6\text{D}_6$ .

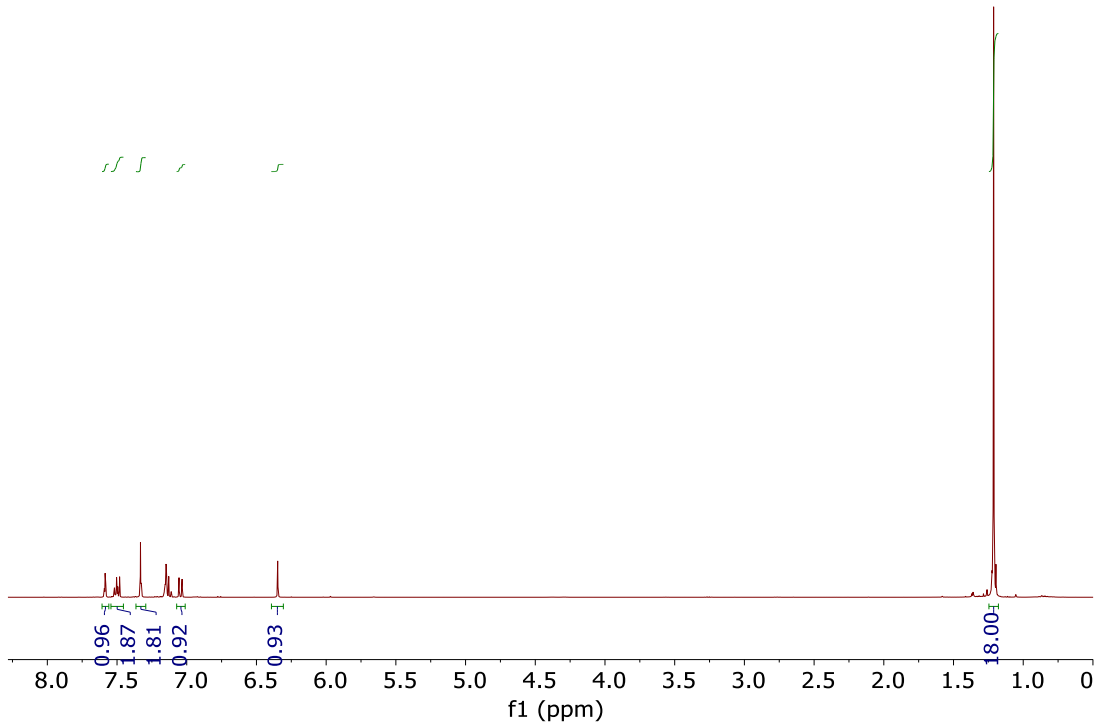


**Figure S2.4.**  $^1\text{H}$  NMR Spectrum of **D** in  $\text{C}_6\text{D}_6$ .

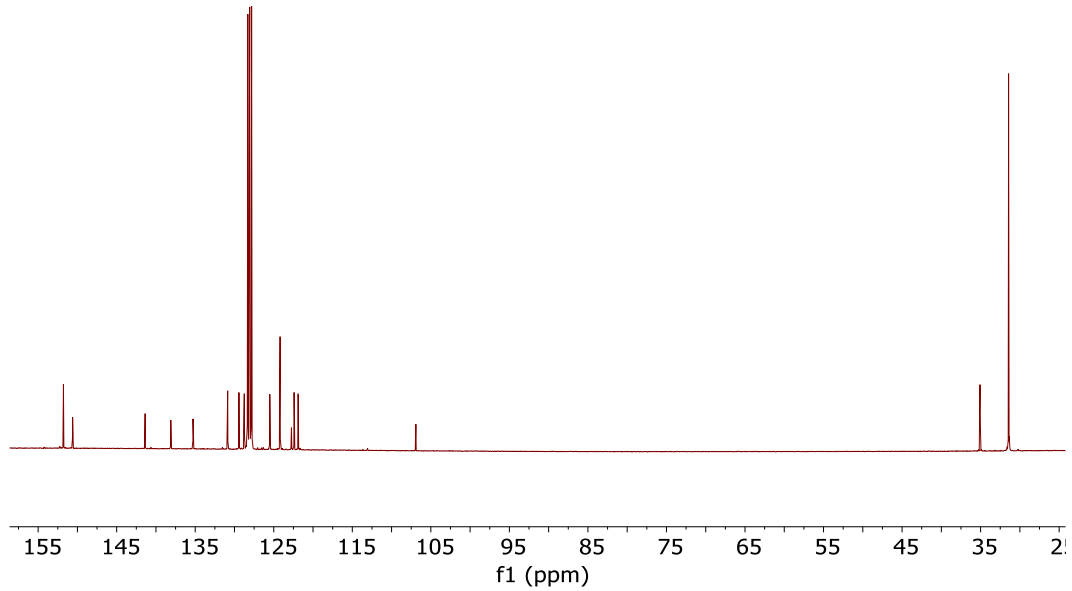


**Figure S2.5.**  $^{13}\text{C}\{\text{H}\}$  NMR Spectrum of **D** in  $\text{C}_6\text{D}_6$ .

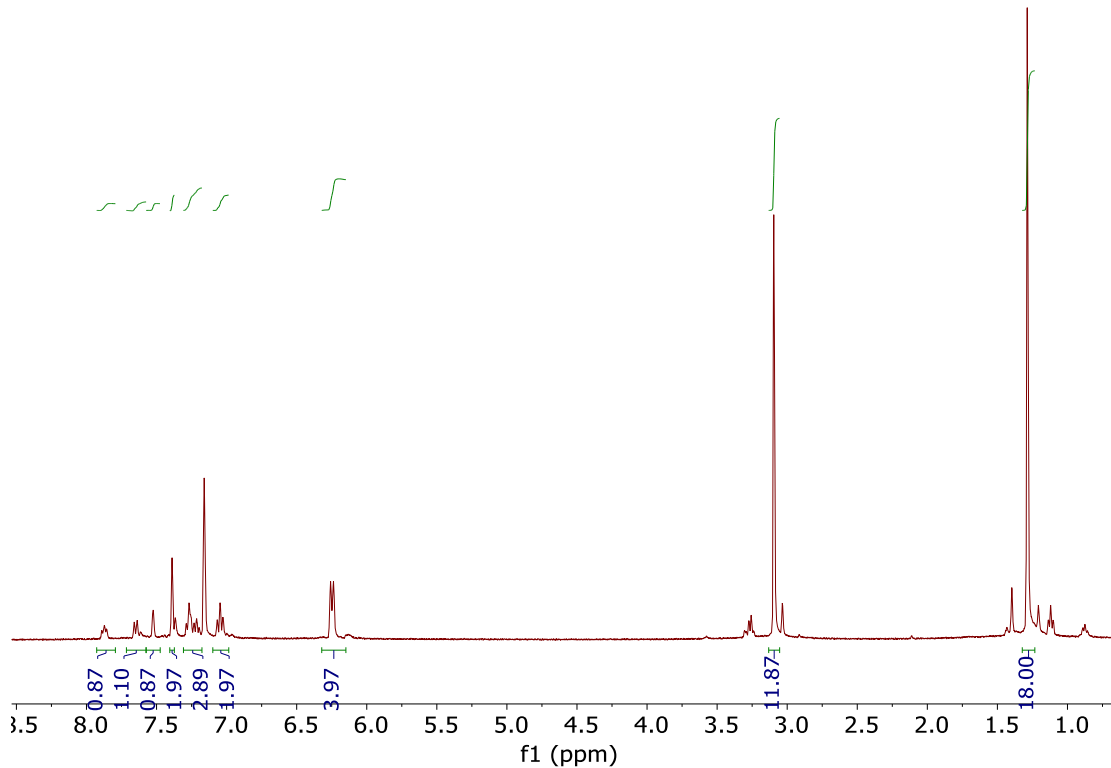


**Figure S2.6.**  $^1\text{H}$  NMR Spectrum of **PONapH** in  $\text{C}_6\text{D}_6$ .

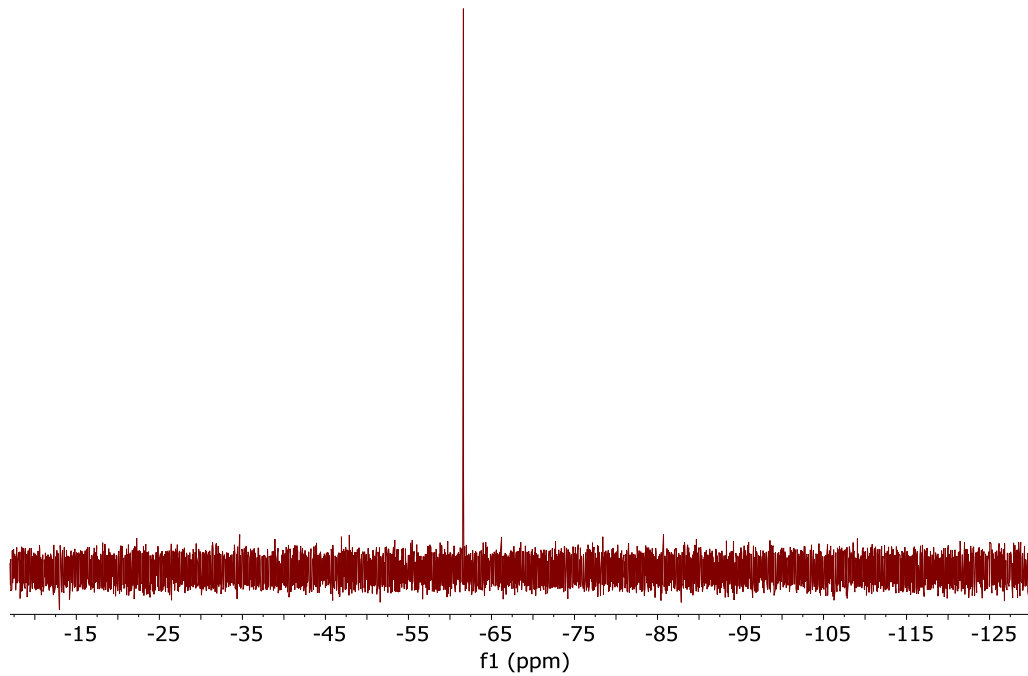


**Figure S2.7.**  ${}^3\text{P}\{{}^1\text{H}\}$  NMR spectrum of **PONapH** in  $\text{C}_6\text{D}_6$ .

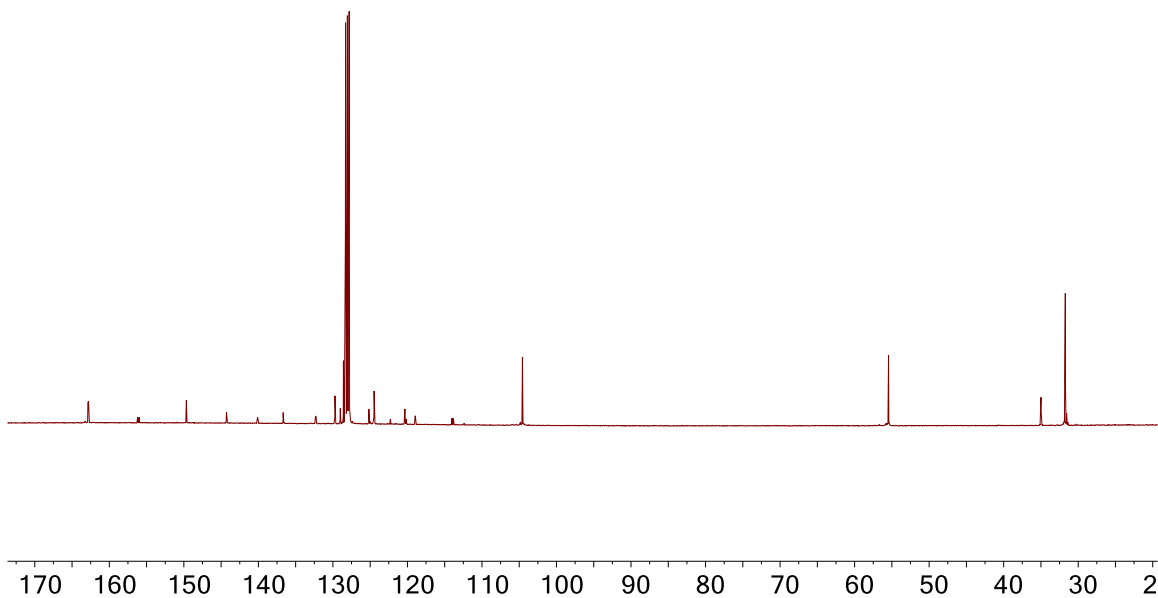


**Figure S2.8.**  ${}^{13}\text{C}\{{}^1\text{H}\}$  NMR spectrum of **PONapH** in  $\text{C}_6\text{D}_6$ .

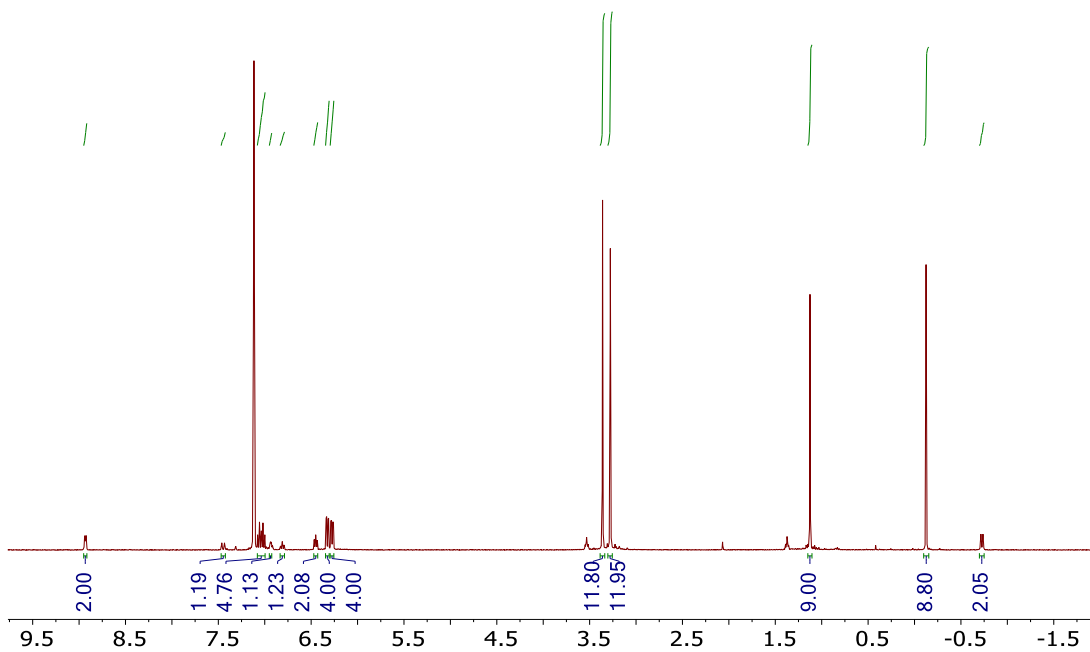


**Figure S2.9.**  $^1\text{H}$  NMR spectrum of **1** in  $\text{C}_6\text{D}_6$ .

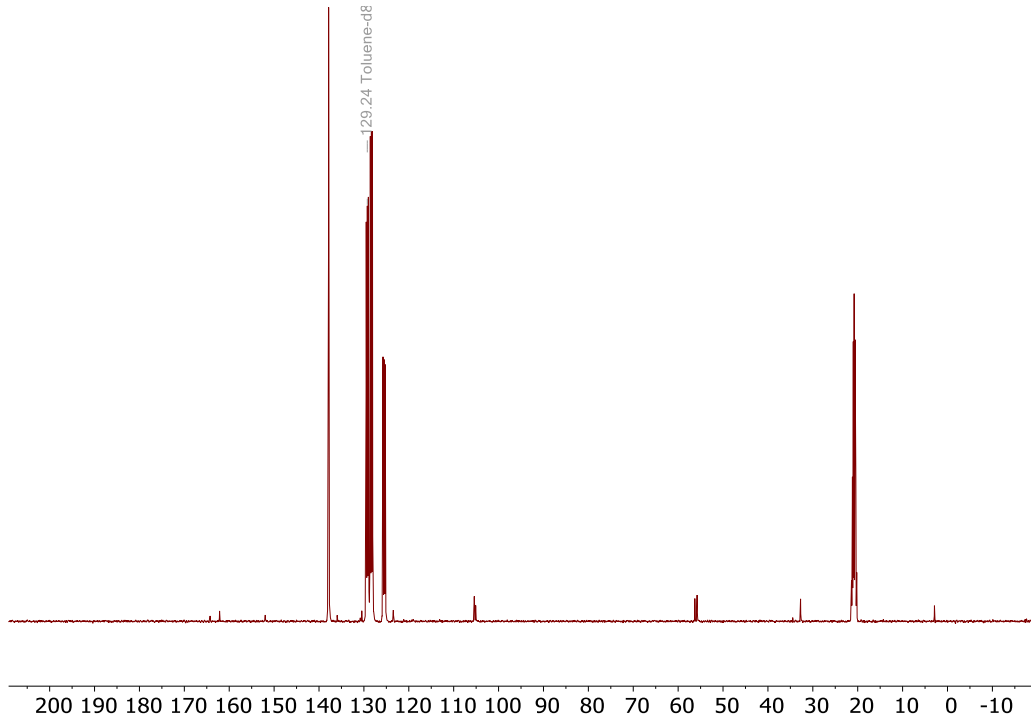


**Figure S2.10.**  $^{13}\text{C}\{^1\text{H}\}$  NMR spectrum of **1** in  $\text{C}_7\text{D}_8$ .

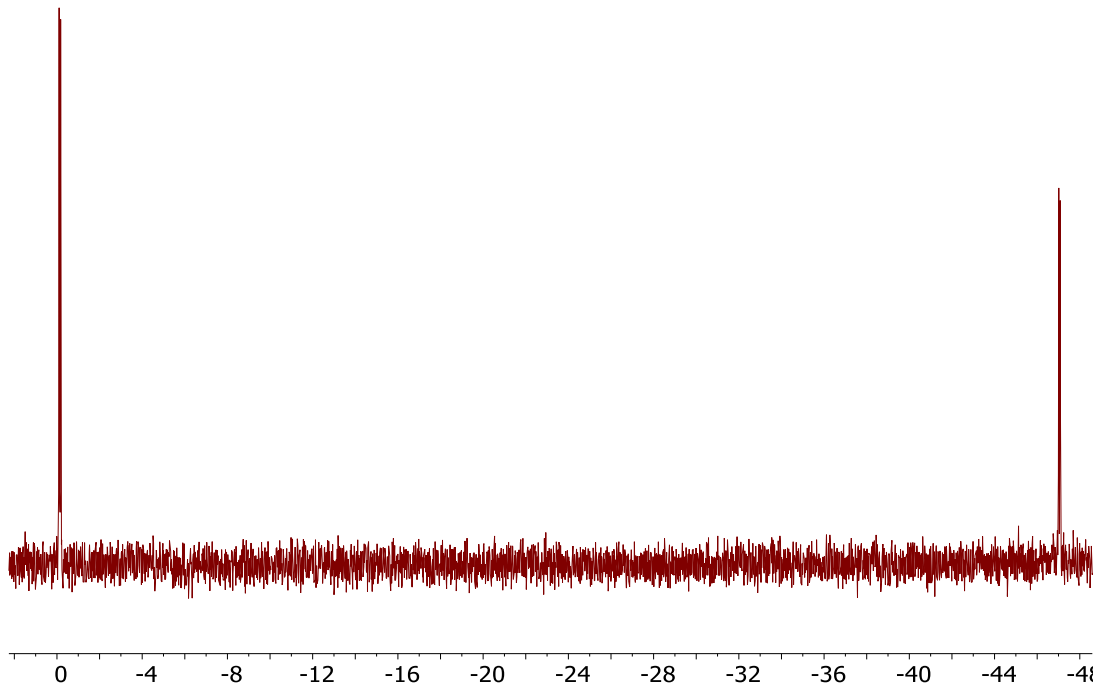


**Figure S2.11.**  $^{31}\text{P}\{\text{H}\}$  NMR spectrum of **1** in  $\text{C}_6\text{D}_6$ .

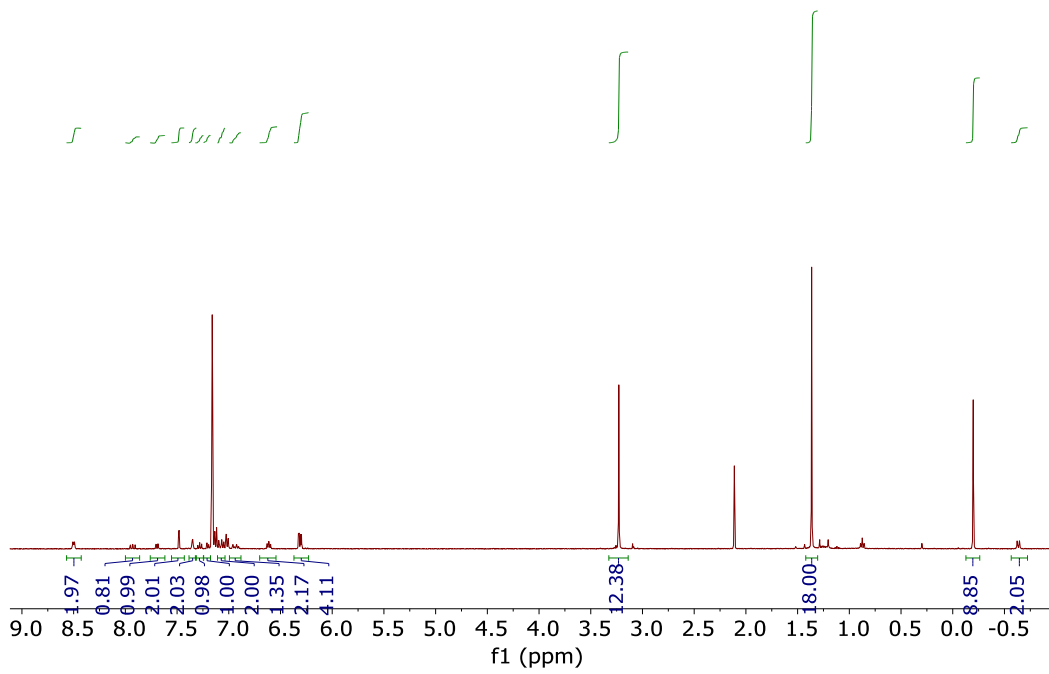


**Figure S2.12.**  $^1\text{H}$  NMR spectrum of **2** in  $\text{C}_6\text{D}_6$ .

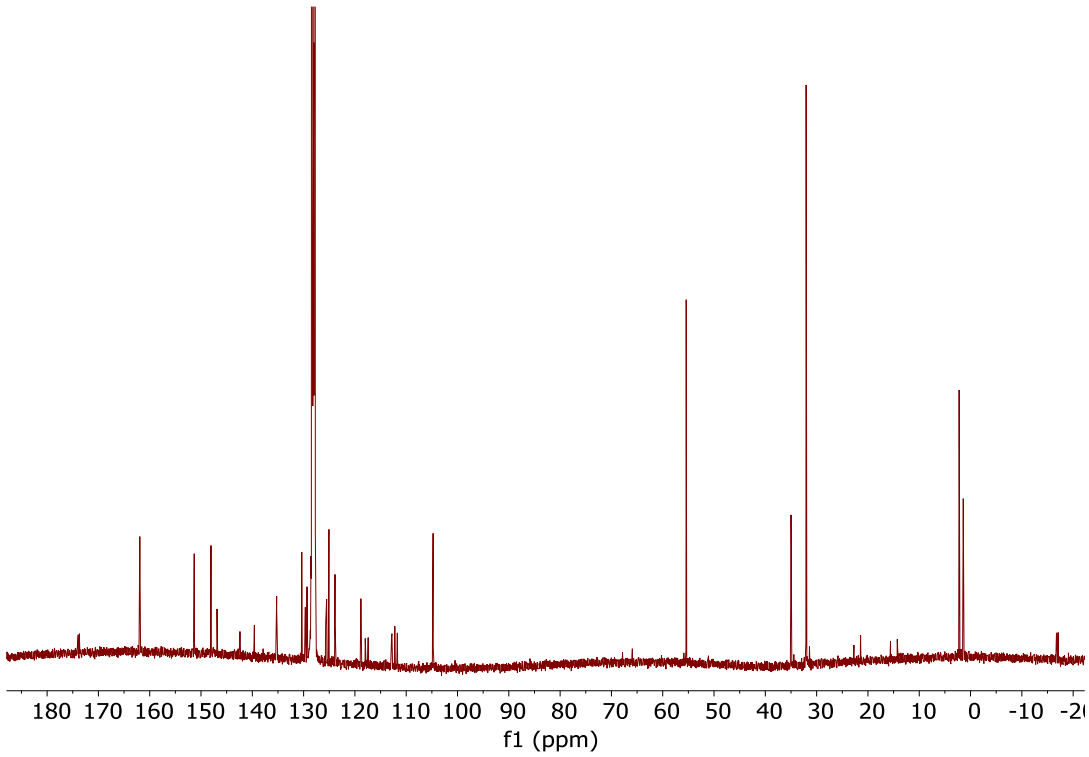


**Figure S2.13.**  $^{13}\text{C}\{^1\text{H}\}$  NMR spectrum of **2** in  $\text{C}_6\text{D}_6$ .

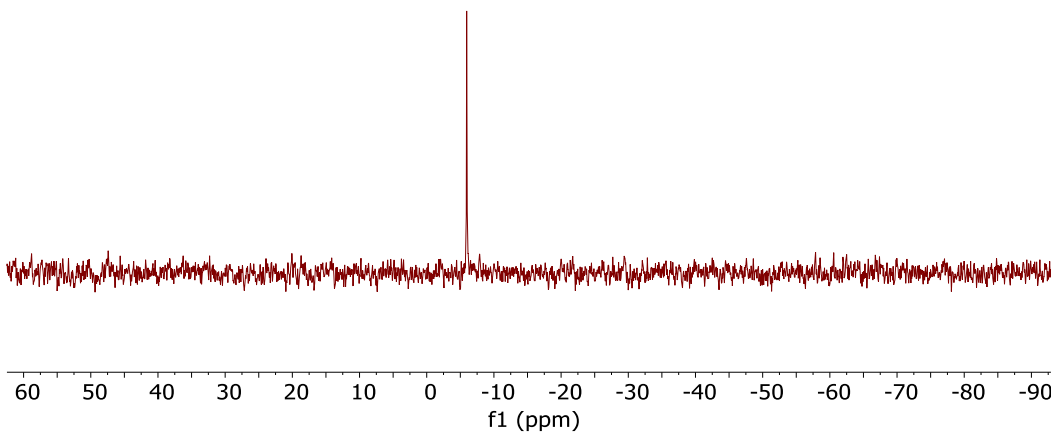


**Figure S2.14.**  $^{31}\text{P}\{^1\text{H}\}$  NMR spectrum of **2** in  $\text{C}_6\text{D}_6$ .

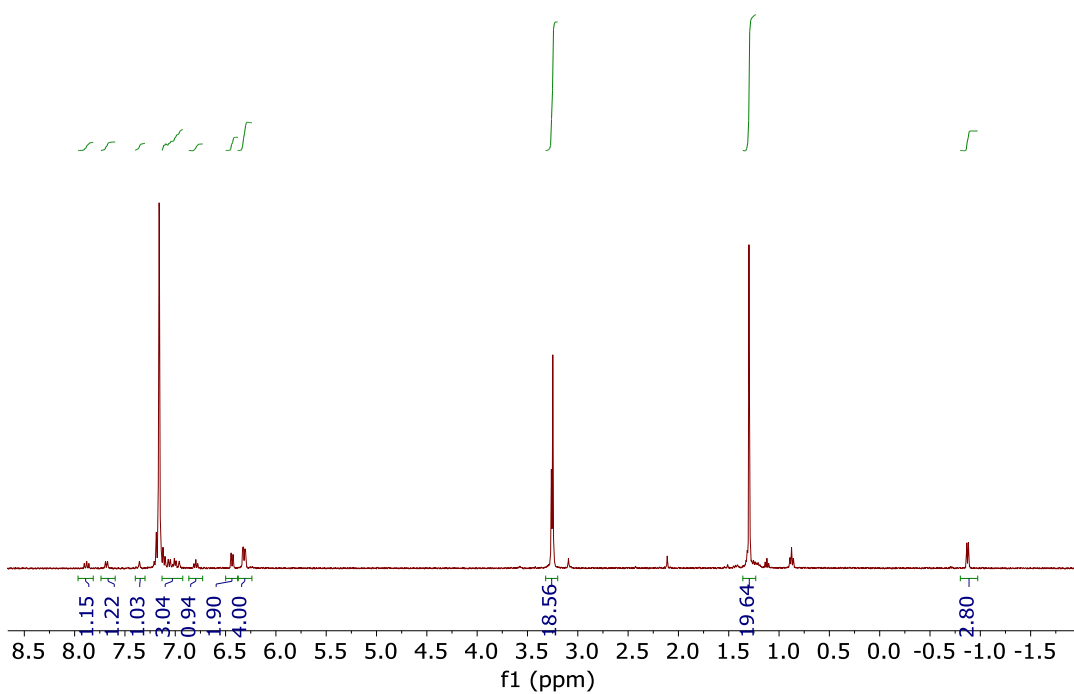


**Figure S2.15:**  $^1\text{H}$  NMR spectrum of **2-lut** in  $\text{C}_6\text{D}_6$ .

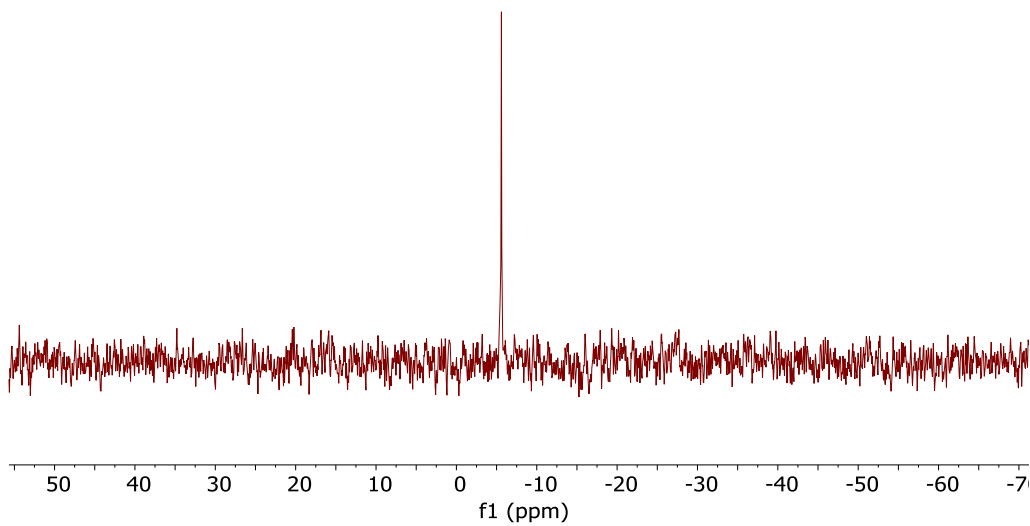


**Figure S2.16:**  $^{31}\text{P}\{^1\text{H}\}$  NMR spectrum of **2-lut** in  $\text{C}_6\text{D}_6$ .

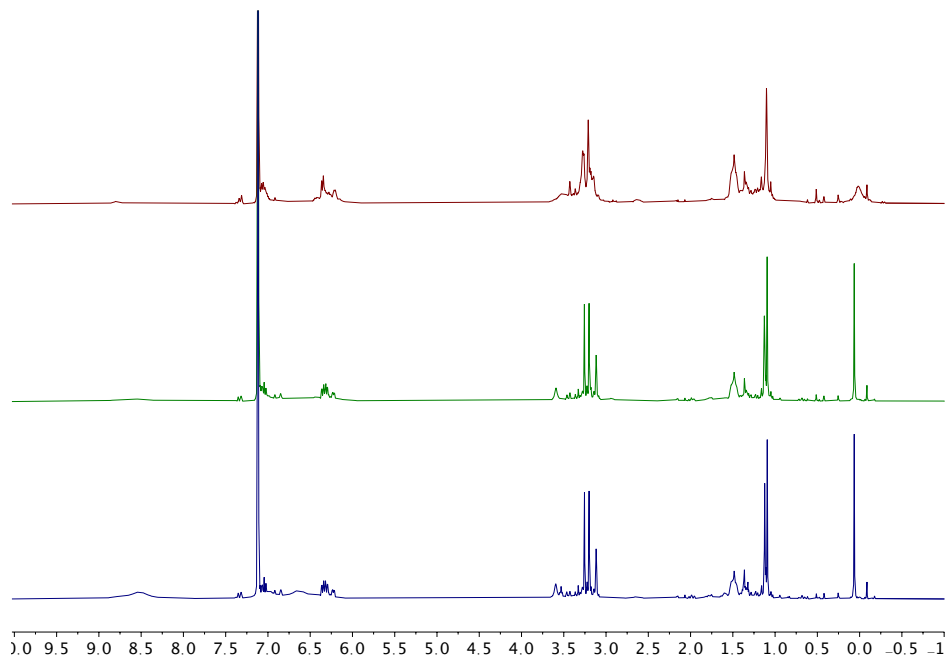


**Figure S2.17.**  $^1\text{H}$  NMR spectrum of **3** in  $\text{C}_6\text{D}_6$  (top).  $^1\text{H}$  NMR spectrum of **3** + 1 equiv. pyridine in  $\text{C}_6\text{D}_6$  (middle).  $^1\text{H}$  NMR spectrum of **3** + 5 equiv. pyridine in  $\text{C}_6\text{D}_6$  (bottom).

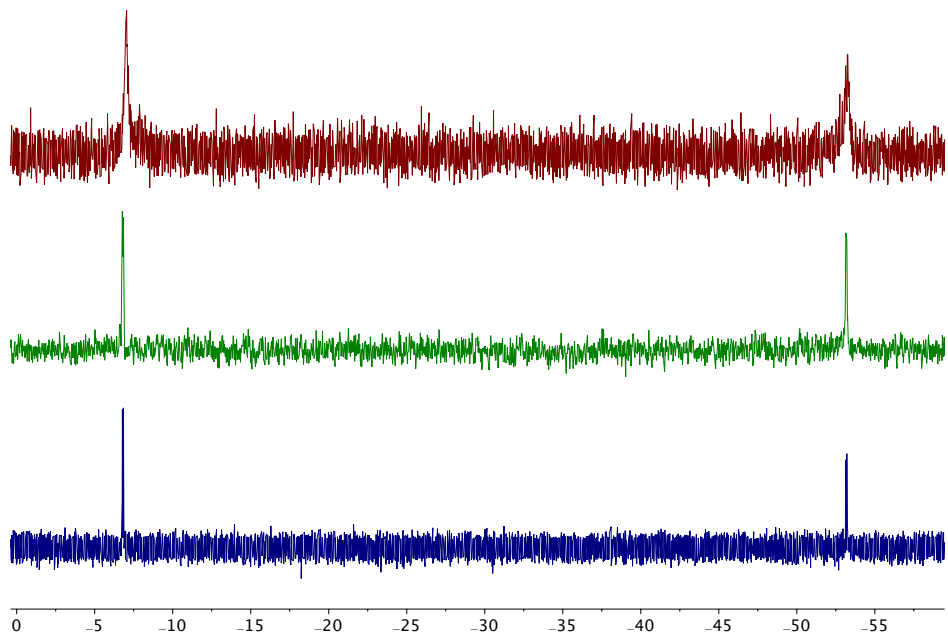


**Figure S2.18.**  $^{31}\text{P}\{^1\text{H}\}$  NMR spectrum of **3** in  $\text{C}_6\text{D}_6$  (top).  $^{31}\text{P}\{^1\text{H}\}$  NMR spectrum of **3** + 1 equiv. pyridine in  $\text{C}_6\text{D}_6$  (middle).  $^{31}\text{P}\{^1\text{H}\}$  NMR spectrum of **3** + 5 equiv. pyridine in  $\text{C}_6\text{D}_6$  (bottom).

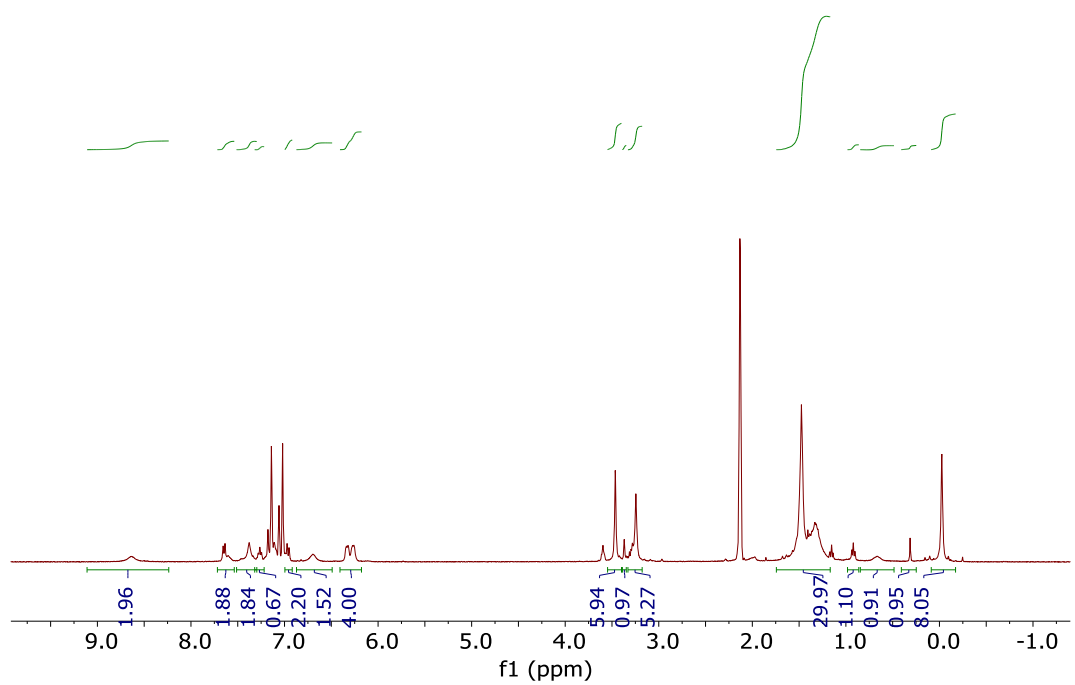


**Figure S2.19.**  $^1\text{H}$  NMR spectrum of **4** in  $\text{C}_6\text{D}_6$ .

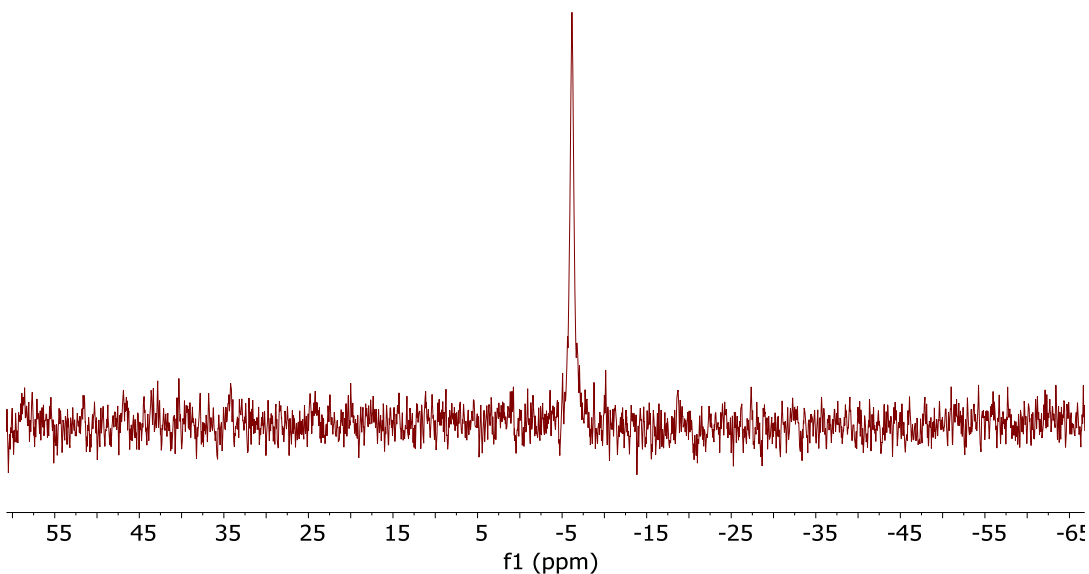


**Figure S2.20.**  $^{31}\text{P}\{\text{H}\}$  NMR spectrum of **4** in  $\text{C}_6\text{D}_6$ .

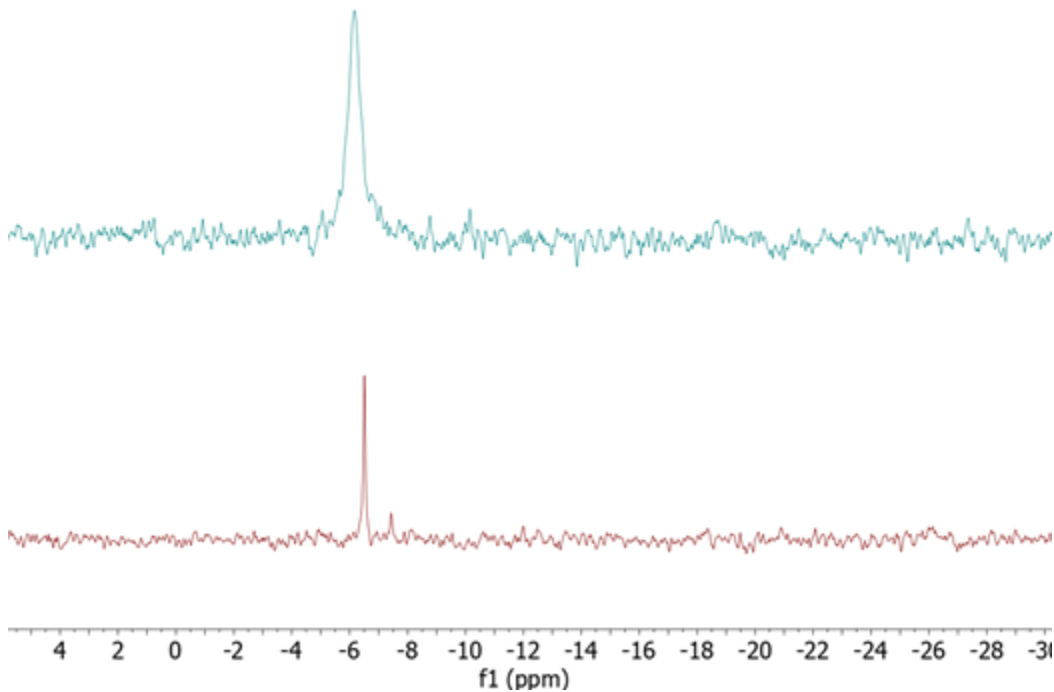


**Figure S2.21.**  $^{31}\text{P}\{\text{H}\}$  NMR spectrum of **4** in  $\text{C}_7\text{D}_8$ (top).  $^{31}\text{P}\{\text{H}\}$  NMR spectrum **4 + 10** equivalents of pyridine in  $\text{C}_6\text{D}_6$ (bottom).

### 3 Solution-State NMR Characterization and Discussion of 5

Encouraged by the structural confirmation of the chelate resulting from 2,1-insertion of acrylate in the solid-state, further NMR studies were performed to address the solution structure. The room temperature  $^1\text{H}$  NMR spectrum of **5** shows the expected number of aromatic resonances as well as broad peaks corresponding to the two methoxy resonances in a 1:1 ratio. A broad resonance ( $\delta$  1.56) and a sharp resonance ( $\delta$  1.48) are assigned to the tert-butyl groups from the phosphine naphthoxide ligand and the ester group, respectively. Resonances for the Ni-bound alkyl moiety are observed at  $\delta$  2.1 as a broad multiplet for the methine, overlapping resonances at  $\delta$  0.76, and 1.19 for the diastereotopic methylene protons, and at  $\delta$  0.81 for the methyl protons, which were identified using multiplicity edited  $^1\text{H}$ - $^{13}\text{C}\{\text{H}\}$  HSQC.  $^{13}\text{C}\{\text{H}\}$  NMR (Figure S3.2) display five aliphatic resonances corresponding to the Ni-bound alkyl moiety. The resonances at  $\delta$  14.3, 19.7, and 21.3 are consistent with methyl, methylene, and methine groups, respectively. This assignment is further supported by higher magnitude  $J_{\text{CP}}$  value for the methine resonance (24.8 Hz) and low magnitude  $J_{\text{CP}}$  value for the methylene resonance (3.0 Hz). Furthermore, the multiplicity-edited  $^{13}\text{C}\{\text{H}\}$ - $^1\text{H}$  HSQC identifies the resonance at  $\delta$  19.7 as a methylene resonance with  $^1\text{H}$  cross peaks at  $\delta$  0.76 and 1.19, the latter resonance overlapping with the tert-butyl resonances. A cross peak for the methyl peak was observed at  $\delta$  0.81, and for the methine, at  $\delta$  2.12. Although these data do not rule out a solution structure with the carbonyl dissociating, they provide conclusive

support for the Ni-alkyl group connectivity observed in the solid-state. Chain walking through  $\beta$ -H elimination and reinsertion at the other end of the olefin could give isomers in solution. The isomer where Ni walks to the end of the alkyl chain would not display a methyl group, while the remaining one with Ni migrating a single carbon would still have methyl, methylene, and methine motifs but in a different coupling pattern; both can be ruled out based on the NMR data. However, we cannot rule out a dynamic isomerization process with compound **5** as the major, and only detectable component.

Decoalescence of **5** is observed at low temperatures, NMR studies of **5** suggest the existence of two conformers in exchange, which in part elucidate the broadness observed of the resonances in the room-temperature  $^1\text{H}$  and  $^{31}\text{P}\{^1\text{H}\}$  NMR spectra of **5**. Complex **5** was investigated further toward gleaned additional insights into potential isomerization processes. The  $^{31}\text{P}\{^1\text{H}\}$  NMR spectrum of **5** shows a single broad resonance at  $\delta$  -6.36 with a  $W_{1/2} = 58.1$  Hz. Variable temperature  $^{31}\text{P}\{^1\text{H}\}$  NMR spectra show the appearance of two sharp peaks upon cooling to 0 °C in a 10 to 1 ratio, at approximately  $\delta$  -6.1 and -8.5, respectively. Upon further cooling to -60 °C, the ratio decreases to approximately 4.3:1. Cooling to -80 °C further decreases the ratio (3.1:1) and significant broadening is observed in the major isomer, but not the minor isomer (Figure S3.5). Cooling to -90 °C shows further broadening and chemical shift change with both resonances overlapped. This observation could indicate the presence of two isomers stemming from reversible  $\beta$ -H elimination and reinsertion processes; alternatively, it could also indicate the presence of conformers which are not fluxional on the NMR time scale at low temperatures. The  $^1\text{H}$  NMR shows sharpening of several resonances up-on cooling, as well as the decoalescence of the tert-butyl resonances on the naphthoxide ligand. Chemical shift changes are also observed for many of the resonances including the methoxy, the aromatic, and the Ni-alkyl groups. The apparent overlap of many of these resonances upon decoalescence render the interpretation of the low temperature  $^1\text{H}$  NMR spectra inconclusive. Because isomerization via chain walking would result in five- or six-membered chelates likely more stable than the alkyl species observed at room temperature, we favor the interpretation that the isomers observed at low temperatures are conformers.

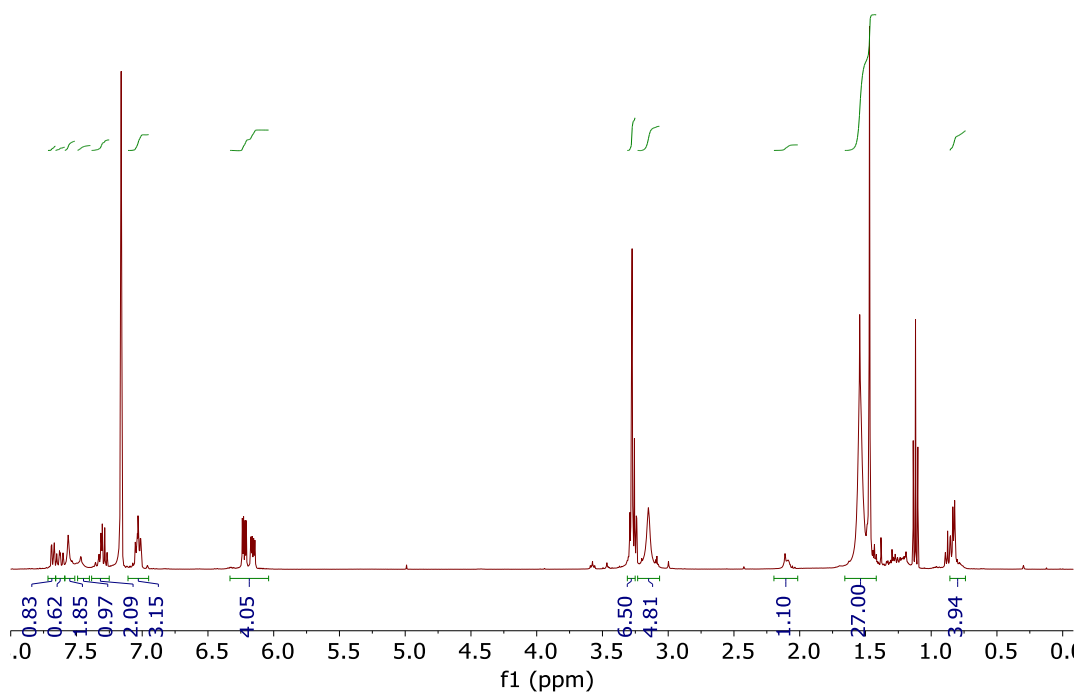


**Figure S3.1.**  $^1\text{H}$  NMR spectrum of **5** in  $\text{C}_6\text{D}_6$

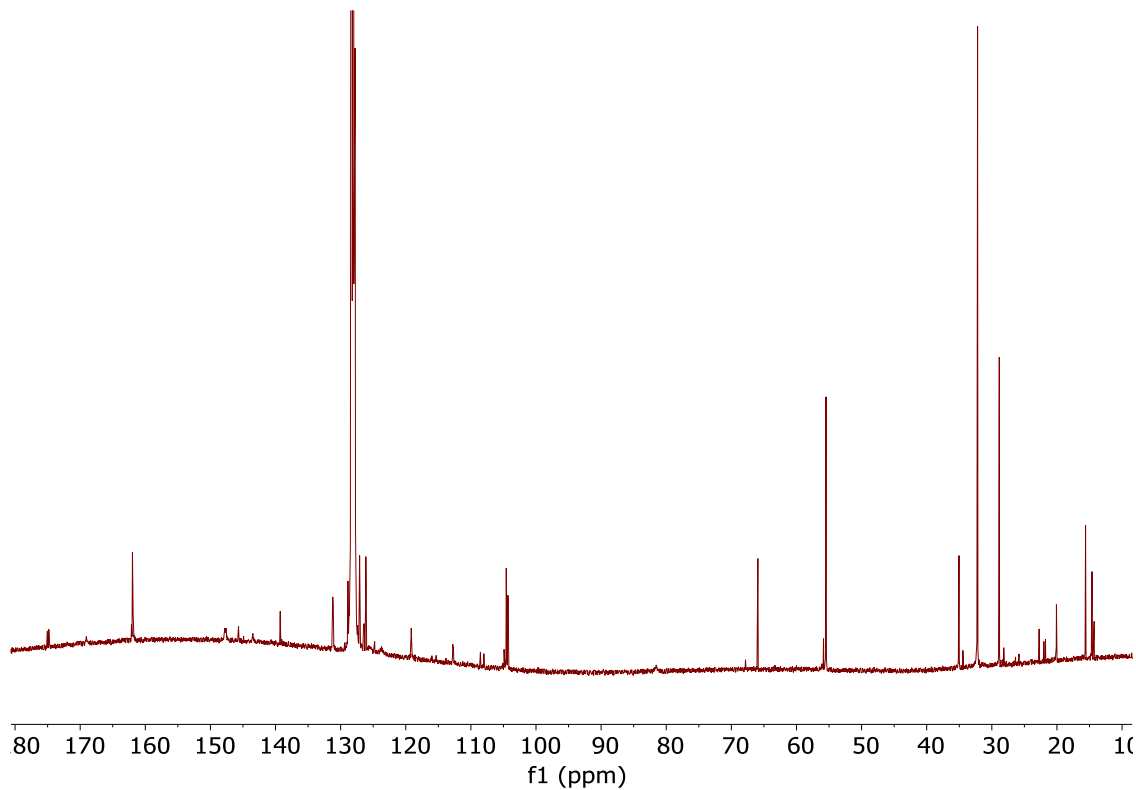


**Figure S3.2.**  $^{13}\text{C}\{^1\text{H}\}$  NMR spectrum of **5** in  $\text{C}_6\text{D}_6$

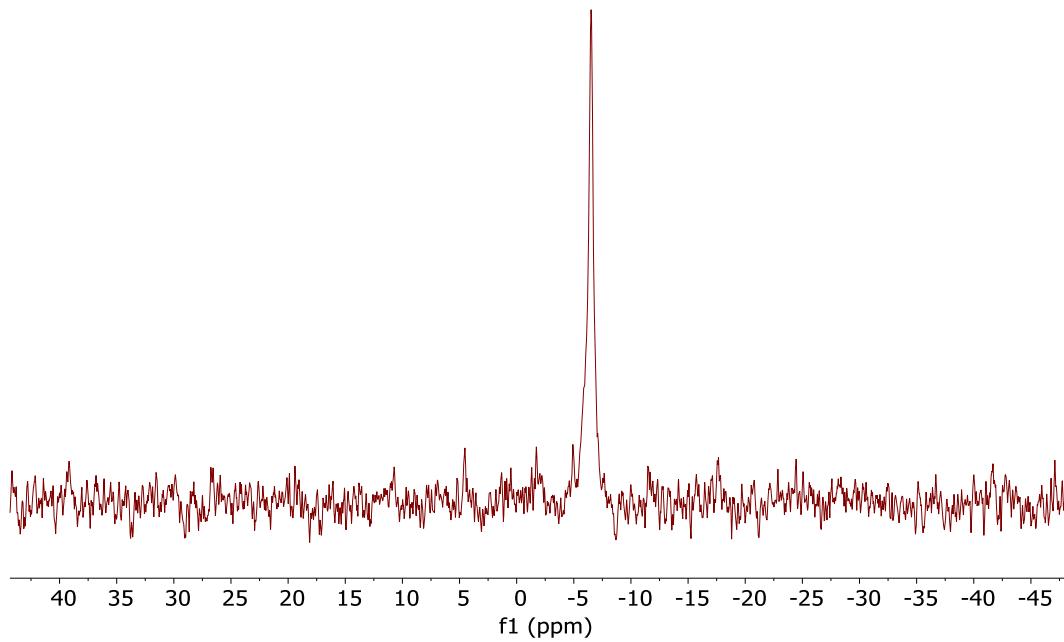


**Figure S3.3.**  $^{31}\text{P}\{\text{H}\}$  NMR spectrum of **5** in  $\text{C}_6\text{D}_6$

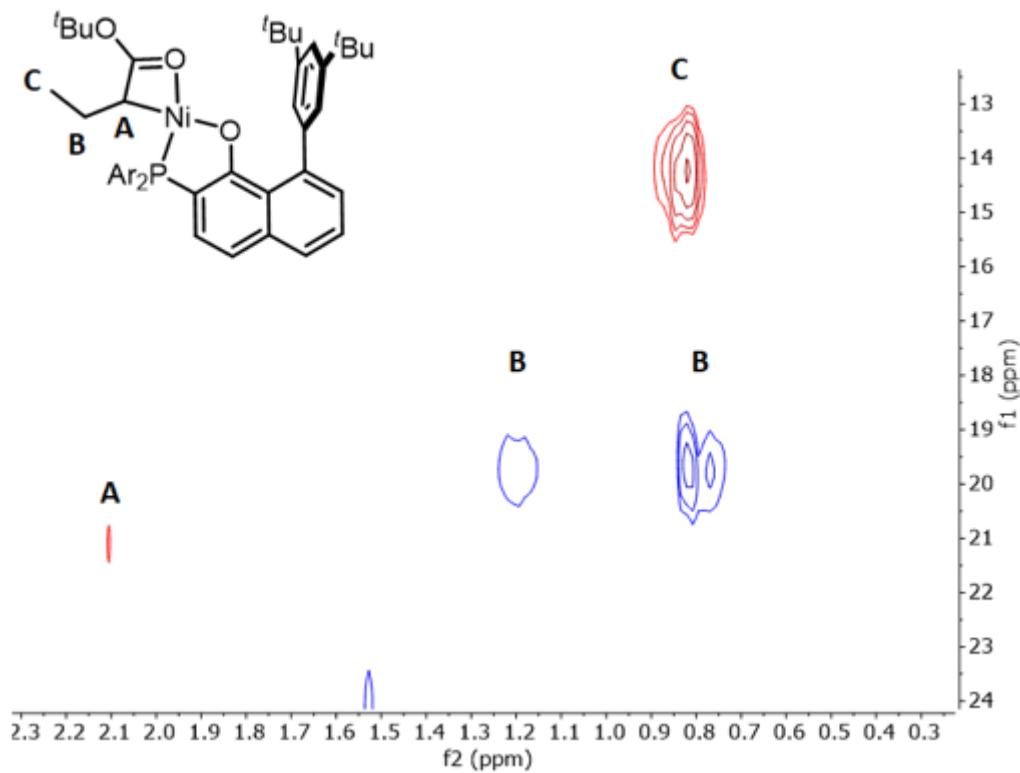


**Figure S3.4.**  $^{13}\text{C}\{\text{H}\}$ - $^1\text{H}$  HSQC NMR Spectrum of **5** in  $\text{C}_7\text{D}_8$

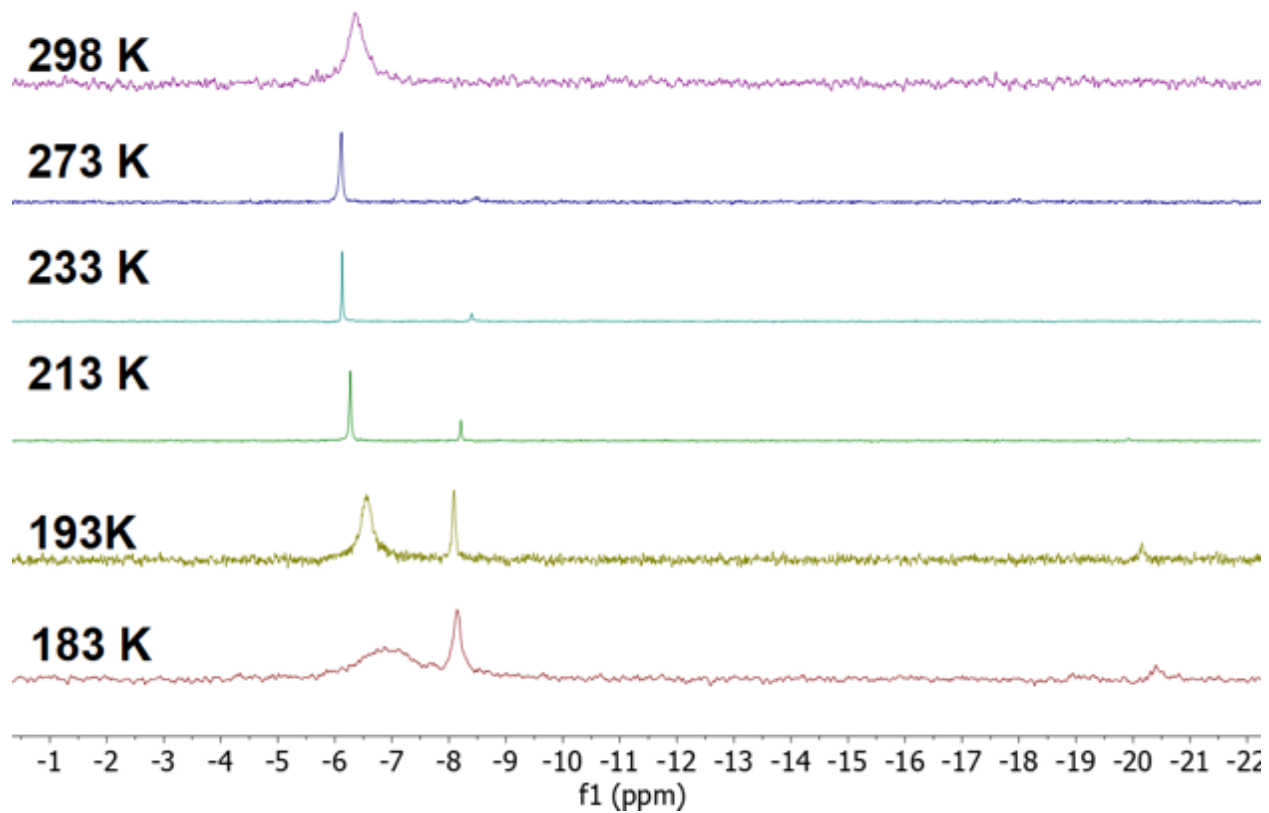


**Figure S3.5.**  $^{31}\text{P}\{\text{H}\}$  Variable-Temperature NMR Spectra of **5** in  $\text{C}_7\text{D}_8$

#### 4 Crystallographic Information

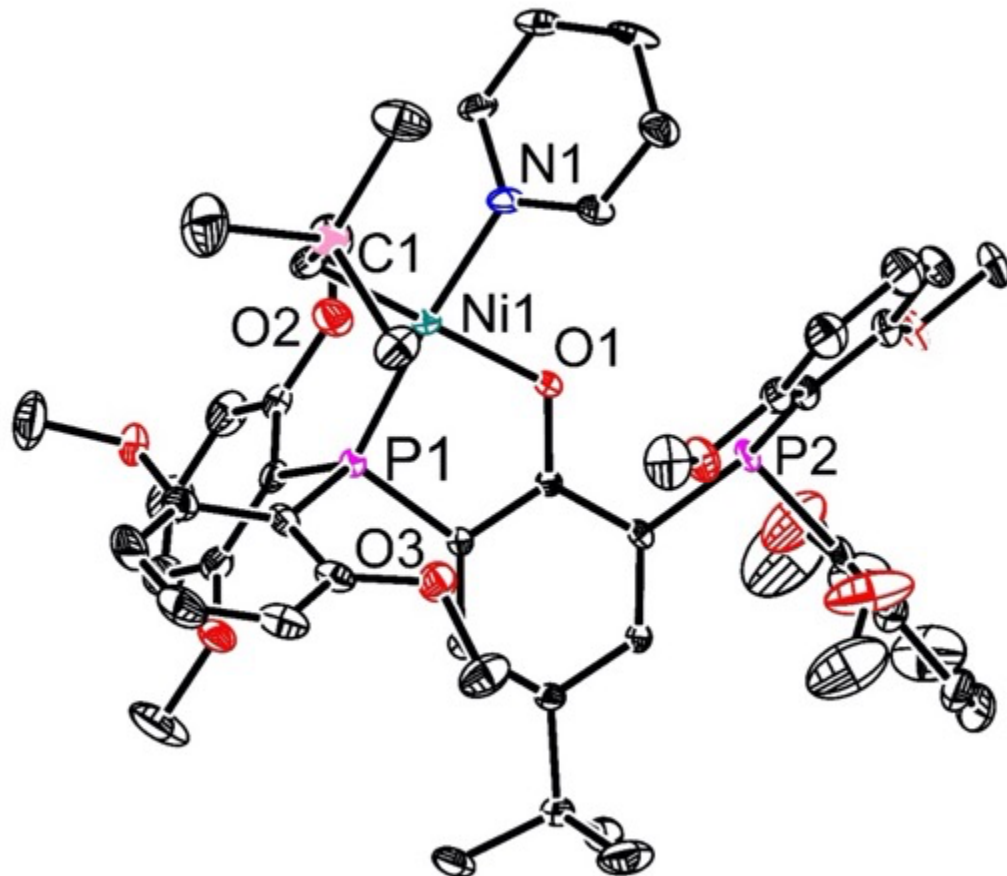


**Figure S4.1.** Solid-State Structure of **1**. Ellipsoids are show at the 50% probability level. Hydrogen atoms and solvent molecules excluded for clarity. Disordered SiMe<sub>3</sub> and OMe group excluded for clarity.

**Special Refinement Details for **1**:** Complex **1** crystallizes in a P-1 space group with the full molecule in the asymmetric unit. The SiMe<sub>3</sub> group is modelled with two-site disorder with occupancies of 0.78 and 0.22. One of the methoxy groups is also modelled with two-site disorder with occupancies of 0.78 and 0.22. The carbon on the lower occupancy disordered methoxy group is refined isotropically to prevent an NPD. A disordered benzene molecule is observed and is refined isotropically to prevent NPDs. There is likely disorder on the benzene molecule, despite efforts, it could not be modelled.

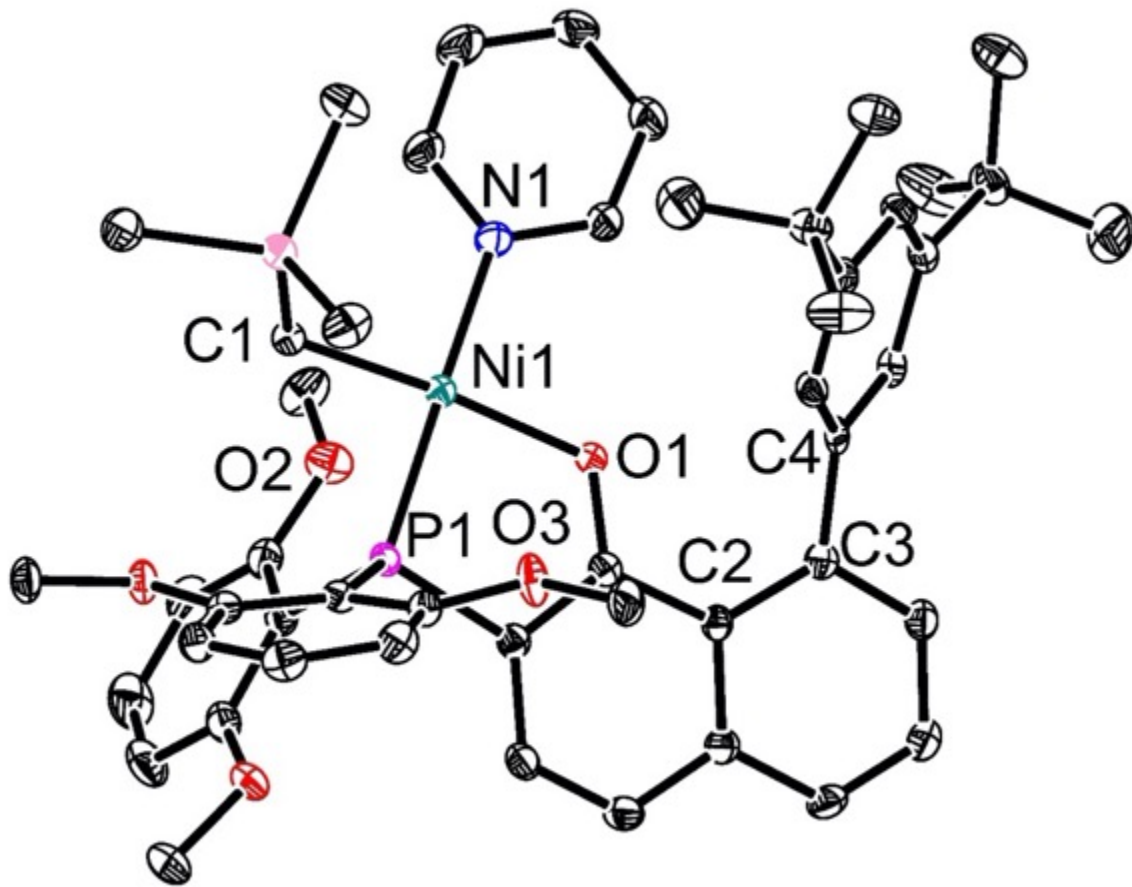


**Figure S4.2.** Solid-State Structure of **2**. Ellipsoids are show at the 50% probability level. Hydrogen atoms and solvent molecules excluded for clarity.

**Special Refinement Details for **2**:** Complex **2** crystallizes as a twin in a **P-1** space group with the full molecule and half of a benzene molecule in the asymmetric unit.

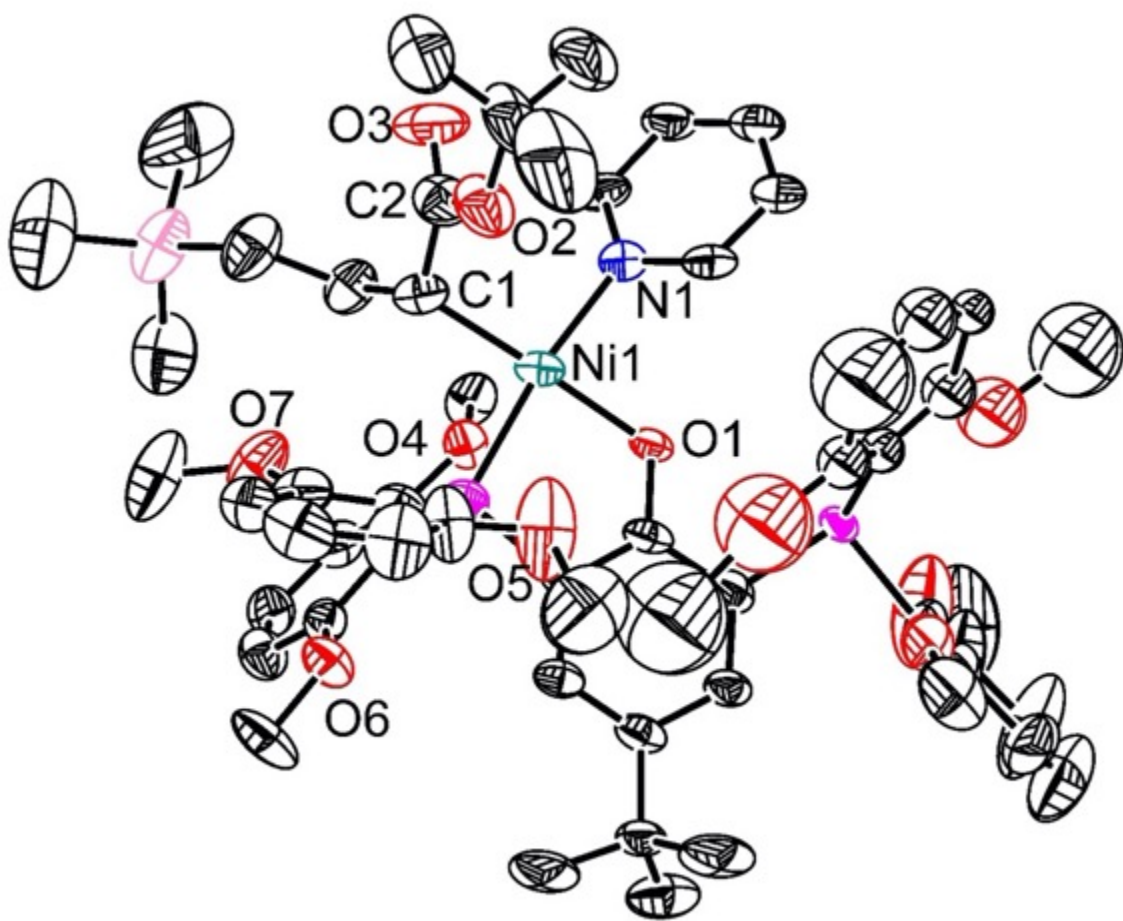


**Figure S4.3.** Solid-State Structure of **3**. Ellipsoids are show at the 50% probability level. Hydrogen atoms and solvent molecules excluded for clarity.

**Special Refinement Details for **3**:** Complex **3** crystallizes in a P-1 space group with the full molecule in the asymmetric unit. The SiMe<sub>3</sub> group is modelled with two-site disorder with occupancies of 0.54 and 0.46. The unbound P center and the 2,6 dimethoxy aryl groups are modelled with two-site disorder with occupancies of 0.76 and 0.24. The data collected on this sample produces a moderate quality solid-state structure.

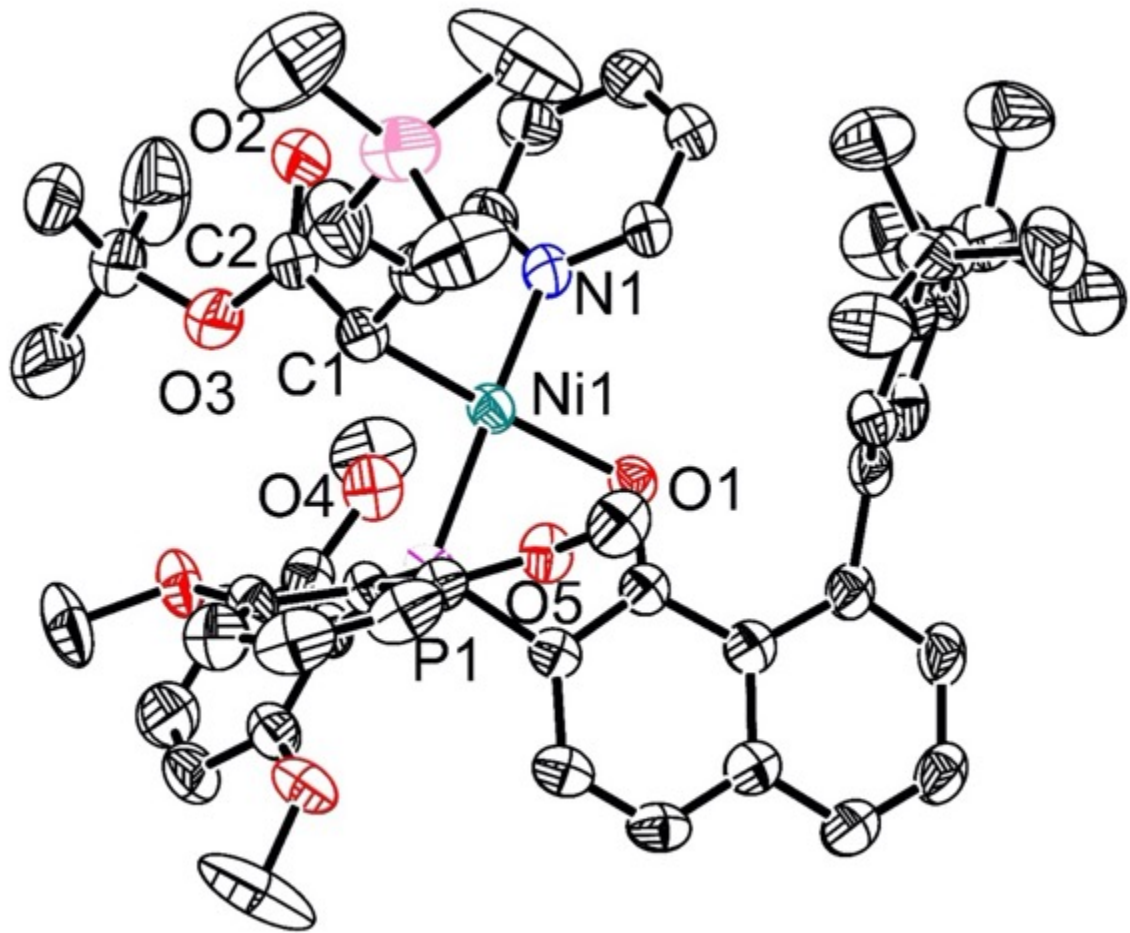


**Figure S4.4.** Solid-State Structure of **4**. Ellipsoids are show at the 50% probability level. Hydrogen atoms and solvent molecules excluded for clarity. Disorder also excluded for clarity.

**Special Refinement Details for **4**:** Complex **4** crystallized in a  $P_{21/c}$  space group with the full molecule in the asymmetric unit. Two-site disorder was modelled for the entire tert-butyl aryl group with relative occupancies of 0.78 and 0.22. Additional two site disorder was modelled for one of the dimethoxy aryl rings with relative occupancies of 0.78 and 0.22. Two of the carbons on the less-occupied dimethoxy ring were refined isotropically to prevent NPDs.

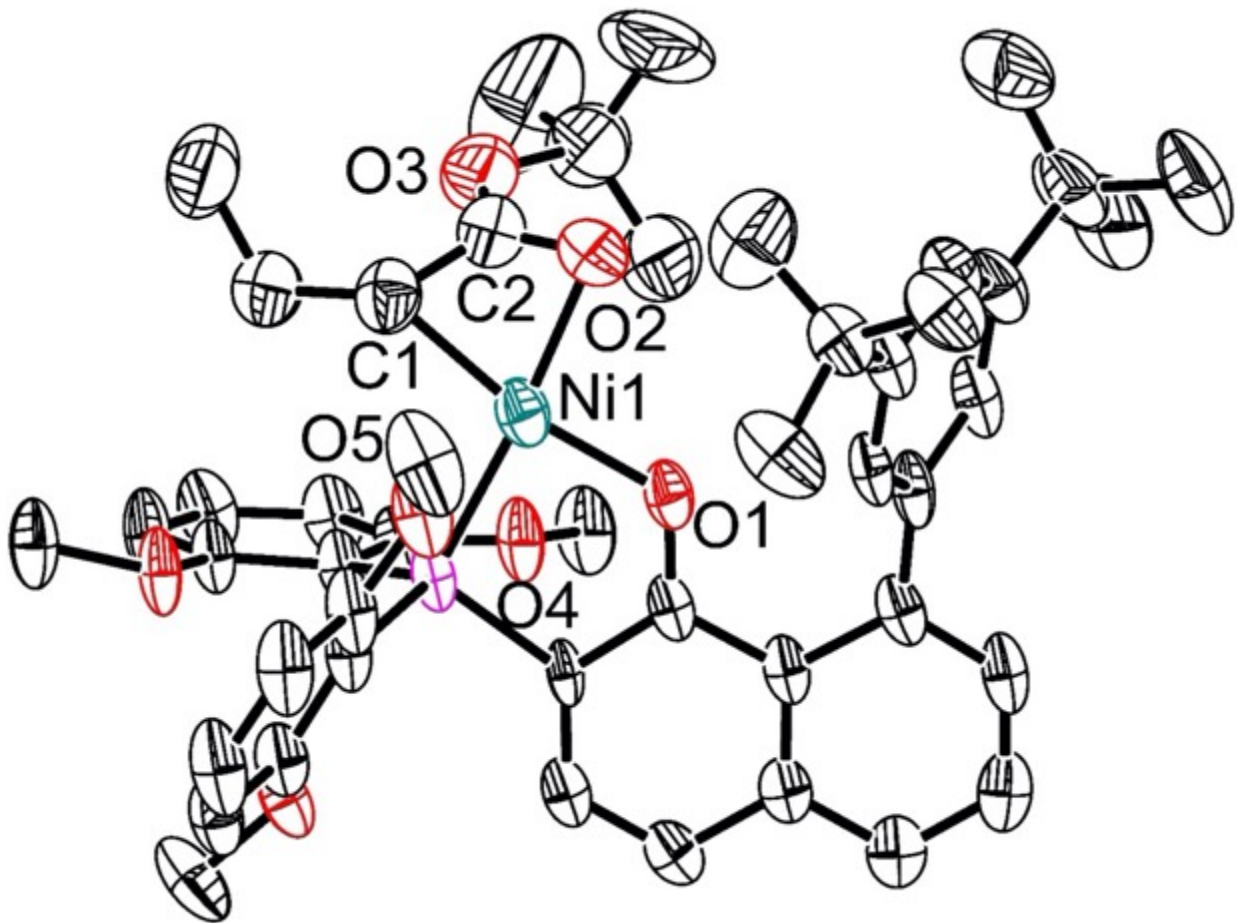


**Figure S4.5.** Solid-State Structure of **5**. Ellipsoids are show at the 50% probability level. Hydrogen atoms and solvent molecules excluded for clarity. Disorder of tert-butyl aryl also excluded for clarity.

**Special Refinement Details for **5**:** Complex **5** crystallizes in a  $P_{21/n}$  space group with an outer sphere ether molecule, all of which are present in the asymmetric unit. Two-site disorder is present in one of the tertbutyl groups on the aryl ring, with occupancies of 0.52 and 0.48. Additional solvent disorder could not be modelled successfully and was masked using SQUEEZE.

Crystallographic Information

**Table S4.1.** Crystal and refinement data for complexes **1-3**

	<b>1</b>	<b>2</b>	<b>3</b>
CCDC	2056541	2056542	2056543
Empirical formula	C <sub>58</sub> H <sub>63.9</sub> NNiO <sub>8</sub> P <sub>2</sub> Si	C <sub>52</sub> H <sub>63</sub> NNiO <sub>5</sub> PSi	C <sub>60.57</sub> H <sub>78.28</sub> NNiO <sub>11.34</sub> P <sub>2</sub> Si <sub>1.8</sub> 2
Formula weight	1067.7	899.78	1173.71
Temperature/K	100 K	100 K	100 K
Crystal system	Triclinic	Triclinic	Triclinic
Space group	P-1	P-1	P-1
a/Å	13.272(4)	11.2840(9)	13.366 (8)
b/Å	13.914(7)	12.9467(10)	16.184(5)
c/Å	15.221(5)	16.3826(13)	16.570(5)
α/°	90.282(18)	91.142(5)	90.72(2)
β/°	101.120(14)	103.578(4)	97.09(2)
γ/°	90.58(2)	92.791(4)	101.70(2)
Volume/Å <sup>3</sup>	2757.8(19)	2322.5	3480(3)
Z	2	2	2
ρ <sub>calc</sub> g/cm <sup>3</sup>	1.286	1.287	1.120
μ/mm <sup>-1</sup>	0.487	1.552	1.555
F(000)	1125.8	955.40	1246
Radiation	CuKα (λ = 1.54178)	CuKα (λ = 1.54178)	CuKα (λ = 1.54178)
Reflections collected	61600	9890	70100
Independent reflections	9916	9095	8812
Goodness-of-fit on F <sup>2</sup>	1.141	1.059	1.077
Final R indexes [I>=2σ (I)]	R <sub>1</sub> = 8.42 % R <sub>2</sub> = 19.44 %	R <sub>1</sub> = 3.66 % R <sub>2</sub> = 9.78 %	R <sub>1</sub> = 11.48 % R <sub>2</sub> = 32.87 %

**Table S4.2:** Crystal and refinement data for complexes **4** and **5**

	<b>4</b>	<b>5</b>
CCDC	2056544	2056545
Empirical formula	C <sub>56</sub> H <sub>71.78</sub> NNiO <sub>7</sub> PSi	C <sub>52</sub> H <sub>68</sub> NiO <sub>8</sub> P
Formula weight	988.67	910.72
Temperature/K	100 K	100 K
Crystal system	Monoclinic	Triclinic
Space group	P <sub>21/C</sub>	P <sub>21/n</sub>
a/Å	17.811(5)	15.546(4)
b/Å	20.024(6)	14.863(4)
c/Å	15.761(5)	23.621(9)
α/°	90	90
β/°	104.164(13)	103.26(2)
γ/°	90	90
Volume/Å <sup>3</sup>	5450(3)	5312(3)
Z	4	4
ρ <sub>calc</sub> g/cm <sup>3</sup>	1.205	1.139
μ/mm <sup>-1</sup>	1.394	1.189
F(000)	2111.1	1948
Radiation	CuKα ( $\lambda = 1.54178$ )	CuKα ( $\lambda = 1.54178$ )
Reflections collected	101836	63894
Independent reflections	9392	4944
Goodness-of-fit on F <sup>2</sup>	1.018	1.041
Final R indexes [I>=2σ (I)]	R <sub>1</sub> = 7.00 % R <sub>2</sub> = 20.59 %	R <sub>1</sub> = 10.84 % R <sub>2</sub> = 30.15 %

## ***Part B: Ethylene/tBA Copolymerization***

### **5. Conditions and results**

#### **5.1 Procedures for polymerizations**

##### **5.1.1 General procedure for high throughput parallel polymerization reactor (PPR) runs for preparation of polyethylene and ethylene/tBA copolymers.**

Polyolefin catalysis screening was performed in a high throughput parallel polymerization reactor (PPR) system. The PPR system was comprised of an array of 48 single cell (6 x 8 matrix) reactors in an inert atmosphere glovebox. Each cell was equipped with a glass insert with an internal working liquid volume of approximately 5 mL. Each cell had independent controls for pressure and was continuously stirred at 800 rpm. Catalyst, ligand, and metal precursor solutions, unless otherwise noted, were prepared in toluene. Ligands were metallated with 1:1 ligand:metal (L:M) ratio by premixing a solution of metal precursor with a solution of the ligand. All liquids (i.e., solvent, tBA, and catalyst solutions) were added via robotic syringes. Gaseous reagents (i.e., ethylene) were added via a gas injection port. Prior to each run, the reactors were heated to 50 °C, purged with ethylene, and vented.

All desired cells were injected with tBA followed with a portion of toluene (This step was skipped for ethylene homopolymerization). The reactors were heated to the run temperature and then pressured to the appropriate psig with ethylene. Catalyst or in situ metallated ligands were then added to the cells. Each catalyst addition was chased with a small amount of toluene so that after the final addition, a total reaction volume of 5 mL was reached. Upon addition of the catalyst, the PPR software began monitoring the pressure of each cell. The desired pressure (within approximately 2-6 psig) was maintained by the supplemental addition of ethylene gas by opening the valve at the set point minus 1 psi and closing it when the pressure reached 2 psi higher. All drops in pressure were cumulatively recorded as “Uptake” or

“Conversion” of the ethylene for the duration of the run or until the uptake or conversion requested value was reached, whichever occurred first. Each reaction was then quenched by addition of 1% oxygen in nitrogen for 30 seconds at 40 psi higher than the reactor pressure. The shorter the “Quench Time”, the more active the catalyst. In order to prevent the formation of too much polymer in any given cell, the reaction was quenched upon reaching a predetermined uptake level of 80psig. After all the reactors were quenched they were allowed to cool to about 60 °C. They were then vented and the tubes were removed. The polymer samples were then dried in a centrifugal evaporator at 60 °C for 12 hours, weighed to determine polymer yield and submitted for IR (tBA incorporation) and GPC (molecular weight) analysis.

#### **5.1.2 General procedure for batch reactor runs for preparation of ethylene/tBA copolymers. (Table 1, entry 8 & 9)**

Polymerization reactions were conducted in a 2-L Parr batch reactor. The reactor was heated by an electrical heating mantle and cooled by an internal serpentine cooling coil containing cooling water. The water was pre-treated by passing through an Evoqua water purification system. Both the reactor and the heating/cooling system were controlled and monitored by a Camile TG process computer. The bottom of the reactor was fitted with a dump valve, which empties the reactor contents into a lidded dump pot, which was pre-filled with a catalyst-kill solution (typically 5 mL of an Irgafos / Irganox / toluene mixture). The lidded dump pot was vented to a 15-gal. blowdown tank, with both the pot and the tank N<sub>2</sub> purged. All chemicals used for polymerization or catalyst makeup are run through purification columns to remove any impurities that may affect polymerization. The toluene was passed through two columns, the first containing A2 alumina, the second containing Q5 reactant. The

tert-butyl acrylate was filtered through activated alumina. The ethylene was passed through two columns, the first containing A204 alumina and 4 Å molecular sieves, the second containing Q5 reactant. The N<sub>2</sub> used for transfers was passed through a single column containing A204 alumina, 4 Å molecular sieves and Q5 reactant.

The reactor was loaded first from the shot tank that contained toluene and tBA. The shot tank was filled to the load set points by use of a differential pressure transducer. After solvent/acrylate addition, the shot tank was rinsed twice with toluene. Then the reactor was heated up to the polymerization temperature set point. The ethylene was added to the reactor when the reaction temperature was reached to maintain the reaction pressure set point. Ethylene addition amounts were monitored by a micro-motion flowmeter.

The catalysts were handled in an inert atmosphere glovebox and were prepared as a solution in toluene. The catalyst was drawn into a syringe and pressure-transferred into the catalyst shot tank. This was followed by 3 rinses of toluene, 5 mL each. Catalyst was added when the reactor pressure set point was reached.

Immediately after catalyst addition the run timer was started. Usually within the first 2 min. of successful catalyst runs an exotherm was observed, as well as decreasing reactor pressure. Ethylene was then added by the Camile to maintain reaction pressure set point in the reactor. These polymerizations were run for 75 min or until 40 g of ethylene uptake. Then the agitator was stopped, and the bottom dump valve was opened to empty reactor contents into the lidded dump pot. The lidded dump pot was closed and the contents were poured into trays placed in a lab hood where the solvent was evaporated off overnight. The trays containing the remaining polymer were then transferred to a vacuum oven, where they were heated up to 140 °C under

vacuum to remove any remaining solvent. After the trays cooled to ambient temperature, the polymers were weighed for yield/efficiencies and submitted for polymer testing if so desired.

## **5.2 General procedure for polymer characterization**

### **5.2.1 Gel permeation chromatography (GPC)**

High temperature GPC analysis was performed using a Dow Robot Assisted Delivery (RAD) system equipped with a Polymer Char infrared detector (IR5) and Agilent PLgel Mixed A columns. Decane (10  $\mu$ L) was added to each sample for use as an internal flow marker. Samples were first diluted in 1,2,4-trichlorobenzene (TCB) stabilized with 300 ppm butylated hydroxyl toluene (BHT) at a concentration of 10 mg/mL and dissolved by stirring at 160°C for 120 minutes. Prior to injection the samples are further diluted with TCB stabilized with BHT to a concentration of 3 mg/mL. Samples (250  $\mu$ L) are eluted through one PL-gel 20  $\mu$ m (50 x 7.5 mm) guard column followed by two PL-gel 20  $\mu$ m (300 x 7.5 mm) Mixed-A columns maintained at 160 °C with TCB stabilized with BHT at a flowrate of 1.0 mL/min. The total run time was 24 minutes. To calibrate for molecular weight (MW) Agilent EasiCal polystyrene standards (PS-1 and PS-2) were diluted with 1.5 mL TCB stabilized with BHT and dissolved by stirring at 160 °C for 15 minutes. These standards are analyzed to create a 3rd order MW calibration curve. Molecular weight units are converted from polystyrene (PS) to polyethylene (PE) using a daily Q-factor calculated to be around 0.4 using the average of 5 Dowlex 2045 reference samples.

### **5.2.2 Fourier-transform infrared spectroscopy (FTIR)**

The 10 mg/mL samples prepared for GPC analysis are also utilized to quantify tert butyl acrylate (tBA) incorporation by Fourier Transform infrared spectroscopy (FTIR). A Dow robotic preparation station heated and stirred the samples at 160°C for 60 minutes then

deposited 130  $\mu$ L portions into stainless wells promoted on a silicon wafer. The TCB was evaporated off at 160°C under nitrogen purge. IR spectra were collected using a Nexus 6700 FT-IR equipped with a DTGS KBr detector from 4000-400 cm<sup>-1</sup> utilizing 128 scans with a resolution of 4. Ratio of tBA (C=O: 1762-1704 cm<sup>-1</sup>) to ethylene (CH<sub>2</sub>: 736-709 cm<sup>-1</sup>) peak areas were calculated and fit to a linear calibration curve to determine total tBA.

### **5.2.3 Differential scanning calorimetry (DSC)**

Differential scanning calorimetry analyses was performed on solid polymer samples using a TA Instruments, Inc. Discovery Series or TA Instruments, Inc., DSC2500, programmed with the following method:

Equilibrate at 175.00 °C

Isothermal for 3 minutes

Ramp 30.00 °C/min to 0.00 °C

Ramp 10.00 °C/min to 175.00 °C

Data was analyzed using TA Trios software.

### **5.2.4 NMR characterization**

NMR spectra of ethylene/tBA copolymers were recorded on a Bruker 400 MHz using o-dichlorobenzene at 120 °C. <sup>1</sup>H NMR analysis of copolymers were done using a relaxation time (0.2 s), and an acquisition time (1.8 s) with the number of FID's collected per sample (512). <sup>13</sup>C{<sup>1</sup>H} NMR analysis of copolymers were done using 90° pulse of 17.2  $\mu$ s, a relaxation time (22.0 s), an acquisition time (5.3 s), and inverse-gated decoupling with the number of FID's collected per sample (1536).

### 5.3 Ethylene homopolymerization in high throughput parallel polymerization reactors (PPR)

Table S5.1 show a set of ethylene homopolymerization trials with **1**. In general, **1** showed extremely high activity ( $\sim 400000 \text{ kg}/(\text{mol}\cdot\text{h})$ ) at 90 °C. These trials were stopped in  $\sim 10$ s to protect the reactor, and therefore resulting polyethylene features relatively low Mw and high PDI. This may not represent **1**'s typical performance.

**Table S5.1.** Ethylene/tBA copolymerization with in-situ mixed ligand **POPH** and  $\text{py}_2\text{Ni}(\text{CH}_2\text{SiMe}_3)_2$  (**Ni**)

Entry <sup>a</sup>	time (s)	temp. (°C)	Act. (kg/(mol·h))	$M_w/10^3$	PDI	Tm (°C)
1	11	90	378947	9.3	5.3	123.9
2	10	90	417000	27.4	9.4	106.9
3	10	90	411429	16.8	6.5	107.0

<sup>a</sup>V(total)=5 mL, [Ni]=0.25 μmol, ethylene pressure=400 psi.

#### 5.4 Supplemental data for ethylene/tBA copolymerization in high throughput parallel polymerization reactors (PPR)

Table S5.2~S5.4 show original analytic data of ethylene/tBA copolymerization with **1** and **2**. Table 1 shows average of representative replicated runs presented in these three tables.

**Table S5.2.** Ethylene/tBA copolymerization with in-situ mixed ligand **POPH** and  $\text{py}_2\text{Ni}(\text{CH}_2\text{SiMe}_3)_2$  (**Ni**)

Entry <sup>a</sup>	tBA (M)	T (°C)	Act. (kg/(mol·h))	t (min)	$M_w/10^3$	PDI	%Mol t-BA	Tm (°C)
1	0.05	70	304	60	97.2	2.25	2.58	107.3
2	0.05	70	324	60	91.5	2.25	2.57	106.9
3	0.05	70	300	60	93.0	2.26	2.56	107.0
4	0.05	70	328	60	95.8	2.30	2.49	107.8
5	0.05	70	348	60	93.6	2.25	2.34	108.7
6	0.05	90	482	55	60.8	2.26	2.21	110.5
7	0.05	90	629	52	58.6	2.25	1.94	111.9
8	0.05	90	644	38	58.9	2.22	2.26	110.5
9	0.05	90	639	44	59.5	2.27	2.18	110.8
10	0.1	90	244	60	38.7	2.33	5.40	93.6
11	0.1	90	248	60	43.4	2.38	4.99	94.7
12	0.1	90	240	60	40.9	2.30	4.99	94.8
13	0.1	90	248	60	40.2	2.23	4.85	95.2
14	0.15	90	116	60	28.4	2.29	8.60	81.9
15	0.15	90	108	60	27.7	2.36	7.96	82.2
16	0.15	90	120	60	30.3	2.27	7.97	83.3
17	0.15	90	128	60	29.3	2.32	8.16	82.2
18	0.15	100	104	60	22.2	2.31	7.97	81.1
19	0.15	100	120	60	22.6	2.31	7.64	80.9
20	0.15	100	132	60	22.9	2.22	8.19	81.4
21	0.15	100	120	60	22.8	2.17	7.63	81.8
22	0.15	100	88	60	22.9	2.19	7.47	83.2
23	0.2	100	84	60	19.0	2.31	12.49	68.4
24	0.2	100	80	60	19.1	2.10	11.42	68.4

<sup>a</sup>V(total)=5 mL, [Ni]=0.25 μmol, ethylene pressure=400 psi. Polymerization runs were stopped when t=1 h or ethylene uptake reached a level of 80.13 psig (to prevent formation of too much polymer in the reactor), which ever occurred first (see section S5.1 for more details).

**Table S5.3.** Ethylene/tBA copolymerization with isolated nickel complex **1**

Entry <sup>a</sup>	T (°C)	t (min)	Act. (kg/(mol·h))	M <sub>w</sub> /10 <sup>3</sup>	PDI	%Mol t-BA	Tm (°C)
1	90	37	618	54.7	2.07	2.17	110.8
2	90	37	595	54.3	2.17	2.20	109.4
3	90	37	659	53.1	2.20	2.24	109.9
4	90	54	517	55.9	2.08	2.10	111.4
5	90	45	604	55.8	2.12	2.06	111.3
6	90	44	575	50.6	2.31	2.26	109.6
7	90	33	848	56.5	2.12	2.01	110.3
8	90	32	871	58.7	2.13	1.97	110.2

<sup>a</sup>V(total)=5 mL, [1]=0.25 μmol, [tBA]=0.05 M, ethylene pressure=400 psi. Polymerization runs were stopped when ethylene uptake reached a level of 80.13 psig to prevent formation of two much polymer in the reactor.

**Table S5.4.** Ethylene/tBA copolymerization with isolated nickel complex **2**

Entry <sup>a</sup>	Cat. (μmol)	tBA (M)	T (°C)	t (min)	Act. (kg/(mol·h))	Mw	PDI	%Mol t-BA	Tm (°C)
1	0.25	0.05	70	60	204	16.1	2.30	0.72	120.9
2	0.25	0.05	70	60	208	16.2	2.16	0.71	121.4
3	0.25	0.05	70	60	204	17.3	2.29	0.83	121.0
4	0.25	0.05	70	60	208	16.3	2.28	0.74	120.9
5	0.25	0.05	90	60	404	10.6	2.10	0.71	120.6
6	0.25	0.05	90	60	444	10.0	2.04	0.73	120.7
7	0.25	0.05	90	22	595	10.3	2.26	0.72	121.2
8	0.25	0.05	90	56	481	9.6	2.30	0.75	121.0
9	0.25	0.05	100	47	657	8.2	2.01	0.72	121.0
10	0.25	0.05	100	50	620	8.2	2.22	0.73	120.2
11	0.25	0.05	100	46	634	8.0	2.12	0.64	120.6
12	0.5	0.1	90	60	262	9.0	2.28	1.40	115.5
13	0.5	0.1	90	60	262	9.0	1.99	1.36	115.0
14	0.5	0.15	90	60	210	7.9	1.97	1.97	110.6
15	0.5	0.15	90	60	200	7.4	2.24	2.04	109.8
16	0.5	0.15	90	60	204	7.5	2.30	1.98	111.6

<sup>a</sup>V(total)=5 mL, [Ni]=0.25 μmol, ethylene pressure=400 psi. Polymerization runs were stopped when t=1 h or ethylene uptake reached 80.13 psi (<1 h), which ever occurred first.

## 5.5 Supplemental figures for ethylene/tBA copolymerizatin with different tBA concentration

Data for these figures are extracted from Table S5.2~S5.4 (Red: **1**, blue: **2**)

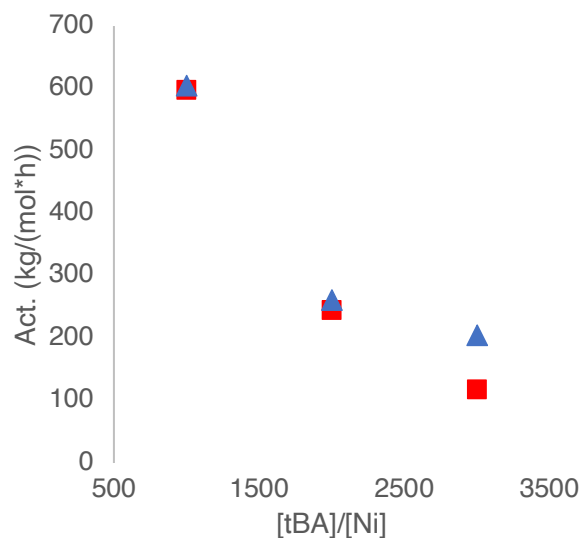


**Figure S5.1.** Catalytic activity of **1/2** with different equiv. of tBA

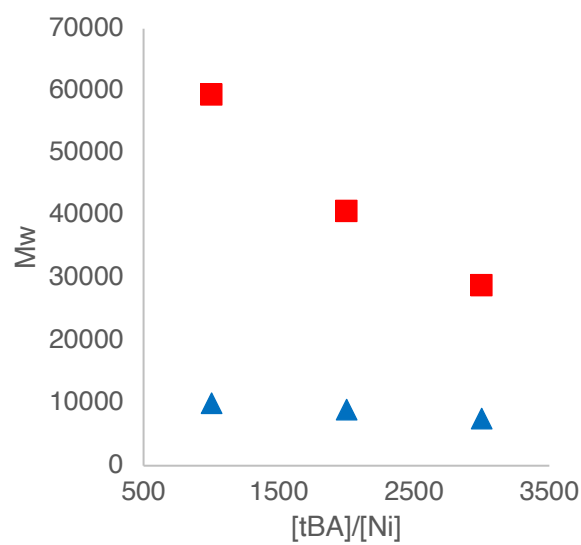


**Figure S5.2.** Molecular weights of ethylene/tBA copolymers with different equiv. of tBA

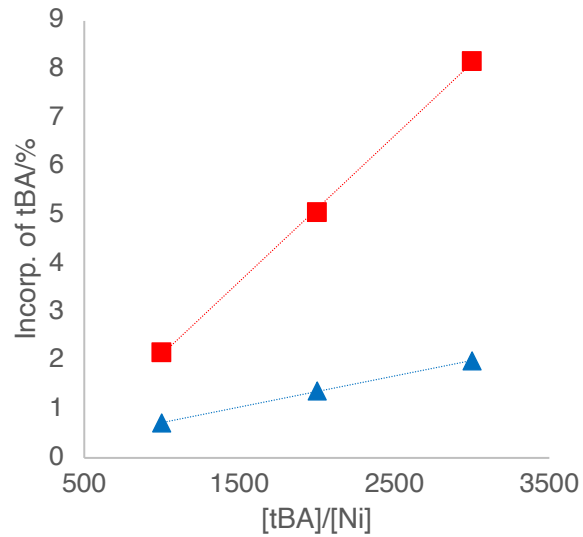


**Figure S5.3.** tBA incorporation of ethylene/tBA copolymers with different equiv. of tBA

**6. NMR Characterization of ethylene/tBA copolymers**

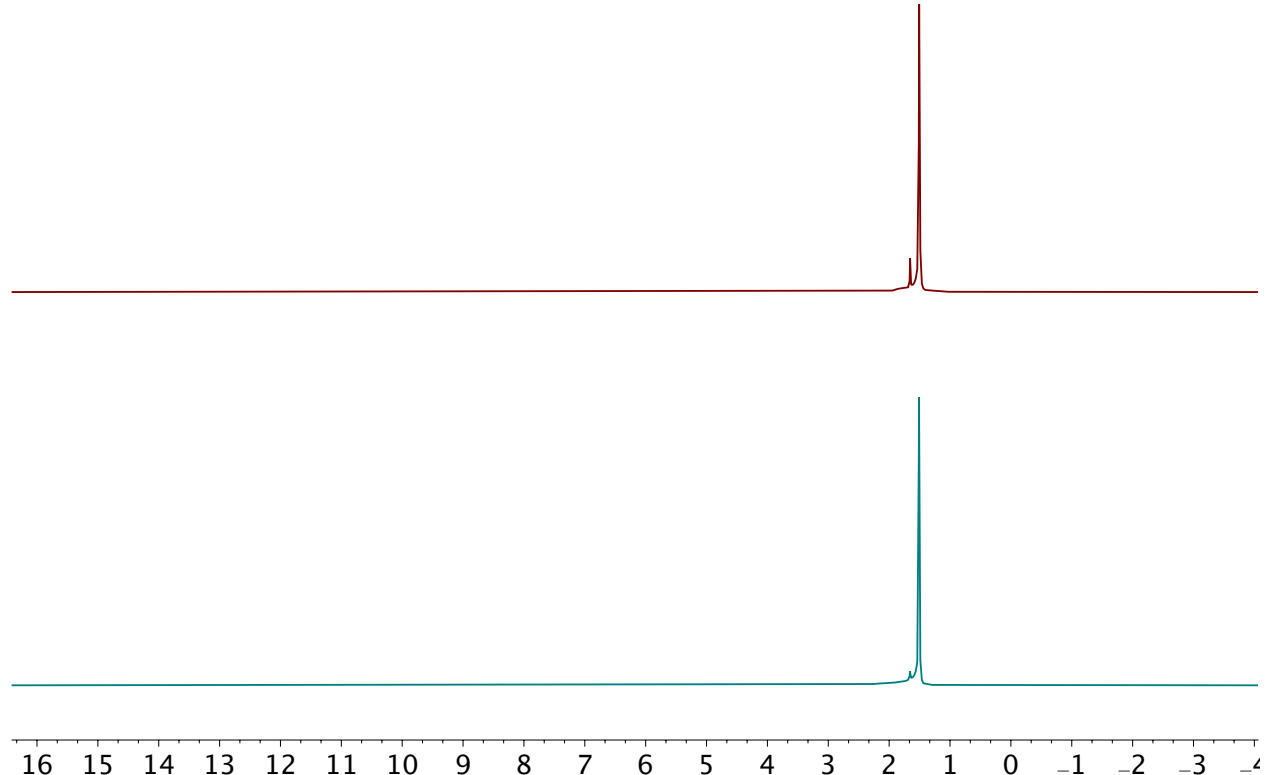


**Figure S6.1.**  $^1\text{H}$  NMR spectra of ethylene/tBA copolymer P1 (top, collected from table S5.3, entry 2) and P2 (bottom, collected from table S5.4, entry 7)

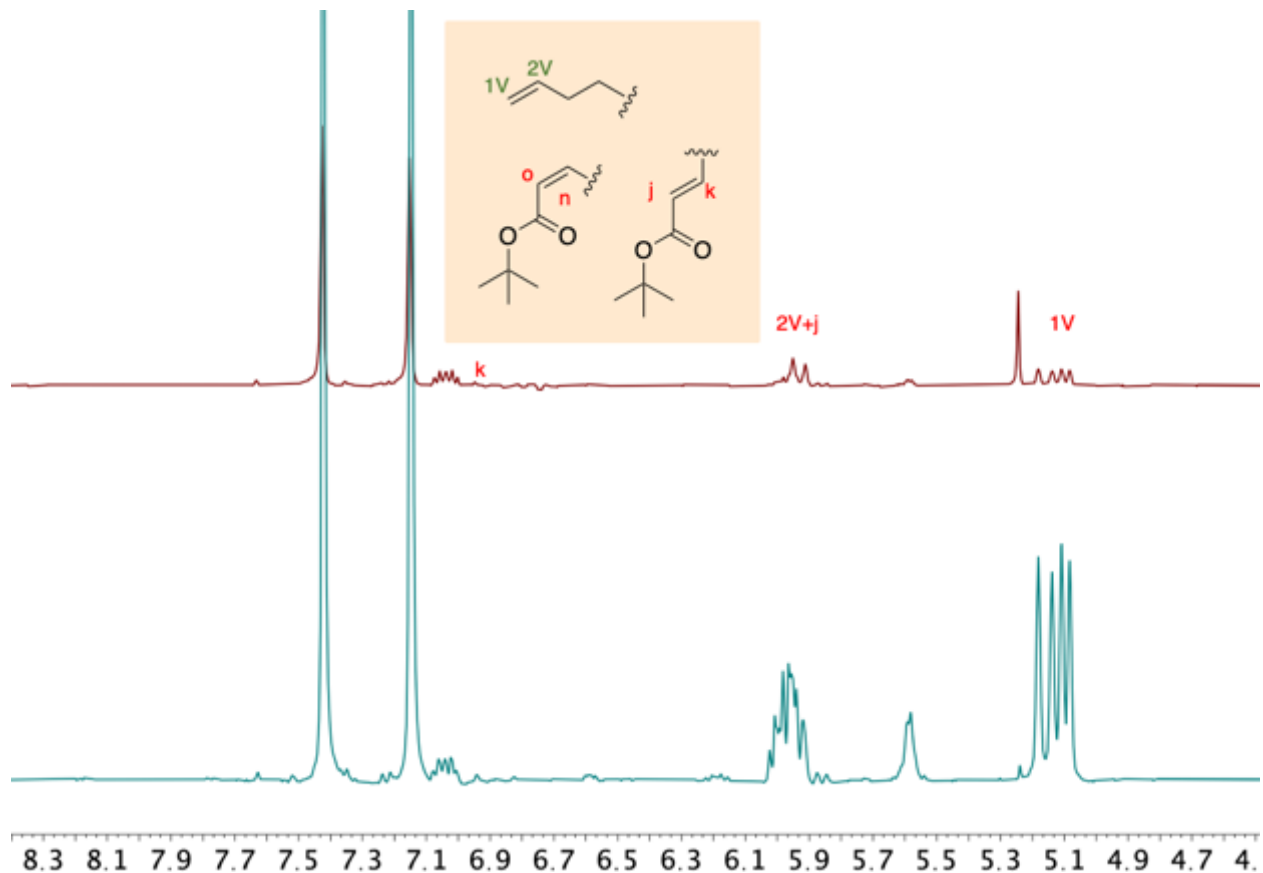


**Figure S6.2.** <sup>1</sup>H NMR spectra of ethylene/tBA copolymer P1 (top, collected from table S5.3, entry 2) and P2 (bottom, collected from table S5.4, entry 7): Part 2. Assignment is based on <sup>1</sup>H-<sup>1</sup>H COSY NMR spectrum (Figure S6.3) and ref 37.

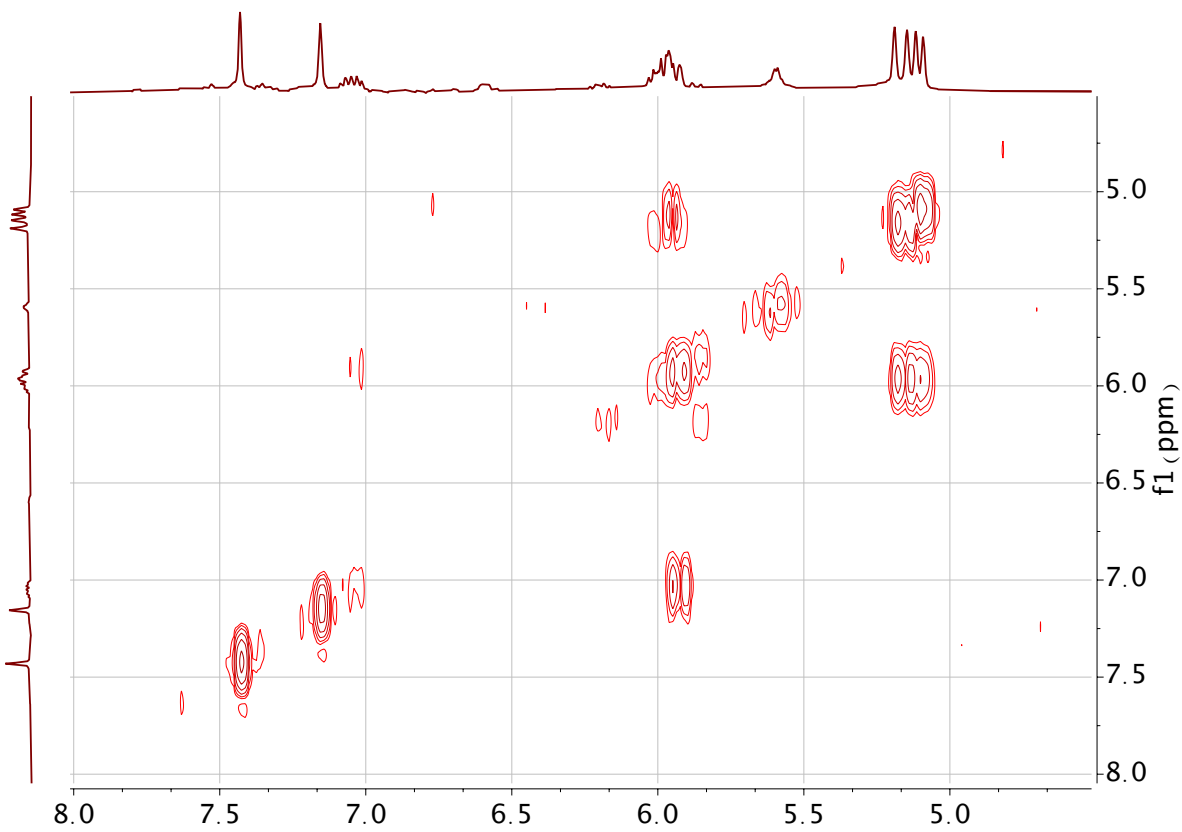


**Figure S6.3.**  $^1\text{H}$ - $^1\text{H}$  COSY NMR spectrum of ethylene/tBA copolymer P2 (collected from table S5.4, entry 7)

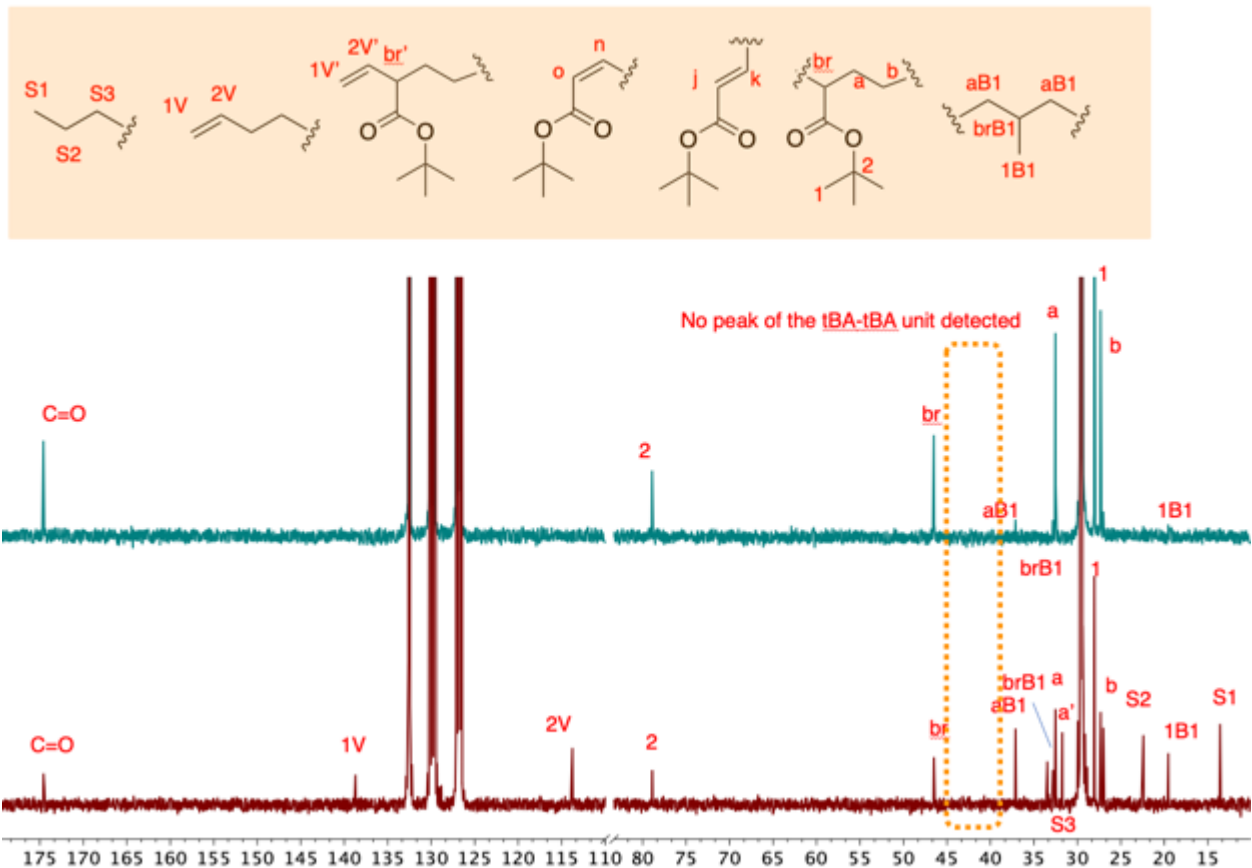


**Figure S6.4.**  $^{13}\text{C}\{\text{H}\}$  NMR spectra of ethylene/tBA copolymer P1 (top, collected from table S5.3, entry 2) and P2 (bottom, collected from table S5.4, entry 7). Assignment is based on ref 37.

## 7. GPC curves of ethylene/tBA copolymers

Conventional GPC & Composition Results					
LIMS #:	19-3295	Description:	Library 370217 Vial 1f		Date:
Project:		Report by:			5/7/19 13:03
For:	FileProc	Method:	Not Selected		
MWD Results: Conventional GPC		Quadrant Analysis		Run Parameters:	
Mn	43,280	25%	202260	Conc	1.8000
M <sub>p</sub>	77,200	50%	94690	Inj. Vol.	480.0
M <sub>v</sub>	88,500	75%	53950	Mass Inj.	0.0550
M <sub>w</sub>	97,160	100%	20980	MassRec.	98.93%
M <sub>z</sub>	178,790	Whole	67560	System Parameters:	
PDI	2.25	50% Ratio	3.96	Flow Rate	1.0008
			271.64	Flow Marker	18.296
Comonomer Type	Octene			Ref Flow Marker	18.192
Avg SCB/1000TC	24.37			Rec. Flow Rate	
Avg Wt% Comonomer	19.7				
Avg Corrected Wt%	19.49				

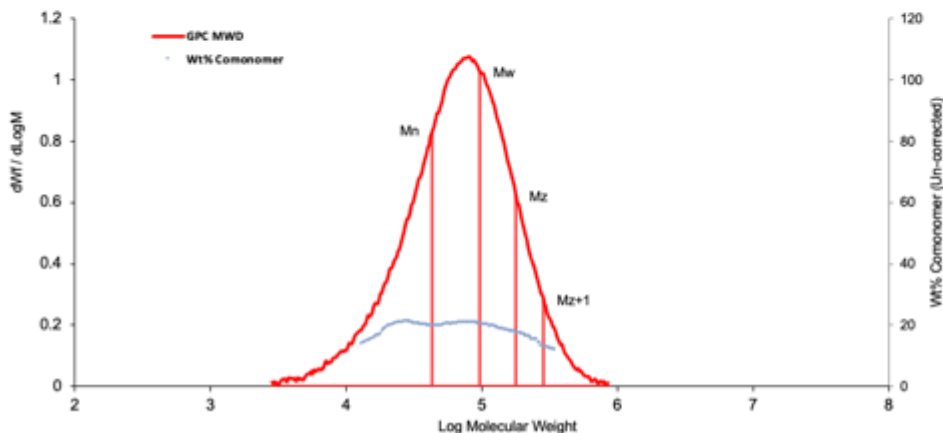


**Figure S7.1.** GPC curve of ethylene/tBA copolymer (table S5.2, entry 1).

<u><b>Conventional GPC &amp; Composition Results</b></u>					
LIMS #:	19-6521	Description:	Library 371847 Vial 43	Date:	8/27/19 5:06
Project:		Report by:			
For:	FileProc	Method:	Not Selected		
<b>MWD Results: Conventional GPC</b>		<b>Quadrant Analysis</b>		<b>Run Parameters:</b>	
Mn	26,270	25%	112300	Conc	1.8000
M <sub>p</sub>	48,930	50%	55950	Inj. Vol.	480.0
M <sub>v</sub>	51,300	75%	32590	Mass Inj.	0.8550
M <sub>w</sub>	55,810	100%	12700	MassRec.	76.95%
M <sub>z</sub>	96,690	Whole	40040	System Parameters:	
PDI	2.12	50% Ratio	3.71	Flow Rate	0.9989
			-60	Flow Marker	18.182
Comonomer Type	Octene		271.64	Ref Flow Marker	18.201
Avg SCB/1000TC	4.06			Rec. Flow Rate	
Avg Wt% Comonomer	3.57				
Avg Corrected Wt%	3.25				

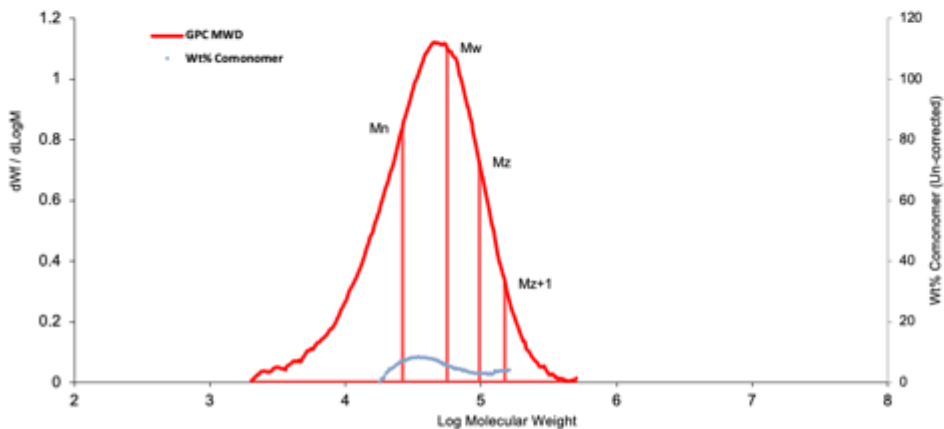


**Figure S7.2.** GPC curve of ethylene/tBA copolymer (table S5.3, entry 5).

<b><i>Conventional GPC &amp; Composition Results</i></b>					
LIMS #:	19-6834	Description:	Library 372462 Vial 10	Date:	9/3/19 12:57
Project:		Report by:			
For:	FileProc	Method:	Not Selected		
<b>MWD Results: Conventional GPC</b>					
Mn	3,670	Quadrant Analysis		Run Parameters:	
M <sub>p</sub>	7,530	25%	16640	Conc	1.8000
M <sub>v</sub>	7,480	50%	8190	Inj. Vol.	480.0
M <sub>w</sub>	8,170	75%	4650	Mass Inj.	0.8550
M <sub>z</sub>	14,600	100%	1780	MassRec.	114.47%
PDI	2.22	Whole	5760	System Parameters:	
		50% Ratio	3.86	Flow Rate	0.9980
			-60	Flow Marker	18.182
			271.64	Ref Flow Marker	18.219
Comonomer Type	Octene			Rec. Flow Rate	
Avg SCB/1000TC	9.47				
Avg Wt% Comonomer	9.36				
Avg Corrected Wt%	7.58				

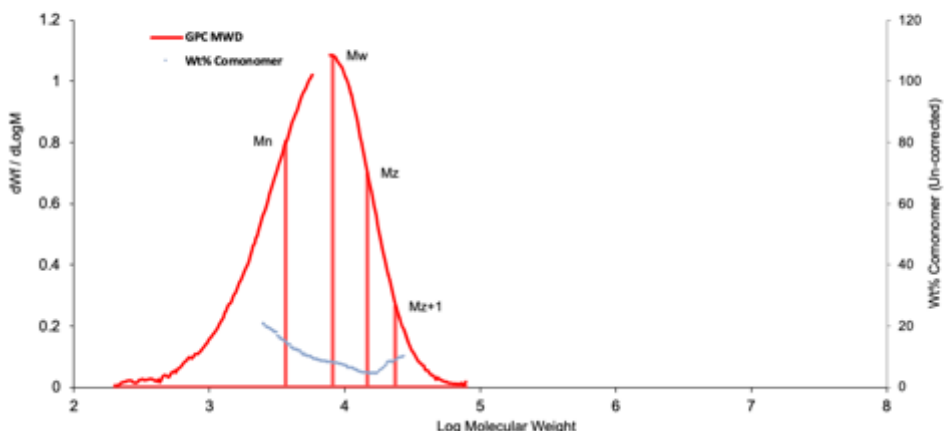


**Figure S7.3.** GPC curve of ethylene/tBA copolymer (table S5.4, entry 10).

## ***Part C:Experimental details for Kinetic Studies***

### ***8. Kinetic Measurements***

#### ***8.1 Procedures***

***Ethylene insertion(e1&e2).*** Unless specified, 0.0118 mmol of nickel complexes prepared using the above procedure was dissolved in C<sub>6</sub>D<sub>5</sub>Cl with pyridine in the glove box. The mixture was transferred to a J-Young tube and frozen in a liquid nitrogen bath. Then ethylene was added quantitatively via a gas bulb attached to the high vacuum line<sup>6</sup> pre-filled with ethylene. The resulting mixture was warmed up to thawing temperature and shaken vigorously prior to pre-heated NMR probe for acquisition of spectra at specified temperature. Solvent residues were used as an internal standard. The decay of the concentration of the nickel (trimethylsilyl)methyl pyridine complex as well as the decay of the concentration of ethylene was recorded based on the ratio of the integration of bound phosphine to that of the internal standard accordingly.

***tBA insertion (a1&a3).*** Unless specified, 0.0118 mmol of nickel complexes prepared using the above procedure was dissolved in protio-PhCl or 90% protio-PhCl/10% C<sub>6</sub>D<sub>5</sub>Cl with pyridine in the glove box. The mixture was frozen in the coldwell pre-cooled by a liquid nitrogen bath, and *t*-butyl acrylate (tBA, or PhCl solution of tBA) was added via syringe (Total volume=0.75 ml). The resulting mixture was warmed up to thawing temperature and shaken vigorously prior to transferring to pre-heated NMR probe for acquisition of spectra at 50 °C. NMR monitoring of tBA insertion were performed with a capillary insert with CDCl<sub>3</sub> solution of MePPh<sub>3</sub><sup>+</sup>Br<sup>-</sup> inside as an external standard and the decay of the concentration of the nickel (trimethylsilyl)methyl pyridine complex was recorded based on the ratio of the integration of bound phosphine to that of the external standard accordingly.

**tBA insertion into ethylene inserted species (a2).** Unless specified, 0.0118 mmol of nickel complexes prepared using the above procedure was dissolved in C<sub>6</sub>D<sub>5</sub>Cl with pyridine in the glove box (total volume = Y mL, see below for clarification). The mixture was transferred to a J-Young tube, degassed via three freeze-pump-thaw cycles and kept frozen in a liquid nitrogen bath. Then ethylene was added via a gas bulb attached to the high vacuum line<sup>6</sup> pre-filled with ethylene. The mixture was then warm up to room temperature and shaken vigorously. Decay of ethylene and decay of the nickel trimethylsilyl methyl complex were monitored via <sup>1</sup>H and <sup>31</sup>P NMR. Roughly at ~50% conversion of the nickel trimethylsilyl methyl complex, the mixture was frozen in a liquid nitrogen bath. Then residue ethylene was removed via four freeze-pump-thaw-backfill (with Ar or N<sub>2</sub>) cycles. Complete removal of ethylene (>99.95%) was confirmed by <sup>1</sup>H NMR. Then the mixture was transferred to pre-heated NMR probe for acquisition of one sample spectrum at 50 °C. Then the mixture was transferred into a glove box and frozen in the coldwell pre-cooled by a liquid nitrogen bath. Then *t*-butyl acrylate (tBA, or PhCl solution of tBA, X mL) was added via a syringe or micro-syringe (X+Y=0.75 mL) and the mixture was frozen again. The resulting mixture was warmed up to thawing temperature and shaken vigorously prior to transferring to pre-heated NMR probe. Spectra was collected immediately after reaching the desired temperature. NMR monitoring of tBA insertion were performed with P(O)Ph<sub>3</sub> (0.2~0.4 equiv. to the nickel complex) as an internal standard and the decay of the concentration of the nickel (trimethylsilyl)methyl pyridine complex was recorded based on the ratio of the integration of bound phosphine to that of the internal standard in <sup>31</sup>P NMR accordingly.

**Ethylene insertion into tBA inserted species (e3).** Unless specified, 0.0059 mmol of the nickel complex **3** prepared using the above procedure was dissolved in C<sub>7</sub>D<sub>8</sub> with pyridine in

the glove box (total volume = 0.75 mL). The mixture was transferred to a J-Young tube, degassed via three freeze-pump-thaw cycles and kept frozen in a liquid nitrogen bath. Then ethylene was added via a gas bulb attached to the high vacuum line<sup>6</sup> pre-filled with ethylene. The resulting mixture was warmed up to thawing temperature prior to pre-heated NMR probe for acquisition of spectra at the specified temperature. Solvent residues were used as an internal standard. The decay of the concentration of the nickel (trimethylsilyl)methyl pyridine complex as well as the decay of the concentration of ethylene was recorded based on the ratio of the integration of bound phosphine to that of the internal standard accordingly.

## 8.2 Kinetic Plots of tBA Insertion into Nickel (Trimethylsilyl)methyl Pyridine Complexes

(a1)

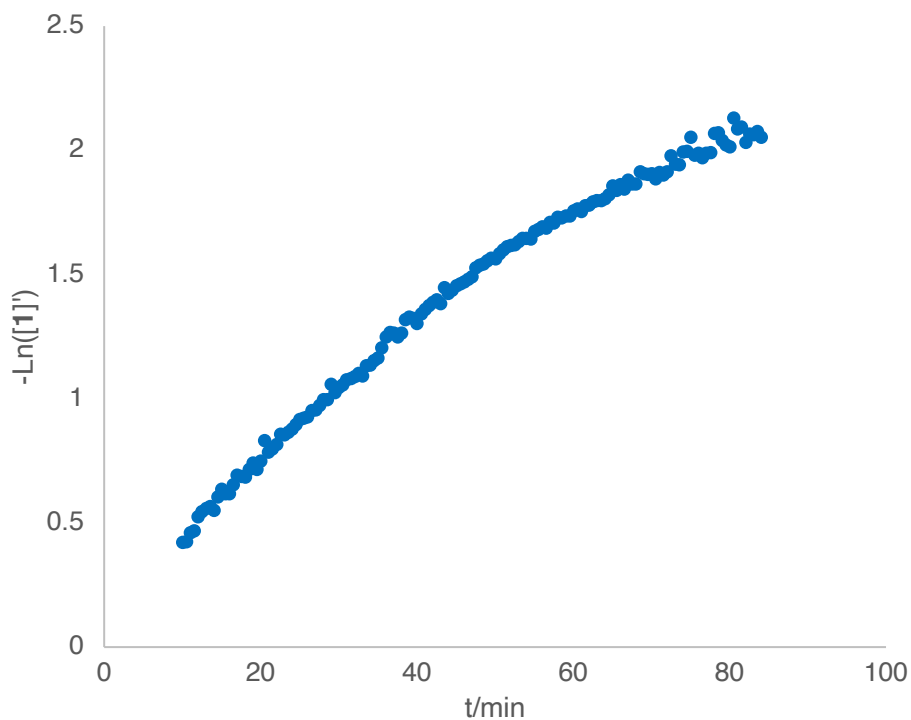


**Figure S8.1.** Log plot of relative concentration of **1** ( $[1']= [1]/[\text{St}]$ , St: internal standard) vs time as monitored by  $^1\text{H}$  NMR spectroscopy.

(Note for Figure S8.1) Procedure: In the glove box, **1** (0.0059 mmol, 5.8 mg) was dissolved in  $\text{C}_6\text{D}_6$  and the mixture was frozen in the coldwell pre-cooled by a liquid nitrogen bath, and *t*-butyl acrylate (100 equiv., 0.086 ml) was added via syringe (Total volume=0.75 ml). The resulting mixture was warmed up to thawing temperature prior to pre-heated NMR probe for acquisition of spectra at 30°C. No capillary was used the decay of the concentration of the nickel (trimethylsilyl)methyl pyridine complex was recorded based on the ratio of the integration of bound pyridine to that of the solvent residue.

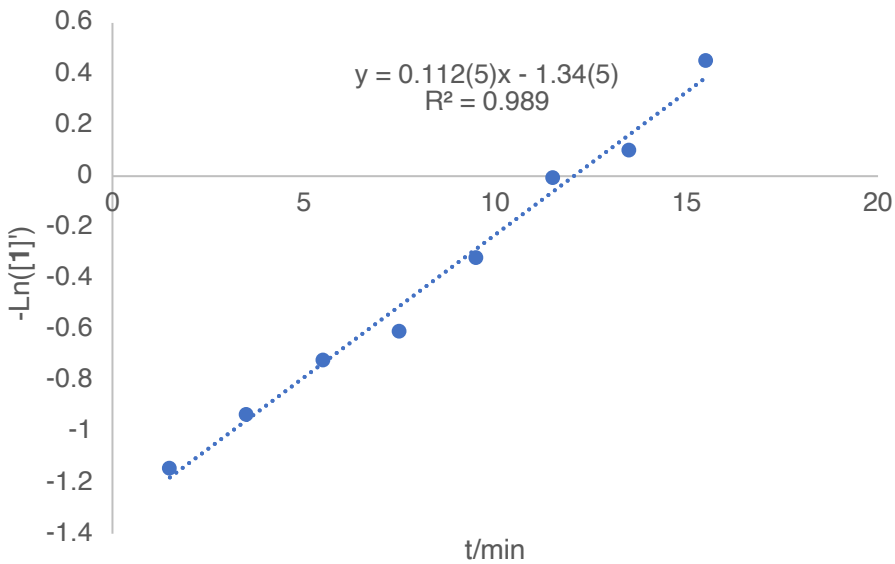


**Figure S8.2.** Log plot of relative concentration of **1** ( $[1'] = [1]/[\text{St}]$ , St: external standard) vs time as monitored by  $^{31}\text{P}$  NMR spectroscopy. Solvent: PhCl-H<sub>5</sub>. Temperature: 50 °C. Initial concentration:  $[1]_0 = 0.0157 \text{ M}$ ;  $[\text{tBA}]_0 = 1.178 \text{ M}$  (75 equiv.);  $[\text{py}]_0 = 0.0315 \text{ M}$  (2 equiv.).

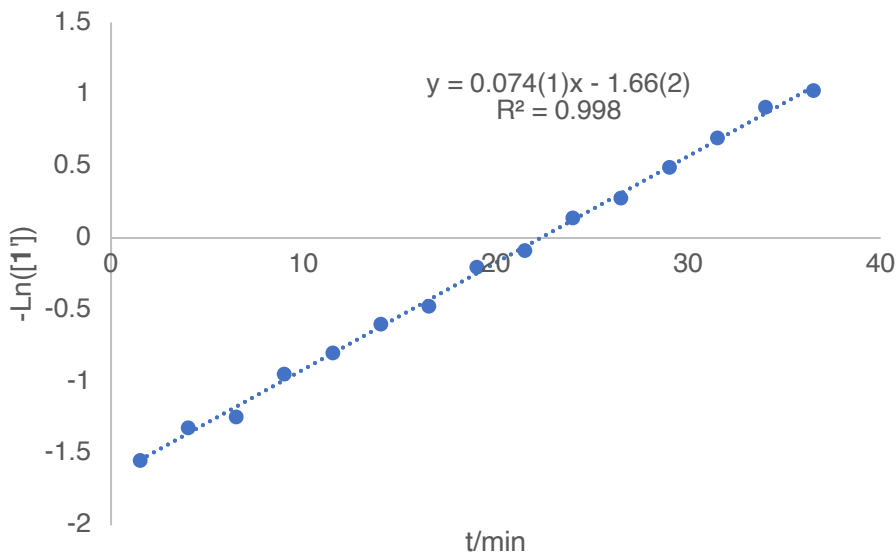


**Figure S8.3.** Log plot of relative concentration of **1** ( $[1'] = [1]/[\text{St}]$ , St: external standard) vs time as monitored by  $^{31}\text{P}$  NMR spectroscopy. Solvent: PhCl-H<sub>5</sub>. Temperature: 50 °C. Initial concentration:  $[1]_0 = 0.0157 \text{ M}$ ;  $[\text{tBA}]_0 = 0.785 \text{ M}$  (50 equiv.);  $[\text{py}]_0 = 0.0315 \text{ M}$  (2 equiv.).

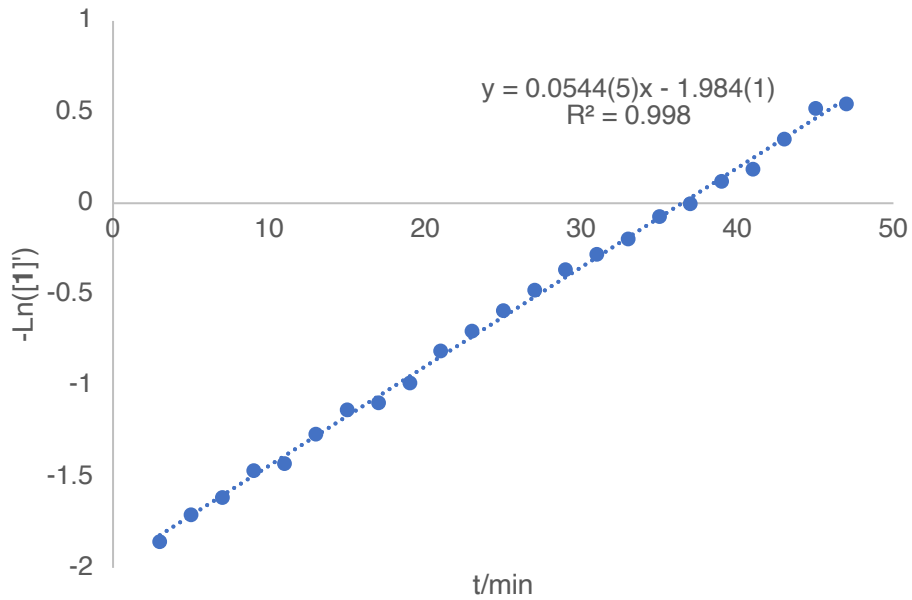


**Figure S8.4.** Log plot of relative concentration of **1** ( $[1']=[1]/[\text{St}]$ , St: external standard) vs time as monitored by  $^{31}\text{P}$  NMR spectroscopy. Solvent: PhCl-H5. Temperature: 50 °C. Initial concentration:  $[1]_0=0.0157 \text{ M}$ ;  $[\text{tBA}]_0=0.550 \text{ M}$  (35 equiv.);  $[\text{py}]_0=0.0315 \text{ M}$  (2 equiv.).

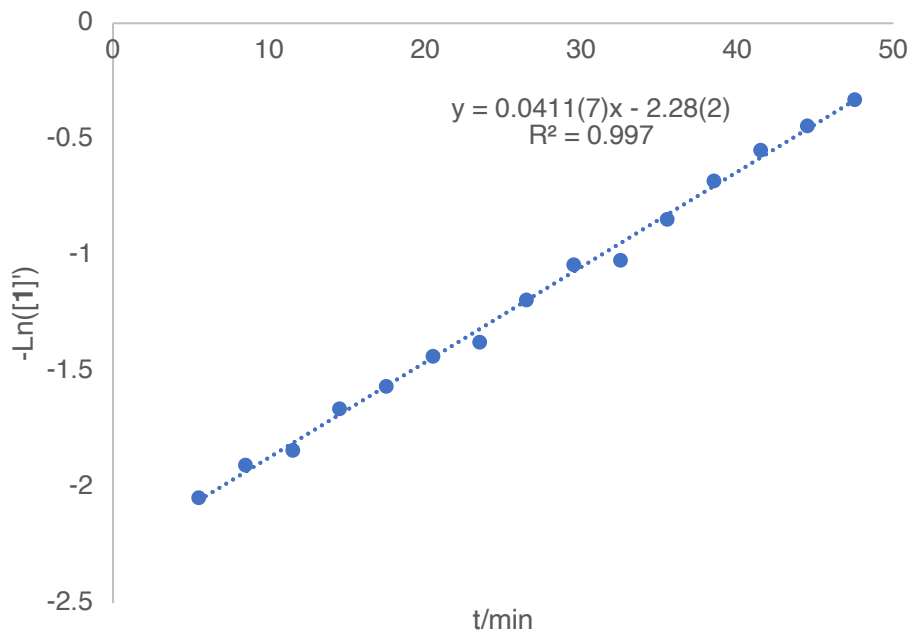


**Figure S8.5.** Log plot of relative concentration of **1** ( $[1']=[1]/[\text{St}]$ , St: external standard) vs time as monitored by  $^{31}\text{P}$  NMR spectroscopy. Solvent: PhCl-H5. Temperature: 50 °C. Initial concentration:  $[1]_0=0.0157 \text{ M}$ ;  $[\text{tBA}]_0=0.393 \text{ M}$  (25 equiv.);  $[\text{py}]_0=0.0315 \text{ M}$  (2 equiv.).

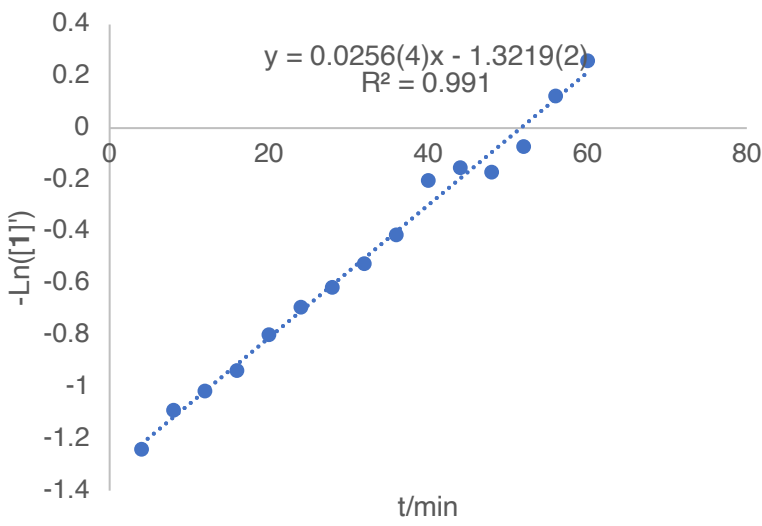


**Figure S8.6.** Log plot of relative concentration of **1** ( $[1']=[1]/[\text{St}]$ , St: external standard) vs time as monitored by  $^{31}\text{P}$  NMR spectroscopy. Solvent: PhCl-H5. Temperature: 50 °C. Initial concentration:  $[1]_0=0.0157 \text{ M}$ ;  $[\text{tBA}]_0=0.393 \text{ M}$  (25 equiv.);  $[\text{py}]_0=0.0471 \text{ M}$  (3 equiv.).

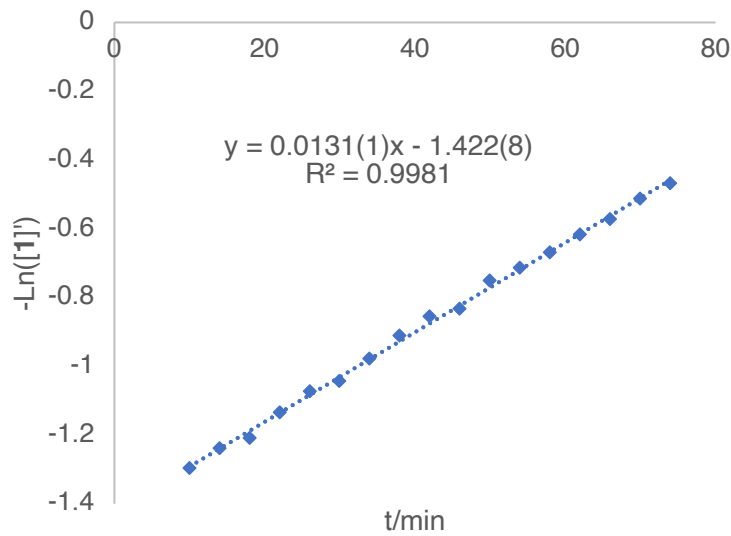


**Figure S8.7.** Log plot of relative concentration of **1** ( $[1']=[1]/[\text{St}]$ , St: external standard) vs time as monitored by  $^{31}\text{P}$  NMR spectroscopy. Solvent: PhCl-H5. Temperature: 50 °C. Initial concentration:  $[1]_0=0.0157 \text{ M}$ ;  $[\text{tBA}]_0=0.393 \text{ M}$  (25 equiv.);  $[\text{py}]_0=0.0942 \text{ M}$  (6 equiv.).

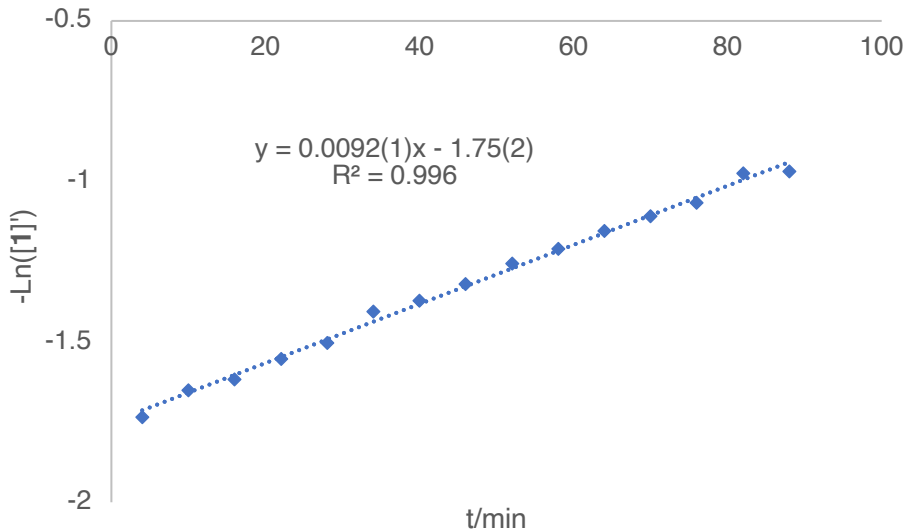


**Figure S8.8.** Log plot of relative concentration of **1** ( $[1']=[1]/[\text{St}]$ , St: external standard) vs time as monitored by  $^{31}\text{P}$  NMR spectroscopy. Solvent: PhCl-H5. Temperature: 50 °C. Initial concentration:  $[1]_0=0.0157 \text{ M}$ ;  $[\text{tBA}]_0=0.393 \text{ M}$  (25 equiv.);  $[\text{py}]_0=0.142 \text{ M}$  (9 equiv.).

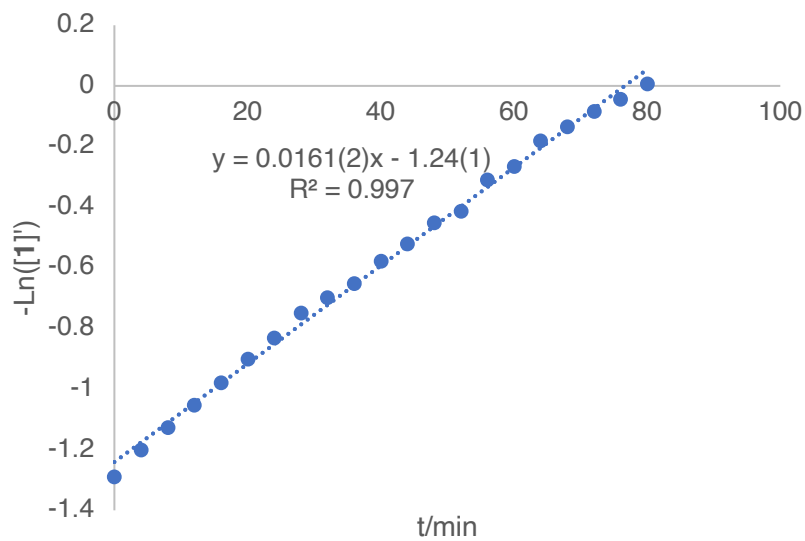


**Figure S8.9.** Log plot of relative concentration of **1** ( $[1']=[1]/[\text{St}]$ , St: external standard) vs time as monitored by  $^{31}\text{P}$  NMR spectroscopy. Solvent: PhCl-H5. Temperature: 50 °C. Initial concentration:  $[1]_0=0.0157 \text{ M}$ ;  $[\text{tBA}]_0=0.157 \text{ M}$  (10 equiv.);  $[\text{py}]_0=0.0315 \text{ M}$  (2 equiv.).

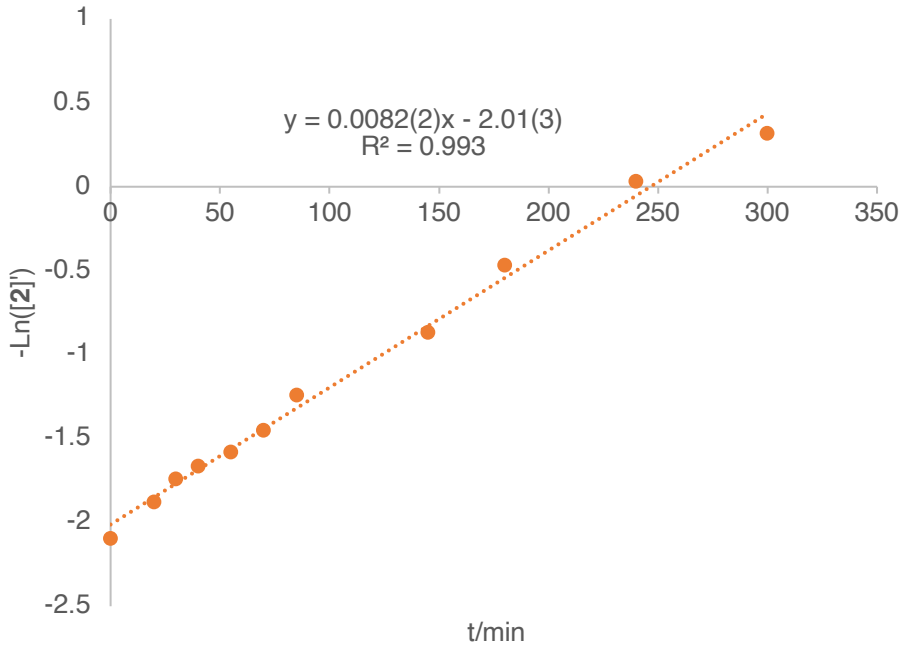


**Figure S8.10.** Log plot of relative concentration of **2** ( $[2'] = [2]/[\text{St}]$ , St: external standard) vs time as monitored by  $^{31}\text{P}$  NMR spectroscopy. Solvent: PhCl-H<sub>5</sub>. Temperature: 50 °C. Initial concentration:  $[2]_0 = 0.0157 \text{ M}$ ;  $[\text{tBA}]_0 = 1.57 \text{ M}$  (100 equiv.);  $[\text{py}]_0 = 0.157 \text{ M}$  (10 equiv.).

### 8.3 Kinetic Plots of Ethylene Insertion into Nickel Alkyl Pyridine Complexes ( $e1/e2$ )

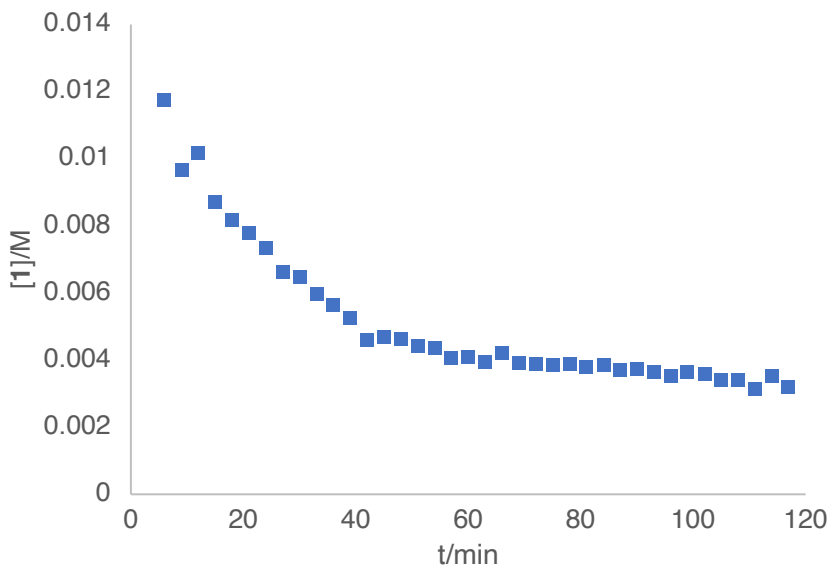


**Figure S8.11.** Plot of concentration of **1** vs time as monitored by  $^{31}\text{P}$  NMR spectroscopy.

Solvent: PhCl-D5. Temperature: 50 °C. Initial concentration:  $[\mathbf{1}]_0=0.0157 \text{ M}$ ;  
 $[\text{Ethylene}]_0=0.236 \text{ M}$  (15 equiv.);  $[\text{py}]_0=0.0315 \text{ M}$  (2 equiv.).

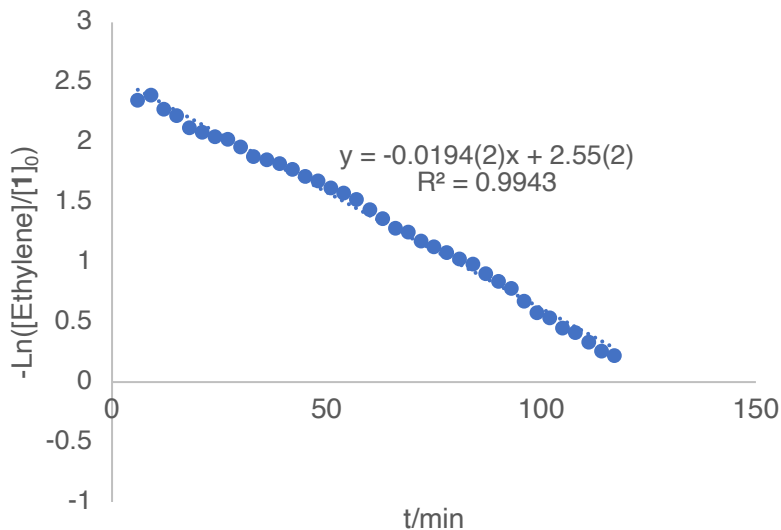


**Figure S8.12.** Log plot of relative concentration of ethylene ( $[\text{Ethylene}']=[\text{Ethylene}]/[\mathbf{1}]_0$ ) vs time as monitored by  $^1\text{H}$  NMR spectroscopy. Solvent: PhCl-D5. Temperature: 50 °C. Initial concentration:  $[\mathbf{1}]_0=0.0157 \text{ M}$ ;  $[\text{Ethylene}]_0=0.236 \text{ M}$  (15 equiv.);  $[\text{py}]_0=0.0315 \text{ M}$  (2 equiv.).

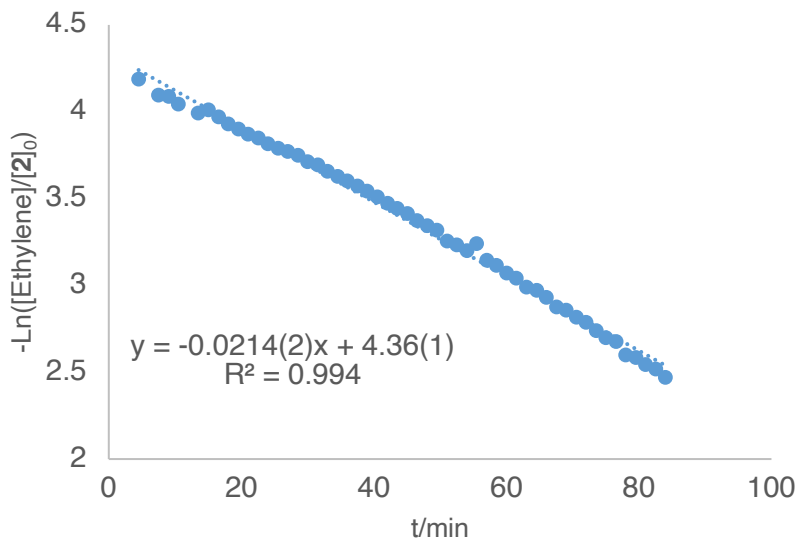


**Figure S8.13.** Log plot of relative concentration of ethylene ( $[{\text{Ethylene}}'] = [{\text{Ethylene}}]/[{\text{2}}]_0$ ) vs time as monitored by  $^1\text{H}$  NMR spectroscopy. Solvent: PhCl-D5. Temperature: 50 °C. Initial concentration:  $[{\text{1}}]_0 = 0.0157 \text{ M}$ ;  $[{\text{Ethylene}}]_0 = 0.236 \text{ M}$  (15 equiv.);  $[{\text{py}}]_0 = 0.0315 \text{ M}$  (2 equiv.).

#### 8.4 tBA Insertion into Ethylene Inserted Species (a2)

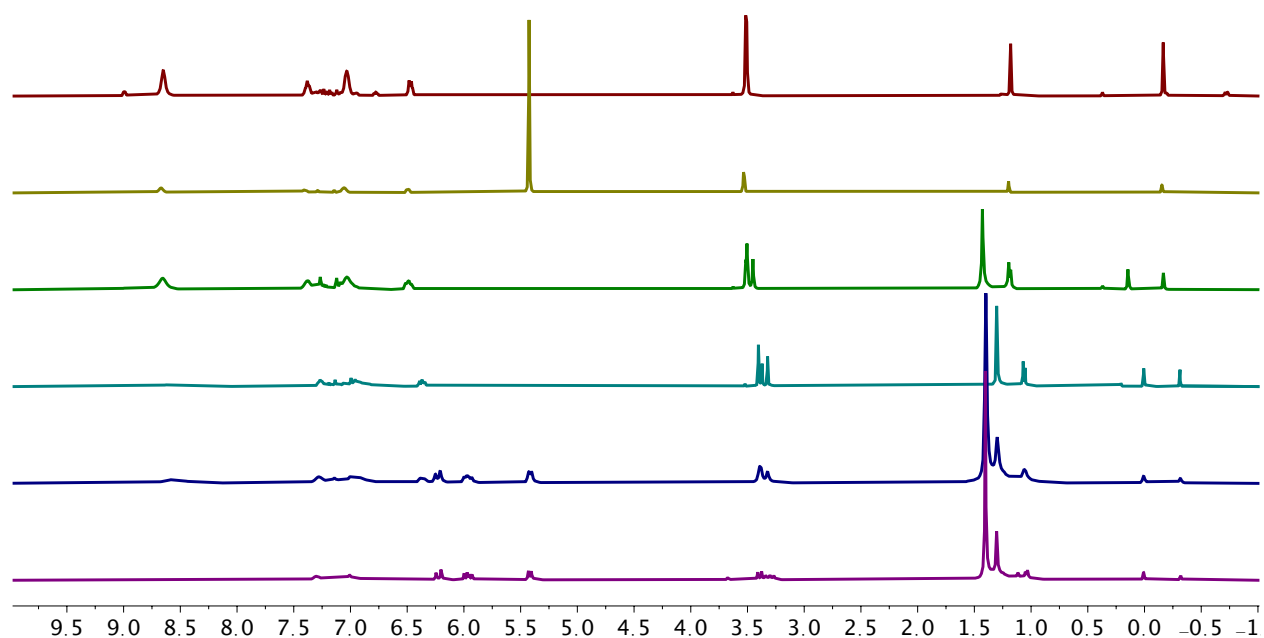


**Figure S8.14.** <sup>1</sup>H NMR spectra of (from top to bottom, C<sub>6</sub>D<sub>5</sub>Cl): a) **1** +10 equiv. of pyridine; b) after addition of 25 equiv. of ethylene; c) after removal of ethylene; d) spectrum recollected at 50 °C; e) after addition of 15 equiv. of tBA; f) after quantitative conversion of ethylene inserted species. Solvent: PhCl-D5. Initial concentration: [1]<sub>0</sub>=0.0157 M; [py]<sub>0</sub>=0.157 M (10 equiv.).

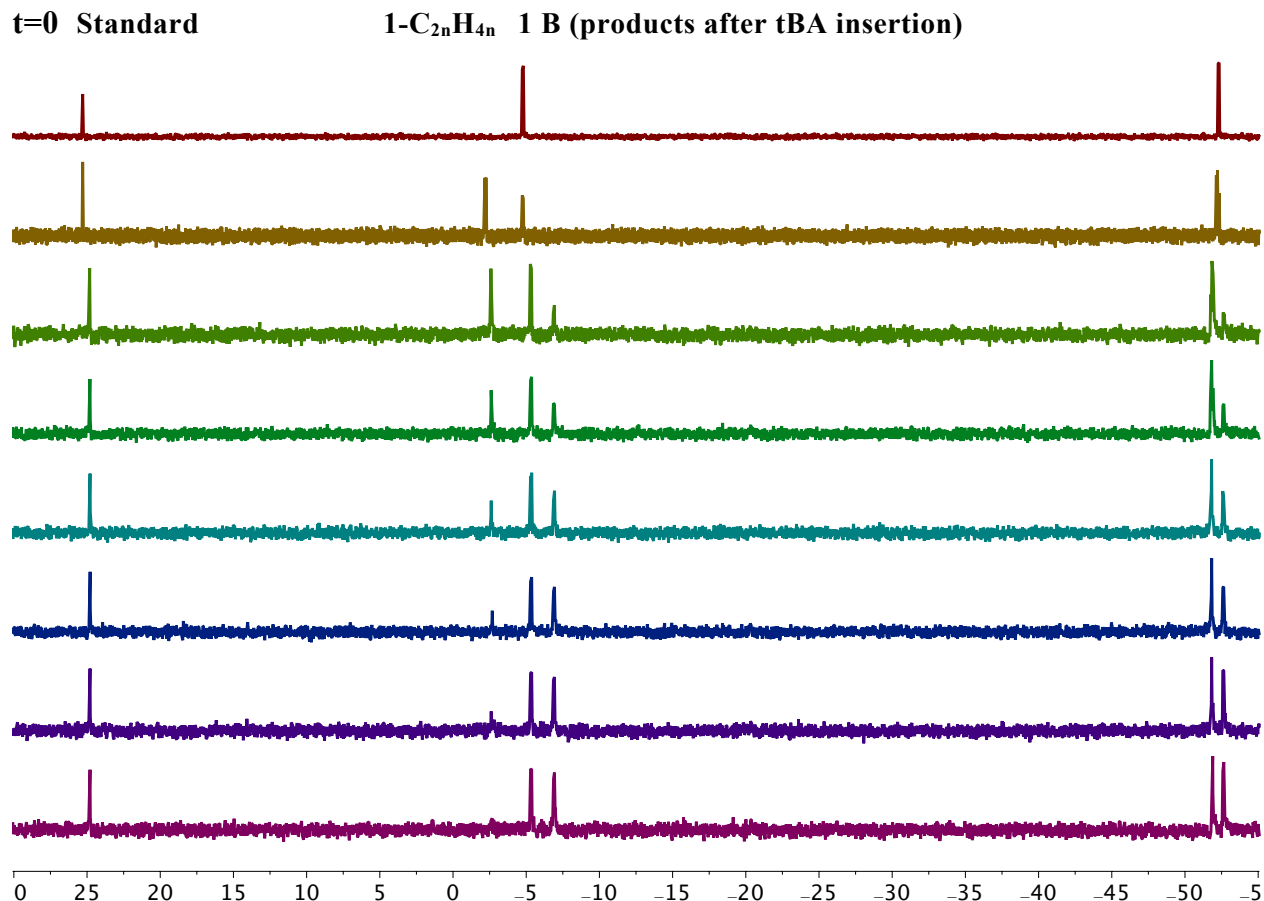


**Figure S8.15.**  $^{31}\text{P}$  NMR monitoring of decay of ethylene inserted species (from top to bottom, C<sub>6</sub>D<sub>5</sub>Cl): a) A +10 equiv. of pyridine; b) before addition of tBA; c) after addition of 25 equiv. of ethylene; d) (last five) spectra collected every 20 s. Solvent: PhCl-D<sub>5</sub>. Temperature: 50 °C. Initial concentration: [1]<sub>0</sub>=0.0157 M; [tBA]<sub>0</sub>=0.236 M (15 equiv.); [py]<sub>0</sub>=0.157 M (10 equiv.).

## Kinetic Plot

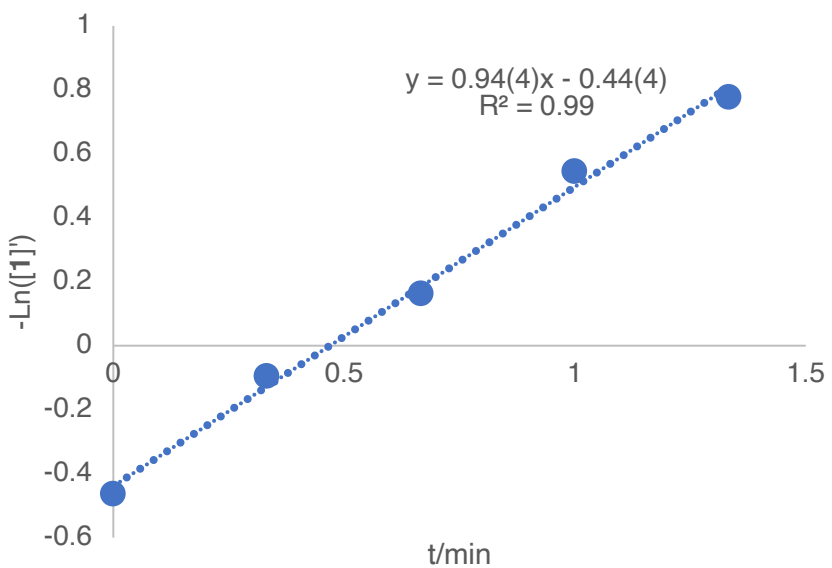


**Figure S8.16.** Log plot of relative concentration of 1 ( $[1']=[1]/[St]$ , St: internal standard) vs time as monitored by  $^{31}\text{P}$  NMR spectroscopy. Solvent: PhCl-D5. Temperature: 50 °C. Initial concentration:  $[1]_0=0.0157\text{ M}$ ;  $[\text{tBA}]_0=0.236\text{ M}$  (15 equiv.);  $[\text{py}]_0=0.157\text{ M}$  (10 equiv.).

## 8.5 Ethylene Insertion into tBA Inserted Species (e3)

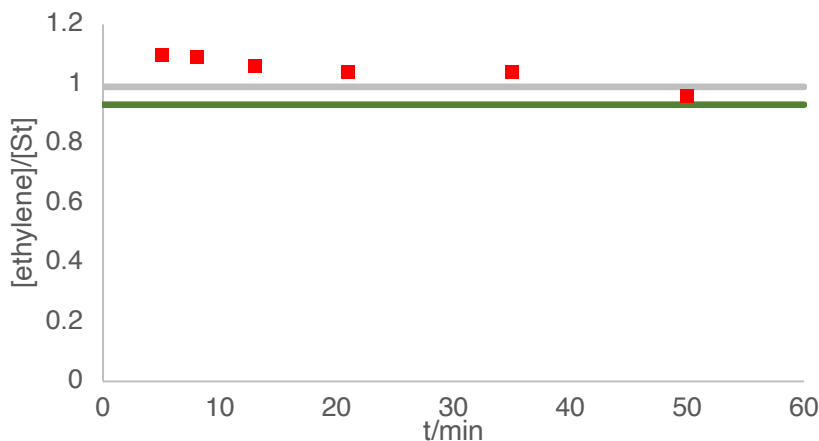


**Figure S8.17.** Plot of relative concentration of Ethylene ( $[\text{Ethylene}]/[\text{St}]$ , St: external standard) vs time as monitored by  $^1\text{H}$  NMR spectroscopy. Solvent: Tol-d8. Temperature: 50 °C. Initial concentration:  $[\mathbf{1}]_0=0.0079 \text{ M}$ ;  $[\text{Ethylene}]_0=0.099 \text{ M}$  (12.5 equiv.);  $[\text{py}]_0=0.079 \text{ M}$  (10 equiv.). (red spots: measured value, grey line: 90% of initial concentration, green line: 85% of initial concentration)

As shown above, only 15% decrease of the concentration of ethylene in solution was observed. Therefore, ethylene concentration could be treated as a constant in first 50 minutes, which fits pseudo 1<sup>st</sup> order condition. A preliminary kinetic plot based on data collected in first 50 minutes was shown below (only the first half-life period involved).

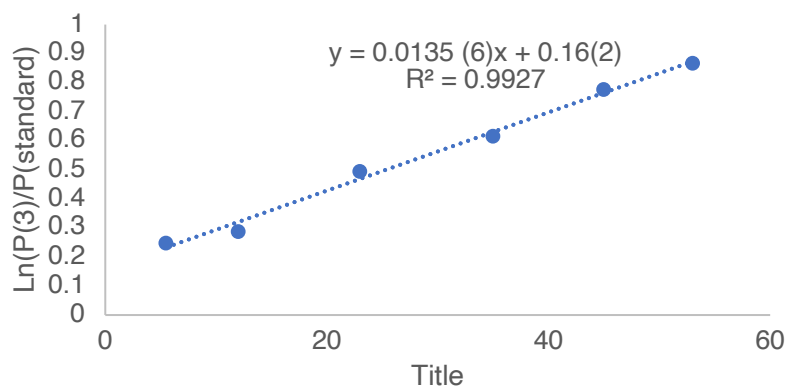
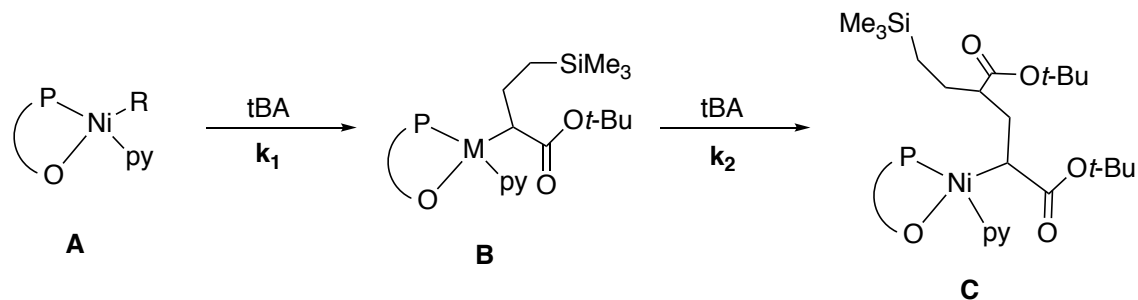


**Figure S8.18.** Log plot of relative concentration of 1 ( $[\mathbf{1}']=[\mathbf{1}]/[\text{St}]$ , St: internal standard) vs time as monitored by  $^1\text{H}$  NMR spectroscopy. Solvent: Tol-d8. Temperature: 50 °C. Initial concentration:  $[\mathbf{1}]_0=0.0079 \text{ M}$ ;  $[\text{Ethylene}]_0=0.099 \text{ M}$  (12.5 equiv.),  $[\text{py}]_0=0.079 \text{ M}$  (10 equiv.).

## 8.8 tBA Insertion into tBA Inserted Species

### Discussion of Methods

Unless specified, data shown below come from experiments in part 2. As shown in Fig S4.1, phosphines in nickel (trimethylsilyl)methyl pyridine complex (**A**) and acylated nickel alkyl complex (**B**, product of first tBA insertion) feature distinguished chemical shifts in  $^{31}\text{P}$  NMR and they are also different from that of further inserted species. Based on changes of  $[\text{A}]$  and  $[\text{B}]$  over time, overall insertion rate of the second acrylate insertion can be obtained, which is shown below.



$$\frac{d[A]}{dt} = -k_1 \cdot [A] \quad (\text{i})$$

$$[A] = [A]_0 \cdot e^{-k_1 t} \quad (\text{ii})$$

$$\frac{d[B]}{dt} = k_1 \cdot [A] - k_2 \cdot [B] \quad (\text{iii})$$

Based on (ii) and (iii),

$$k_2 \cdot [B] + \frac{d[B]}{dt} = k_1 \cdot [A]_0 \cdot e^{-k_1 t} \quad (\text{iv}) \rightarrow$$

$$k_2 \cdot e^{k_2 t} \cdot [B] + e^{k_2 t} \cdot \frac{d[B]}{dt} = k_1 \cdot [A]_0 \cdot e^{k_2 t} \cdot e^{-k_1 t} \quad (\text{v}) \rightarrow$$

$$\frac{d}{dt}(e^{k_2 t} \cdot [B]) = k_1 \cdot [A]_0 \cdot e^{(k_2 - k_1)t} \quad (\text{vi}) \rightarrow$$

$$e^{k_2 t} \cdot [B] = \frac{k_1}{k_2 - k_1} \cdot [A]_0 \cdot e^{(k_2 - k_1)t} + C \quad (\text{vii}) \rightarrow$$

$$[B] = \frac{k_1}{k_2 - k_1} \cdot [A]_0 \cdot e^{-k_1 t} + C \cdot e^{k_2 t} \quad (\text{viii})$$

$$t=0, [B]=0, \therefore C = -\frac{k_1}{k_2 - k_1} \cdot [A]_0 \quad (\text{ix})$$

Based on (viii) and (ix),

$$[B] = \frac{k_1}{k_2 - k_1} \cdot [A]_0 \cdot (e^{-k_1 t} - e^{k_2 t}) \quad (\text{xi})$$

$$(\text{viii})/(\text{iii}) \rightarrow \frac{[B]}{[A]} = \frac{k_1}{k_2 - k_1} \cdot (1 - e^{-(k_2 - k_1)t}) \quad (\text{xii})$$

If  $p = k_2 - k_1$ ,  $\frac{[B]}{[A]} = \frac{k_1}{p} \cdot (1 - e^{-pt}) \quad (\text{xiii})$

$[B]/[A]$  can be obtained from spectra, thereby  $p$  is solved via minimizing the difference of calculated curve (y axis:  $[B]/[A]$ , x axis: time) and curve generated from exp in excel (“solver” add-on)

## Sample Spectra

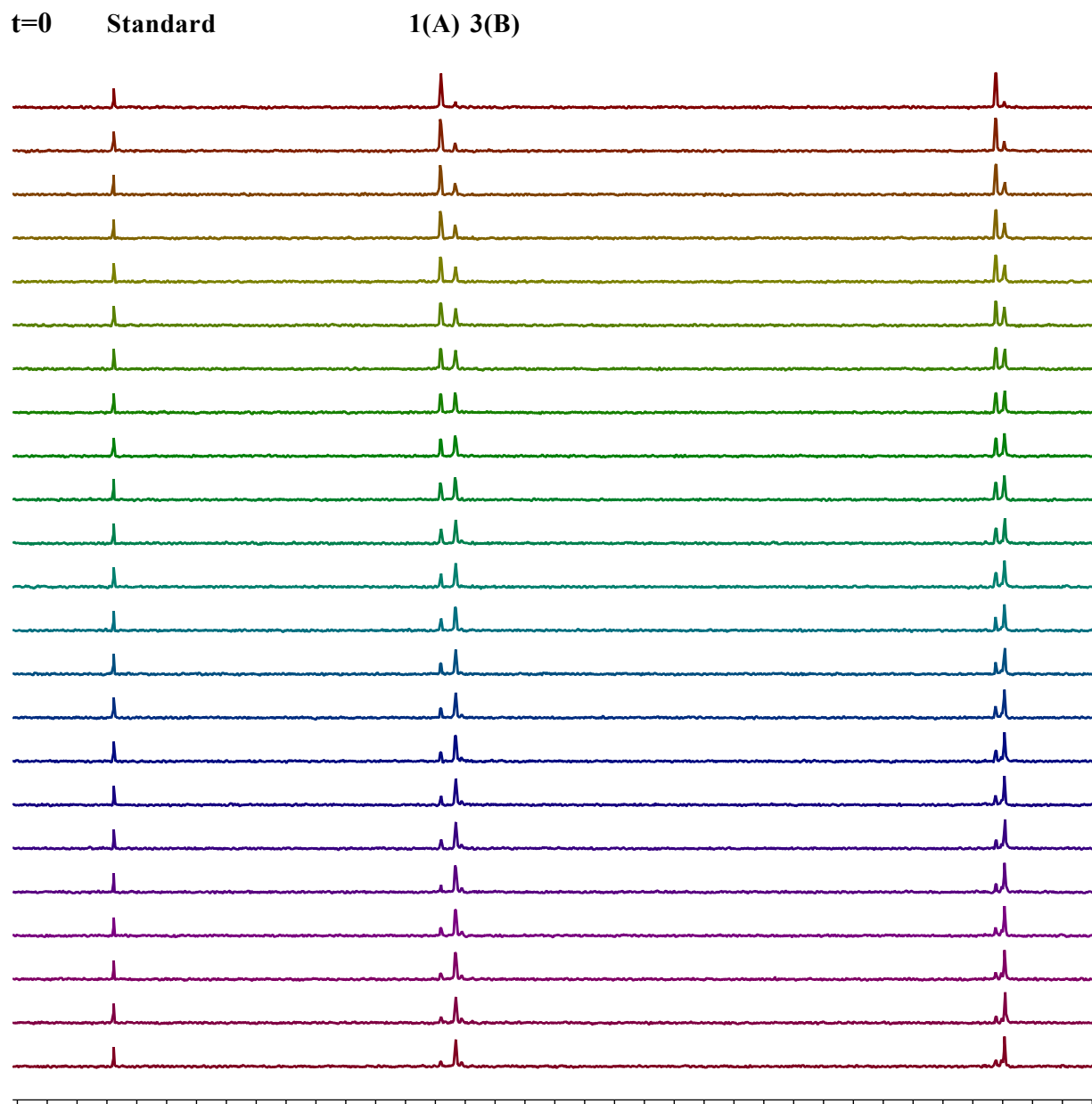


**Figure S8.19,**  $^{31}\text{P}$  Plot of NMR monitoring of tBA insertion into **1**. Solvent: PhCl-H<sub>5</sub>.

Temperature: 50 °C. Initial concentration:  $[1]_0=0.0157 \text{ M}$ ;  $[\text{tBA}]_0=0.550 \text{ M}$  (35 equiv.);  $[\text{py}]_0=0.0315 \text{ M}$  (2 equiv.).

## Kinetic Plots

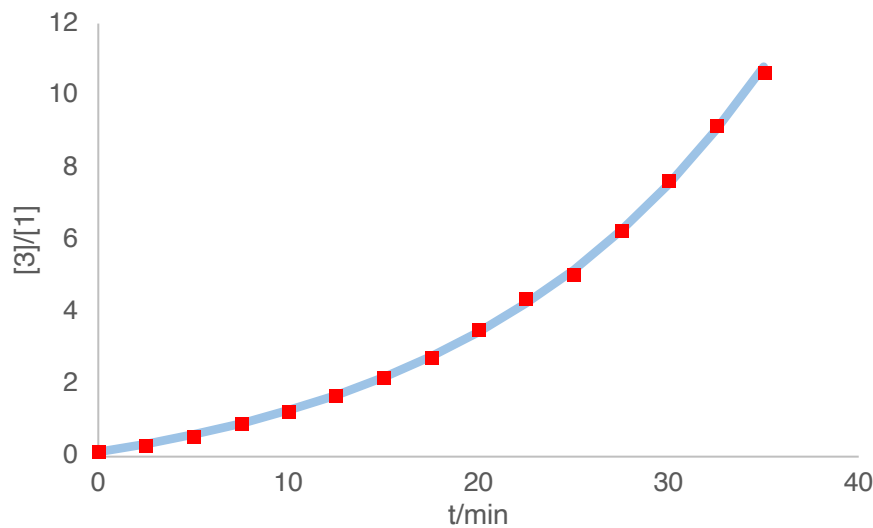


**Figure S8.20.** Plot of  $[3]/[1]$  v.s. time during tBA insertion. Solvent: PhCl-H5.

Temperature: 50 °C. Initial concentration:  $[1]_0=0.0157 \text{ M}$ ;  $[t\text{BA}]_0=0.785 \text{ M}$  (50 equiv.);  
 $[\text{py}]_0=0.0315 \text{ M}$  (2 equiv.). Red spots: experimental data; blue line: fitted curve.

- $p=-0.0635$ , SSR (sum of squared residues) =0.0979,  $k_2=0.0107$

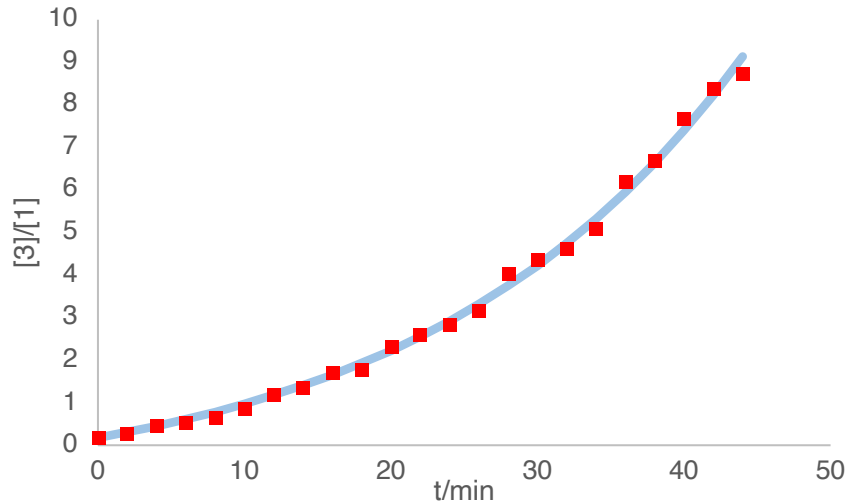


**Figure S8.21.** Plot of  $[3]/[1]$  v.s. time during tBA insertion Solvent: PhCl-H5. Temperature: 50 °C. Initial concentration:  $[1]_0=0.0157 \text{ M}$ ;  $[t\text{BA}]_0=0.550 \text{ M}$  (35 equiv.);  $[\text{py}]_0=0.0315 \text{ M}$  (2 equiv.). Red spots: experimental data, blue line: fitted curve.

- $p=-0.0461$ , SSR=0.588,  $k_2=0.0083$

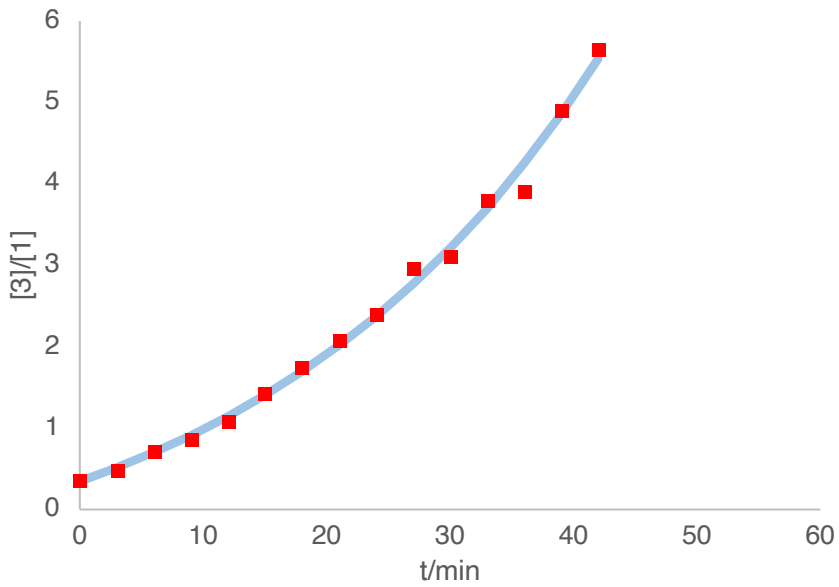


**Figure S8.22.** Plot of  $[3]/[1]$  v.s. time during tBA insertion Solvent: PhCl-H5. Temperature: 50 °C. Initial concentration:  $[1]_0=0.0157$  M;  $[tBA]_0=0.393$  M (25 equiv.);  $[py]_0=0.0315$  M (2 equiv.). Red spots: experimental data, blue line: fitted curve.

- $p=-0.0356$ ,  $SSR=0.206$ ,  $k_2=0.0055$

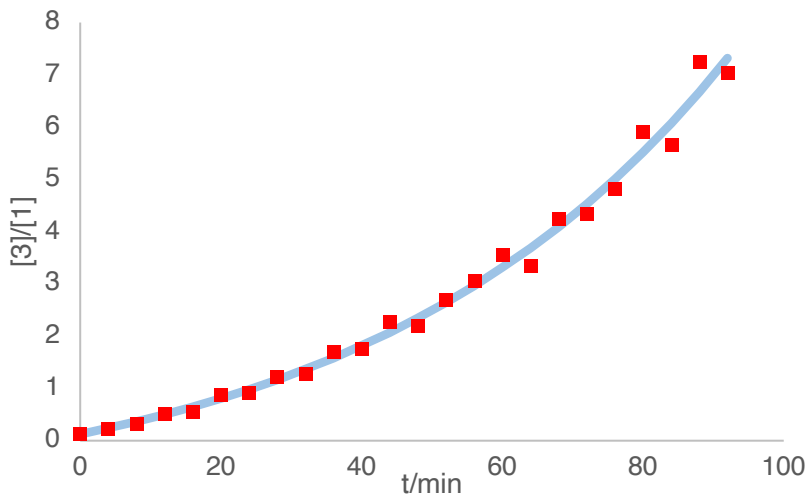


**Figure S8.23.** Plot of  $[3]/[1]$  v.s. time during tBA insertion. Solvent: PhCl-H5. Temperature: 50 °C. Initial concentration:  $[1]_0=0.0157$  M;  $[tBA]_0=0.393$  M (25 equiv.);  $[py]_0=0.0471$  M (3 equiv.). Red spots: experimental data, blue line: fitted curve.

- $p=-0.0195$ ,  $SSR=1.133$ ,  $k_2=0.0061$

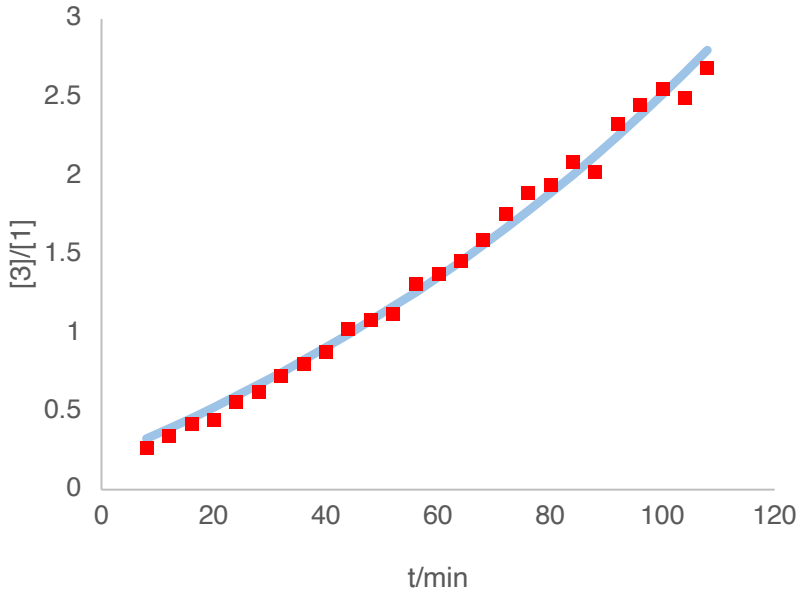


**Figure S8.24.** Plot of  $[3]/[1]$  v.s. time during tBA insertion. Solvent: PhCl-H5.

Temperature: 50 °C. Initial concentration:  $[1]_0=0.0157$  M;  $[tBA]_0=0.393$  M (25 equiv.);  $[py]_0=0.0942$  M (6 equiv.). Red spots: experimental data, blue line: fitted curve.

- $p=-0.0083$ ,  $SSR=0.118$ ,  $k_2=0.0048$

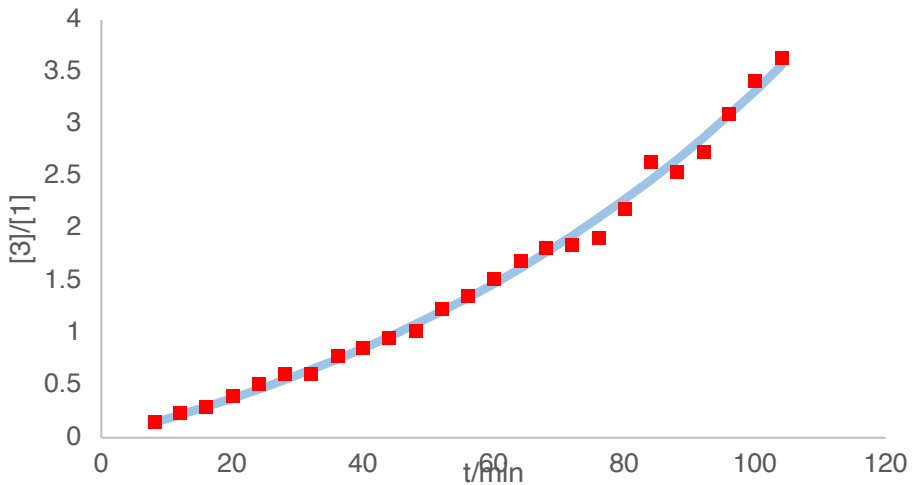


**Figure S8.25.** Plot of  $[3]/[1]$  v.s. time during tBA insertion Solvent: PhCl-H5. Temperature: 50 °C. Initial concentration:  $[1]_0=0.0157$  M;  $[tBA]_0=0.157$  M (10 equiv.);  $[py]_0=0.0315$  M (2 equiv.). Red spots: experimental data, blue line: fitted curve.

- $p=-0.0129$ ,  $SSR=0.153$ ,  $k_2=0.0032$

## Summary

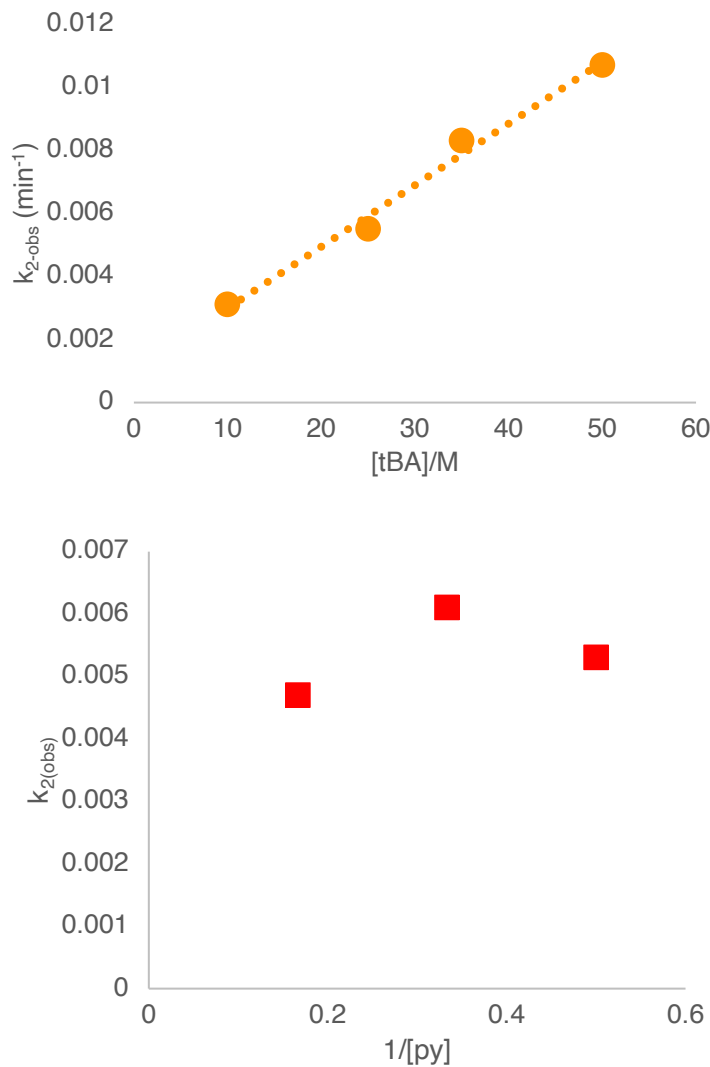


**Figure S8.26.** Plots (top:  $k_{\text{obs}}$  vs [tBA]; bottom:  $k_{\text{obs}}$  vs  $1/\text{[py]}$ ) of coordination insertion of tBA into **3** (See Figure S8.20~S8.25 for details).

## **9. DFT calculation**

### **9.0 Computational Methods**

Geometry optimizations in the gas phase were initially carried out using the GFN1-xTB method<sup>8</sup> as implemented in Entos Qcore Version 0.7.<sup>9</sup> The resulting structures were further optimized using hybrid meta-generalized gradient-approximation (hybrid meta-GGA) M06 functional<sup>10</sup> with Karlsruhe-family basis set of double- $\zeta$  valence def2-SVP<sup>11,12</sup> for all atoms as implemented in *Gaussian 16* rev. A.03.<sup>13</sup> Where possible, available X-ray crystal structures were used as an initial guess. The M06 functional was chosen as it performs better than many other functionals (e.g.  $\omega$ B97X-D and TPSS) in predicting transition metal (TM) reaction barrier heights (TMBH21 dataset)<sup>14-16</sup> for reactions involving TMs.<sup>3,17</sup> M06 has also been employed to study similar TM-catalyzed systems with excellent agreement with experimental results.<sup>18,19</sup> Minima and transition structures on the potential energy surface (PES) were confirmed as such by harmonic frequency analysis, showing respectively zero and one imaginary frequency, at the same level of theory. Where appropriate, intrinsic reaction coordinate (IRC) analyses<sup>20,21</sup> were performed to confirm that the found TSs connect to the right reactants and products.

Single point (SP) corrections were performed using M06 functional and def2-TZVP<sup>11</sup> basis set for all atoms. The implicit SMD continuum solvation model<sup>22</sup> was used to account for the solvent effect of chlorobenzene on the Gibbs energy profile. Gibbs energies were evaluated at the reaction temperature of 323.15 K, using a quasi-RRHO treatment of vibrational entropies.<sup>23,24</sup> Vibrational entropies of frequencies below 100 cm<sup>-1</sup> were obtained according to a free rotor description, using a smooth damping function to interpolate between the two limiting descriptions. The free energies were further corrected using standard concentration of 1 mol/L, which was used in solvation calculations. SMD(chlorobenzene)-M06/def2-TZVP//M06/def2-SVP Gibbs energies are given and quoted in kcal mol<sup>-1</sup> throughout. *Unless otherwise stated, these solvent-corrected values are used for discussion throughout the main text and in this supporting information.*

Non-covalent interactions (NCIs) were analyzed using NCIPILOT<sup>25</sup> calculations. The .wfn files for NCIPILOT were generated at M06/DGDZVP<sup>26,27</sup> level of theory. NCI indices calculated with NCIPILOT were visualized at a gradient isosurface value of  $s = 0.5$  au. These are colored according to the sign of the second eigenvalue ( $\lambda_2$ ) of the Laplacian of the density ( $\nabla^2\rho$ ) over the range of -

0.1 (blue = attractive) to +0.1 (red = repulsive). Molecular orbitals are visualized using an isosurface value of 0.05 throughout. All molecular structures and molecular orbitals were visualized using *PyMOL* software.<sup>28</sup> Geometries of all optimized structures (in .xyz format with their associated energy in Hartrees) are included in a separate folder named *structures\_xyz* with an associated README file. All these data have been deposited with this Supporting Information. All Python scripts used for data analysis are taken from <https://github.com/bobbypaton>.

### 9.0.1 Conformational considerations

Where available, experimentally obtained X-ray crystal structures were used as initial guess for geometry optimization. Where different conformers exist in the X-ray structures, all available conformers were used for geometry optimization and the final optimized, lowest energy structure is used. The ligand backbone from the lowest energy conformer is then kept fixed for all subsequent reaction paths. For olefin insertions, all possible coordination modes/orientations were considered in the geometry optimization and the lowest energy conformers are used for discussion.

## 9.1 Reaction pathways leading from POP-Ni-py (1)

### 9.1.1 The starting structure of POP-Ni-py (1)

The starting structure for the optimization of **POP-Ni-py** complex was taken from the experimentally obtained X-ray crystal structure. The henceforth optimized structure **1-c2** is shown in Figure S9.1. We found another optimized structure (**1**) that is lower in energy than **1-c2** and we take this as the zero energy reference for this reaction (Figure S9.1). Note that these two structures are essentially conformers and they differ in the spatial orientation of the trialkylsilylated polymer chain.

<b>1</b>	<b>1-c2</b>
$\Delta G = 0.0$	$\Delta G = 9.8$

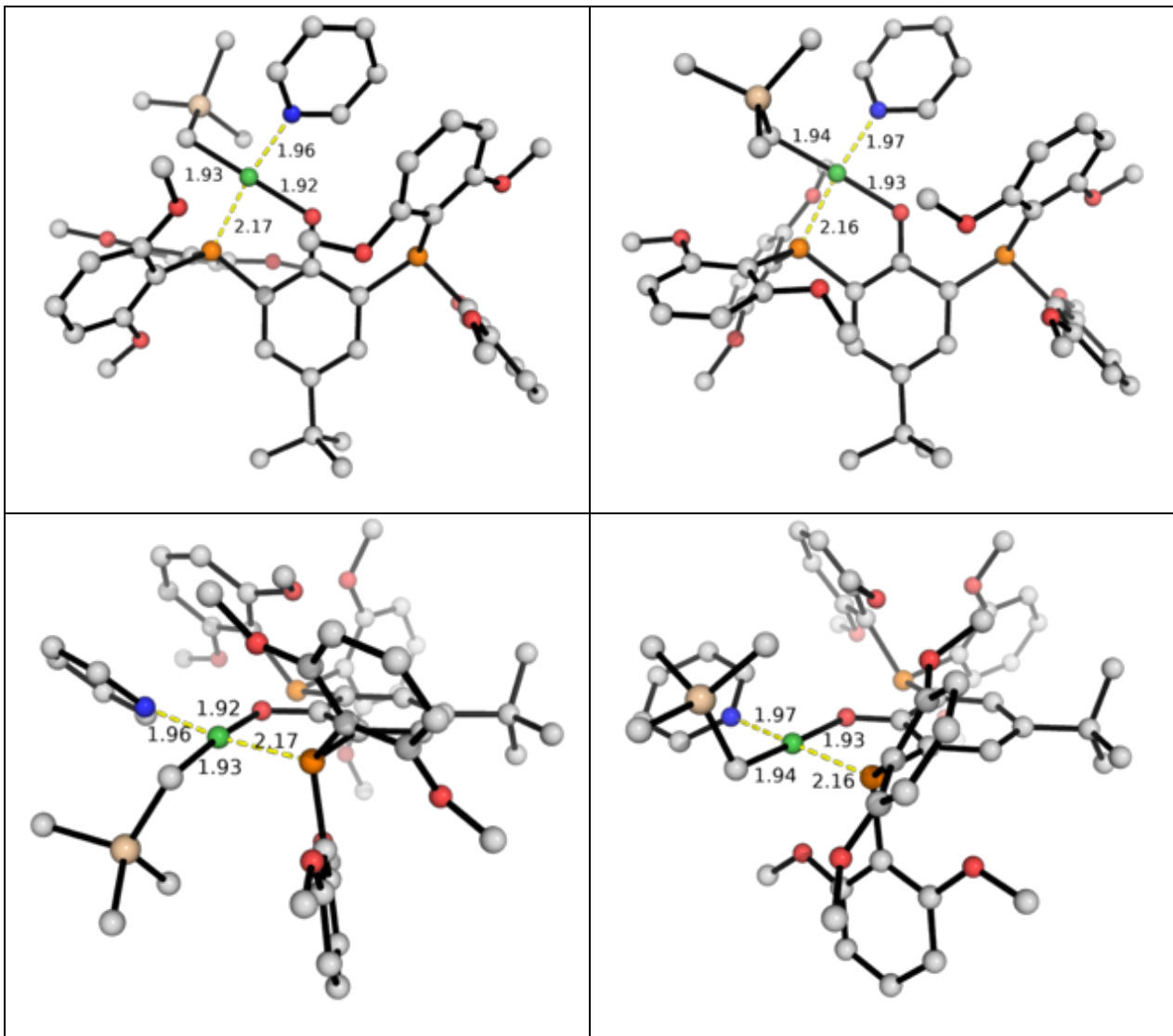


**Figure S9.1.** Optimized structures for the Ni(II) complex **POP-Ni-py**. The Gibbs energies are calculated at SMD (chlorobenzene)-M06/def2-TZVP//M06/def2-SVP level of theory and measured relative to the most stable species (**1**). Key bond distances are given in Å. Gibbs energy units are given in kcal mol<sup>-1</sup>.

### 9.1.2 Ethylene-bound Ni(II) complex – displacement of pyridine by ethylene in POP-Ni-py

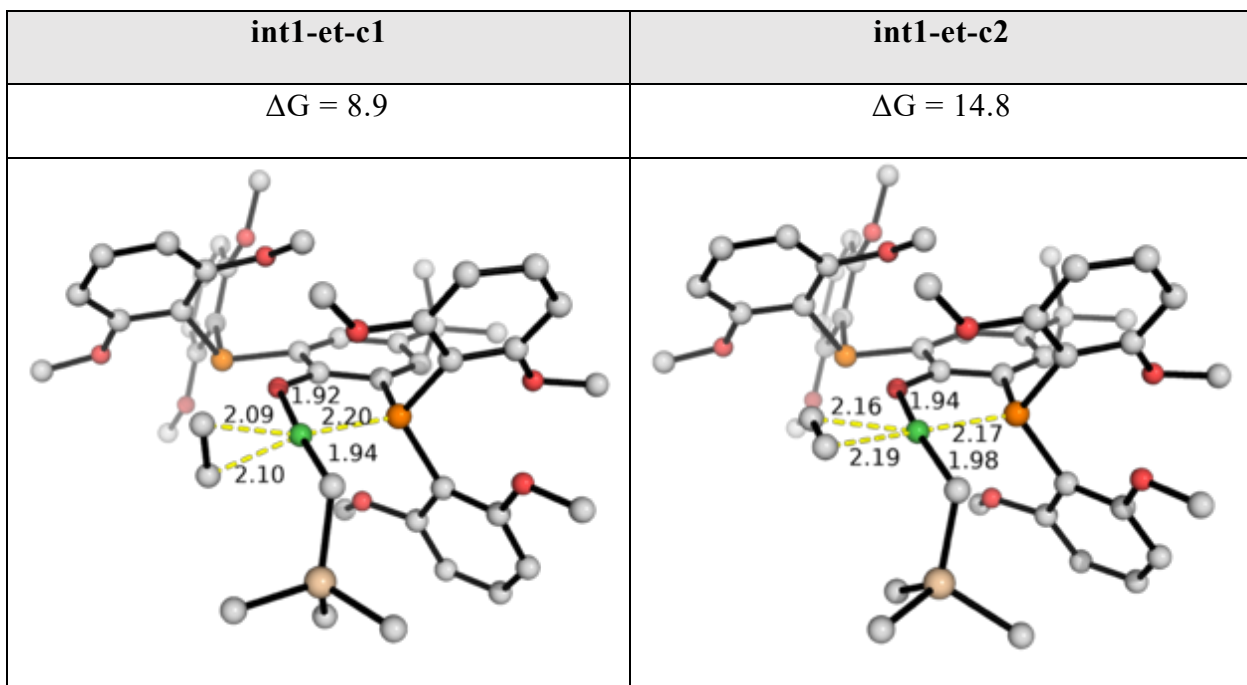


**Figure S9.2.** Optimized structures for the Ni(II) complex **POP-Ni-et**. The Gibbs energies are calculated relative to **POP-Ni-py** (**1**). Key bond distances are given in Å. Gibbs energy units are given in kcal mol<sup>-1</sup>.

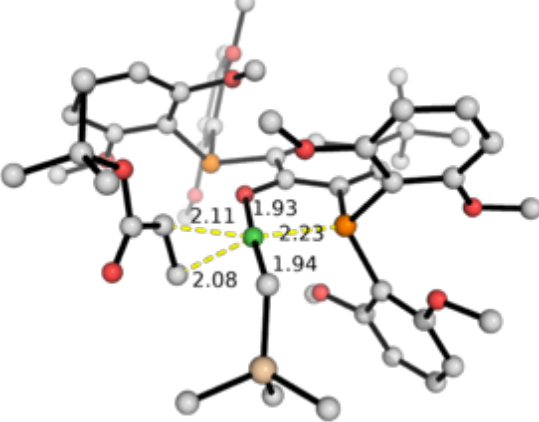
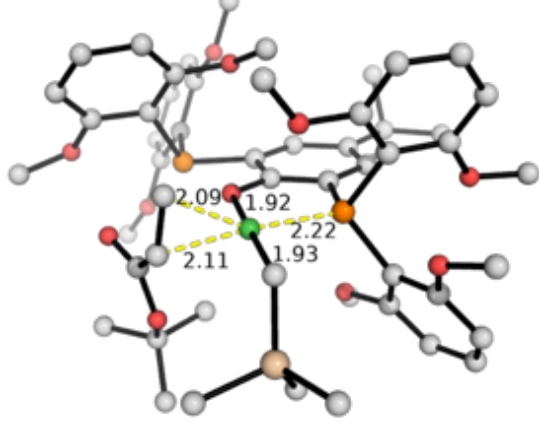
Herein we show the optimized structures of the Ni(II) complex where the pyridine ligand gets displaced by ethylene substrate. We denote these as **POP-Ni-et** complexes where the suffix “et” denotes ethylene. Two structures can be found (Figure S9.2). These differ in the orientations of the ethylene  $\pi$ -bond that is coordinated to the Ni-center. In **int1-et-c1**, the  $\pi$ -bond is perpendicular to the Ni square plane, whereas in **int1-et-c2**, the  $\pi$ -bond is parallel to and lying on the Ni square plane. Structure **int1-et-c1** is 5.9 kcal mol<sup>-1</sup> more stable than **int1-et-c2**. For the migratory insertion of ethylene substrate into the Ni–C bond, the ethylene has to be in **int1-et-c2** before insertion can occur (*vide infra*).

### 9.1.3 t-butylacrylate (tBA)-bound Ni(II) complex – displacement of pyridine by tBA in **POP-Ni-py**

We similarly show the optimized structures of the Ni(II) complex where the pyridine ligand gets displaced by t-butylacrylate (tBA) substrate. All possibilities were considered while minimizing / avoiding unphysical steric clashes. The optimized structures are given in Figure S9.3. We denote these as **POP-Ni-ac** complexes where the suffix “ac” denotes t-butylacrylate.

tBA can coordinate either via the C=C  $\pi$ -bond or the O-atom of the carbonyl group. For the coordination via C=C  $\pi$ -bond to the Ni-center, both the C=C bond perpendicular (**int1-ac-c1** and **int1-ac-c2**) and parallel (**int1-ac-c3** and **int1-ac-c4**) to the Ni square plane can be found. As in the case of ethylene binding, the tBA binding with C=C  $\pi$ -bond perpendicular to the Ni square plane is lower in energy/more stable (by at least 4.4 kcal mol<sup>-1</sup>) than with C=C  $\pi$ -bond parallel to the Ni square plane. Comparing the latter two structures (**int1-ac-c3** and **int1-ac-c4**) which the reaction must pass prior to migratory insertion, we found that **int1-ac-c3**, forming the observed tBA insertion product, is 5.1 kcal mol<sup>-1</sup> more stable than **int1-ac-c4**, which forms the less favorable regioisomer (*vide infra*).

For tBA insertion, additionally, two structures with O-coordination were found (**int1-ac-o1** and **int1-ac-o2**). These differ in the orientation of the *t*-butoxy group. Both these O-coordinated structures have lower energy than C=C  $\pi$ -bond coordinated species (by 2.2 kcal mol<sup>-1</sup> comparing the lowest energy coordination species, **int1-ac-o1** and **int1-ac-c1**), suggesting that the initial coordination of tBA substrate would occur via O-coordination.

Coordination via C=C $\pi$ -bond	
<b>int1-ac-c1</b>	<b>int1-ac-c2</b>
$\Delta G = 13.7$	$\Delta G = 15.6$
	
<b>int1-ac-c3</b>	<b>int1-ac-c4</b>
$\Delta G = 20.0$	$\Delta G = 25.1$

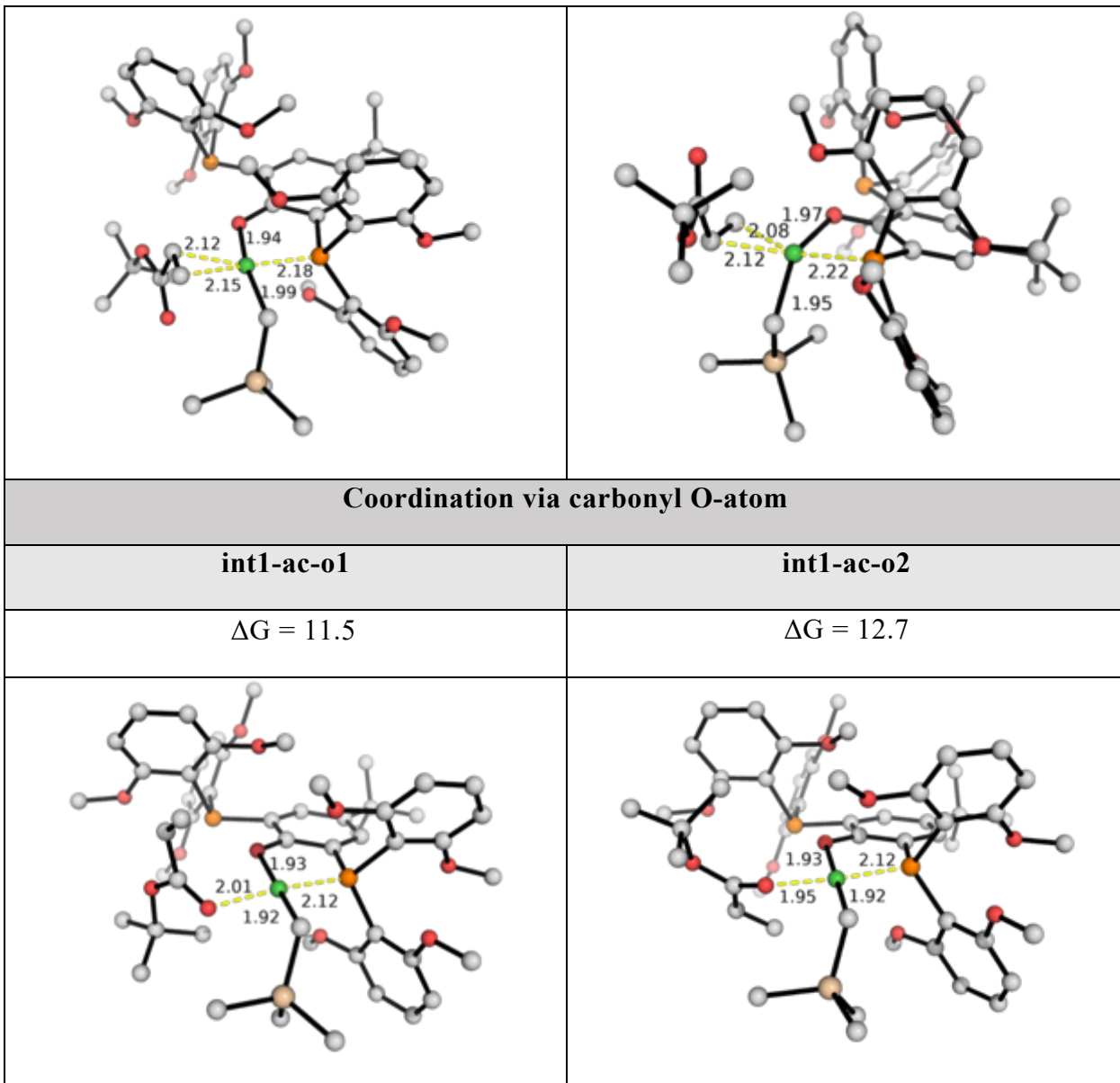


**Figure S9.3.** Optimized structures for the Ni(II) complex **POP-Ni-ac**. The Gibbs energies are calculated relative to **POP-Ni-py (1)**. Key bond distances are given in Å. Gibbs energy units are given in kcal mol<sup>-1</sup>.

#### 9.1.4 First insertion of substrate into **POP-Ni-py (1)**

We investigated the comparative barriers of the insertion of ethylene vs tBA into catalyst **POP-Ni-py (1)**. Figure S9.4 shows the reaction scheme and the Gibbs energy profile for the first insertion. The optimized TS structures and their key bond distances are given in Figure S9.5. From this energy profile, we can see that the 2,1-insertion of acrylate tBA (**ts1-ac**, at 30.5 kcal mol<sup>-1</sup>) has a lower activation barrier, by 2.6 kcal mol<sup>-1</sup>, at the reaction temperature

of 50 °C, than the insertion of ethylene (**ts1-et**, at 33.1 kcal mol<sup>-1</sup>); the regioisomeric 1,2-insertion of tBA (**ts1-ac-r**) is the least favorable, with a barrier of 41.5 kcal mol<sup>-1</sup>. Comparing the migratory insertion site selectivity of tBA (2,1-insertion vs 1,2-insertion), our calculation is in agreement with the observation that the migratory insertion of acrylate occurs at the β-carbon site of an α,β-unsaturated carbonyl, akin to conjugate addition.<sup>29-31</sup> Using simple transition state theory (TST), this translates to a rate of roughly **ts1-ac : ts1-et : ts1-ac-r = 1 : 57 : 27** million. With this energy profile, it implicates that the insertion of acrylate can occur more easily than the insertion of ethylene, which is contradictory to the experimental observation that the first insertion of ethylene proceeds *ca.* 50 times faster than the tBA insertion. In addition, the overall barriers of 30.5 kcal mol<sup>-1</sup> for tBA insertion and 33.1 kcal mol<sup>-1</sup> for ethylene insertion seem pretty high. We anticipate that the Ni-catalyst **POP-Ni-py (1)** can undergo an isomerization before subsequent first insertion occurs, giving a lower activation barrier and correct substrate selectivity (see section 7.2).

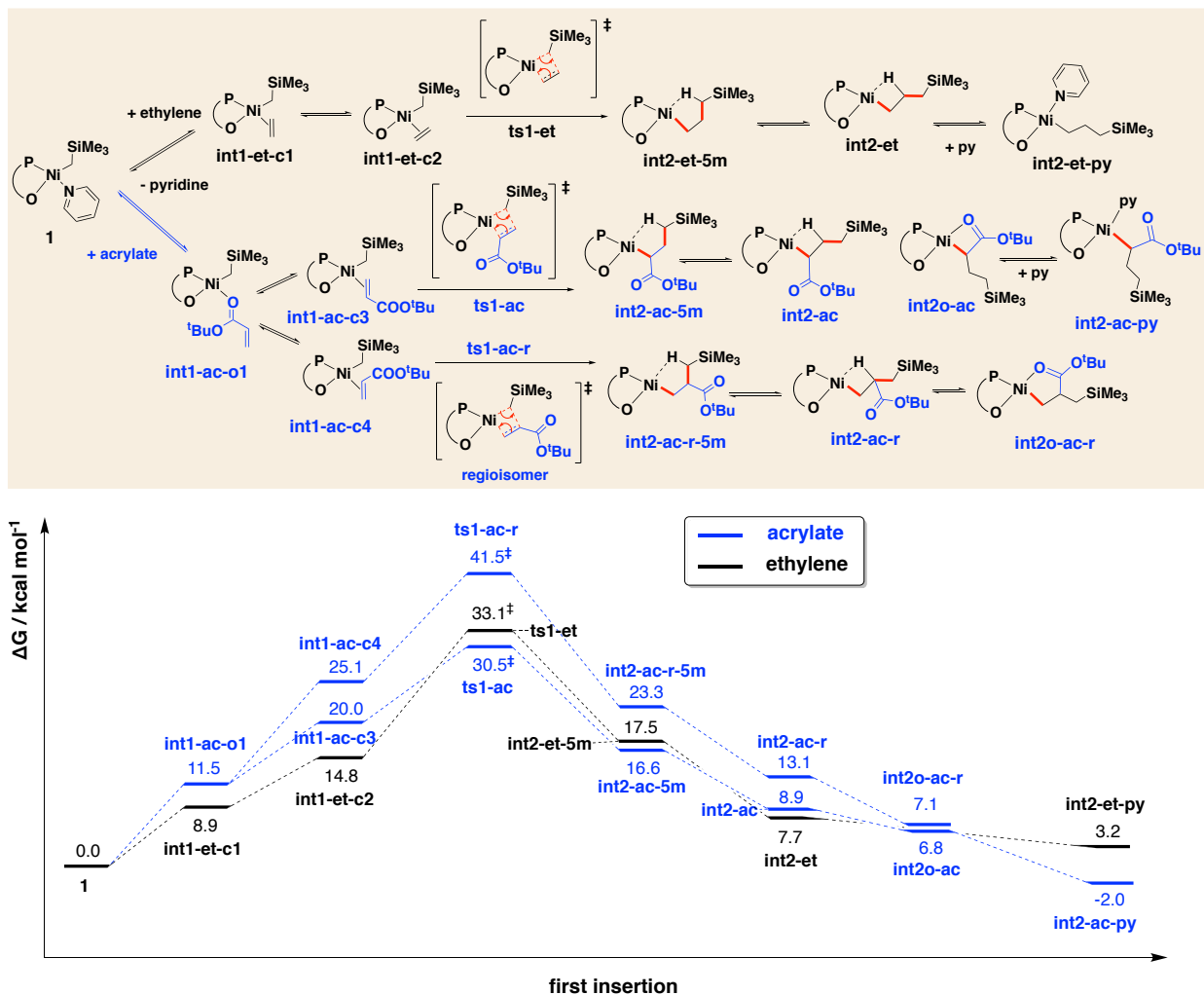


**Figure S9.4.** Gibbs energy profile for the first insertion of ethylene vs *t*-butylacrylate into catalyst **POP-Ni-py** (**1**). The Gibbs energies are calculated at SMD(chlorobenzene)-M06/def2-TZVP//M06/def2-SVP level of theory. The energy of the species **POP-Ni-py** (**1**) is taken as a reference.

The first insertion products have the  $\beta$ -H atom coordinated to the Ni-center, forming 4-membered nickelacycles (**int2-et**, **int2-ac** and **int2-ac-r**). These 4-m nickelacycles are lower in energy than the 5-m nickelacycles formed via  $\gamma$ -H atom coordination (**int2-et-5m**, **int2-ac-5m** and **int2-ac-r-5m**), as located by IRC analysis.

<b>ts1-et</b>	<b>ts1-ac</b>
$\Delta G^\ddagger = 33.1$	$\Delta G^\ddagger = 30.5$

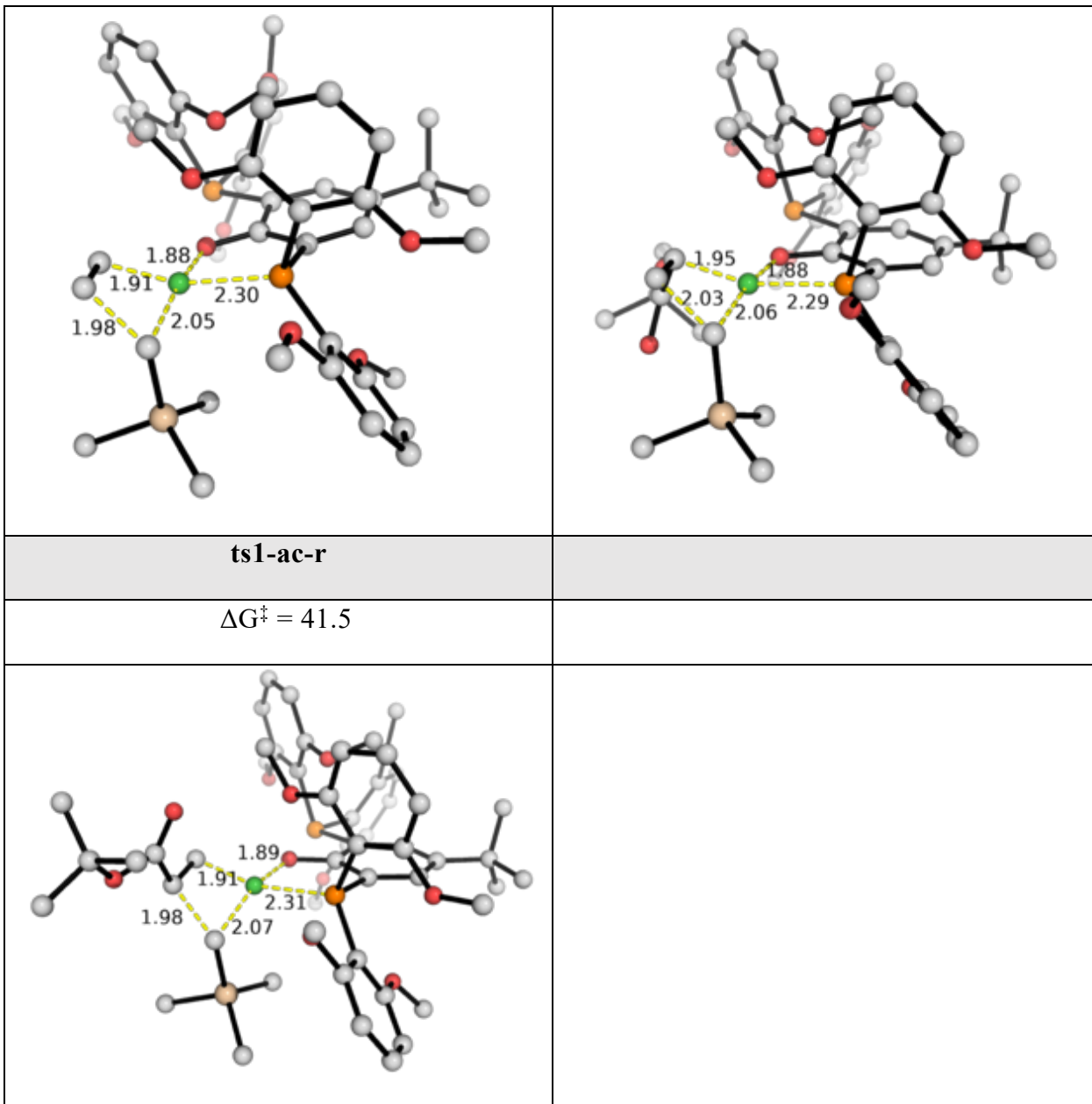
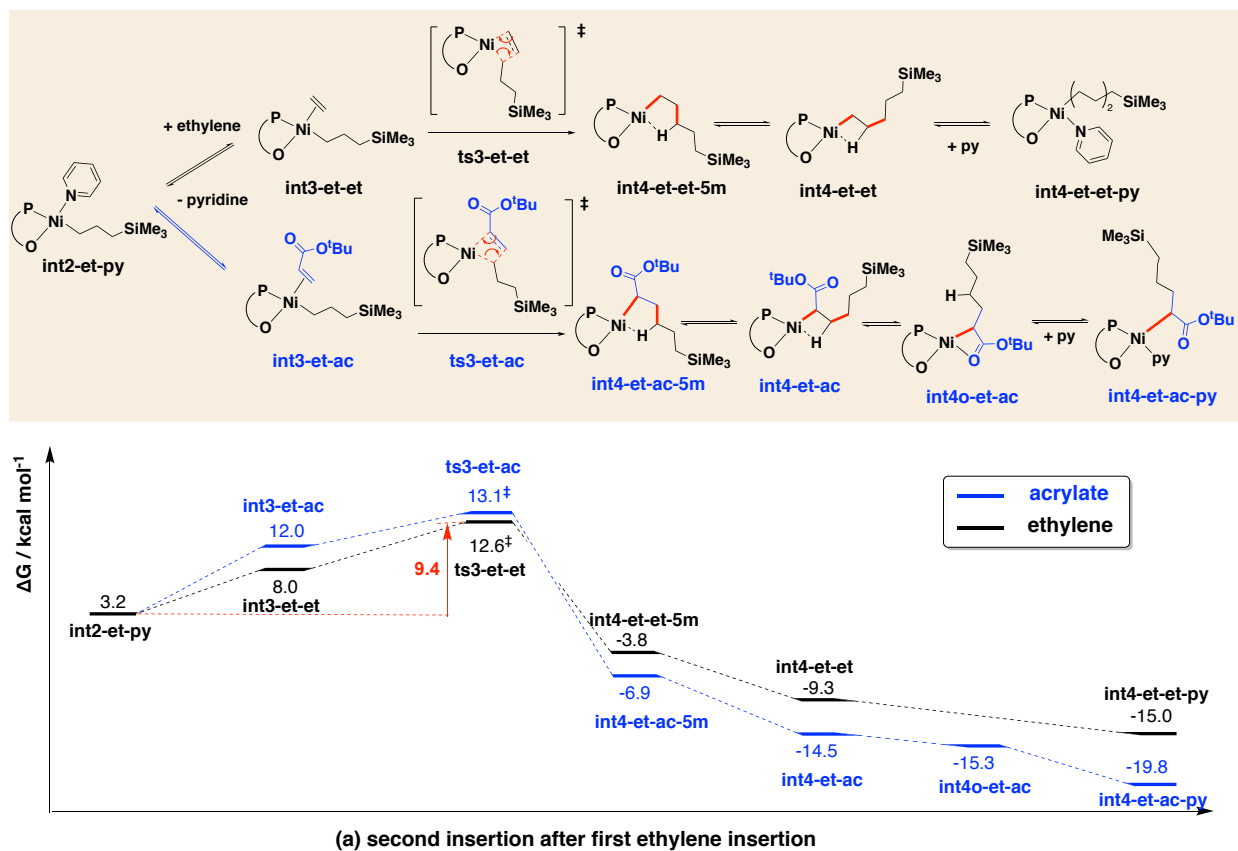


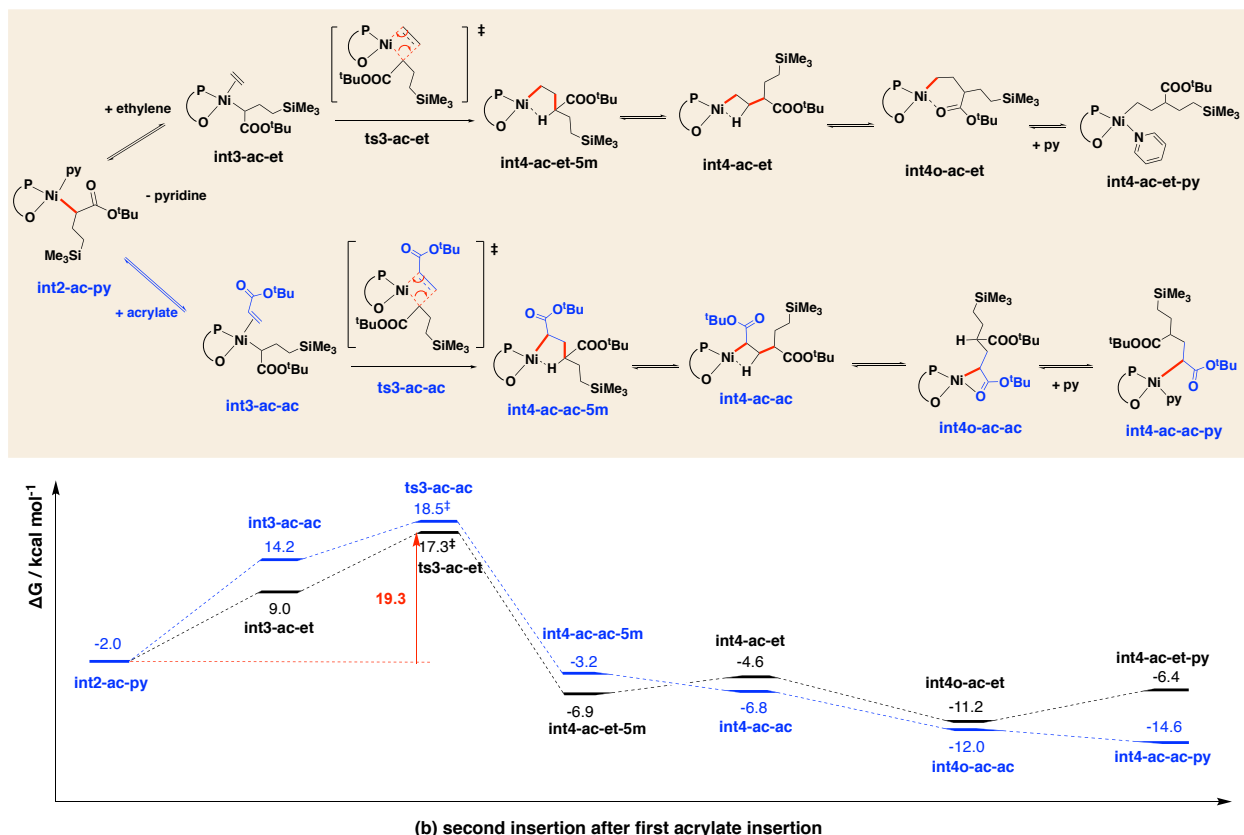
**Figure S9.5.** Optimized TS structures of first insertion of ethylene/tBA into Ni(II) complex **POP-Ni-ac 1**. Key bond distances are given in Å. Gibbs energy units are given in kcal mol<sup>-1</sup>.

### 9.1.5 Second insertion of monomer into first insertion product of POP-Ni-py (1)

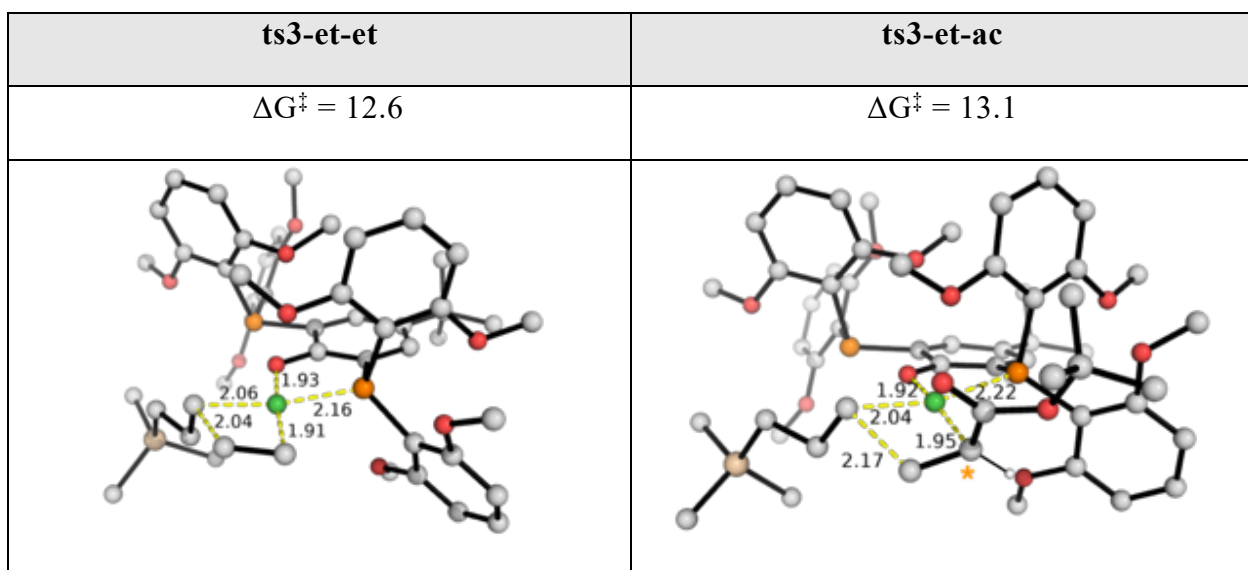
The insertion of second monomer after the first insertion of ethylene vs tBA into catalyst **POP-Ni-py 1** was studied. Figure S9.6 presents the Gibbs energy profile for the second insertion; optimized TS structures are given in Figure S9.7. In Figure S9.6 (a), we see that the second insertion of ethylene to first ethylene-inserted product has a rather low activation barrier of 9.4 kcal mol<sup>-1</sup> (**ts3-et-et**, at 12.6 kcal mol<sup>-1</sup>). The second insertion of tBA into first

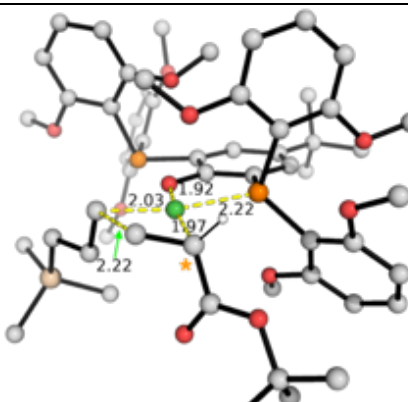
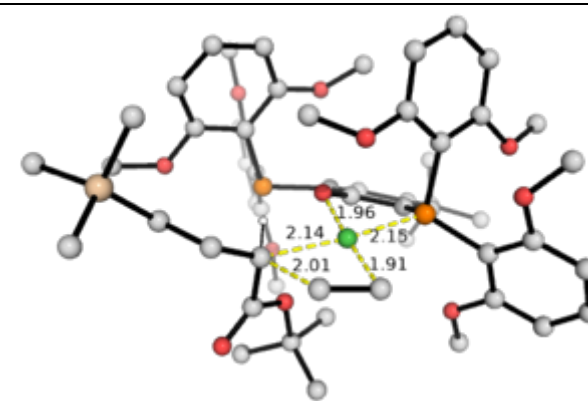
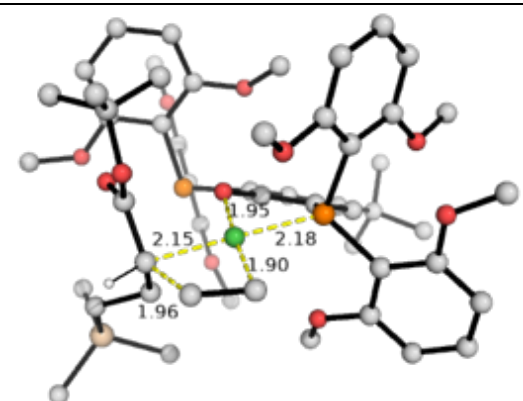
ethylene-inserted product has a slightly higher activation barrier, by 0.5 kcal mol<sup>-1</sup> (**ts3-et-ac**, at 13.1 kcal mol<sup>-1</sup>). This energetic difference is rather small and typically falls within the numerical accuracy of DFT. This implies that the rate of second insertion of ethylene would be rather similar to that of acrylate into first ethylene-inserted product. The insertion products having 4-membered nickelacycles via  $\beta$ -H agostic interaction with the Ni-center (**int4-et-et** and **int4-et-ac**) have lower energies than the 5-m nickelacycles formed via  $\gamma$ -H atom coordination (**int4-et-et-5m** and **int4-et-ac 5m**), as located by IRC analysis. We note that, however, these energetic differences do not affect the overall conclusion of the kinetic analyses as these species are not involved in turnover-frequency determining steps.





**Figure S9.6.** Gibbs energy profile for the second insertion of ethylene vs *t*-butylacrylate into first inserted product resulting from catalyst **POP-Ni-py (1)**. The energy of the species **POP-Ni-py (1)** is taken as a reference. **(a)** Second insertion after first ethylene insertion product and **(b)** second insertion after first acrylate insertion product.



<b>ts3-et-ac-c2</b>	
$\Delta G^\ddagger = 14.0$	
	
<b>ts3-ac-et</b>	<b>ts3-ac-et-c2</b>
$\Delta G^\ddagger = 17.3$	$\Delta G^\ddagger = 26.9$
	
<b>ts3-ac-ac</b>	<b>ts3-ac-ac-c2</b>
$\Delta G^\ddagger = 18.5$	$\Delta G^\ddagger = 18.5$

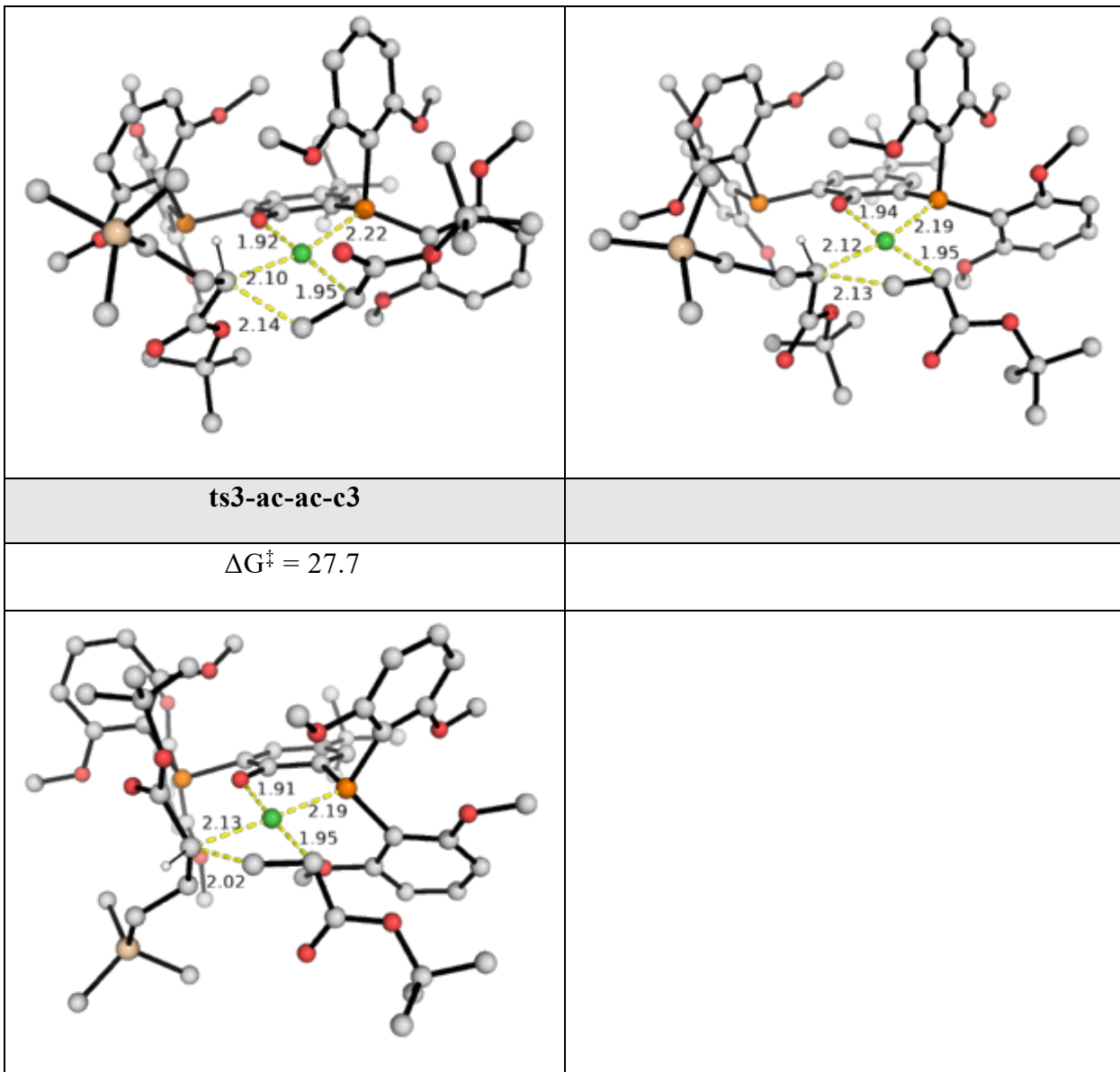


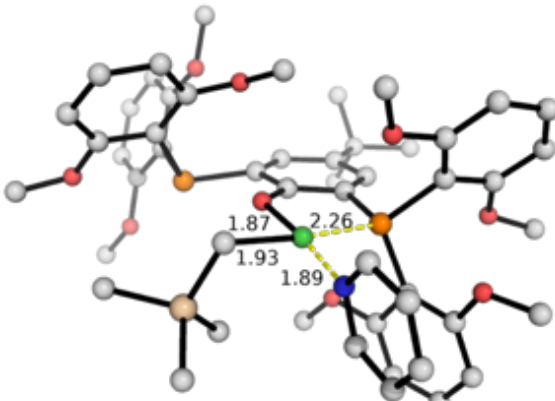
**Figure S9.7.** Optimized TS structures of second insertion of ethylene/tBA into first inserted product arising from Ni(II) complex **POP-Ni-ac 1**. Key bond distances are given in Å. Gibbs energy units are given in kcal mol<sup>-1</sup>.

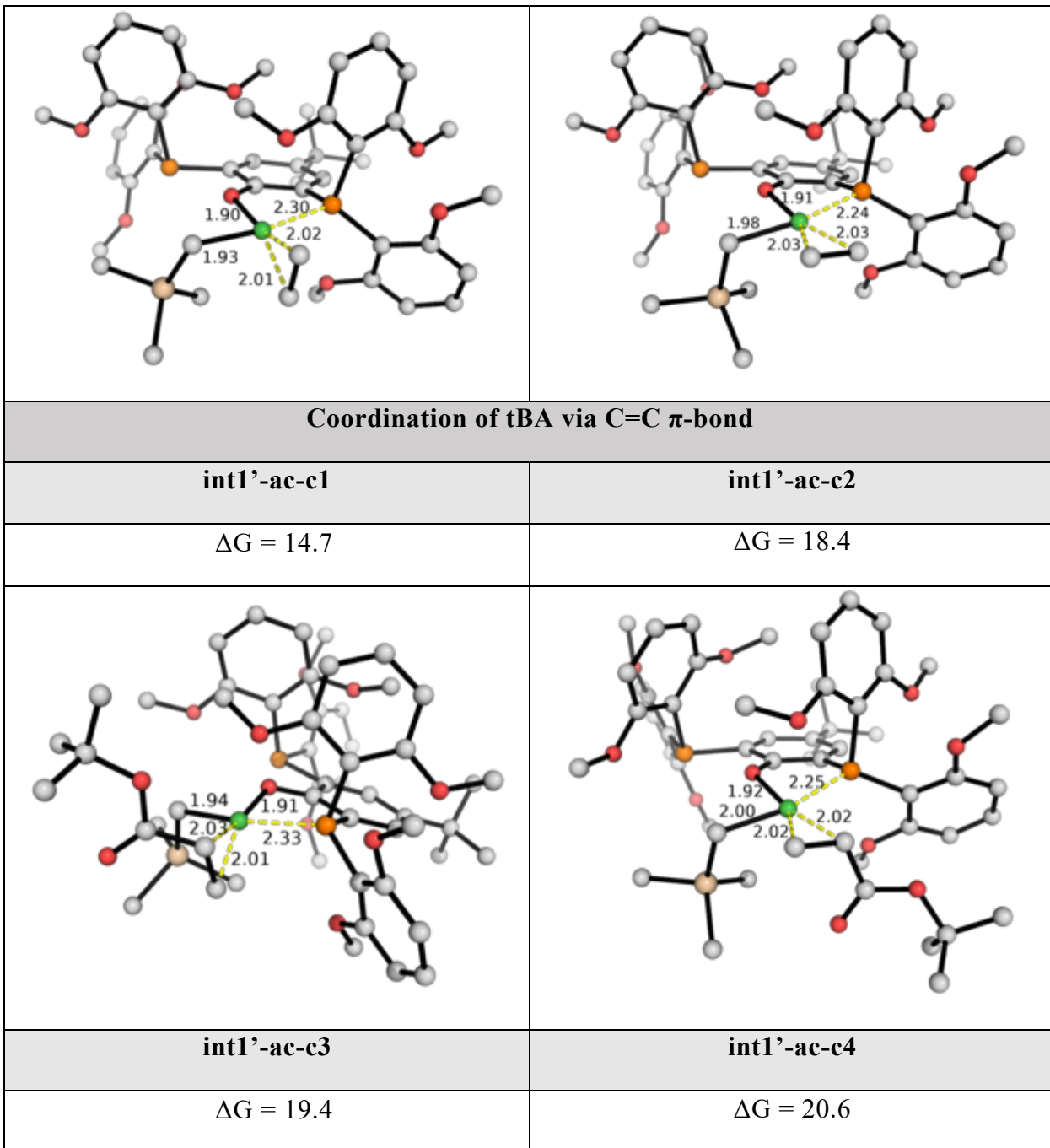
For the second insertion of monomer into first acrylate-inserted product (Figure S9.6 (b)), the insertion of ethylene (**ts3-ac-et**, at 17.3 kcal mol<sup>-1</sup>) has a barrier that is 1.2 kcal mol<sup>-1</sup> lower than the second insertion of tBA (**ts3-ac-ac**, at 18.5 kcal mol<sup>-1</sup>). The overall barrier for the second insertion into tBA-inserted product (28.9 kcal mol<sup>-1</sup>) is much higher than the overall barrier for the second insertion into ethylene-inserted (9.4 kcal mol<sup>-1</sup>), suggesting that the second insertion into acrylate-inserted product will be much more difficult than the second insertion into ethylene-inserted product.

## 9.2 Reaction pathways leading from the geometric isomer of the catalyst POP-Ni-py (1')

### 9.2.1 Geometric isomer POP-Ni-py (1') and its relevant substrate-bound complexes

Previous report by Morokuma and Nozaki on Pd phosphine-sulfonate-catalyzed polymerization<sup>31</sup> suggests that the olefin can insert to the growing polymer chain that is *trans* to the phosphorus atom. We herein consider the insertion to the geometric isomeric form of the **POP-Ni-py** catalyst, denoted as **1'**. The optimized structures of this pyridine-bound catalyst and the relevant substrate-bound complexes are shown in Figure S9.8. The relative energies are given with respect to the most stable form **POP-Ni-py 1**.

<b>1'</b>	
$\Delta G = 4.4$	
	
<b>Coordination of ethylene via C=C π-bond</b>	
<b>int1'-et-c1</b>	<b>int1'-et-c2</b>
$\Delta G = 11.7$	$\Delta G = 14.6$



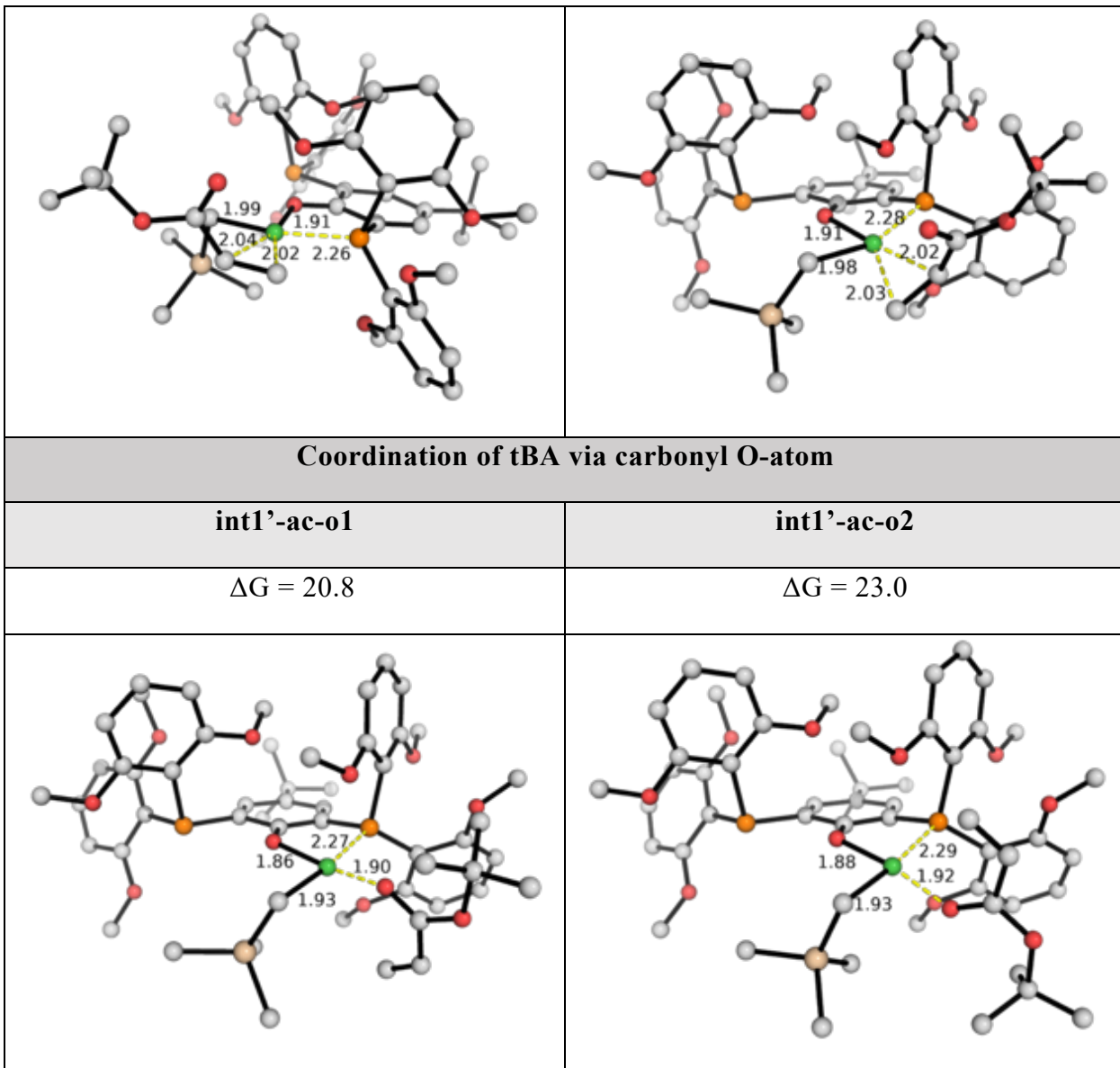
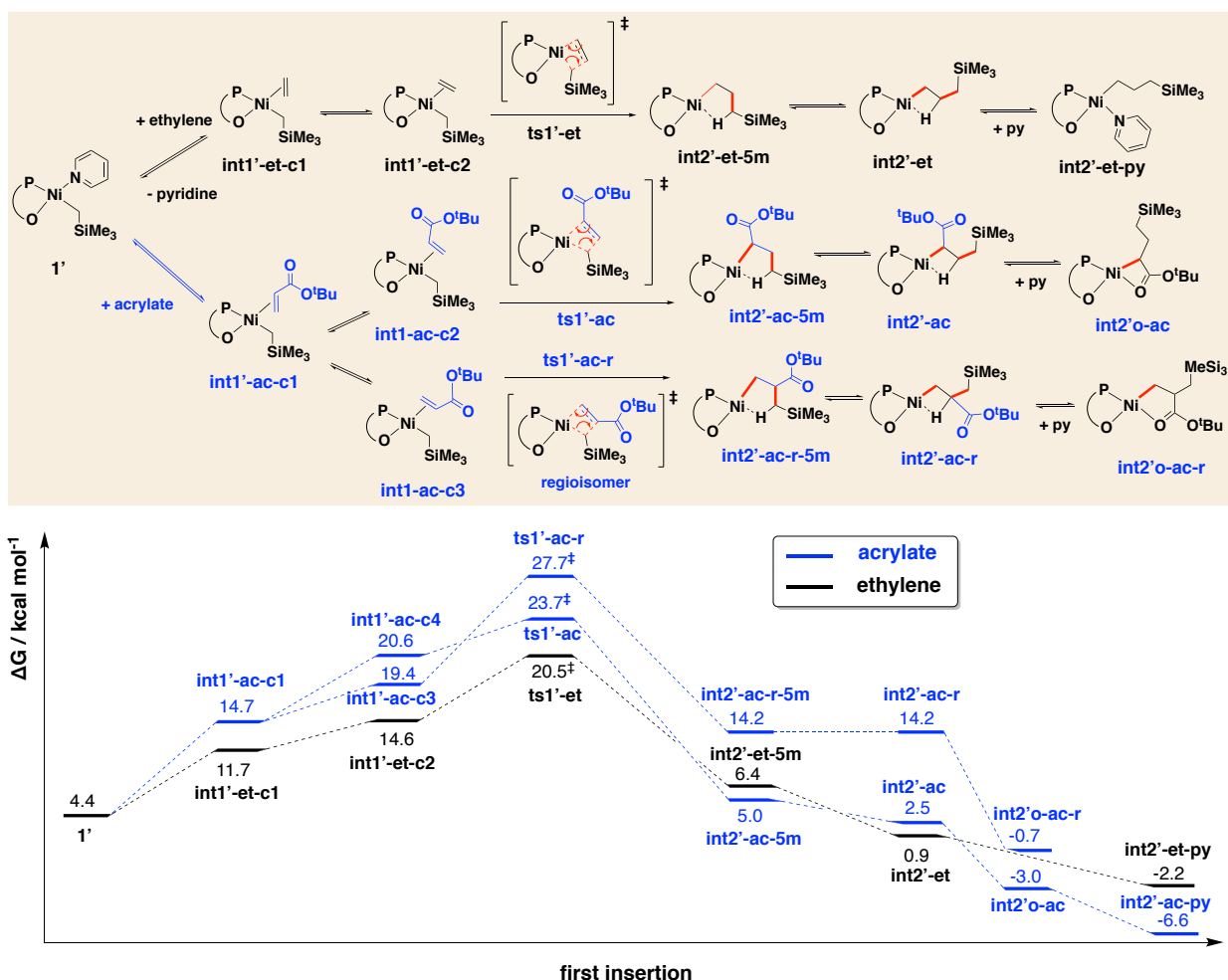


**Figure S9.8.** Optimized structures for the coordination complexes of the isomeric Ni-catalyst **1'**. The Gibbs energies are calculated relative to **POP-Ni-py (1)**. Key bond distances are given in Å. Gibbs energy units are given in kcal mol<sup>-1</sup>.

It is interesting to note here that, for the coordination complex with tBA monomer, the coordination via  $\pi_{CC}$  bond (**int1'-ac-c1**, at 14.7 kcal mol<sup>-1</sup>) is much more stable, by 6.1 kcal mol<sup>-1</sup>, than the coordination via oxygen atom (**int1'-ac-o1**, at 20.8 kcal mol<sup>-1</sup>) (cf Figure S9.3). This differences possibly arise due to the electronic differences at Ni-metal relative to the ligand coordination from phenoxy-O and phosphine-P atoms. Herein the  $\pi$  donation is more favored than lone pair donation *cis* to P-atom, compared to the other way when tBA coordinates *trans* to P-atom (Figure S9.3).

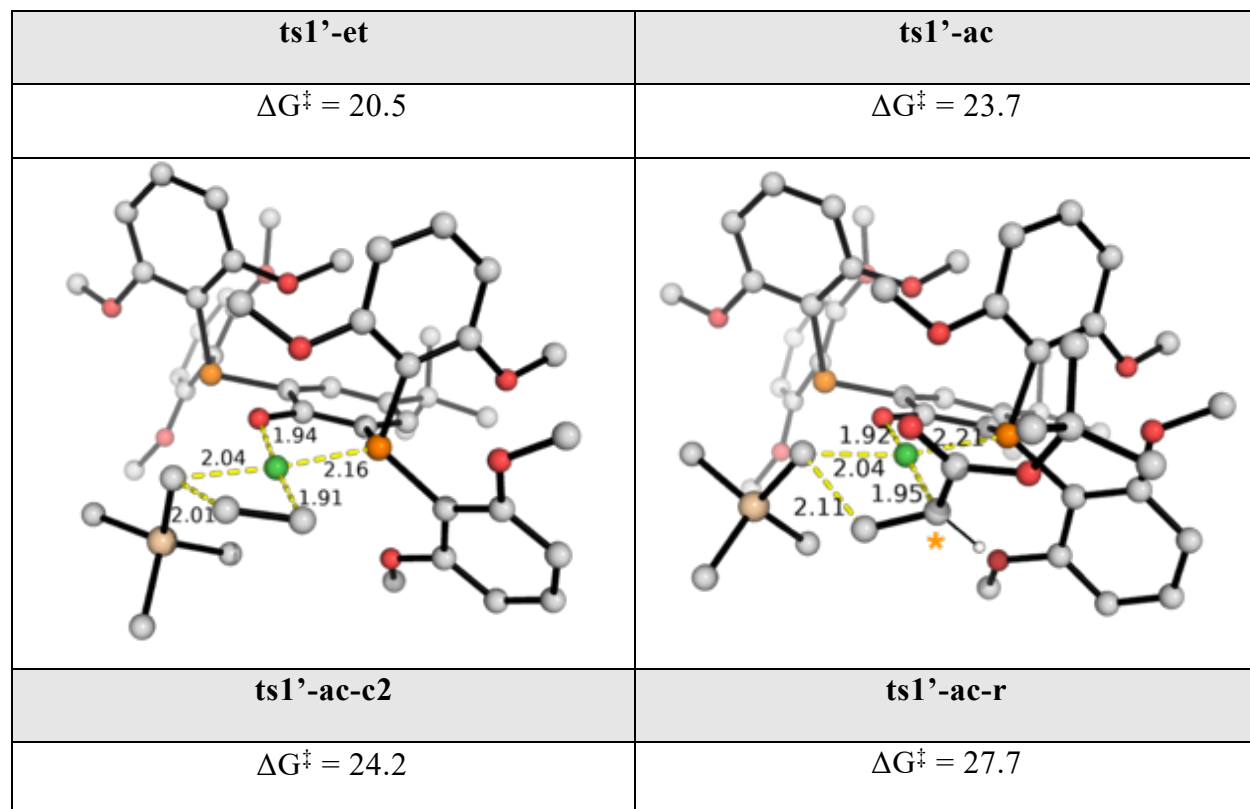
### 9.2.3 First insertion of substrate into isomeric POP-Ni-py (1')

The insertion of ethylene vs tBA into isomeric **POP-Ni-py 1'** was calculated. The Gibbs energy profile is shown in Figure S9.9 and the optimized TS structures are given in Figure S9.10. All values are given in kcal mol<sup>-1</sup> and take the energy of the catalyst **POP-Ni-py 1** as a reference. From this energy profile, we can see that the insertion of ethylene into the isomeric form of the Ni-catalyst has the lowest activation barrier (**ts1'-et**, at 20.5 kcal mol<sup>-1</sup>). The insertion of tBA in either ways (**ts1'-ac**, at 23.7 kcal mol<sup>-1</sup> and **ts1'-ac-r**, at 27.7 kcal mol<sup>-1</sup>) are both less favorable. In particular, the insertion of ethylene is 3.2 kcal mol<sup>-1</sup> more favorable than the 2,1-insertion of tBA, translating to a selectivity in favor of ethylene insertion by about 146 folds using simple TST.



**Figure S9.9.** Gibbs energy profile for the first insertion of ethylene vs *t*-butylacrylate into isomeric form of the Ni-catalyst POP-Ni-py (1'). The Gibbs energies are calculated at SMD(chlorobenzene)-M06/def2-TZVP//M06/def2-SVP level of theory. The energy of the species POP-Ni-py (1) is taken as a reference

More importantly, the overall barrier of  $20.5 \text{ kcal mol}^{-1}$  for ethylene insertion (taking the most stable catalyst **1** as the energy reference, assuming that the geometric isomers **1** and **1'** can interconvert rather easily) is much lower (by at least  $10 \text{ kcal mol}^{-1}$ ) than the activation barriers observed for the insertion into catalyst **1** (Figure S9.4). In other words, if the isomerization of **1** to **1'** can occur easily (*vide infra*), then the insertion of ethylene will occur through the isomeric form of the catalyst via **ts1'-et**. This is in agreement with prior DFT studies of Pd-catalyzed ethylene polymerization<sup>24</sup> where the migratory insertion of the growing polymer chain can occur more readily when it is *trans* to P-atom (*trans* effect).



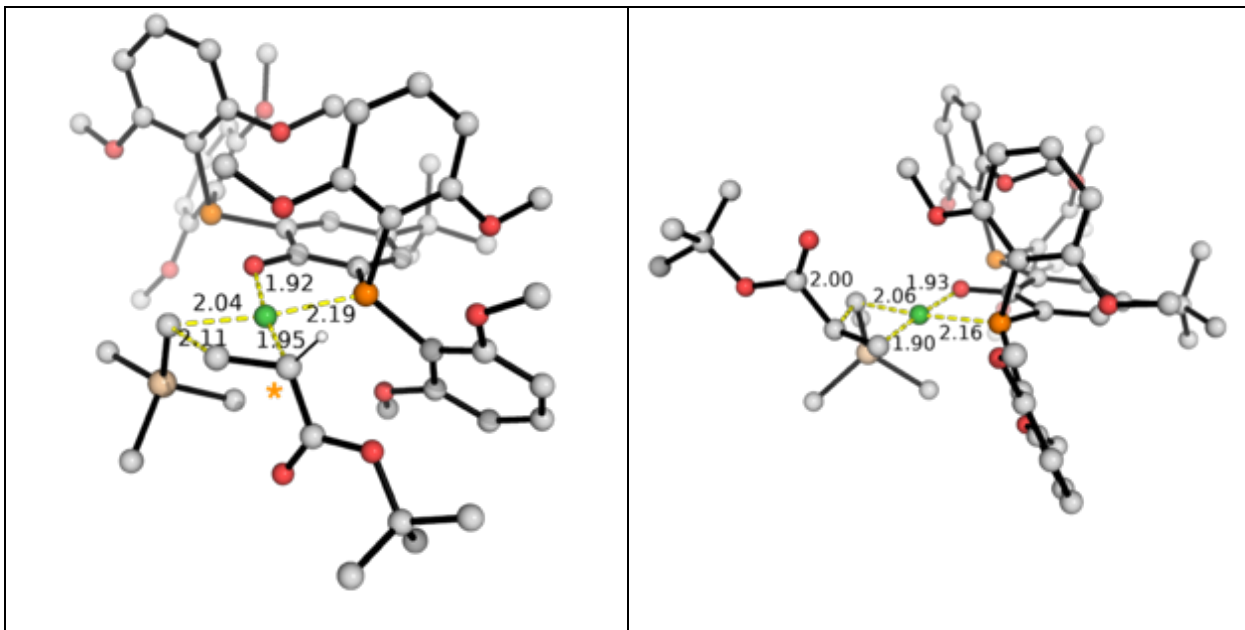


**Figure S9.10.** Optimized structures for the TS structures of first insertion of ethylene/tBA into Ni(II) complex **POP-Ni-ac 1**. Stereocenters in **ts1'-ac** and **ts1'-ac-c2** are marked with yellow asterisk (\*). Key bond distances are given in Å. Gibbs energy units are given in kcal mol<sup>-1</sup>.

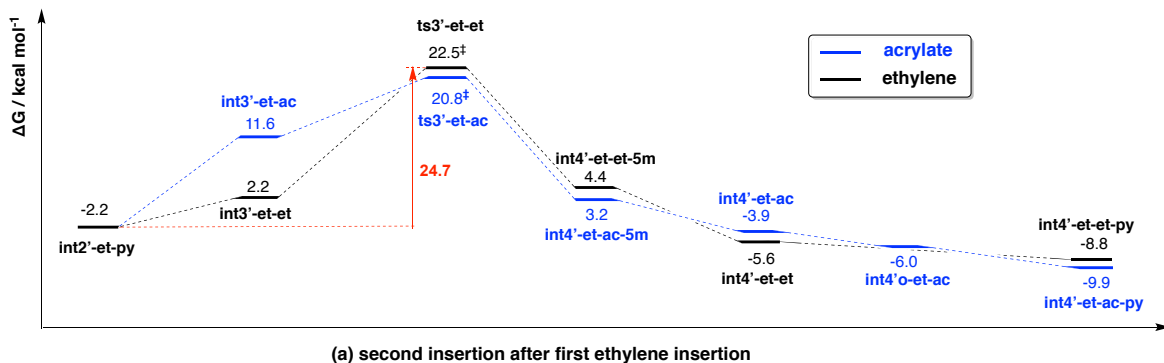
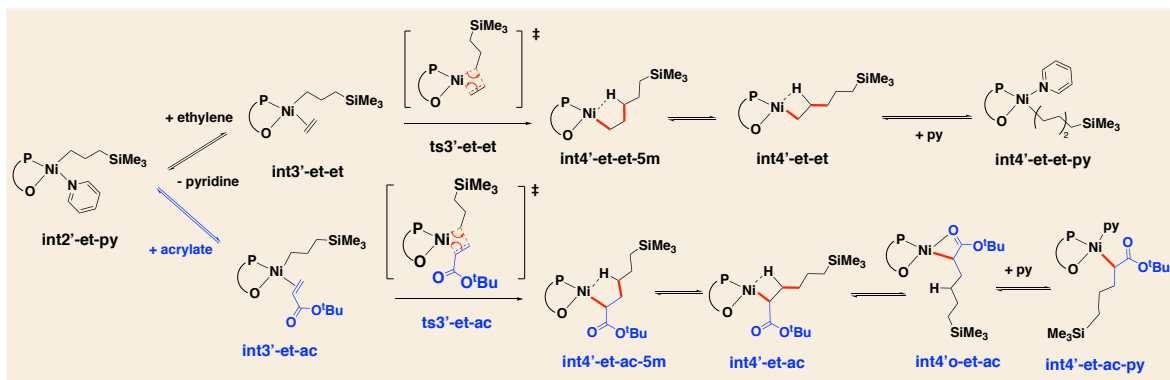
Comparing the migratory insertion site selectivity of tBA, herein the migratory insertion of acrylate occurs more readily, by 4.0 kcal mol<sup>-1</sup>, at the  $\beta$ -carbon site of the  $\alpha,\beta$ -unsaturated carbonyl (**ts1'-ac**, at 23.7 kcal mol<sup>-1</sup>) than at the  $\alpha$ -carbon site (**ts1'-ac-r**, at 27.7 kcal mol<sup>-1</sup>), as previously. For the migratory insertion at the  $\beta$ -carbon, two possibilities can occur (**ts1'-ac** and **ts1'-ac-c2**), giving a stereocenter at the  $\alpha$ -carbon (Figure S9.10). We took the lowest TS for all subsequent second insertion.

### 9.2.3 Second insertion of monomer into first insertion product of isomeric POP-Ni-py (1')

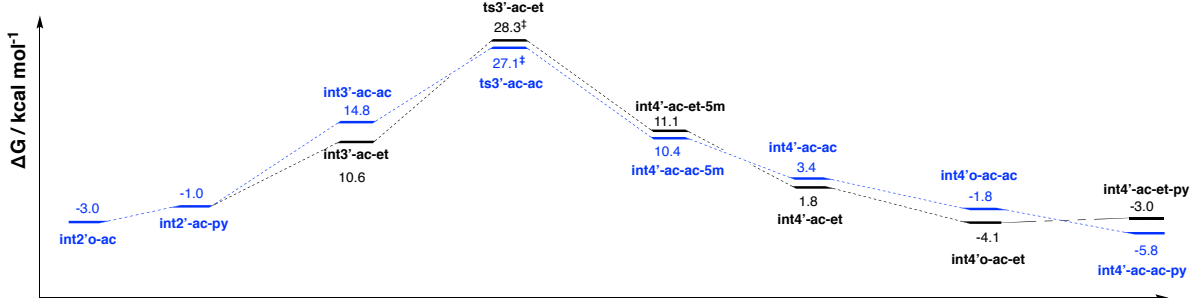
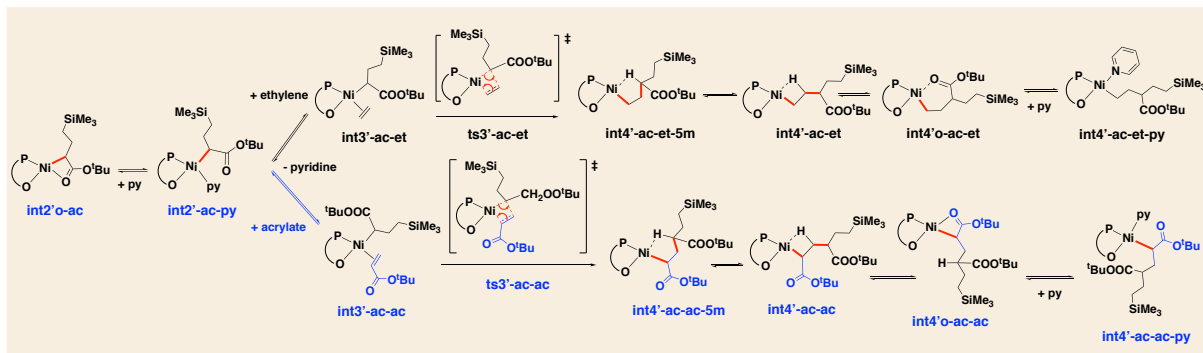
The insertion of second monomer after the first insertion of ethylene vs tBA into the geometric isomeric catalyst **POP-Ni-py 1'** was studied. Figure S9.11 presents the Gibbs energy profile for the second insertion and Figure S9.12 gives the optimized TS structures. In Figure S9.11 (a), we can see that the second insertion of ethylene to first ethylene-inserted product has a slightly higher barrier, by 1.7 kcal mol<sup>-1</sup> (**ts3'-et-et**, at 22.5 kcal mol<sup>-1</sup>) than the second insertion of acrylate tBA into first ethylene-inserted product (**ts3'-et-ac**, at 20.8 kcal mol<sup>-1</sup>).

This implies that the second insertion of tBA is predicted to occur more rapidly via this pathway, which is inconsistent with experimental observation that the second insertion of ethylene after first ethylene insertion occurs more rapidly than the second insertion of tBA. We note that, similar to first insertion, these second insertions where the growing chain originate from Ni-coordination site *cis* to the P-atom of the ligand have higher activation barriers than the corresponding second insertions where the growing polymer chain is *trans* to the P-atom (Figure S9.6 (a)). Again, we hypothesize that the initial catalyst **1** having growing polymer chain *cis* to the P-atom of the ligand can isomerize to its geometric isomer **1'** where the growing polymer chain is *trans* to the P-atom of the ligand before first insertion occurs (Figure S9.9). The ethylene insertion product **int2'-et-py** at -2.2 kcal mol<sup>-1</sup> can undergo another isomerization to **int2-et-py**, at 3.2 kcal mol<sup>-1</sup> before the second insertion of ethylene occurs. The isomerization serves to place the growing polymer chain *trans* to the P-atom of the ligand so that it can take advantage of the *trans* effect of the ligand, making the migratory insertion step easier to occur.

In the second insertion of monomer into the first acrylate-inserted product (Figure S9.11 (b)), we note that the insertion of tBA again has a lower barrier (**ts3'-ac-ac**, at 27.1 kcal mol<sup>-1</sup>), by 1.2 kcal mol<sup>-1</sup>, than the insertion of ethylene (**ts3'-ac-et**, at 28.3 kcal mol<sup>-1</sup>), similar to that observed for the second insertion into first ethylene-inserted product in Figure S9.11 (a). This TS for the tBA insertion into tBA-inserted product (**ts3'-ac-ac**, activation barrier of 30.1 kcal mol<sup>-1</sup>) has a very close activation barrier to TS **ts3-ac-ac** with an activation barrier of 29.7 kcal mol<sup>-1</sup> (Figure S9.6 (b)).

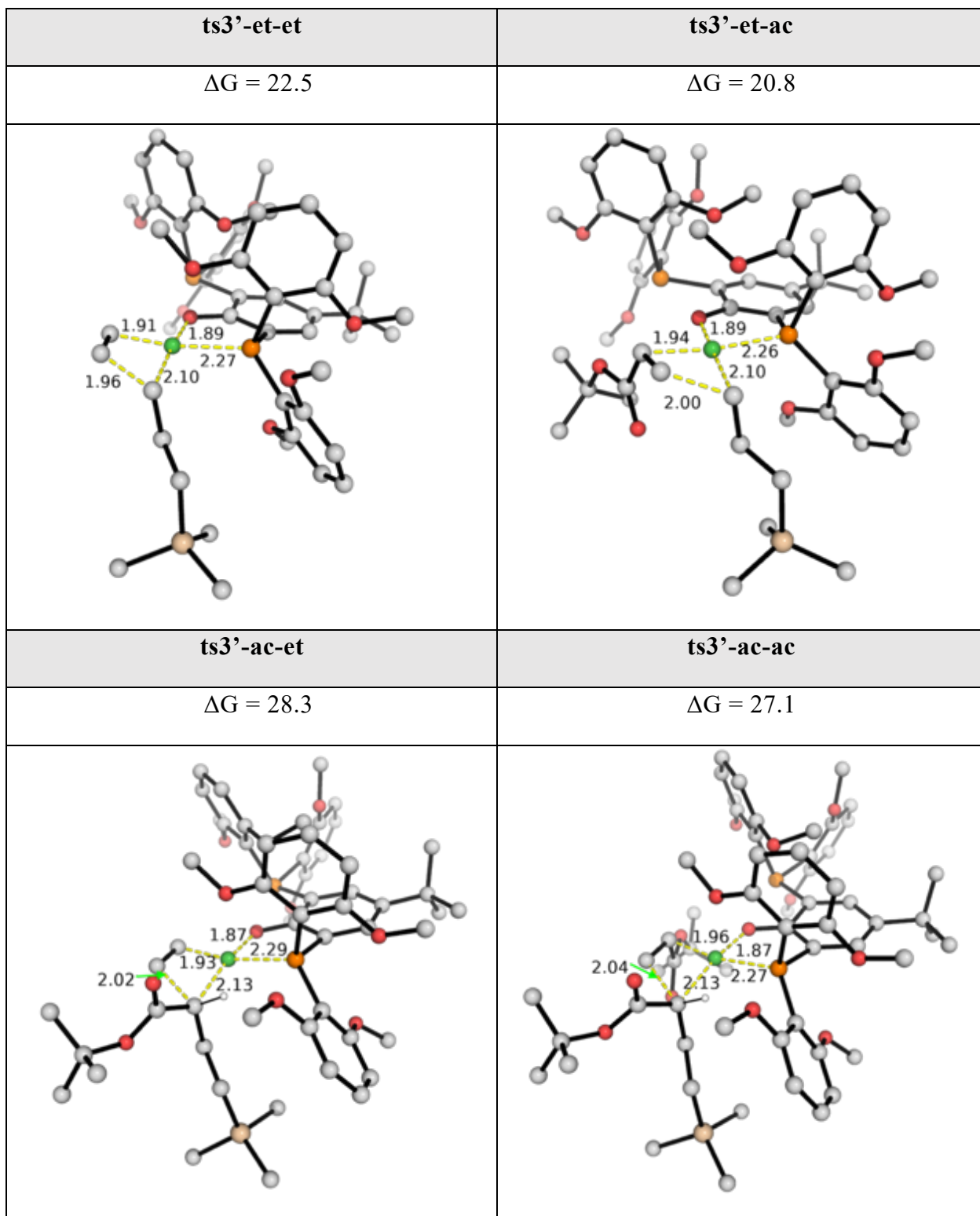


(a) second insertion after first ethylene insertion



(b) second insertion after first acrylate insertion

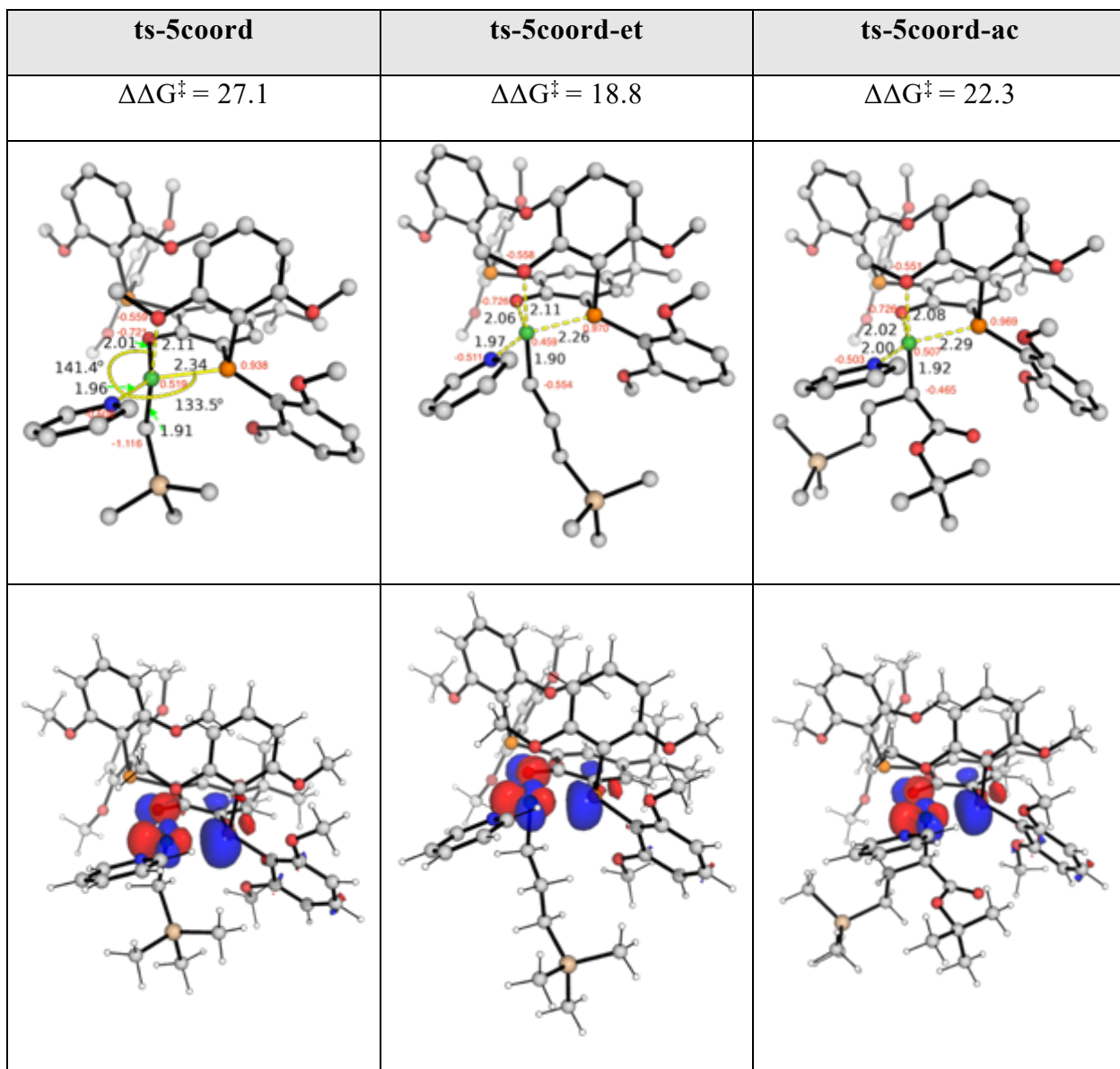
**Figure S9.11.** Gibbs energy profile for the second insertion of ethylene vs *t*-butylacrylate into first inserted product resulting from isomeric catalyst **POP-Ni-py 1'**. The Gibbs energies are calculated at SMD(chlorobenzene)-M06/def2-TZVP//M06/def2-SVP level of theory. The energy of the species **POP-Ni-py (1)** is taken as a reference. (a) Second insertion after first ethylene insertion product and (b) second insertion after first acrylate insertion product.

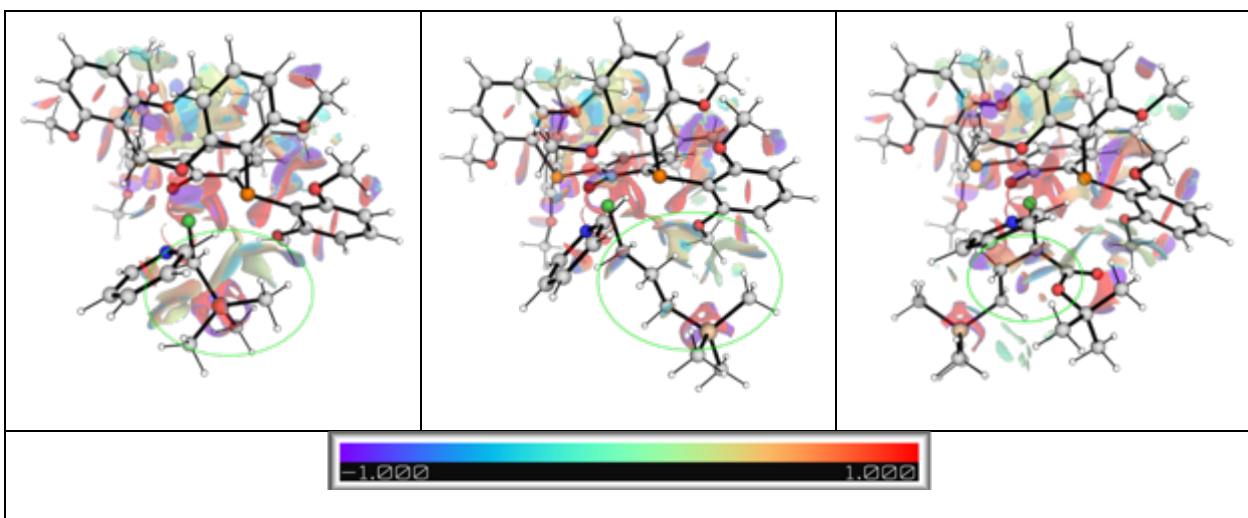


**Figure S9.12.** Optimized TS structures of second insertion of ethylene/tBA into first inserted product arising from isomeric Ni(II) complex **POP-Ni-ac 1'**. Key bond distances are given in Å. Gibbs energy units are given in kcal mol<sup>-1</sup>.

### 9.3 Sterics and electronics effects in key transition states

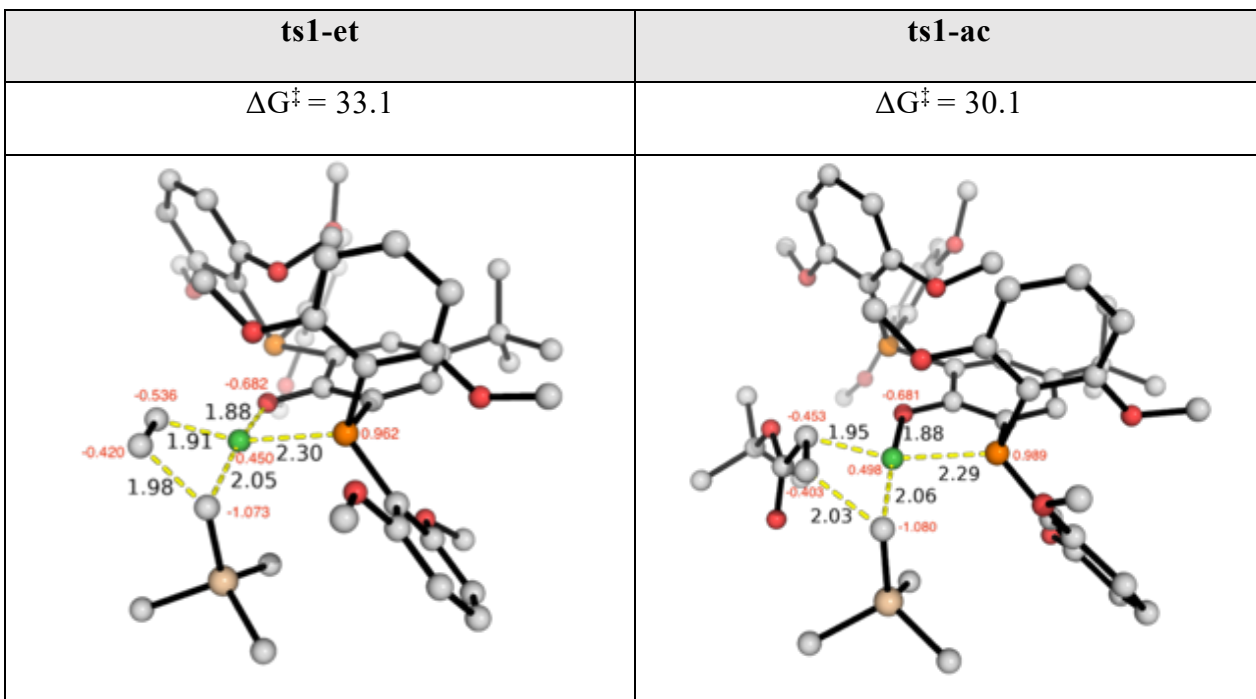
#### 9.3.1 Comparison of sterics and electronics of first and second isomerization

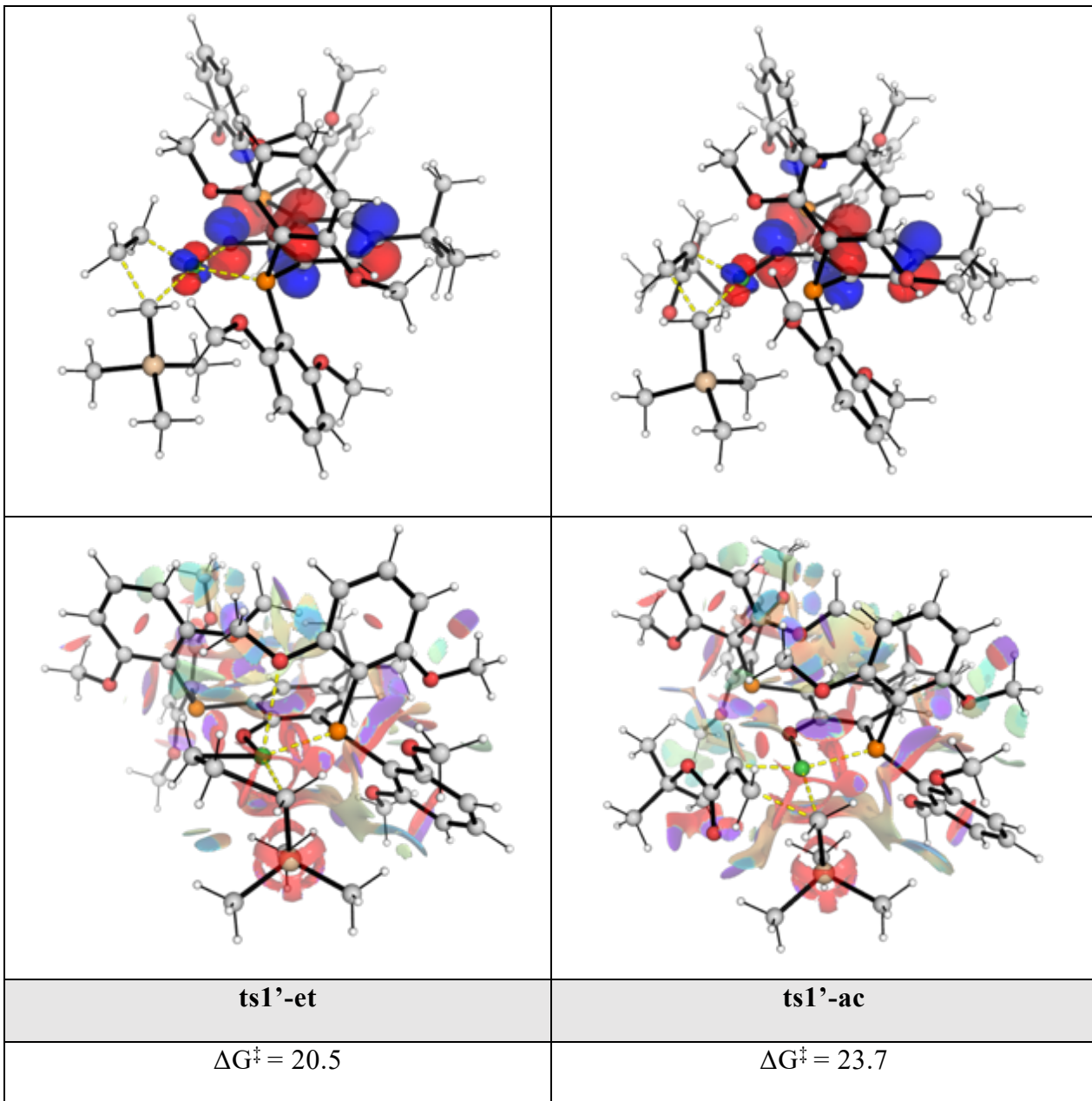


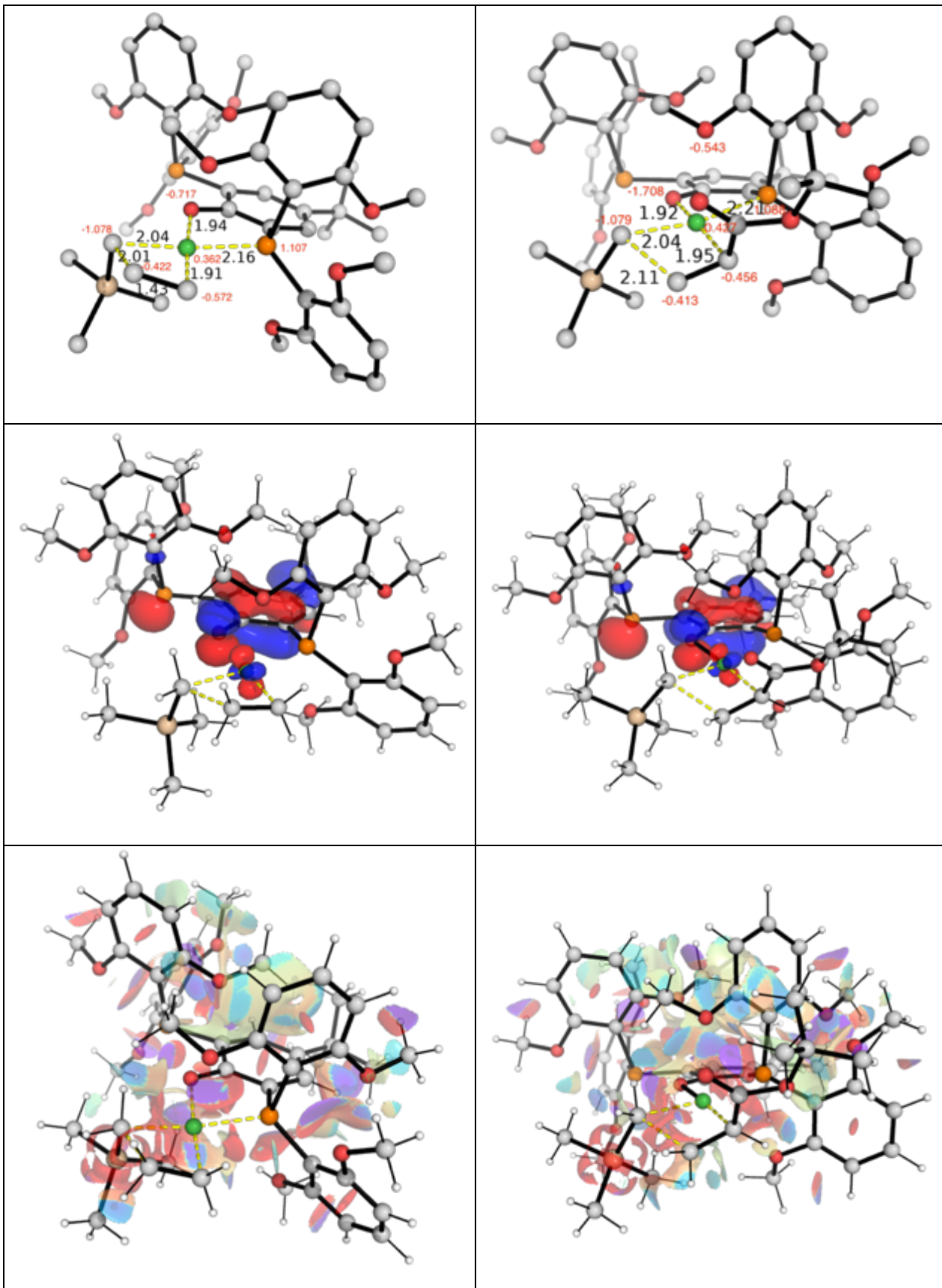


**Figure S9.13.** Optimized TS structures (first row), HOMO (middle row) and NCI plots (last row) for the isomerization of catalyst (**ts-5coord**), the isomerization of first ethylene-insertion product (**ts-5coord-et**) and the isomerization of first tBA-insertion product (**ts-5coord-ac**). Natural bond orbital (NBO) charges are given in red in the first row. Key bond distances are given in Å and angles are given in degrees. Isomerization barriers are given in kcal mol<sup>-1</sup>.

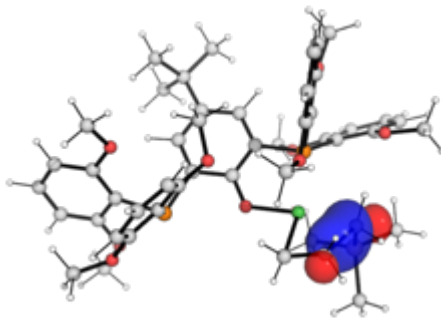
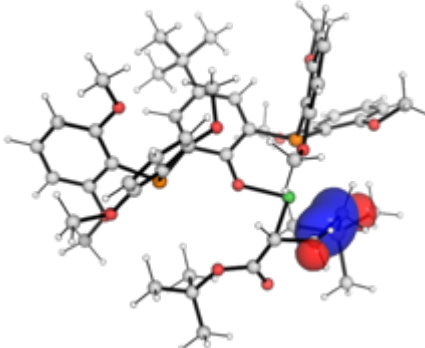
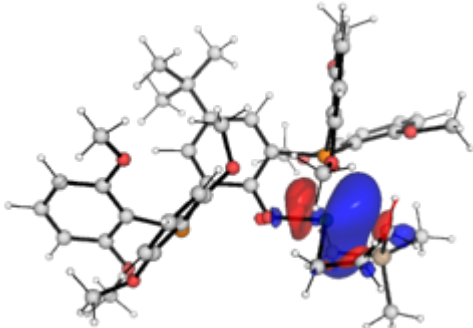
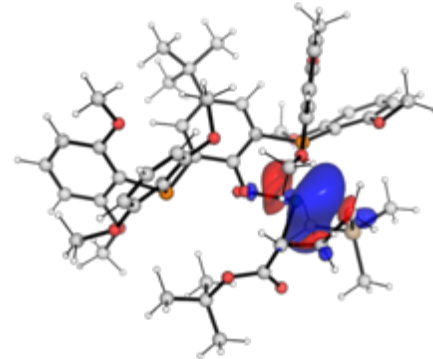
### 9.3.2 Comparison of sterics and electronics of first insertion

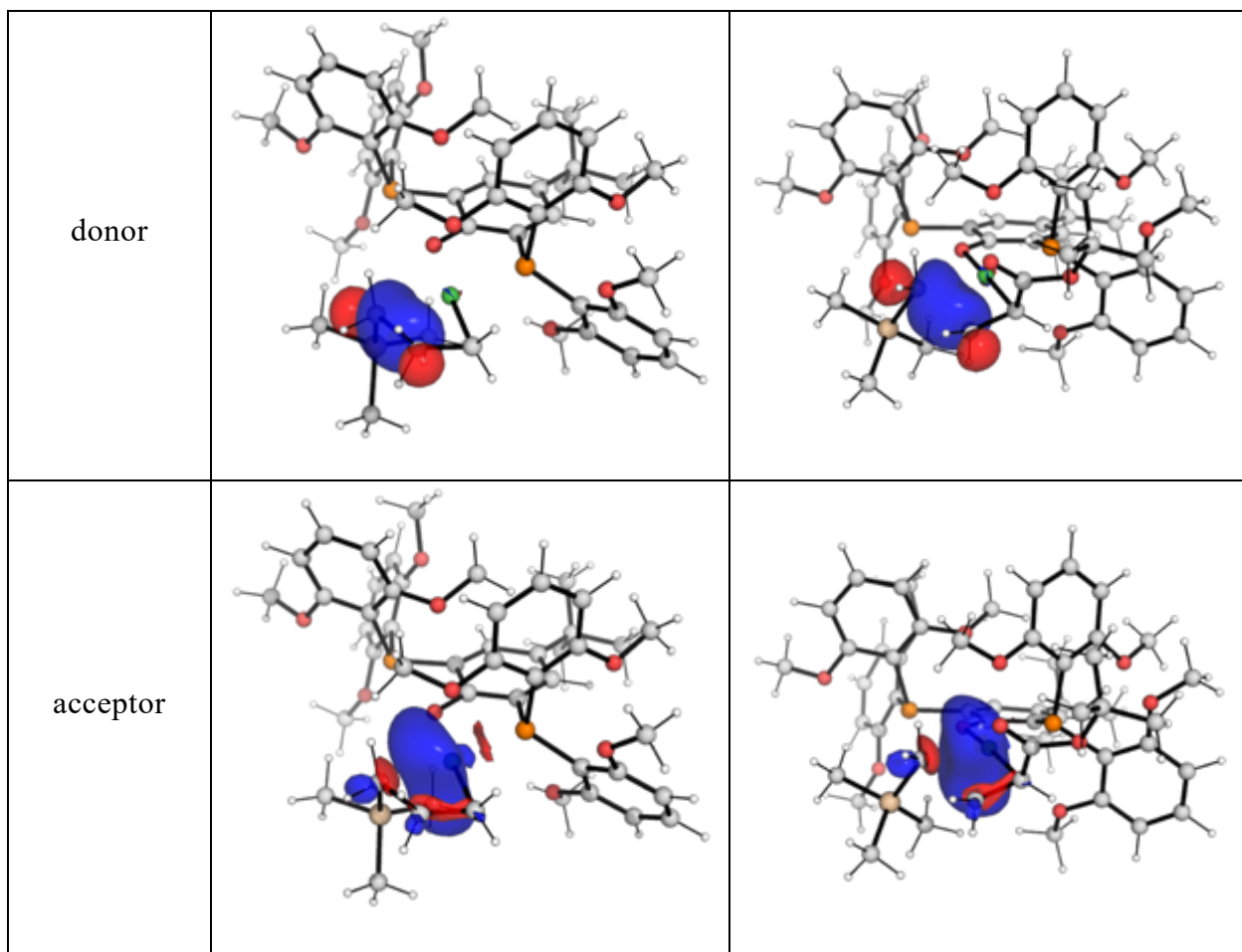






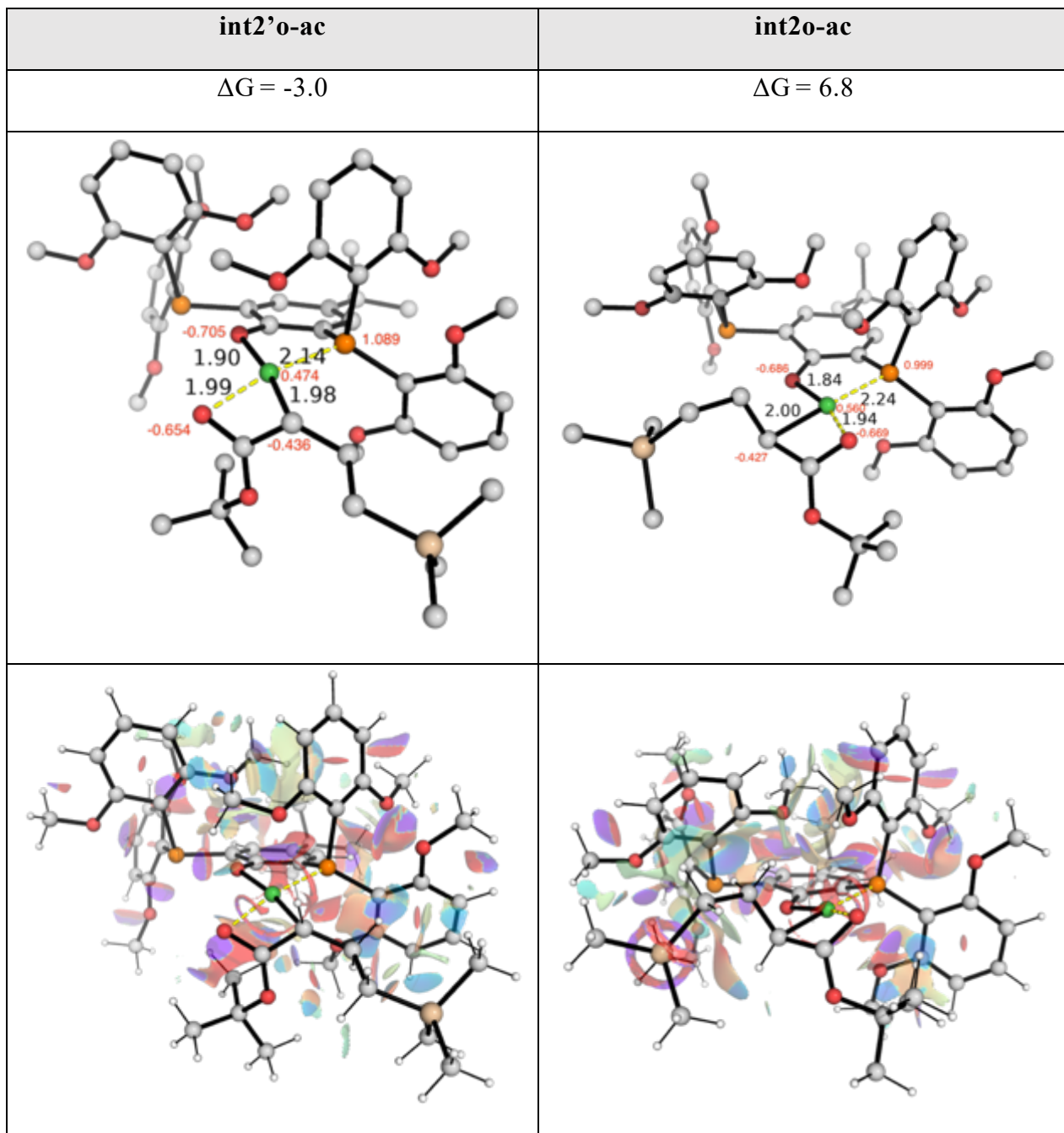
**Figure S9.14.** Optimized TS structures (first row), HOMO (middle row) and NCI plots (last row) for the first insertion into catalyst **1** and **1'**. Natural bond orbital (NBO) charges are given in red in the first row. TS free energies are relative to catalyst **1** and are given in kcal mol<sup>-1</sup>. Key bond distances are given in Å.

	ts1-et	ts1-ac
$\Delta E^{(2)}$	-58.8	-66.2
donor		
acceptor		
	ts1'-et	ts1'-ac
$\Delta E^{(2)}$	-76.8	-89.1

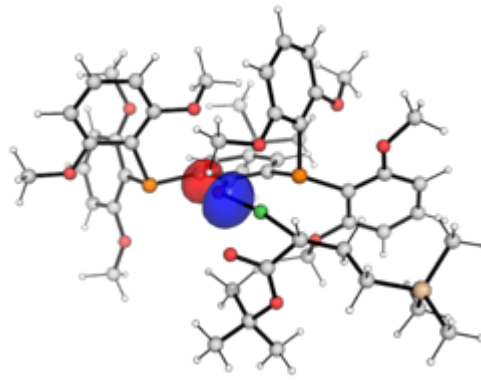
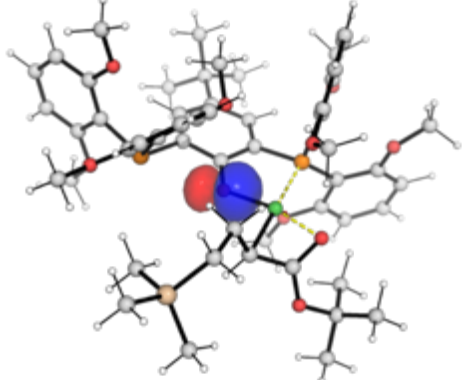
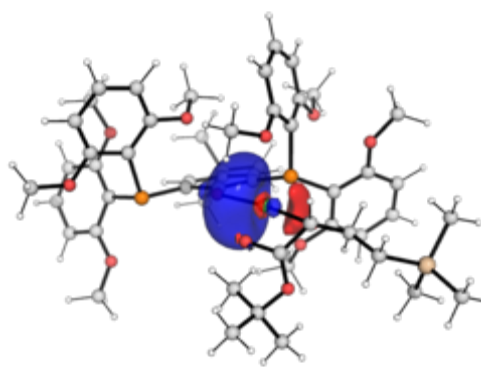
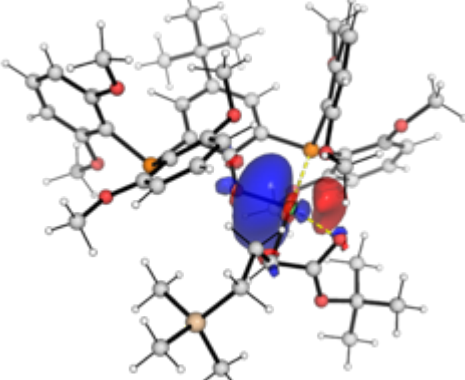


**Figure S9.15.** Natural bonding orbital (NBO) analysis using second-order perturbative stabilization energy ( $\Delta E^{(2)}$ ), which gives the dominant bonding interactions between the nascently formed C–C  $\sigma$ -bond and the metal (Ni d\* orbital). Energies are given in kcal mol<sup>-1</sup>.

### 9.3.3 Comparison of sterics and electronics of O-chelates



**Figure S9.16.** Optimized O-chelate structures from catalyst 1 and 1' after first insertion of tBA monomer (first row) and their associated NCI plots (last row). Natural bond orbital (NBO) charges are given in red in the first row. Free energies are relative to catalyst 1 and are given in  $\text{kcal mol}^{-1}$ . Key bond distances are given in Å.

	<b>int2'o-ac</b>	<b>int2o-ac</b>
$\Delta E^{(2)}$	-90.2	-90.7
donor		
acceptor		

**Figure S9.17.** Natural bonding orbital (NBO) analysis using second-order perturbative stabilization energy ( $\Delta E^{(2)}$ ), which gives the dominant bonding interactions between the ligand (O lone pair) and the metal (Ni d\* orbital). Energies are given in kcal mol<sup>-1</sup>.

#### 9.4 Optimized geometries

Geometries of all optimized structures (in .xyz format with their associated energy in Hartrees) are included in a separate folder named *ESI\_final\_structures\_xyz* with an associated README file. All these data have been deposited with this Supporting Information and uploaded to zenodo.org (DOI: 10.5281/zenodo.4593551).

## 9.5 Absolute energies, zero-point energies

Absolute values (in Hartrees) for SCF energy, zero-point vibrational energy (ZPE), enthalpy (H), entropy (T.S), Gibbs energy (G) and quasi-harmonic Gibbs energy (qh-G) (at 363K) for optimized structures are given below. Single point corrections in SMD chlorobenzene (PhCl) using M06/def2-TZVPP is also included.

Structure	E/au	ZPE/au	H/au	T.S/au	G/au	qh-G/au	SP M06 (PhCl)
<b>pyridine</b>	-247.909697	0.088228	-247.81546	0.032832	-247.848294	-247.848297	-248.1904562
<b>acrylate</b>	-423.819507	0.17752	-423.62895	0.04875	-423.677704	-423.676995	-424.3033801
<b>ethylene</b>	-78.455265	0.050271	-78.400563	0.02478	-78.425344	-78.425344	-78.54851714
<b>1</b>	-5189.241603	1.036085	-5188.1233	0.198768	-5188.3221	-5188.305872	-5192.797515
<b>1-c2</b>	-5189.236897	1.036548	-5188.1183	0.197557	-5188.31588	-5188.3003	-5192.782739
<b>1a</b>	-5189.212702	1.034707	-5188.0954	0.199746	-5188.29511	-5188.279103	-5192.765101
<b>1b</b>	-5189.185522	1.034698	-5188.0679	0.205235	-5188.27313	-5188.253497	-5192.75056
<b>1c</b>	-5189.186621	1.035603	-5188.0688	0.200136	-5188.26894	-5188.25173	-5192.748144
<b>1d</b>	-5189.194589	1.034687	-5188.0778	0.196656	-5188.27445	-5188.259757	-5192.744988
<b>1e</b>	-5189.196931	1.034702	-5188.0798	0.200321	-5188.28009	-5188.263164	-5192.75054
<b>1'</b>	-5189.231303	1.036112	-5188.1132	0.197377	-5188.31058	-5188.295063	-5192.791076
<b>1'-c2</b>	-5189.23134	1.03661	-5188.113	0.196555	-5188.30957	-5188.29421	-5192.791052
<b>1-et</b>	-5267.706362	1.088281	-5266.5311	0.209256	-5266.7404	-5266.723044	-5271.353245
<b>1'-et</b>	-5267.694985	1.091389	-5266.5188	0.201332	-5266.72017	-5266.705166	-5271.333264
<b>1-5coord</b>	-5189.242184	1.037125	-5188.1233	0.196911	-5188.32024	-5188.304669	-5192.796841
<b>ts-5coord</b>	-5189.199468	1.035075	-5188.0832	0.194773	-5188.27798	-5188.263332	-5192.754707

<b>ts-5coord-c2</b>	-5189.201204	1.036326	-5188.0839	0.195138	-5188.27908	-5188.26383	-5192.75408
<b>ts-tet</b>	-5189.18503	1.033482	-5188.069	0.201988	-5188.27094	-5188.253244	-5192.744506
<b>ts-tet-c2</b>	-5189.184899	1.034553	-5188.0682	0.200527	-5188.26873	-5188.251449	-5192.744486
<b>1-3coord</b>	-4941.274167	0.944664	-4940.2542	0.184598	-4940.43882	-4940.423931	-4944.560212
<b>ts-3coord</b>	-4941.235107	0.943599	-4940.2156	0.18711	-4940.40269	-4940.387171	-4944.526758
<b>1'-3coord</b>	-4941.267226	0.945768	-4940.2459	0.184686	-4940.43058	-4940.416053	-4944.555098
<b>int1-et-c1</b>	-5019.769048	0.999264	-5018.6903	0.192846	-5018.88313	-5018.867915	-5023.13828
<b>int1-et-c2</b>	-5019.755394	0.999292	-5018.6765	0.193086	-5018.86955	-5018.854351	-5023.128822
<b>ts1-et</b>	-5019.732137	0.99937	-5018.6543	0.190634	-5018.84495	-5018.829914	-5023.100743
<b>int2-et-5m</b>	-5019.759654	1.001171	-5018.6801	0.189694	-5018.86977	-5018.855275	-5023.127892
<b>int2-et</b>	<b>-5019.774032</b>	<b>1.000902</b>	<b>-5018.6949</b>	<b>0.190244</b>	<b>-5018.88517</b>	<b>-5018.870031</b>	<b>-5023.143109</b>
<b>int2-et-py</b>	-5267.720861	1.091861	-5266.5437	0.205831	-5266.74954	-5266.732392	-5271.363807
<b>int3-et-et</b>	-5098.259105	1.056309	-5097.121	0.196427	-5097.31747	-5097.302357	-5101.713874
<b>ts3-et-et</b>	-5098.254169	1.056623	-5097.1167	0.193558	-5097.31023	-5097.296119	-5101.707965
<b>int4-et-et-</b>							
<b>5m</b>	-5098.286035	1.059077	-5097.1461	0.193002	-5097.33914	-5097.325121	-5101.736877
<b>int4-et-et</b>	-5098.278376	1.057475	-5097.1391	0.201245	-5097.34036	-5097.322692	-5101.740405
<b>int4-et-et-py</b>	-5346.233736	1.147978	-5344.9972	0.215569	-5345.2128	-5345.193162	-5349.963406
<b>int3-et-ac-</b>							
<b>o1</b>	-5443.613849	1.181021	-5442.3407	0.218123	-5442.55883	-5442.541496	-5447.455874
<b>ts3-et-ac-c2</b>	-5443.629067	1.18354	-5442.3555	0.211645	-5442.56719	-5442.551629	-5447.467354
<b>int3-et-ac</b>	-5443.634197	1.184165	-5442.3597	0.211941	-5442.57163	-5442.556291	-5447.471049

<b>ts3-et-ac</b>	-5443.632409	1.183665	-5442.3589	0.211135	-5442.57005	-5442.554611	-5447.469085
<b>int4-et-ac-</b>							
<b>5m</b>	-5443.666668	1.185743	-5442.3908	0.211901	-5442.60274	-5442.58715	-5447.502749
<b>int4-et-ac</b>	-5443.663361	1.182787	-5442.3889	0.2225	-5442.61135	-5442.591162	-5447.507477
<b>int4o-et-ac</b>							
<b>py</b>	-5691.613601	1.275918	-5690.2402	0.234284	-5690.47448	-5690.452908	-5695.726293
<b>int1-ac-o1</b>	-5365.14382	1.126406	-5363.929	0.20859	-5364.13755	-5364.122284	-5368.896838
<b>int1-ac-o2</b>	-5365.139406	1.126901	-5363.9242	0.209643	-5364.13388	-5364.117481	-5368.895341
<b>int1-ac-c2</b>	-5365.14134	1.127254	-5363.9264	0.206149	-5364.13255	-5364.117725	-5368.892272
<b>int1-ac-c1</b>	-5365.137787	1.126468	-5363.9227	0.211357	-5364.13409	-5364.116908	-5368.892686
<b>int1-ac-c4</b>	-5365.124659	1.127448	-5363.9095	0.206261	-5364.11579	-5364.101063	-5368.877123
<b>ts1-ac-r</b>	-5365.095363	1.125928	-5363.8818	0.209193	-5364.09102	-5364.074341	-5368.848503
<b>int2-ac-r-</b>							
<b>5m</b>	-5365.122976	1.126293	-5363.9083	0.212228	-5364.12057	-5364.102883	-5368.876551
<b>int2-ac-r</b>	-5365.140289	1.129117	-5363.9245	0.205681	-5364.13022	-5364.114439	-5368.898534
<b>int2o-ac-r</b>	-5365.151173	1.128006	-5363.9356	0.208853	-5364.14442	-5364.127689	-5368.905791
<b>int1-ac-c3</b>	-5365.132432	1.12721	-5363.9174	0.20718	-5364.12455	-5364.109338	-5368.884794
<b>ts1-ac</b>	-5365.117188	1.126246	-5363.9033	0.20831	-5364.11158	-5364.095714	-5368.866499
<b>int2-ac-5m</b>	-5365.145081	1.129101	-5363.9289	0.206478	-5364.1354	-5364.119609	-5368.892552
<b>int2-ac</b>	-5365.150976	1.128597	-5363.935	0.20689	-5364.14186	-5364.126473	-5368.903844
<b>int2o-ac</b>	-5365.152768	1.128034	-5363.9367	0.209688	-5364.14642	-5364.129761	-5368.905835
<b>int2-ac-py</b>	-5613.11037	1.218904	-5611.7974	0.222257	-5612.01966	-5612.001677	-5617.134478

<b>int3-ac-et</b>	-5443.631637	1.183465	-5442.3573	0.214522	-5442.5718	-5442.555477	-5447.473936
<b>ts3-ac-et</b>	-5443.619682	1.183437	-5442.3462	0.212359	-5442.55852	-5442.542498	-5447.461815
<b>ts3-ac-et-c2</b>	-5443.6109	1.184377	-5442.3369	0.209489	-5442.54643	-5442.531757	-5447.448411
<b>int4-ac-et-</b>							
<b>5m</b>	-5443.663307	1.184668	-5442.3881	0.213211	-5442.60126	-5442.585479	-5447.500983
<b>int4-ac-et</b>	-5443.645335	1.181883	-5442.3726	0.22009	-5442.59264	-5442.572673	-5447.492232
<b>int4o-ac-et</b>	-5443.674743	1.186755	-5442.3989	0.207929	-5442.60685	-5442.592145	-5447.512689
<b>int4-ac-et-</b>							
<b>py</b>	-5691.603271	1.274271	-5690.2308	0.238781	-5690.46956	-5690.445934	-5695.723481
<b>int3-ac-ac</b>	-5789.00125	1.308686	-5787.5919	0.234642	-5787.82652	-5787.808407	-5793.22464
<b>ts3-ac-ac</b>	-5788.997784	1.309946	-5787.5885	0.229713	-5787.81824	-5787.801633	-5793.221201
<b>ts3-ac-ac-c2</b>	-5788.99554	1.309709	-5787.5861	0.232168	-5787.81826	-5787.800354	-5793.220172
<b>ts3-ac-ac-c3</b>	-5788.983713	1.310518	-5787.5739	0.23197	-5787.80589	-5787.787367	-5793.206716
<b>int4-ac-ac-</b>							
<b>5m</b>	-5789.029337	1.311337	-5787.618	0.232981	-5787.85102	-5787.832913	-5793.256034
<b>int4-ac-ac</b>	-5789.037769	1.311353	-5787.6271	0.231676	-5787.85875	-5787.840622	-5793.262425
<b>int4o-ac-ac</b>	-5789.057057	1.313791	-5787.645	0.226446	-5787.87144	-5787.855275	-5793.275367
<b>int4-ac-ac-</b>							
<b>py</b>	-6036.986375	1.401863	-6035.4776	0.251979	-6035.72956	-6035.706971	-6041.486186
<b>int1'-ac-o1</b>	-5365.123621	1.125321	-5363.9096	0.211759	-5364.12132	-5364.103989	-5368.880059
<b>int1'-ac-o2</b>	-5365.119695	1.125119	-5363.9058	0.210161	-5364.11599	-5364.099864	-5368.876718
<b>int1'-ac-c1</b>	-5365.136514	1.125243	-5363.9225	0.210529	-5364.13305	-5364.116795	-5368.889853
<b>int1'-ac-c2</b>	-5365.135934	1.127289	-5363.9208	0.206553	-5364.12738	-5364.112707	-5368.887566

<b>int1'-ac-c3</b>	-5365.129584	1.126723	-5363.9147	0.211079	-5364.12577	-5364.108177	-5368.884062
<b>ts1'-ac-r</b>	-5365.118221	1.12636	-5363.9044	0.208669	-5364.11311	-5364.096233	-5368.871442
<b>int2'-ac-r-</b>							
<b>5m</b>	-5365.141155	1.128051	-5363.9255	0.209702	-5364.13519	-5364.117982	-5368.894135
<b>int2'-ac-r</b>	-5365.142024	1.129869	-5363.9253	0.20607	-5364.13142	-5364.115458	-5368.89758
<b>int2'o-ac-r</b>	-5365.161022	1.128933	-5363.9447	0.20854	-5364.15325	-5364.136533	-5368.919239
<b>int1'-ac-c4</b>	-5365.132373	1.127515	-5363.9171	0.207739	-5364.12482	-5364.109235	-5368.88387
<b>ts1'-ac</b>	-5365.128369	1.127405	-5363.9139	0.205761	-5364.11964	-5364.10461	-5368.879545
<b>ts1'-ac-c2</b>	-5365.13104	1.128037	-5363.9163	0.20397	-5364.12024	-5364.105858	-5368.880289
<b>int2'-ac-5m</b>	-5365.159411	1.128809	-5363.943	0.207833	-5364.15084	-5364.135078	-5368.91004
<b>int2'-ac</b>	-5365.159959	1.128007	-5363.9443	0.208652	-5364.15294	-5364.136532	-5368.912959
<b>int2'o-ac</b>	-5365.167805	1.127878	-5363.9518	0.211468	-5364.16327	-5364.145649	-5368.920537
<b>int2'-ac-py</b>	-5613.113548	1.218963	-5611.8	0.225777	-5612.0258	-5612.006061	-5617.140639
<b>ts-5coord-ac</b>	-5613.072434	1.216883	-5611.7611	0.226015	-5611.98715	-5611.967451	-5617.096872
<b>int3'-ac-et</b>	-5443.626601	1.182244	-5442.3525	0.218262	-5442.57076	-5442.552981	-5447.468885
<b>ts3'-ac-et</b>	-5443.598075	1.181525	-5442.3256	0.216397	-5442.54195	-5442.524543	-5447.4407
<b>int4'-ac-et-</b>							
<b>5m</b>	-5443.629021	1.183632	-5442.3544	0.216486	-5442.57087	-5442.553354	-5447.470218
<b>int4'-ac-et</b>	-5443.634584	1.18283	-5442.3603	0.221897	-5442.5822	-5442.561955	-5447.481968
<b>int4'o-ac-et</b>	-5443.64984	1.183962	-5442.3749	0.219313	-5442.5942	-5442.574868	-5447.493738
<b>int4'-ac-et-</b>							
<b>py</b>	-5691.588782	1.275829	-5690.2158	0.232709	-5690.44847	-5690.427263	-5695.707557

<b>int3'-ac-ac</b>	-5789.004047	1.310423	-5787.5935	0.232865	-5787.82635	-5787.808218	-5793.226696
<b>ts3'-ac-ac</b>	-5788.981456	1.309115	-5787.5723	0.234356	-5787.80663	-5787.78763	-5793.205127
<b>int4'-ac-ac-</b>							
<b>5m</b>	-5789.012895	1.310839	-5787.6026	0.232658	-5787.83529	-5787.816658	-5793.234135
<b>int4'-ac-ac</b>							
<b>int4'o-ac-ac</b>	-5789.017714	1.310426	-5787.6071	0.236439	-5787.84356	-5787.823463	-5793.243263
<b>int4'o-ac-ac</b>	-5789.034041	1.311631	-5787.6225	0.235154	-5787.8577	-5787.838042	-5793.253317
<b>int4'-ac-ac-</b>							
<b>py</b>	-6036.974438	1.402495	-6035.4657	0.249163	-6035.71486	-6035.693067	-6041.474135
<b>int1'-et-c1</b>	-5019.76831	0.998667	-5018.6903	0.191812	-5018.88207	-5018.86728	-5023.133637
<b>int1'-et-c2</b>	-5019.761944	0.999589	-5018.6833	0.191266	-5018.87456	-5018.859808	-5023.130173
<b>ts1'-et</b>	-5019.752934	0.998849	-5018.6755	0.191288	-5018.86675	-5018.851419	-5023.120112
<b>int2'-et-5m</b>	-5019.776492	1.000064	-5018.6974	0.1929	-5018.89025	-5018.874367	-5023.143195
<b>int2'-et</b>	-5019.783341	1.000021	-5018.7043	0.193669	-5018.89794	-5018.881715	-5023.151533
<b>int2'-et-c1</b>	-5019.780706	1.000697	-5018.7014	0.191526	-5018.89294	-5018.877463	-5023.152537
<b>int2'-et-c2</b>	-5019.780994	1.000541	-5018.7018	0.19144	-5018.89321	-5018.877944	-5023.148888
<b>int2'-et-py</b>	-5267.730378	1.092304	-5266.553	0.206432	-5266.75943	-5266.741747	-5271.372532
<b>ts-5coord-et</b>	-5267.699152	1.091151	-5266.5236	0.204065	-5266.72767	-5266.7107	-5271.342345
<b>int3'-et-et</b>	-5098.268091	1.055728	-5097.1302	0.197407	-5097.32765	-5097.31252	-5101.722032
<b>ts3'-et-et</b>	-5098.232948	1.056302	-5097.0954	0.196573	-5097.29193	-5097.276314	-5101.690656
<b>int4'-et-et-</b>							
<b>5m</b>	-5098.263033	1.056901	-5097.1243	0.197586	-5097.32192	-5097.306427	-5101.71945
<b>int4'-et-et</b>	-5098.268635	1.055862	-5097.1305	0.204279	-5097.33474	-5097.315819	-5101.731631

**int4'-et-et-**

<b>py</b>	-5346.223791	1.149681	-5344.9866	0.209814	-5345.19644	-5345.179198	-5349.957613
-----------	--------------	----------	------------	----------	-------------	--------------	--------------

**int3'-et-ac**

<b>int3'-et-ac</b>	-5443.630788	1.183882	-5442.3561	0.2133	-5442.56941	-5442.553492	-5447.470966
--------------------	--------------	----------	------------	--------	-------------	--------------	--------------

<b>ts3'-et-ac</b>	-5443.617916	1.183706	-5442.344	0.213136	-5442.55709	-5442.540818	-5447.456116
-------------------	--------------	----------	-----------	----------	-------------	--------------	--------------

**int4'-et-ac-**

<b>5m</b>	-5443.647073	1.184454	-5442.372	0.214202	-5442.58616	-5442.569823	-5447.484278
-----------	--------------	----------	-----------	----------	-------------	--------------	--------------

<b>int4'-et-ac</b>	-5443.650879	1.184302	-5442.3758	0.217637	-5442.59342	-5442.575112	-5447.494123
--------------------	--------------	----------	------------	----------	-------------	--------------	--------------

<b>int4'o-et-ac</b>	-5443.654172	1.184072	-5442.3789	0.217757	-5442.59663	-5442.578655	-5447.497208
---------------------	--------------	----------	------------	----------	-------------	--------------	--------------

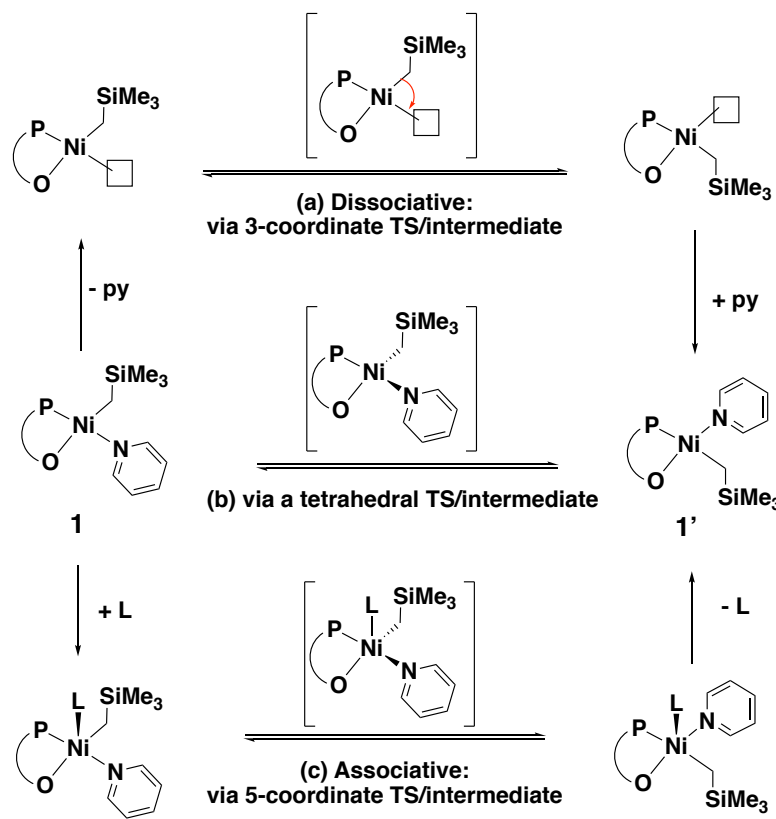
**int4'-et-ac-**

<b>py</b>	-5691.610865	1.275926	-5690.2379	0.229741	-5690.46767	-5690.448546	-5695.719416
-----------	--------------	----------	------------	----------	-------------	--------------	--------------

---

## 10. Computational investigation in isomerization

The isomerization of the square planar catalyst between **POP-Ni-py (1)** and its isomeric form **POP-Ni-py 1'** can occur via one of the three possible mechanisms: associative, dissociative or twisting through a tetrahedral TS and then back to square planar. This step is essential for the insertion of ethylene into the Ni–C bond via the lower TS **ts1'-et**, at 20.5 kcal mol<sup>-1</sup>, rather than via **ts1-et**, at 33.1 kcal mol<sup>-1</sup>. We herein consider these possibilities computationally:



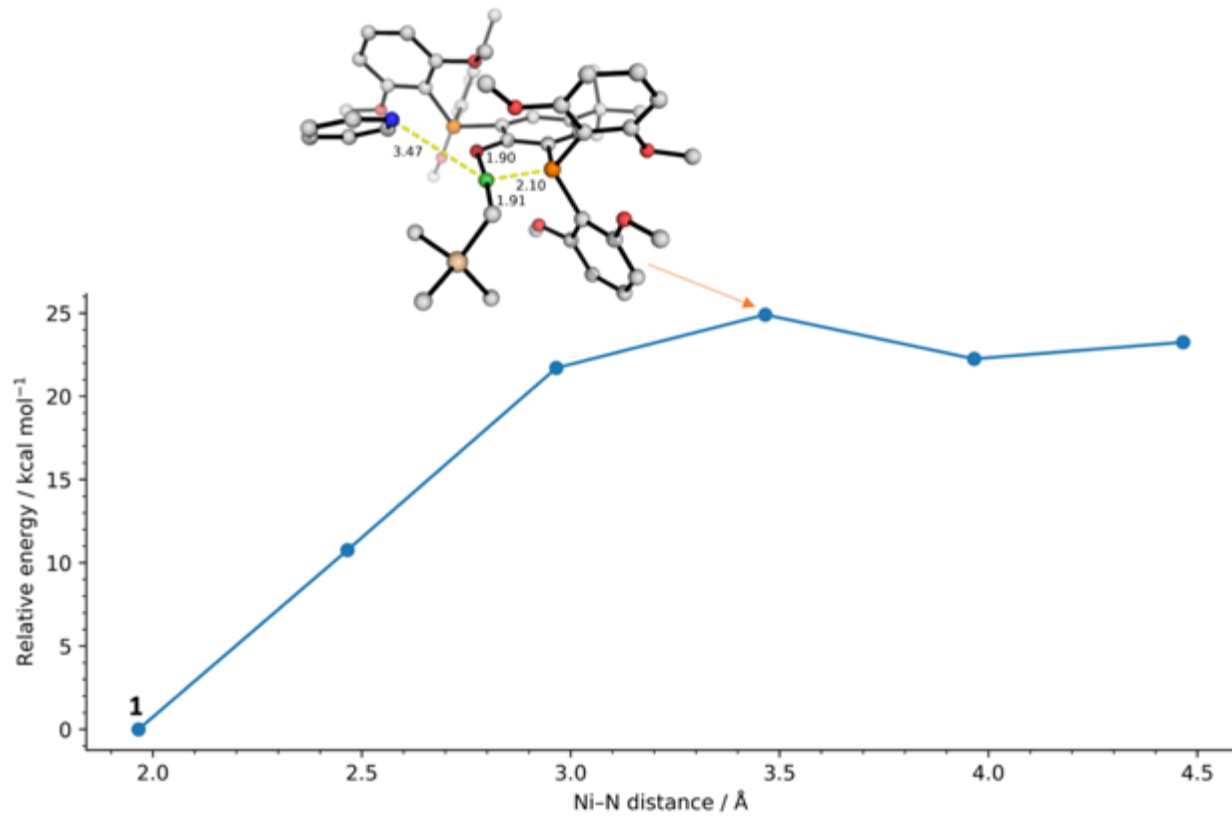
Scheme S10.1. Possible mechanisms of isomerization between two geometric isomeric forms of the Ni-catalyst.

### 10.1 Dissociative mechanism

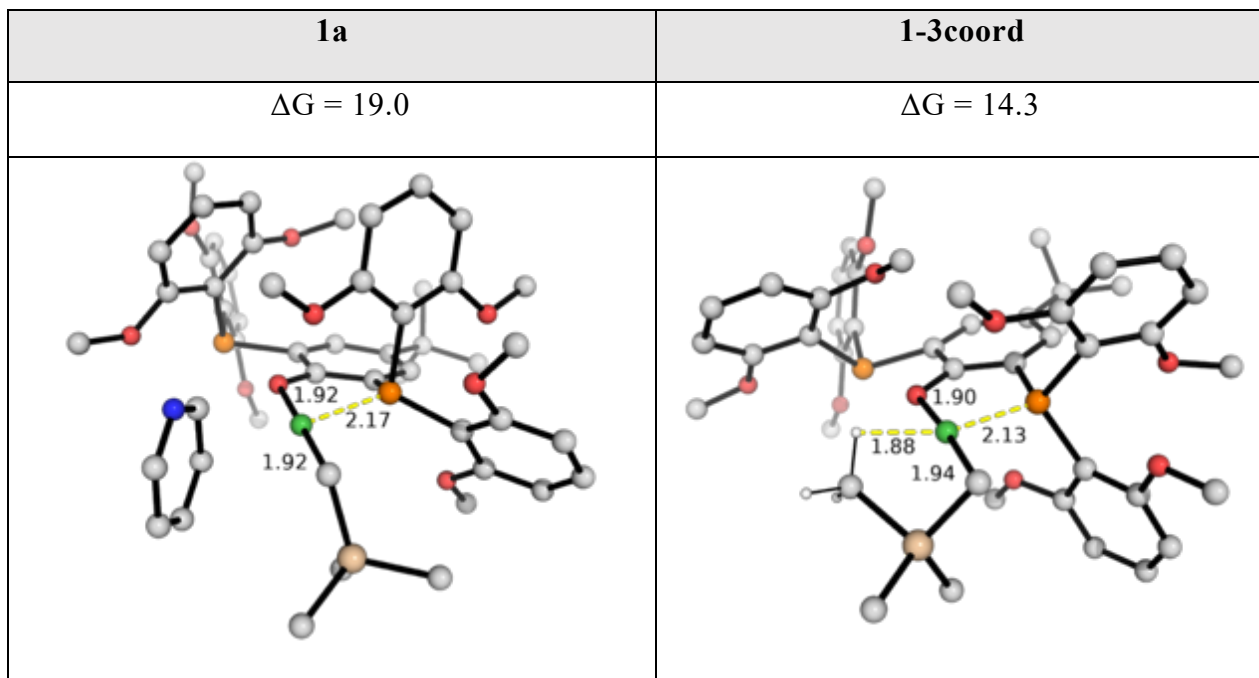
In a dissociative mechanism, the coordinating pyridine ligand leaves, giving a vacant site on Ni metal. Subsequently, the growing polymer chain can isomerize by moving from its original coordinating site to its adjacent, newly vacated coordination site. This is followed by

recoordination of pyridine ligand at the site previously occupied by the growing polymer chain, giving the geometric isomeric form of the catalyst (Scheme S10.1a).

We first try to estimate the barrier to pyridine dissociation by doing a relaxed PES scan along the Ni–N(pyridine) bond. The gas phase energy scan is given in Figure S10.1. We can see that the loss of pyridine ligand is unfavorable and reversible. This is consistent with geometry optimization starting from initial guess structure of long (3.70 Å) Ni–N(pyridine) bond (by manually increasing this distance in catalyst **1** while maintaining the square plane of the Ni-center) which optimized back to catalyst **1**. To obtain the accurate Gibbs energy with solvent correction for the resulting structure after loss of pyridine coordination, we took the structure at point 5 in Figure S10.1 and subjected it to geometry optimization. The final structure, **1a**, is 19.0 kcal mol<sup>-1</sup> uphill (Figure S10.2). This gives the estimate of the dissociation barrier of pyridine as *ca.* 22 kcal mol<sup>-1</sup> (this is nonetheless smaller than the isomerization barrier, *vide infra*). The loss of pyridine from this species, displaced by an agnostic interaction from the C–H group on trimethylsilyl, gives **1-3coord** which is 14.3 kcal mol<sup>-1</sup> uphill (Figure S10.2). This species can further undergo isomerization to give the species **1-3coord** at 18.1 kcal mol<sup>-1</sup> relative to catalyst **Ni-POP-py 1**.



**Figure S10.1.** Relaxed PES scan along phenoxide O-Ni-C angle going from one 3-coordinate isomer to another. Relative energy values are computed at M06/def2-SVP in gas phase and used without further corrections. Key bond distances are given in Å.



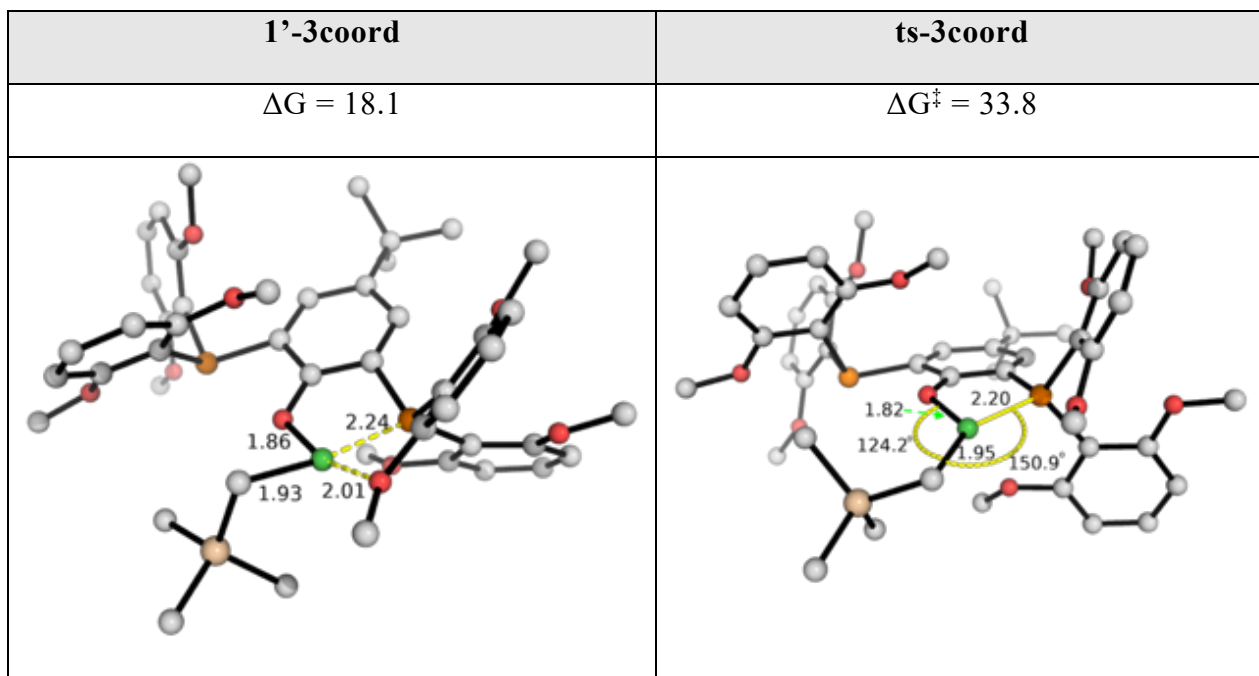


**Figure S10.2.** Optimized structures for the coordination complexes of the isomeric Ni-catalyst **1** and **1'** after losing pyridine coordination to give 3-coordinate species and the TS structure for the isomerization via 3-coordinate TS. The Gibbs energies are calculated relative to **POP-Ni-py** (**1**). Key bond distances are given in Å and angles are given in degrees. Gibbs energy units are given in kcal mol<sup>-1</sup>.

Therefore, the loss of pyridine from catalyst **1** gives **1-3coord**, at 14.3 kcal mol<sup>-1</sup>. We next set out to find the TS for the isomerization from **1-3coord** to **1'-3coord**. We initially tried direct TS search using the guess structure of placing the polymer chain in between the two Ni-coordination sites and QST2 method (in Gaussian 16 software, both *opt=modredundant* and *opt=qst2* methods) to no avail. We can, however, do a relaxed PES scan sweeping out the angle from one geometric isomer to the other to get an estimate of the barrier for such isomerization. This relaxed PES scan in gas phase is given in Figure S10.3, allowing us to estimate that the barrier for the isomerization from **1-3coord** to **1'-3coord** is about 24 kcal mol<sup>-1</sup>. This estimate is valid since the energy difference between **1-3coord** and **1'-3coord** in the gas phase ( $\Delta\Delta E = 4.4$  kcal mol<sup>-1</sup>) is very similar to their Gibbs energy difference in solvent ( $\Delta\Delta G = 3.8$  kcal mol<sup>-1</sup>). Given that species **1-3coord** is 14.3 kcal mol<sup>-1</sup> uphill with respect to **Ni-POP-py** **1**, we estimate that the barrier for isomerization of catalyst **Ni-POP-py** **1** to its geometric isomer **Ni-POP-py** **1'** via a 3-coordinate TS has an upper bound activation barrier

of 38 kcal mol<sup>-1</sup>, which is much higher than the barriers for the migratory insertion of monomer into Ni–C bond of catalyst **Ni-POP-py 1** (Figure S9.4).

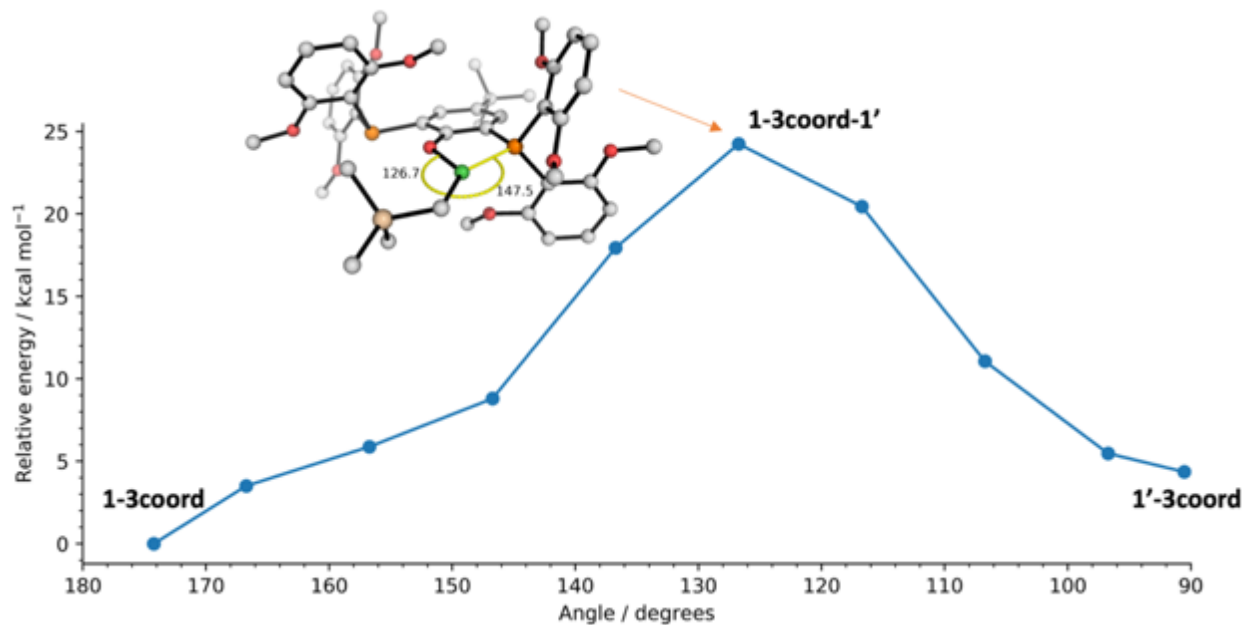


**Figure S10.3.** Relaxed PES scan along phenoxide O–Ni–C angle going from one 3-coordinate isomer to another. Relative energy values are computed at M06/def2-SVP in gas phase and used without further corrections. Key bond distances are given in Å.

Next, we took the structure with the highest energy from this PES scan (Figure S10.3) as an initial guess for the 3-coordination isomerization TS search. We are able to locate the true TS **ts-3coord** (Figure S10.4, verified by IRC) having a barrier of 33.8 kcal mol<sup>-1</sup> relative to the catalyst **Ni-POP-py 1**.

In **1'-3coord** we see that the oxygen atom of an adjacent methoxy group on the ligand can coordinate to the Ni-metal. We wonder if this coordination can displace pyridine ligand in catalyst **1**, thus giving the isomeric **1'**. The optimized structures and their associated energetics are shown in Figure S10.4. The displacement of pyridine ligand by OMe group gives structure **1b**, which is endergonically uphill, at 27.1 kcal mol<sup>-1</sup>. This requires an activation barrier of at least 27.1 kcal mol<sup>-1</sup> and is unfavorable. This is perhaps unsurprising as a strong Ni–N(pyridine) interaction is lost and replaced by a weaker Ni–O(methoxy) interaction.

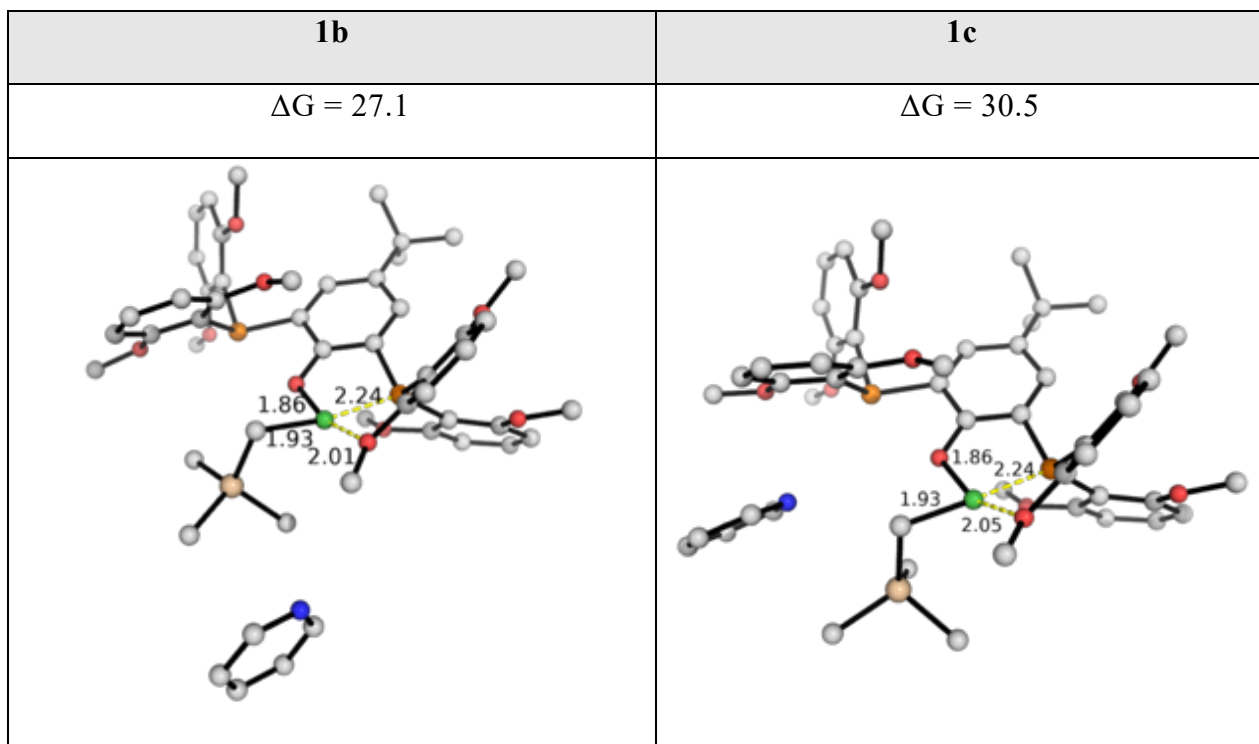


**Figure S10.4.** Optimized structures for the coordination complexes of the isomeric Ni-catalyst **1** and **1'** after losing pyridine coordination to give 3-coordinate species. The Gibbs energies are calculated relative to **POP-Ni-py (1)**. Key bond distances are given in Å. Gibbs energy units are given in kcal mol<sup>-1</sup>.

This dissociative mechanism has an overall barrier of 33.8 kcal mol<sup>-1</sup> which is higher than the isomerization barriers for the other two mechanistic possibilities (*vide infra*) and is thus unlikely for the isomerization of catalyst **1** to its geometric isomer **1'**.

## 10.2 Twisting mechanism via tetrahedral TS/intermediate

A similar dihedral angle scan mapping out one geometric isomer to the other passing through the tetrahedral TS/intermediate, to estimate how big the barrier is, was not successful due to the difficulties in defining the scanning coordinates. However, the direct TS search for the putative TS structure gives two TS conformers, **ts-tet** and **ts-tet-c2**, with the lowest activation barrier of 30.8 kcal mol<sup>-1</sup> (**ts-tet**, Figure S10.5). This TS has been verified to be the true TS for the isomerization via tetrahedral TS using IRC analyses.

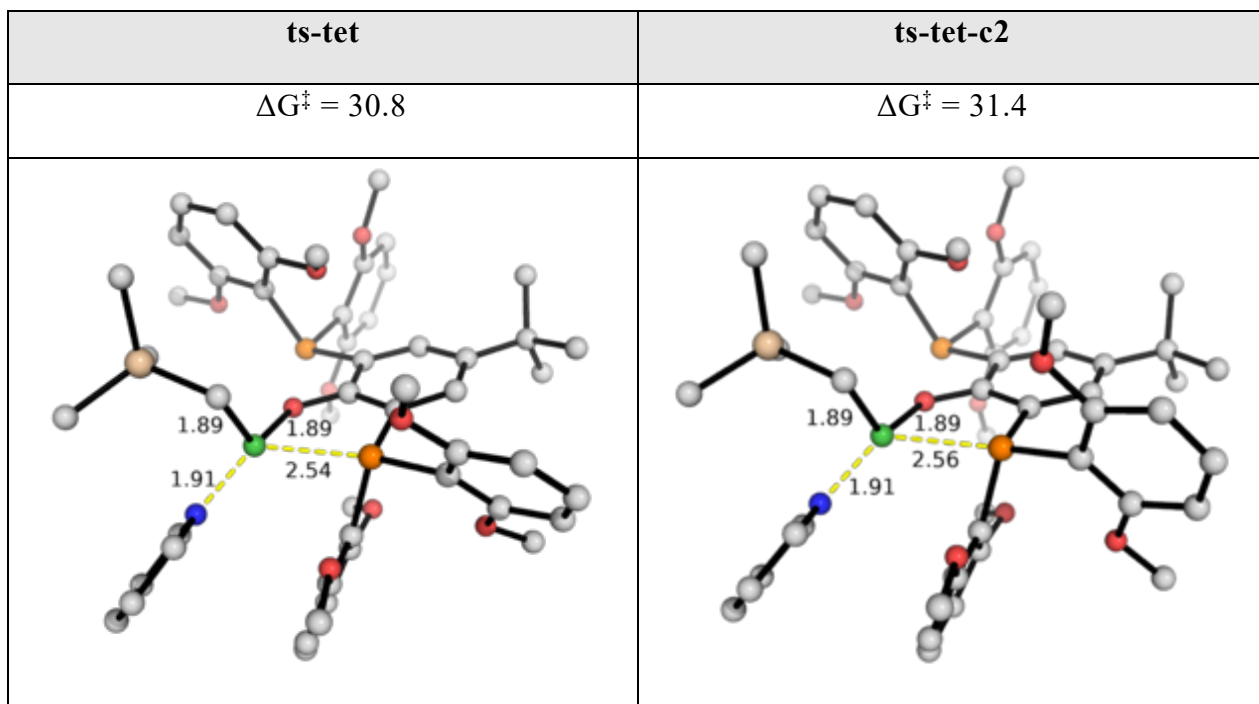


**Figure S10.5.** Optimized TS structures for the isomerization of catalyst **1** to **1'** via tetrahedral transition state. Two TS conformers were found. Key bond distances are given in Å. Gibbs energy units are given in kcal mol<sup>-1</sup>.

### 10.3 Associative mechanism

In an associative mechanism, a fifth ligand coordinates to Ni-center, giving a 5-coordinate species. This can then undergo a Berry pseudorotation to isomerize the catalyst from one geometric isomer to the other, before finally one ligand leaves to give back to the square planar species (Scheme S10.1c).

We first consider if an external ethylene molecule could serve as the fifth ligand by binding to the Ni-center. The direct optimization using ethylene binding to the Ni-center as an initial guess structure did not yield a stable 5-coordinate species. This species **1-et**, with ethylene unbound (Figure S10.6), is 6.6 kcal mol<sup>-1</sup> uphill with respect to the most stable form of the catalyst **Ni-POP-py 1**. This is due to the unfavorable entropic effect associated with bringing in an additional ethylene molecule to the inner coordination shell of the Ni-metal. The absence of a stable 5-coordinate Ni-species with ethylene bound suggest that the coordination of ethylene to form 5-coordinate species is unlikely.

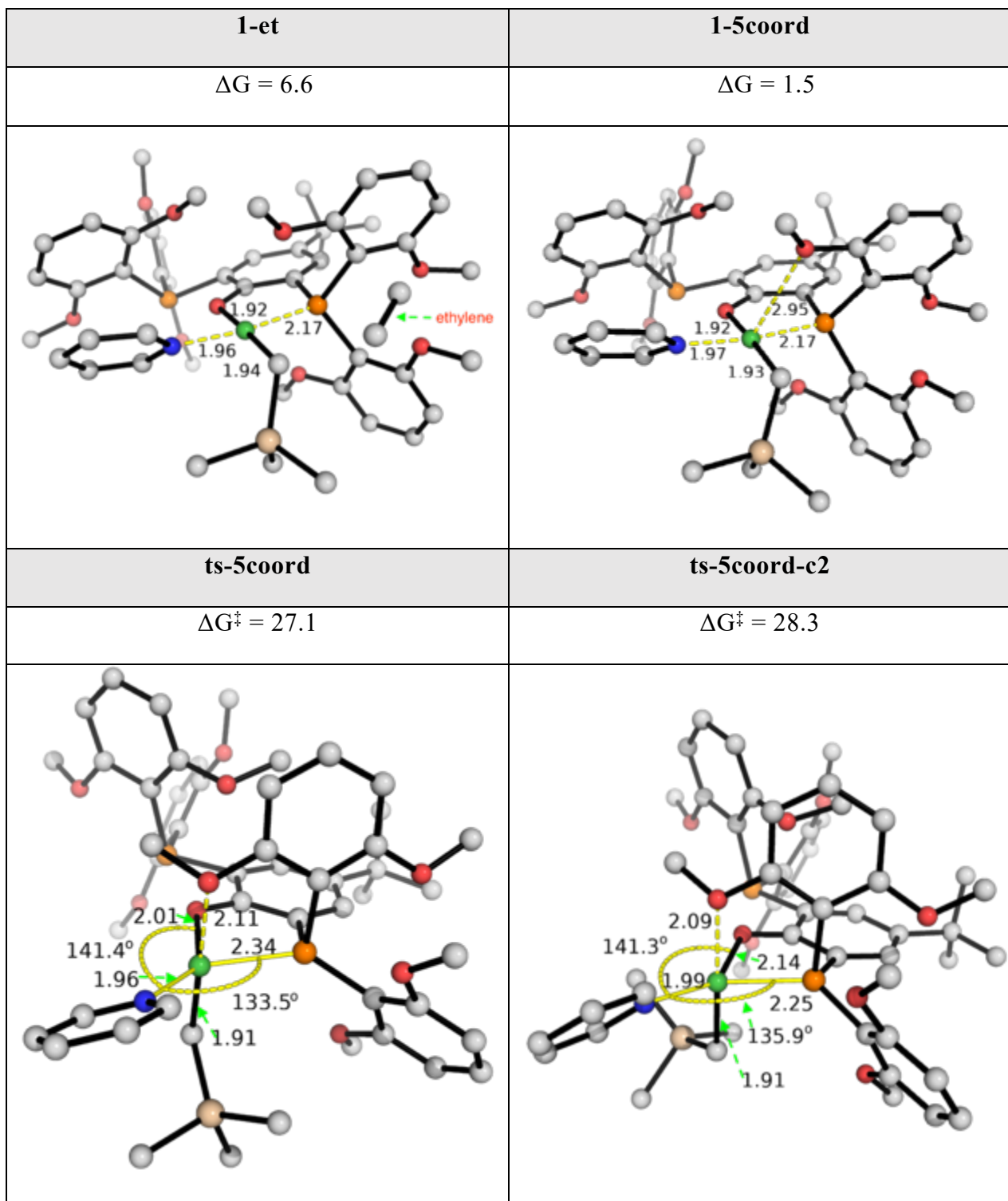


**Figure S10.6.** Optimized structures species involved in isomerization pathway via 5-coordinate Ni-complex. The Gibbs energies are calculated relative to **POP-Ni-py (1)**. Key bond distances are given in Å and angles are given in degrees. Gibbs energy units are given in kcal mol<sup>-1</sup>.

We found that the O-atom of the methoxy group on the ligand can serve as a fifth ligand in coordinating the Ni-center. This species, **1-5coord** (Figure S10.6), is 1.5 kcal mol<sup>-1</sup> higher than catalyst **Ni-POP-py 1** (it is in fact a conformer of catalyst **1**). Two TS conformers for the pseudorotational barriers (**ts-5coord** and **ts-5coord-c2**, Figure S10.6) were found and verified by IRC to be the true TS structures for the isomerization of one catalyst form (catalyst **1**) to its geometric isomer (catalyst **1'**). The lowest energy conformer **ts-5coord** has a barrier of 27.1 kcal mol<sup>-1</sup>, which is lower than the barriers via either 3-coordinate TS (**ts-3coord** at 33.8 kcal mol<sup>-1</sup>, Figure S10.2) or tetrahedral TS (**ts-tet** at 30.8 kcal mol<sup>-1</sup>, Figure S10.5). This is therefore the most likely mechanism: the isomerization of catalyst **Ni-POP-py 1** to its regioisomeric form **Ni-POP-py 1'** occurs via associative mechanism with a proximal OMe group serving as a binding ligand on the fifth coordination site before a pseudoroational TS gives the isomeric catalyst.

#### 10.4 Other possibilities

The loss of P-coordination replaced by methoxy O-coordination was considered. However, the resulting species, **1d** and **1e**, both have very high energy such that their formation is highly endergonic and unfavorable (Figure S10.7). This is perhaps expected as the loss of stronger Ni–P coordination was replaced by weaker Ni–O(methoxy) interaction.

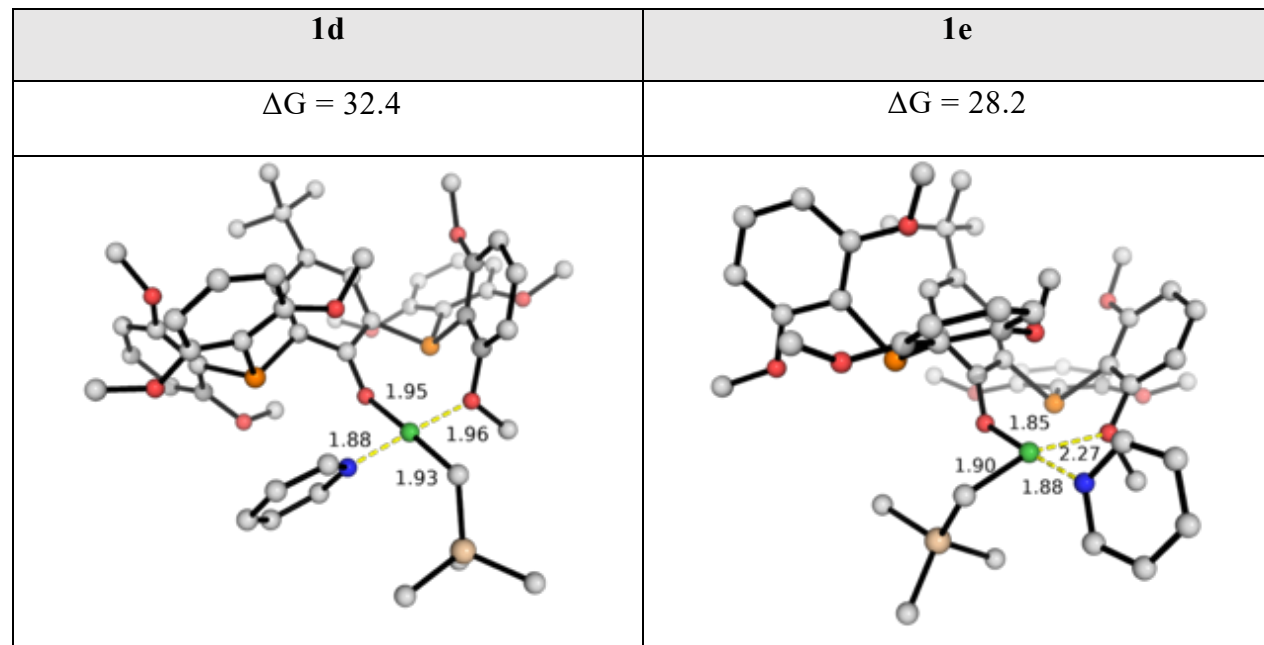
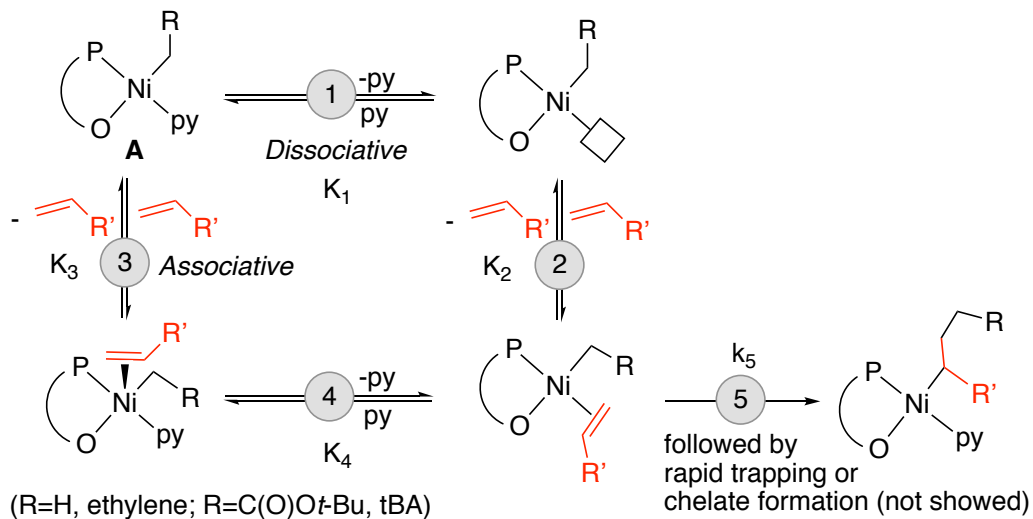


**Figure S10.7.** Optimized structures for the coordination complexes of Ni-catalyst **1** and **1'** where Ni–P interaction is displaced by Ni–O interaction. The Gibbs energies are calculated relative to **POP-Ni-py (1)**. Key bond distances are given in Å. Gibbs energy units are given in kcal mol<sup>-1</sup>.

## 11. Discussion of experimental and computational kinetic studies

### 11.1 Discussion of Enchainment Kinetics (Excluding Potential Isomerization)

The linear dependence indicates that pseudo-1<sup>st</sup> order rate constant ( $k_{obs-1}$ , rate= $k_{obs-1}[Ni]$ ) is proportional to the concentration of tBA and inversely proportional to the concentration of pyridine in the range of concentrations studied. To evaluate this behavior, we considered five mechanistic pathways: **A**: Dissociative mechanism and rate determining step pyridine dissociation; **B**: Dissociative mechanism and rate determining step migratory insertion; **C**: Associative mechanism and rate determining step tBA coordination; **D**: Associative mechanism and rate determining step pyridine dissociation; **E**: Associative mechanism and rate determining step migratory insertion. Corresponding rate equation and expressions of rate constants are shown below:



**Path A:** Dissociative mechanism & Rate determining step: pyridine dissociation (Note: tBA is used as the model monomer in this section and following sections. However, the conclusion also works for ethylene or other monomers)

$$\frac{d[A]}{dt} = -k_1 \cdot \frac{k_2[tBA]}{k_{-1}[py] + k_2[tBA]} \cdot [A]$$

$$k_{obs} = k_1 \cdot \frac{k_2[tBA]}{k_{-1}[py] + k_2[tBA]}$$

In this case,

- 1) If  $k_{-1}[py] \gg k_2[tBA]$ ,  $k_{obs} \propto [tBA]/[py]$
- 2) Upper limit of  $k_{obs}$  is  $k_1$
- 3) In the double reciprocal plot (y axis:  $1/k_{obs}$ , x axis:  $[py]/[tBA]$ ), slope =  $1/(k_2 K_1)$ ,

Intercept =  $1/k_1$

**Path B:** Dissociative mechanism & Rate determining step: migratory insertion

$$\frac{d[A]}{dt} = -K_1 K_2 \cdot \frac{k_5[tBA]}{[py]} \cdot [A]$$

$$k_{obs} = -K_1 K_2 \cdot \frac{k_5[tBA]}{[py]}$$

$$K_{tBA/py} = -K_1 K_2$$

In this case,

- 1)  $k_{obs} \propto [tBA]/[py]$
  - 2) In the double reciprocal plot (y axis:  $1/k_{obs}$ , x axis:  $[py]/[tBA]$ ), slope =  $1/(K_{tBA/py} k_3)$ ,
- Intercept = 0

**Path C:** Associative mechanism & Rate determining step: tBuAc coordination

$$\frac{d[A]}{dt} = -k_3 \cdot \frac{k_4[tBA]}{k_{-3} + k_4} \cdot [A]$$

$$k_{obs} = k_3 \cdot \frac{k_4[tBA]}{k_{-3} + k_4}$$

In this case,

- 1)  $k_{obs}$  is not related to  $[py]$
- 2)  $k_{obs} \propto [tBA]$
- 3) In the double reciprocal plot (y axis:  $1/k_{obs}$ , x axis:  $[py]/[tBA]$ ), slope =  $1/K_3 k_4$ ,  
Intercept = 0 (for different  $[tBA]$ ); or slope = 0, Intercept =  $1/(K_3 k_4 [tBA]) + 1/(k_3 [tBA])$  (for different  $[py]$ )

**Path D:** Associative mechanism & Rate determining step: py dissociation

$$\frac{d[A]}{dt} = -K_3 k_4 \cdot \frac{k_5 [tBA]}{k_{-4} [py] + k_5} \cdot [A]$$

$$k_{obs} = K_3 k_4 \cdot \frac{k_5 [tBA]}{k_{-4} [py] + k_5}$$

In this case,

- 1) If  $k_{-4}[py] \gg k_5[tBA]$ ,  $k_{obs} \propto [tBA]/[py]$
- 2) If  $k_{-4}[py] \ll k_5[tBA]$ ,  $k_{obs}$  is proportional to  $[tBA]$  but not related to  $[py]$
- 3) In the double reciprocal plot (y axis:  $1/k_{obs}$ , x axis:  $[py]/[tBA]$ ), slope =  $1/(K_3 K_4 k_5)$ ,

Intercept =  $1/(K_3 k_4)$

**Path E:** Associative mechanism & Rate determining step: migratory insertion

$$\frac{d[A]}{dt} = -K_3 K_4 \cdot \frac{k_5 [tBA]}{[py]} \cdot [A]$$

$$k_{obs} = -K_3 K_4 \cdot \frac{k_5 [tBA]}{[py]}$$

$$K_{tBA/py} = -K_3 K_4$$

In this case,

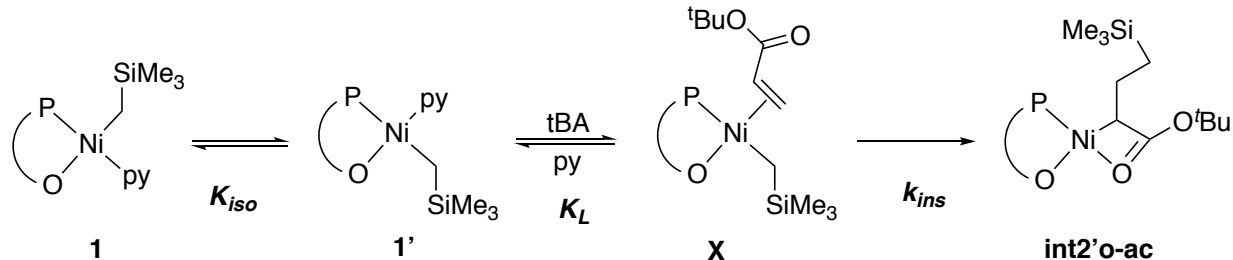
- 1)  $k_{obs} \propto [tBA]/[py]$
- 2) In the double reciprocal plot (y axis:  $1/k_{obs}$ , x axis:  $[py]/[tBA]$ ), slope =  $1/(K_{tBA/py} k_3)$ ,  
Intercept = 0

Notably, double reciprocal plot is not enough to differentiate path B and path E

Mechanisms A, C, and D are expected to result in non-zero intercepts and therefore are inconsistent with the data. Mechanisms B and E both predict zero intercepts and are consistent with the data. Both of these reaction pathways implicate olefin insertion is slow comparing to ligand exchange (pyridine dissociation + olefin coordination). Note that an isomerization process that moves the alkyl group to the position trans to the phosphine, as previously proposed for asymmetric ligand systems cannot be addressed experimentally as it results in the same dependence on substrate concentration as the above cases (see below).

## 11.2 Discussion of Enchainment Kinetics (Including Isomerization)

Consider the first insertion of either ethylene or tBA. Herein we use tBA as an illustration; note that the case for ethylene will be the same.



The overall rate of the formation of insertion product **int2'o-ac** is given by

$$\text{rate} = k_{ins} \cdot [\mathbf{X}] \quad (\text{A})$$

The isomerization step has the highest barrier for this transformation whereas the insertion step is rate-limiting after the isomerization. Applying the steady-state approximation to species **1'**, we have

$$0 = \frac{d[\mathbf{1}']} {dt} = k_{iso} [\mathbf{1}] - k_{-iso} [\mathbf{1}'] + k_{-L} [\mathbf{X}] [\text{py}] - k_L [\mathbf{1}'] [\text{tBA}] \quad (\text{B})$$

Consistent with experimental finding, the insertion step has a slower rate than olefin coordination such that a fast equilibrium exists between species **1'** and **X**. We then have

$$K_L = \frac{[\text{py}][\mathbf{X}]}{[\text{tBA}][\mathbf{1}']} \implies [\mathbf{1}'] = \frac{[\text{py}][\mathbf{X}]}{[\text{tBA}]K_L} \quad (\text{C})$$

where  $K_L$  is the equilibrium constant between species **1'** and **X**.

Substituting Equation (C) into (B), we have

$$0 = k_{iso} [\mathbf{1}] - k_{-iso} \frac{[\text{py}][\mathbf{X}]}{[\text{tBA}]K_L} + k_{-L} [\mathbf{X}] [\text{py}] - k_L \frac{[\text{py}][\mathbf{X}]}{[\text{tBA}]K_L} [\text{tBA}]$$

$$\implies [\mathbf{X}] = \frac{k_{iso}[\mathbf{1}][\text{tBA}]K_L}{k_{-iso}[\text{py}]} = K_{iso}K_L [\mathbf{1}] \frac{[\text{tBA}]}{[\text{py}]} \quad (\text{D})$$

Putting Equation (D) in (A), we have the rate of insertion as

$$\begin{aligned} \text{rate} &= k_{ins} \cdot [\mathbf{X}] = k_{ins}K_{iso}K_L [\mathbf{1}] \frac{[\text{tBA}]}{[\text{py}]} \\ &= k_{ins(\text{tBA})}K_{iso}K_{L(\text{tBA})} [\mathbf{1}] \frac{[\text{tBA}]}{[\text{py}]} \end{aligned} \quad (\text{E})$$

Similarly, the rate of insertion of ethylene is given by

$$\text{rate} = k_{ins(\text{et})}K_{iso}K_{L(\text{et})} [\mathbf{1}] \frac{[\text{et}]}{[\text{py}]} \quad (\text{F})$$

Note that equation (E) is consistent with the findings of experiment measurement of tBA enchainment that pseudo-1<sup>st</sup> order rate constant ( $k_{obs-1}$ ,  $\text{rate}=k_{obs-1}[\text{Ni}]$ ) is proportional to the concentration of tBA and inversely proportional to the concentration of pyridine in the range of concentrations studied.

### 11.3 Comparison of Ethylene and tBA Enchainment

Based on (E) and (F), the relative rate of insertions is then given by

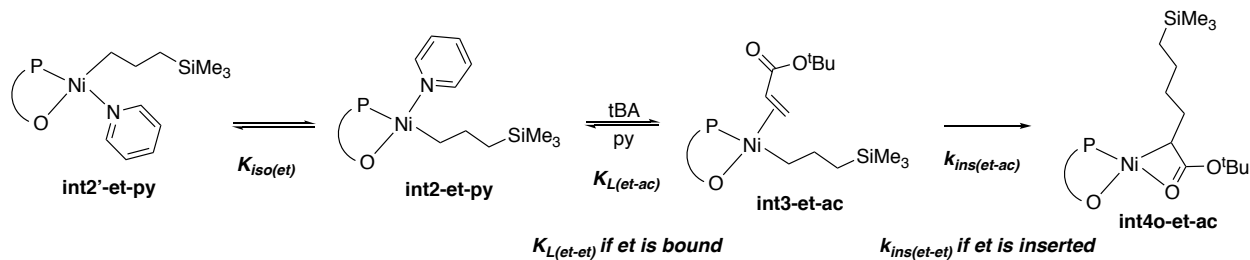
$$\begin{aligned} \frac{\text{rate}(\text{et})}{\text{rate}(\text{tBA})} &= \frac{k_{ins(\text{et})}K_{iso}K_{L(\text{et})} [\mathbf{1}] [\text{et}]}{k_{ins(\text{tBA})}K_{iso}K_{L(\text{tBA})} [\mathbf{1}] [\text{tBA}]} \\ &= \frac{k_{ins(\text{et})}K_{L(\text{et})} [\text{et}]}{k_{ins(\text{tBA})}K_{L(\text{tBA})} [\text{tBA}]} \\ &= \exp[-\Delta\Delta G^\ddagger/RT] \cdot \exp[-\Delta\Delta G/RT] \frac{[\text{et}]}{[\text{tBA}]} \end{aligned} \quad (\text{G})$$

where  $\Delta\Delta G^\ddagger = \Delta G_{ins(\text{et})}^\ddagger - \Delta G_{ins(\text{tBA})}^\ddagger$  is the difference between the activation barriers of the insertions and  $\Delta\Delta G = \Delta G_{ins(\text{et})} - \Delta G_{ins(\text{tBA})}$  is the difference between the

complexation/ coordination energies. Note that the barriers are measured for each *elementary step* in this analysis.

For the first insertion of ethylene (Figure S9.9), the barrier of insertion is 5.9 kcal mol<sup>-1</sup> (from **int1'-et-c2** to **ts1'-et**), while the coordination energy is 10.2 kcal mol<sup>-1</sup> (from **1'** to **int1'-et-c2**). For the first insertion of tBA, the barrier of insertion is 3.1 kcal mol<sup>-1</sup> (from **int1'-ac-c4** to **ts1'-ac**), while the coordination energy is 16.2 kcal mol<sup>-1</sup> (from **1'** to **int1'-ac-c4**). Therefore, this gives the difference between the activation barriers of insertion as 2.8 kcal mol<sup>-1</sup> and the difference between the coordination energies as -6.0 kcal mol<sup>-1</sup>. The overall difference in the first insertions of ethylene and tBA is thus  $(2.8 + (-6.0)) = -3.2$  kcal mol<sup>-1</sup>, i.e., the insertion of ethylene has a barrier that is 3.2 kcal mol<sup>-1</sup> lower than the insertion of tBA. This is consistent with the energetic span model<sup>25,26</sup> where the concept of turnover frequency (TOF) determining intermediate (TDI) and TOF-determining transition state (TDTs) is used. For both insertions, the TDI is the catalyst **1'** whereas the insertion step is the TDTs. The barrier differences between the insertion of ethylene (16.1 kcal mol<sup>-1</sup> from **1'** to **ts1'-et**) and the insertion of tBA (19.3 kcal mol<sup>-1</sup> from **1'** to **ts1'-ac**) is 3.2 kcal mol<sup>-1</sup>, consistent with the kinetic analysis above.

Using similar analysis for the second insertion (shown below second insertion of tBA into first ethylene-inserted product as an example), where the key rate-determining steps are the same as for the first insertion,



the relative rates for the second insertion of ethylene (et) vs tBA (ac) into first ethylene-inserted product is given by

$$\begin{aligned}
\frac{\text{rate(et-et)}}{\text{rate(et-ac)}} &= \frac{k_{ins(\text{et-et})} K_{iso(\text{et})} K_{L(\text{et-et})} [\text{int2'-et-py}] [\text{et}]}{k_{ins(\text{et-ac})} K_{iso(\text{et})} K_{L(\text{et-ac})} [\text{int2'-et-py}] [\text{tBA}]} \\
&= \frac{k_{ins(\text{et-et})} K_{L(\text{et-et})} [\text{et}]}{k_{ins(\text{et-ac})} K_{L(\text{et-ac})} [\text{tBA}]} \\
&= \exp[-\Delta\Delta G^\ddagger/RT] \cdot \exp[-\Delta\Delta G/RT] \frac{[\text{et}]}{[\text{tBA}]}
\end{aligned} \tag{H}$$

where again the differences between the Gibbs energy of activation  $\Delta\Delta G^\ddagger = \Delta G_{ins(\text{et-et})}^\ddagger - \Delta G_{ins(\text{et-ac})}^\ddagger$  and of complexation/ coordination  $\Delta\Delta G = \Delta G_{ins(\text{et-et})} - \Delta G_{ins(\text{et-ac})}$  are similarly defined.

#### 11.4 Comparison of initiation vs propagation of ethylene (or tBA)

The rates of first insertion (initiation) and second insertion (propagation) can be similarly compared. For example, the relative rates of first insertion of ethylene into catalyst **1** and second insertion of ethylene into ethylene-inserted product **int2'-et-py** is given by

$$\begin{aligned}
\frac{\text{rate(et)}}{\text{rate(et-et)}} &= \frac{k_{ins(\text{et})} K_{iso} K_{L(\text{et})} [\mathbf{1}] [\text{et}]}{k_{ins(\text{et-et})} K_{iso(\text{et})} K_{L(\text{et-et})} [\text{int2'-et-py}] [\text{et}]} \\
&= \frac{k_{ins(\text{et})}}{k_{ins(\text{et-et})}} \frac{K_{iso}}{K_{iso(\text{et})}} \frac{K_{L(\text{et})}}{K_{L(\text{et-et})}} \frac{[\mathbf{1}]}{[\text{int2'-et-py}]} \\
&= \exp[-\Delta\Delta G_{ins}^\ddagger/RT] \cdot \exp[-\Delta\Delta G_{iso}/RT] \cdot \exp[-\Delta\Delta G_{coord}/RT] \cdot \frac{[\mathbf{1}]}{[\text{int2'-et-py}]}
\end{aligned} \tag{I}$$

From the energy profile in Figure S9.9, we see that the barrier for insertion of ethylene into catalyst **1'** (elementary step) is 5.9 kcal mol<sup>-1</sup>; the insertion barrier of ethylene into **int2'-et-py** (Figure S9.11(a)) is 4.6 kcal mol<sup>-1</sup>. This gives a barrier difference in the insertion of 1.3 kcal mol<sup>-1</sup>. Similarly, the barrier difference in isomerization is 22.7 – 18.8 = 3.9 kcal mol<sup>-1</sup>. The difference in the coordination energies is 10.2 – 4.8 = 5.4 kcal mol<sup>-1</sup>. This gives a total barrier difference of 10.6 kcal mol<sup>-1</sup>. Using the energetic span model, the barrier for first insertion is 16.1 kcal mol<sup>-1</sup> from the TDI (**1'**) to TDTs (**ts1'-et**); the barrier for second insertion into first ethylene-inserted product is 9.4 kcal mol<sup>-1</sup> from the TDI (**int2'-et-py**) to TDTs (**ts3'-et**). This gives a barrier difference of 6.7 kcal mol<sup>-1</sup> which is the sum of the

differences in the coordination and insertion energies given by the elementary steps above ( $1.3 + 5.4$ ) =  $6.7 \text{ kcal mol}^{-1}$ .

### 11.5 Comparison of propagation of ethylene (or tBA) into ethylene-initiated vs tBA-initiated species

The rates of second insertion (propagation) of each olefin into first ethylene- or tBA-inserted product can be similarly compared. The difference in the rates will arise from the first insertion of ethylene vs tBA, followed by the isomerization in each insertion product, as well as the second insertion into each first insertion product. We consider the insertion of ethylene into ethylene-inserted product vs into tBA-inserted product as an example; the insertion of tBA into ethylene-inserted product vs into tBA-inserted product is similar. The first insertion of ethylene (**ts1'-et**) is more favorable than the insertion of tBA (**ts1'-ac**) by  $3.2 \text{ kcal mol}^{-1}$ . Then, the isomerization of first ethylene-inserted product (**ts-5coord-et**, with a barrier of  $18.8 \text{ kcal mol}^{-1}$ ) is in addition more favorable than the isomerization of first tBA-inserted product (**ts-5coord-ac**, with a barrier of  $22.3 \text{ kcal mol}^{-1}$ ) by  $3.5 \text{ kcal mol}^{-1}$ . The subsequent ethylene insertion into first ethylene-inserted product (**ts3-et-et**, with a barrier of  $9.4 \text{ kcal mol}^{-1}$ ) is in addition more favorable than the tBA insertion into first ethylene-inserted product (**ts3-et-ac**, with a barrier of  $19.3 \text{ kcal mol}^{-1}$ ) by  $9.9 \text{ kcal mol}^{-1}$ . Taken together, this implies that the insertion of ethylene into ethylene-inserted product is *ca.* 10 orders of magnitude faster than into tBA-inserted product.

For the insertion of tBA into first ethylene-inserted vs tBA-inserted product, the insertion of tBA into first ethylene-inserted product (**ts3-et-ac**) has a barrier of  $9.9 \text{ kcal mol}^{-1}$ ; the insertion of tBA into first tBA-inserted product has a barrier of  $20.5 \text{ kcal mol}^{-1}$ . This gives a difference in the insertion step of  $10.6 \text{ kcal mol}^{-1}$ , which is very similar to the difference of insertion of ethylene into first ethylene-inserted and first tBA-inserted product ( $9.9 \text{ kcal mol}^{-1}$  above). The differences in the first insertion of ethylene vs tBA and their subsequent isomerization are the same as above ( $3.2 \text{ kcal mol}^{-1}$  and  $3.5 \text{ kcal mol}^{-1}$  respectively). Thus, we expect the insertion of tBA into tBA-inserted product to be *ca.* 10 orders of magnitude faster than into tBA-inserted product.

## **References**

- 1) Pangborn, A. B.; Giardello, M. A.; Grubbs, R. H.; Rosen, R. K.; Timmers, F. J. Safe and convenient procedure for solvent purification. *Organometallics* **1996**, *15*, 1518-1520.
- 2) Neuwald, B.; Caporaso, L.; Cavallo, L.; Mecking, S. Concepts for stereoselective acrylate insertion. *J. Am. Chem. Soc.* **2013**, *135*, 1026-1036.
- 3) Low, C. H.; Rosensberg, J. N.; Lopez, M. A.; Agapie, T. Oxidative Coupling with Zr (IV) Supported by a Noninnocent Anthracene-Based Ligand: Application to the Catalytic Cotrimerization of Alkynes and Nitriles to Pyrimidines. *J. Am. Chem. Soc.* **2018**, *140*, 11906-11910.
- 4) Connor, E. F.; Younkin, T. R.; Henderson, J. I.; Waltman, A. W.; Grubbs, R. H. Synthesis of neutral nickel catalysts for ethylene polymerization—the influence of ligand size on catalyst stability. *Chem. Commun.* **2003**, 2272-2273.
- 5) Palmer, W. N.; Zarate, C.; Chirik, P. J. Benzyltriboronates: Building Blocks for Diastereoselective Carbon–Carbon Bond Formation. *J. Am. Chem. Soc.* **2017**, *139*, 2589-2592.
- 6) Bruger, B. J.; Bercaw, J. E. Vacuum line techniques for handling air-sensitive organometallic compounds. *ACS Publications: Experimental Organometallic Chemistry*, Chapter 4, **1987**, pp79-115.
- 7) **Full reference for Gaussian software:**  
Gaussian 16, Revision A.01, Frisch, M. J.; Trucks, G. W.; Schlegel, H. B.; Scuseria, G. E.; Robb, M. A.; Cheeseman, J. R.; Scalmani, G.; Barone, V.; Mennucci, B.; Petersson, G. A.; Nakatsuji, H.; Caricato, M.; Li, X.; Hratchian, H. P.; Izmaylov, A. F.; Bloino, J.; Zheng, G.; Sonnenberg, J. L.; Hada, M.; Ehara, M.; Toyota, K.; Fukuda, R.; Hasegawa, J.; Ishida, M.; Nakajima, T.; Honda, Y.; Kitao, O.; Nakai, H.; Vreven, T.; Montgomery Jr., J. A.; Peralta, J. E.; Ogliaro, F.; Bearpark, M.; Heyd, J. J.; Brothers, E.; Kudin, K. N.; Staroverov, V. N.; Kobayashi, R.; Normand, J.; Raghavachari, K.; Rendell, A.; Burant, J. C.; Iyengar, S. S.; Tomasi, J.; Cossi, M.; Rega, N.; Millam, J. M.; Klene, M.; Knox, J. E.; Cross, J. B.; Bakken, V.; Adamo, C.; Jaramillo, J.; Gomperts, R.; Stratmann, R. E.; Yazyev, O.; Austin, A. J.; Cammi, R.; Pomelli, C.; Ochterski, J. W.; Martin, R. L.; Morokuma, K.; Zakrzewski, V. G.; Voth, G. A.; Salvador, P.; Dannenberg, J. J.; Dapprich, S.; Daniels, A. D.; Farkas, Ö.; Foresman, J. B.; Ortiz, J. V.; Cioslowski, J.; Fox, D. J. Gaussian, Inc., Wallingford CT, 2016.
- 8) Grimme, S.; Bannwarth, C.; Shushkov, P. A Robust and Accurate Tight-Binding Quantum Chemical Method for Structures, Vibrational Frequencies, and Noncovalent Interactions of Large Molecular Systems Parametrized for All Spd-Block Elements ( $Z = 1\text{--}86$ ). *J. Chem. Theory Comput.* **2017**, *13* (5), 1989–2009.
- 9) Manby, F. R.; Miller, T. F.; Bygrave, P. J.; Ding, F.; Dresselhaus, T.; Buccheri, A.; Bungey, C.; Lee, S. J. R.; Meli, R.; Steinmann, C.; et al. Entos : A Quantum Molecular Simulation Package. *ChemRxiv*. **2019**.
- 10) Zhao, Y.; Truhlar, D. G. The M06 Suite of Density Functionals for Main Group Thermochemistry, Thermochemical Kinetics, Noncovalent Interactions, Excited States, and Transition Elements: Two New Functionals and Systematic Testing of Four M06-Class Functionals and 12 Other Function. *Theor. Chem. Acc.* **2008**, *120* (1), 215–241.

- 11) Weigend, F.; Ahlrichs, R. Balanced Basis Sets of Split Valence, Triple Zeta Valence and Quadruple Zeta Valence Quality for H to Rn: Design and Assessment of Accuracy. *Phys. Chem. Chem. Phys.* **2005**, *7* (18), 3297–3305.
- 12) Weigend, F. Accurate Coulomb-Fitting Basis Sets for H to Rn. *Phys. Chem. Chem. Phys.* **2006**, *8* (9), 1057–1065.
- 13) Frisch, M. J.; Trucks, G. W.; Schlegel, H. B.; Scuseria, G. E.; Robb, M. A.; Cheeseman, J. R.; Scalmani, G.; Barone, V.; Mennucci, B.; Petersson, G. A.; et al. Gaussian 16, Revision A.01. 2016.
- 14) Hu, L.; Chen, H. Assessment of DFT Methods for Computing Activation Energies of Mo/W-Mediated Reactions. *J. Chem. Theory Comput.* **2015**, *11* (10), 4601–4614.
- 15) Sun, Y.; Chen, H. Performance of Density Functionals for Activation Energies of Re-Catalyzed Organic Reactions. *J. Chem. Theory Comput.* **2014**, *10* (2), 579–588.
- 16) Sun, Y.; Chen, H. Performance of Density Functionals for Activation Energies of Zr-Mediated Reactions. *J. Chem. Theory Comput.* **2013**, *9* (11), 4735–4743.
- 17) Yu, H. S.; He, X.; Li, S. L.; Truhlar, D. G. MN15: A Kohn–Sham Global-Hybrid Exchange–Correlation Density Functional with Broad Accuracy for Multi-Reference and Single-Reference Systems and Noncovalent Interactions. *Chem. Sci.* **2016**, *7* (8), 5032–5051.
- 18) O'Duill, M. L.; Matsuura, R.; Wang, Y.; Turnbull, J. L.; Gurak, J. A.; Gao, D. W.; Lu, G.; Liu, P.; Engle, K. M. Tridentate Directing Groups Stabilize 6-Membered Palladacycles in Catalytic Alkene Hydrofunctionalization. *J. Am. Chem. Soc.* **2017**, *139* (44), 15576–15579.
- 19) Liu, Z.; Wang, Y.; Wang, Z.; Zeng, T.; Liu, P.; Engle, K. M. Catalytic Intermolecular Carboamination of Unactivated Alkenes via Directed Aminopalladation. *J. Am. Chem. Soc.* **2017**, *139* (32), 11261–11270.
- 20) Fukui, K. Formulation of the Reaction Coordinate. *J. Phys. Chem.* **2005**, *74* (23), 4161–4163.
- 21) Fukui, K. The Path of Chemical Reactions - The IRC Approach. *Acc. Chem. Res.* **1981**, *14* (12), 363–368.
- 22) Marenich, A. V.; Cramer, C. J.; Truhlar, D. G. Universal Solvation Model Based on Solute Electron Density and on a Continuum Model of the Solvent Defined by the Bulk Dielectric Constant and Atomic Surface Tensions. *J. Phys. Chem. B* **2009**, *113* (18), 6378–6396.
- 23) Grimme, S. Supramolecular Binding Thermodynamics by Dispersion-Corrected Density Functional Theory. *Chem.: Eur. J.* **2012**, *18* (32), 9955–9964.
- 24) Funes-Ardoiz, I.; Paton, R. S. GoodVibes v1.0.1 <http://doi.org/10.5281/zenodo.56091>.
- 25) Contreras-García, J.; Johnson, E. R.; Keinan, S.; Chaudret, R.; Piquemal, J. P.; Beratan, D. N.; Yang, W. NCIPLOT: A Program for Plotting Noncovalent Interaction Regions. *J. Chem. Theory Comput.* **2011**, *7* (3), 625–632.
- 26) Sosa, C.; Andzelm, J.; Elkin, B. C.; Wimmer, E.; Dobbs, K. D.; Dixon, D. A. A Local Density Functional Study of the Structure and Vibrational Frequencies of Molecular Transition-Metal Compounds. *J. Phys. Chem.* **1992**, *96* (16), 6630–6636.

- 27) Godbout, N.; Salahub, D. R.; Andzelm, J.; Wimmer, E. Optimization of Gaussian-Type Basis Sets for Local Spin Density Functional Calculations. Part I. Boron through Neon, Optimization Technique and Validation. *Can. J. Chem.* **1992**, *70* (2), 560–571.
- 28) Schrödinger, L. *The PyMOL Molecular Graphics Development Component, Version 1.8*; 2015.
- 29) Guironnet, D.; Roesle, P.; Rünzi, T.; Göttker-Schnetmann, I.; Mecking, S. Insertion Polymerization of Acrylate. *J. Am. Chem. Soc.* **2009**, *131* (2), 422–423.
- 30) Ito, S.; Munakata, K.; Nakamura, A.; Nozaki, K. Copolymerization of Vinyl Acetate with Ethylene by Palladium/ Alkylphosphine-Sulfonate Catalysts. *J. Am. Chem. Soc.* **2009**, *131* (41), 14606–14607.
- 31) Noda, S.; Nakamura, A.; Kochi, T.; Lung, W. C.; Morokuma, K.; Nozaki, K. Mechanistic Studies on the Formation of Linear Polyethylene Chain Catalyzed by Palladium Phosphine-Sulfonate Complexes: Experiment and Theoretical Studies. *J. Am. Chem. Soc.* **2009**, *131* (39), 14088–14100.
- 32) Amatore, C.; Jutand, A. Mechanistic and Kinetic Studies of Palladium Catalytic Systems. *Journal of Organometallic Chemistry*. Elsevier March 15, 1999, pp 254–278.
- 33) Kozuch, S.; Shaik, S. How to Conceptualize Catalytic Cycles? The Energetic Span Model. *Acc. Chem. Res.* **2011**, *44* (2), 101–110.